INFORMATION TO USERS

This manuscript has been reproduced from the microfilm master. UMI films the text directly from the original or copy submitted. Thus, some thesis and dissertation copies are in typewriter face, while others may be from any type of computer printer.

The quality of this reproduction is dependent upon the quality of the copy submitted. Broken or indistinct print, colored or poor quality illustrations and photographs, print bleedthrough, substandard margins, and improper alignment can adversely affect reproduction.

In the unlikely event that the author did not send UMI a complete manuscript and there are missing pages, these will be noted. Also, if unauthorized copyright material had to be removed, a note will indicate the deletion.

Oversize materials (e.g., maps, drawings, charts) are reproduced by sectioning the original, beginning at the upper left-hand corner and continuing from left to right in equal sections with small overlaps. Each original is also photographed in one exposure and is included in reduced form at the back of the book.

Photographs included in the original manuscript have been reproduced xerographically in this copy. Higher quality 6" x 9" black and white photographic prints are available for any photographs or illustrations appearing in this copy for an additional charge. Contact UMI directly to order.

UMI

A Bell & Howell Information Company
300 North Zeeb Road, Ann Arbor MI 48106-1346 USA
313/761-4700 800/521-0600

STRUCTURAL EVOLUTION OF THE NORWEGIAN-GREENLAND SEA: RESULTS FROM DETAILED ANALYSIS OF SeaMARC II SIDE-SCAN SONAR DATA

by

HANY S. DOSS

A dissertation submitted to the Graduate Faculty in Earth and Environmental Sciences in partial fulfillment of the requirements for the degree of Doctor of Philosophy, The City University of New York.

1997

This manuscript has been read and accepted for the Graduate Faculty in Earth and Environmental Sciences in satisfaction of the dissertation requirement for the degree of Doctor of Philosophy.

Nov. 5 1996
Date

Chair of Examining Committee

11/5/96
Date

Executive Officer

Professor Somdev Bhattacharji
Professor Charlotte Schreiber
Professor Enrico Bonatti
Supervisory Committee

The City University of New York

Table of Contents

LIST OF TABLES

LIST OF ILLUSTRATIONS, CHARTS and DIAGRAMS

CHAPTER 1

Chapter 2:

CHAPTER 1

MORPHOLOGY OF THE SLOW-SPREADING KNIPOVICH RIDGE: RESULTS FROM SeaMARC II SIDE-SCAN/SWATHI-BATHYMETRIC SURVEYS IN THE NORTHERN NORWEGIAN-GREENLAND SEA; Part 1: The Active Plate Boundary*

H. Doss[1], K. Crane[1,2,3], P. Vogt[3], and E. Sundvor[4]

(1) Department of Geology and Geography, Hunter College, 695 Park Avenue, NY, NY 10021, USA

(2) Lamont-Doherty Earth Observatory, Palisades, NY 10964, USA

(3) Code 7420, Naval Research Laboratory, Washington, DC 20375, USA

(4) Department of Solid Earth Physics, University of Bergen, Allegaten 41, Bergen, Norway

(*) submitted for publication

Abstract:

In 1989-1990 the SeaMARC II side-scan sonar (11-12 kHz) and swath bathymetric system imaged more than 80,000 km^2 of the seafloor in the Norwegian-Greenland Sea and southern Arctic Ocean. The data collected encompasses the continental margins along northwestern Norway and western Svalbard, the mid-ocean ridge rift valley along a 150 km long section of the northeastern Mohns Ridge and the entire Knipovich Ridge, the eastern and western flanks of the Knipovich Ridge, the Molloy Transform Fault, the Molloy Deep, and the Molloy Ridge.

Structural evidence for northward rift propagation of the Mohns Ridge into the ancient Spitsbergen Shear Zone (forming the Knipovich Ridge in the process) includes ancient deactivated and migrated transforms, subtle V-shaped-oriented flank faults which have their apex at the present day Molloy Transform, and rift related faults that extend north of the present Molloy Transform Fault. Evidence that the ancient shear zone may still control the overall orientation of the Knipovich Ridge lies in the contrast between the N-S oriented rift walls and the highly oblique en-echelon faults which reside in the rift valley.

The Knipovich Ridge is segmented into predominantly distinct elongate basins; the bathymetric inverse to the more southerly, very-slow spreading Reykjanes Ridge. Present day segment discontinuities coincide with some of the ancient fracture zone faults which are also the locus of large scale volcanism. It is possible that intermittent ponding and leaking of volcanic material occurred along these pre-existing faults creating anomalous belts of shallow bathymetry that cross obliquely onto both flanks of the rift valley. The influence of pre-existing faults on the evolution of the Knipovich Ridge is the primary

reason that the segment discontinuities, rather than the centers of the basinal segments are predominantly volcanic. This contrasts both the punctiform basin and dome segmentation patterns found along most other spreading centers.

Introduction and Background:

The Norwegian-Greenland seafloor is one of very few ocean basins that is young enough to allow us to study the early stages of rifting, spreading, and the development of mid-ocean ridge segmentation. In the case of the Knipovich Ridge, one of the slowest spreading centers in the world (present opening rate ca 1.5 cm/yr), we can observe the development of unusually oblique rifting (~10°-30°), and the en-echelon segmentation of a ridge evolving from a formerly active shear zone (Vogt, 1986).

The Mid-Atlantic Ridge can be traced through Iceland into the Norwegian-Greenland Sea as the Mohns and Knipovich Ridges of which the latter is oriented 70° oblique to the axis of the former (figure 1). The dramatic bend which connects these two spreading centers at 73°30'N is thought to contribute to large scale oblique compression and extension on the rift valley flanks (Crane et al., 1988).

The northern Knipovich Ridge lies in close proximity to the continental margin of the Svalbard Archipelago (figure 1), thereby unequally dividing the northern Norwegian-Greenland seafloor into the eastern Svalbard margin and the western Boreas Basin. At approximately 78°30'N, the Knipovich Ridge rift valley terminates against the Molloy Fracture Zone underneath thick layers of terrestrially and in part biologically derived sediment.

The Knipovich Ridge is thought to be connected to the slow-spreading Nansen Ridge in the Arctic Ocean by a remnant of the Paleo-Spitsbergen Shear Zone (figure 1). It is believed that transtension across this shear zone has led to the creation of several short

spreading centers (pull-apart basins) (Crane et al., 1982; Thiede et al., 1990 and Crane et al., 1991) of which the Molloy Deep Rift is an example. In addition, the more northwesterly section of the Spitsbergen Shear Zone is thought to be undergoing leaky transtensional opening, creating the Lena Trough in the process (figure 1) (Talwani and Eldholm, 1977; Sundvor and Eldholm, 1979; Crane et al., 1981; Eldholm et al., 1986; and Vogt, 1986).

The intricate geometry of the plate boundary, probably dominated by transtension and transpression, is accompanied by an array of off-axial structures that are non-linear and do not trend either orthogonal or parallel to the present day plate motion. These fault blocks and abyssal hills are thought to have been deformed by the substantial deviatoric stress generated across this young plate boundary which was constrained in its early history by inherited structural zones of weakness cutting across former continental crust (Crane et al., 1988 and Crane et al., 1991). Some of these off-axial features are thought to represent: (1) slivers of continental crust separated from the margin by transtension or, (2) fossil transform ridges and troughs which became deactivated as the spreading center propagated northward and the stress field changed from transpression to transtension while the crust underwent rotation, tilting, and bending. Finally, volcanic seamounts were created by ponding and leaking of magma into formally active shear zones leaving linear and oblate hills strewn across the abyssal plain (Crane et al., 1991).

The complexity of the plate boundary in the Norwegian-Greenland Sea reflects the complex opening history in this area. Seafloor spreading in the Norwegian-Greenland Sea and the Arctic Ocean started at approximately anomaly 24 (approximately 54-56 ma. on

the Cande et al., (1992) time scale) (Vogt, 1974, and Talwani et al., 1977). In addition, relative motion between Svalbard and Greenland during the early period was oriented northeast to southwest, with no apparent crustal extension to the north. The plate boundary between the incipient Norwegian-Greenland Sea and the Arctic Ocean was located instead along the broad regional continental Spitsbergen Shear Zone (also called the de Geer Zone) (Johnson, 1967; Harland, 1969; Horsfield et al., 1970; Eldholm et al., 1978; Talwani, 1977; Eldholm, 1980; Vogt et al., 1981; Crane et al., 1982; Dore et al., 1987; Crane et al., 1988)

A change in plate motions is thought to have occurred at about anomaly 13 (34 ma.) as a result of a change in the pole of rotation that increased the east-west component of opening. This marked the beginning of seafloor spreading in the northern Norwegian-Greenland Sea forming the Knipovich Ridge in the process (Talwani et al., 1977) (figure 2). Crane et al. (1988 and 1991) and Okay et al. (1993) proposed that the Knipovich Ridge propagated to the north along one of the major faults which comprised the Paleo-Spitsbergen Shear Zone.

The present Knipovich Ridge rift valley extends from 73°30′N, where it intersects the Mohns Ridge and 78°40′N where it intersects the Molloy Fracture Zone, a major (>100 km offset) transform. The axis of the ridge is characterized by a deep rift valley (greater than 3,000 m deep) which is punctuated by en-echelon belts of shallow bathymetric features (possibly volcanic centers) spaced 48-80 km apart (Vogt, 1986). In the north the rift valley approaches as close as 80 km to the Svalbard coastline making this one of the

closest approaches of a mid-ocean ridge to a continent (figure 1) (except for the Red Sea Rift and the Gulf of California spreading center).

Either an eastward shift in the axis or asymmetric spreading are two hypothesis that have been suggested to explain the asymmetric location of the northern end of the Knipovich Ridge relative to the Svalbard margin and the Greenland margin (Crane et al., 1991; Crane et al., 1982; Vogt et al., 1978; and Desimon, 1979). However, Ohta (1982) used bathymetric flow lines to argue against a geologically young eastward jump of the Knipovich Ridge.

Geophysical Signatures of Northern Norwegian-Greenland Seafloor:

From an analyses of well developed magnetic anomalies across the Mohns Ridge, Talwani and Eldholm (1977) calculated an average half-spreading rate of 0.45 cm/yr (28 to 20 mybp) for this plate boundary. However, the magnetic field is generally quiet over most of the entire Boreas Basin adjacent to the Knipovich Ridge (figure 3) (Sundvor and Eldholm, 1979) making it difficult to determine spreading rates from the magnetic anomaly time scale. Vogt et al., (1982 and 1986) have tentatively identified anomalies 5 and 6 on the western flanks of the Knipovich Ridge (concluding a half-spreading rates of 0.32 cm/yr for the period 36 to 13 mybp). They also suggested that additional anomalies may be identifiable. As figure 3 illustrates, magnetic anomalies are chaotic adjacent to the Knipovich Ridge compared with more normal anomalies along the northeastern section of the Mohns Ridge (Kovacs et al., 1987). Further north, the Nansen Ridge in the Arctic Ocean is characterized by predictable magnetic anomalies as well. Possible mechanisms to explain the chaotic magnetic signatures in the Norwegian-Greenland Sea include

thermal blanketing by sediments in the rift valley combined with a wide diffuse zone of magma injection (Eldholm et al., 1978; and Vogt, 1986), fragmentation due to excessive axial shifting and short lived transforms, and slow oblique spreading (Vogt et al., 1981).

Using heat flow data Crane et al., (1988) determined a half-spreading rate of 0.45 cm/yr. at 75°N and 0.15 -0.31 cm/yr. at 78°N. However, if these spreading rates are correct, they would violate rigid plate tectonics of the area. Crane et al., (1991) revised these spreading rates for the northern Knipovich Ridge after analyzing more than 100 heat flow stations. They determined that spreading was very asymmetric at a rate of approximately 0.7 cm/yr to the northwest and 0.1 cm/yr to the southeast.

Stein et al., (1977) proposed that spreading rate asymmetry could develop when one of the two diverging plates travels faster with respect to the deeper mantle. Thus more crust will be accreted to the slower plate. Minster and Jordan (1978) and Morgan (1981) have suggested that the North American plate has moved much more rapidly than the quasi-stationary Eurasian plate. This would seem to refute the Stein et al. (1977) hypothesis, because crust is apparently accreting more rapidly on the faster North American side (Vogt et al., 1982 and Crane et al, 1991).

Seismic asymmetry is also very pronounced across the Knipovich Ridge, with a region of anomalous seismic activity extending from Nordaustlandet west to the Knipovich Ridge. In contrast, the western Boreas Basin is nearly aseismic. Unfortunately, to date, very few focal depths have been established. However, first motions have been determined for several earthquakes on Svalbard (Chan and Mitchell, 1985). They indicate sinistral strike-slip motion on E-SE striking faults which are fairly oblique to all of the known major

faults in the region. This seismic asymmetry across the Knipovich Ridge suggests widespread tectonic intraplate deformation on the Eurasian plate.

Along the Knipovich Ridge a belt of well defined gravity minima can be found in the rift valley (figure 4) (after Sobczak et al., 1990). The axial gravity anomaly is semi-continuous from the Mohns Ridge to about 76°N where it is right-laterally offset. The continuity of the anomaly suggests a regionally continuous ridge without major offsets. Along the Knipovich Ridge, the western flank has free air gravity values of 10 to 20 mGal higher than the eastern flank (Vogt, et. al., 1982). However, adjacent to the southern Knipovich Ridge, the free air gravity field of the western flank is as much as 60 mGal higher than the eastern flank (figure 4).

Because of a paucity of high resolution data in this area prior to 1989 and the complexity of the magnetic anomaly pattern (figure 3) (Vogt et al., 1980; Vogt et al., 1981; Kovacs et al., 1984) it had been nearly impossible to determine whether or not the Knipovich Ridge was broken into many spreading segments, offset by small transform faults or was rifting across an en-echelon set of extensional grabens. Partly to answer this question, and to clarify many inconsistencies in the published literature (for example Detrick, 1994; who considered the Knipovich Ridge as a transform fault rather than a mid-ocean ridge), our Norwegian-American team mapped the entire axis of the Knipovich Ridge in 1989 and 1990 using the SeaMARC II side-looking sonar system operated out of the Hawaii Institute of Geophysics. The SeaMARC II imagery (figure 5) has provided nearly continuous bathymetric and structural coverage of this once poorly mapped region. In the following sections we present this detailed information and discuss the morphotectonic

evolution and segmentation along the rise axis. The need for high resolution geophysical data to resolve present ridge evolution remains and should be addressed in future surveys.

Instrumentation and Data:

The primary tool used for this survey was the SeaMARC II which was outfitted on the Norwegian research ship "R/V Haakon Mosby". The SeaMARC II is a shallow tow, long range, high resolution seafloor mapping system with the capability of simultaneous recording of digital side-scan sonar images as well as bathymetry across a swath of ensonified seafloor. Bathymetry is determined by measuring phase differences of acoustic arrivals on each of two pairs of transducer arrays, one on each side within the tow vehicle. For deep ocean surveys, it is towed at a depth of approximately 100 m below the surface, which allows it to avoid the high sound velocity gradients near sea surface (Shor, 1990). The system operates at 11 kHz on the port side and 12 kHz on the starboard side. A drogue is attached to the slightly positively buoyant sonar vehicle, providing stability of about 1° in roll and 2-3° for pitch and yaw.

For seafloor depths greater than 1.0 km, the side-scan sonar subsystem is configured to produce a swath of data 10 km wide. Bathymetric data are recorded from nadir to a maximum angle of 60° (a maximum bathymetric swath equal to 3.4 times water depth). The bathymetric swath width is independent of the side-scan swath setting.

The SeaMARC II side-scan images contain 1024 pixels of digital data on either side of the swath with the inner 40 pixels not logged (to avoid interference from multiple sound signals). The individually logged reflectivity values are placed at even spacing across the

track, the bottom being assumed planar and equal to depth directly below the towfish. Pixel spacing was 5 m for the 10 km swath width configured for these surveys. Along-track resolution is a function of the beam width of the system, which is nominally 2° (about 3% of slant range) and therefore widens towards the outer edge of the swath. Side-scan data are slant-range corrected to water depths below the vehicle at the time of collection.

Additionally, the ship was outfitted with a gravimeter, magnetometer, as well as 3.5 kHz and 38 kHz echo-sounders. Unfortunately, during high sea states, equipment failure and poor data quality would not allow reliable use of these data in this paper.

During our 1989 survey, the speed was mostly in the 7-10 knots range, with slower speeds used when maneuvering around or avoiding ice floes (north of latitude 78°30'N). In contrast, the 1990 survey encountered several periods of very rough weather (high sea-state) and system problems occurred. There were several days when the speed averaged less than 1 knot, and the tow vehicle had to be recovered for repairs.

The area covered by the SeaMARC II survey encompasses the entire Knipovich Ridge rift valley, the western ridge flank of the Knipovich Ridge from 76°45'N to the Molloy Transform Fault (extending west and away from the rift valley to a maximum distance of approximately 45 km), the eastern ridge flank of the Knipovich Ridge from 76°15'N to the Molloy Transform Fault (extending east and away from the rift valley to a minimum depth of approximately 1,000 m near the continental margin, the Molloy Transform Fault, the Hovgård Ridge, and the eastern part of the Boreas Basin (figure 6).

Data Interpretation:

Bathymetric contours at 100 m intervals from the SeaMARC II bathymetry as well as lineations from the side-scan imagery were digitized to produce the final product presented here. Where there was a gap in the data, some interpolation was required between closely spaced tracks. Interpolations were limited to gaps between swaths inside the total area mapped.

Recognition of seafloor patterns is a function of the type of feature causing the echo. Linear to semi-linear features (such as faults) are recognized if they have widths of only a few to several tens of meters. Fault escarpments are much easier to identify if they are young, not yet degraded, and offset a uniformly sedimented seafloor. Paradoxically, such lineations may be more difficult to identify where sediments are thin, disturbed, or non-existent. Sediment thickness in the area of study varies from as little as 100m to a few hundred meters (Vogt, 1986) and seafloor expressive of faults are present throughout most of the imaged area near the plate boundary. Between 75°30'N and 76°N, sediment thickness in the rift valley exceeds 400 meters and; fault numbers vary between 0 and 8 (figure 15). As sediment thickness increases on either side of the rift valley, only faults with the largest offset (hundreds of meters) are recognized on the sonar imagery. This possibly contributes to lower fault distribution statistics towards the outer sections of the survey.

Lava flows are easily recognizable due to the greater backscatter they generate (which usually results in darker colors on the records). However, if greater backscatter is observed near the base of the rift valley wall, then it is possible that these darker areas are

rift margin talus slopes instead of lava flows. We interpreted most of these rift margin high backscatter areas to be lava flows due to their characteristic lobate nature, distinctive ripples and draping appearance. While occasionally, high backscatter is correlated with bathymetrically sloping seafloor (for example figures 7A, 7B and 7C; near 73°55'N on the western side of the inner rift valley), more often than not, these areas are nearly flat or very gently sloping (for example figures 7A, 7B and 7C; between 74°20'N and 74°05'N where all high backscatter areas coincide with nearly flat seafloor. Of course, complete certainty of the nature of these areas can only be achieved by future ground truth surveys along the Knipovich Ridge.

Nature of Segmentation:

Macdonald et al. (1991) suggest that segmentation for slow spreading centers can be broken into four orders: Order 1 has a segment length of as much as 400 km and is bounded by a transform fault or rift valley propagator tip. Order 2 has a segment length of 50 km (+/- 30 km) and is bounded by oblique shear zones or rift valley jogs. Order 3 has a segment length of 15 km (+/- 10 km) and is bounded by inter-volcanic lows. Finally, order 4, with a segment length of 7 km (+/- 5 km), is bounded by intra-volcanic lows.

The nature of segmentation of nascent mid-ocean ridges has been studied along the rifted margins of the central Red Sea (Bonatti, 1985; Crane et al, 1987). From these observations, Bonatti (1985) suggested that segmentation of incipient mid-ocean ridges is determined by the spacing between "punctiform" nucleation points where basinal segments form above upwelling asthenosphere. On well developed mid-ocean ridges, axial segmentation has been attributed to a similar Rayleigh-Taylor type of gravitational

instability in a partially molten mantle beneath spreading centers creating volcanic domes on the rise axis (Crane, 1985; and Schouten et al., 1985). In these two gravitational instability models, first and second order segments are thought to mark the locus of rising and melting mantle diapirs. However in the nascent spreading center case, eruption of harmonically spaced magmatic centers creates crust more dense than its surrounding (Crane, 1985), thus creating volcanic basins; the bathymetric inverse to the harmonically spaced volcanic domes located on a well developed mid-ocean ridge.

This paper will attempt to show that along the Knipovich Ridge the above models do not adequately describe its segmentation. There are no obvious harmonically spaced magmatic centers as suggested by Crane (1985) and Schouten (1985). Furthermore, the ridge is dominated by basins rather than rift valley volcanic highs as described by Macdonald (1991).

Bathymetric Analyses:

In general, the Macdonald et al., (1991) scheme suggests that segmentation is a combination of both volcanic and structural/tectonic processes with the two longest segments (1 and 2) defined by greater or lesser transforms or obliquely oriented structures in the rift valley while the two shortest segments (3 and 4) are defined by smaller scale volcanism. In contrast, for fast spreading ridges, Crane (1988) suggested that both deep-seated volcanic and thin-skin structural (short wavelength) segmentation controlled the evolution of the ridge.

Because of the absence of transform faults on the Knipovich Ridge, the entire axis from the bend at the Mohns Ridge to the Molloy Transform Fault (>500 km in length) could be

considered a segment of order 1 according to Macdonald et al (1991) (Vogt et al., 1982; Vogt, 1986).The Knipovich Ridge rift valley is further characterized by basins reaching depths 3,000≥3,500 m, that are for the most part separated by central rift volcanoes oriented obliquely to (and which completely fill up) the rift valley; or by structural highs which obliquely cross the rift valley.

The fact that these bathymetric highs are the locus for oblique faulting (which is the bathymetric inverse to the Macdonald et al., 1991, proposal), poses some difficulties in choosing segment centers and discontinuities. Except for the "punctiform" basin evolution model proposed by Bonatti, 1985; all other segmentation models suggest that a bathymetric (volcanic) high is the center of a segment. Apropos, the boundaries between segments should be cold, deep and often the site of either transform faults or major oblique offsets in the axis. In the case of the Knipovich Ridge, it would be incorrect to choose the bathymetric highs as the centers of its segments. It would be more appropriate to determine whether or not a segment is bounded by lows or highs, by looking at the aspect ratio of either the lows or highs. In the case of the ridges selected by Macdonald et al., (1991), the highs had a much greater length/width ratio than the lows. The inverse is the case along the Knipovich Ridge with the average L/W ratio for basins being far greater than the L/W ratio for highs (10:0.25). Therefore, the highs maybe considered the boundaries to the basinal segments which are not uniform in length, depth or orientation (figure 7C-14C). Thus, we will modify Macdonald's order 2 and 3 segmentation to include those sections of the rift that are bounded by central rift volcanoes or intra rift structural highs that rise 300-400 m above neighboring rift basins.

In general, on the Knipovich Ridge the segment of order 1 is approximately 500 km long and is truncated in the south by the intersection of the Mohns Ridge with the Knipovich Ridge, and to the north by the Molloy Fracture Zone. Order 2 segments are on average 60 km long (+/- 30 km), 3,100 m deep, 8 km wide and are predominantly truncated by rift valley jogs and centralized volcanic activity. These second order segments are comparable to the 40-80 km segmentation wavelength suggested by Vogt (1986). In addition, they are also comparable to Vogt's tentative 50-100 km intermediate wavelength magnetic anomalies which are based on variations in basement topography away from the rift valley.

Order 3 segments are smaller basins on average 30 km long (+/- 10 km), 3,300 m deep, 7 km wide and bounded by a shoaling rift valley (usually extrusive volcanics). Within these segments, there are smaller scale depth and shape variations creating order 4 segments which are on average 20 km long (+/- 5 km), 3450 m deep, and 5 km wide.

The segmentation styles of the Knipovich Ridge are described in detail in the following sections and are summarized in figure 6.

Structural Analyses:

The side-scan imagery (figures 7b-14b) illustrates that there is no easily recognizable pattern of fault distribution within the inner rift or along the flanks of the Knipovich Ridge. For this reason we tabulate fault data using a grid in which a single cell represents one minute of latitude on the N-S axis and 5 km on the E-W axis (at increments of 5 km from the center of the rift valley to 45 km on either side). Fault numbers, spacing, and orientation for the entire Knipovich Ridge axis (figures 15 and 16) and surveyed sections

of rift flanks were entered into the database. The grid's center was chosen as the deepest point of the inner rift and thus required continuous adjustment from one latitude to another. The throw of individual fault escarpments is not easily determined with the SeaMARC II-type data and thus was not entered into the database.

Fault numbers within a given cell were tabulated from the number of faults, regardless of their lengths. Fault orientation was also measured within an individual cell regardless of the overall orientation of the fault. Where the fault radically changed its orientation within a cell, the average of the different orientations for that fault was tabulated.

Fault spacing was tabulated on the eastern and western sides of the axis of the Knipovich Ridge at distances from the axis of 0-5 km, 0-10 km, 0-15 km, 0-20 km, 0-25 km, and 0-45 km. Unfortunately, because the excess sedimentation on the eastern flank has buried many of the major faults in this region, there must be a bias in the statistics. In general, the SeaMARC II side-scan is incapable of detecting features more than few meters below a sedimented seafloor.

Faults vary dramatically in length and they occasionally overlap from one segment to the next (for example see figure 10 B and 10C). Consequently, we decided to measure fault length according to any one bathymetrically defined second order segment.

From south to north, the rise axis can be divided into eight second order segments ranging from 30 km to 60 km in length. These are as follows:

Detailed Along axis segmentation:

1. Order 2 (73°51'N to 74°20'N)

The southern boundary of this segment (figure 7) lies within the 70° bend between the Mohns Ridge and the Knipovich Ridge rift valley. At the segment's northern terminus, the strike of the rift valley changes by another 30° from 010° to 340°(compared to an average fault azimuth of 016°). The segment is a basin defined by the 3,200 m contour; has a length of 52 km, an orientation of 010°, a maximum depth greater than 3,400 m, and an average width of 6.3 km. Fault lengths vary between 0.2 km and 20 km with the majority of faults from 7 km to 9 km in length (figure 14). The average fault density is 1.58 faults/km (total number of faults per 1 km increment of the segment averaged along the entire segment) on the eastern side of the rift valley and 0.95 faults/km on the western side of the rift valley (figure 15). The segment is further subdivided into three sub-segments; (1A, 1B, and 1C).

1A. Order 3 (73°52′N to 73°56′30"N)

Segment 1A is defined by the 3,300 m contour (figure 7). It is 8.1 km in length, exceeds 3,400 m in depth, has an average width of 3 km, an orientation of 035° compared to an average fault azimuth of 024°. Its northern discontinuity lies at 73°58′N where the seafloor shoals to less than 3,000 m and the fault azimuth shifts to 019°. The eastern side of the 1A rift valley segment has an average fault density of 4.66 faults/km (maximum density at 73°51′N of 9.33 faults/km) (figure 15). There are no observable faults on the western side of the rift valley floor.

1B. Order 3 (73°59′N to 74°10′N)

The segment 1B basin is defined by the 3,300 m contour (figure 7). It is 20 km in length, exceeds 3,400 m in depth, has an average width of 3.6 km, and an orientation of 019°. By comparison, fault azimuths average 018°. At its northern discontinuity, the seafloor shoals to 3,200 m and is covered by highly reflective (presumed recent) fresh lava flows where faults trend 023°. Fault density on the eastern rift valley is ~2.6 faults/km compared to a western fault density of 2.3 faults/km (figure 15). Between 74°00'N and 74°04'N the eastern rift valley is heavily faulted (3.88 faults/km). In contrast, higher density faulting in the western rift valley occurs between 74°05'N to 74°08'N (12 faults/km). Between 74°05'N and 74°10'N, lava flows appear to dominate the rift valley.

1C. Order 3 (74°13'N to 74°19'N)

The segment 1C basin is defined by the 3,300 m contour (figure 7). It is 12.6 km in length, varies in width from 1.8 km in the south to 3.6 km in the north, and has an orientation of 018°. By comparison average fault azimuths are 005°. The segment's northern structural discontinuity is characterized by a shift in the strike of the rift valley to 340° where faults trend 013°. Fault density is 3.11 faults/km in the eastern rift valley and 3.48 faults/km in the western rift valley (figure 15). Between 74°15'N and 74°17'N, fault density increases to 4.9 faults/km on both sides of the rift valley.

2. Order 2 (74°19'30"N to 75°52'N)

Segment 2 is bounded by a southern axial structural discontinuity which occurs where the rift valley strike shifts from 010° in the south to 340° (the average strike of the segment)

(figures 7 and 8). The northern boundary is characterized by a reverse axial shift to a trend of 000°. Segment 2 has a length of 165 km, its average width exceeds 10 km (the width of the survey swath) and the maximum depth exceeds 3,700 m (at 75°27'N) (figure 8). Average fault length and azimuth are about 6.5 km (figure 14) and 007°, respectively, while average fault density ranges from 0.25 faults/km on the eastern side of the rift valley to 0.86 faults/km on the western side (figure 15).

Between 74°26'N and 74°45'N, highly reflective acoustic backscatter suggests the presence of relatively fresh and unsedimented lava flows surrounded by older lava flows. Segment 2 is further broken into five smaller segments (2A, 2B, 2C, 2D, and 2E).

2A. Order 3 (74°19'30"N to 74°36'N)

Segment 2A is defined by the 3,200 m contour (figure 7). It is 30 km in length, exceeds 3,400 m in depth, has an average width of 5.4 km, an orientation of 000° compared to an average fault strike of 004°. Its northern boundary/discontinuity of order 3 is a cone shaped volcano that shoals to less than 2,800 m at 74°40'N. The top of the volcano lies ~2 km from the boundary with segment 2B (exact separation distance is not possible to determine as the tip of the segment lies outside the imaged area). The fault density at the southern discontinuity is 0 faults/km and 0.37 faults/km for the eastern and western rift valley respectively while at the northern discontinuity faulting is not observed (figure 15).

There are bathymetric discontinuities of type 4 marked by necking of rift valley walls and the narrowing of rift basins at 74°21'N and 74°32'N which break this segment further into three Order 4 segments (figure 7). These three segments (2A1, 2A2, and 2A3) have the

following maximum depths; 3,200 m, 3,400 m and 3,300 m respectively. Their length to width ratios from south to north are 2.0 km/3.6 km, 19 km/8 km and 11 km/6.3 km respectively. The first segment is cut by a total of only 6 faults. The second segment has a maximum fault number of 8 and 7 at 74°25'N and 74°26'N, respectively (towards the middle of the segment) on the eastern side of the rift valley compared with 7 faults at the northwestern boundary of the segment. The eastern side of the inner rift has an average fault density of 1.18 faults/km compared with 0.75 faults/km on the west. The third segment (2A3) has no observable faults present on the eastern side while on the western side, the fault density is 0.71 faults/km. The highest fault number (8) occurs at 74°34'N (towards the center of the segment).

2B. Order 3 (74°41'N to 74°45'N)

The segment 2B basin is delineated by the 3,200 m contour (figure 7), has a length of 7.2 km, a maximum depth in excess of 3,300 m, an average width of 2.7 km, an orientation of 000°, and an average fault density of less than 0.37 faults/km on both sides of the inner rift. In contrast to the basin orientation, fault azimuths average 021°. The segment is bounded to the north by both a structural and bathymetric discontinuity, where the rift valley changes strike to 060° (with faults striking 036°) and the seafloor shoals to less than 2,900 m at 74°46'N. A somewhat poorly defined triangular crater marks the crest of the inter-segment high which is ~12.7 km in length.

2C. Order 3 (74°47'30"N to 75°22'30"N)

The segment 2C basin is delineated by the 3,400 m contour (figures 7 and 8), has a length of 63 km, a maximum depth in excess of 3,500 m, an average width that exceeds 8 km (the eastern side of the rift valley inner walls are outside of the SeaMARC II track coverage), and a strike of 340°. The segment is truncated in the north by a 030° trending structural high where the seafloor shoals by 400 meters. The structural high is bounded by major faults which completely cross the rift valley at an angle ~30° oblique to the extensional faults which cut the neighboring rift basins. The segment has a fault density of 0.57 faults/km on the eastern side of the rift floor in contrast to 1.33 faults/km on the western side (figure 14).

There are order 4 discontinuities at 74°55'N and 75°16'N which break this segment into three smaller sub-segments (2C1, 2C2, and 2C1) (figure 7 and 8). The three segments have maximum depths in excess of 3,500 m. However, their length and orientation from south to north vary as follows: 13.5 km, 37.8 km, and 11.7 km respectively; and 335°, 000°, and 022°.

Sub-segment 2C1 (figure 7) has no more than 2 faults on the eastern rift valley floor (at 74°54'N) while on the western rift valley floor a maximum of 7 faults can be found in the middle of the segment (at 74°51'N). On both sides of the rift floor, the number of faults is greater towards the center than at the boundaries of the segment. This pattern appears to be independent of the fault density as the western side of the rift has a density of 5 faults/km compared with the eastern density of 0.8 faults/km.

Sub-segment 2C2 (figures 7 and 8) has a maximum of 9 and 13 faults across the rift valley; east and west respectively. From the southern to the central part of the segment, fault numbers change from 1 and 4 (east and west) to 2 and 3 (east and west). At the northern terminus of the segment, fault numbers change again to 6 and 0 east and west respectively. Between 74°59'N and 75°05'N, fresh lava flows cover the eastern floor of the rift valley while both faults and lava flows are recognizable in the western part of the rift valley. The transition between 2C2 and 2C3 is characterized by faults trending 025°on the southern side and lava flows on the northern side of the boundary.

Sub-segment 2C3 (figure 8) has a maximum of 6 and 10 faults across the rift valley; east and west respectively. However, on the eastern side, the maximum fault numbers occur at the distal edges of the segment boundaries and not at its center. On the western side, the number of faults increases from south to north.

2D. Order 3 (75°23'N to 75°43'N)

The segment 2D basin is delineated by the 3,400 m contour (figure 8), has a length of 36 km, a maximum depth in excess of 3,700 m, an average width that exceeds 9.0 km (the western side of the rift valley inner walls are outside of the SeaMARC II track coverage), and an orientation of 000°. In contrast, faults within the segment trend an average of 003°. The segment's northern terminus is bounded by a volcanic high that shoals to a depth shallower than 2,900 m. Superimposed on this high are numerous cones and craters. The segment is cut by a maximum of 22 faults of which 8 and 14 (figure 14) cross through the eastern and western sides; respectively. On either side of the rift valley floor,

the maximum fault numbers occur at opposite segment boundaries (east; 75°41′N and west; 75°27′N). In contrast, the middle of the segment has few or no faults present. On average, eastern fault density is 1.7 faults/km compared to western fault density of 2.6 faults/km. A large highly reflective lava flow covers the middle of the segment.

2E. Order 3 (75°43′N to 75°52′N)

The segment 2E basin is defined by the 3,400 m contour, has a length of 16 km, a maximum depth greater than 3,500 m, an orientation of 005°, an average width of 2.5 km (the floor of which is covered by lava flows). This basin is cut by 9 faults of which 2 occur on the eastern and 7 on the western side (figure 14). On the western side of the rift valley, faults increase in number towards the middle of the segment and decrease towards the boundaries. The few faults on the eastern side occur near the segment's boundaries. Fault density on the eastern side is 0.44 faults/km compared to the western side's 2.8 faults/km. Fault lengths vary between 0.5 km and 0.9 km and their azimuths average 004°.

3. Order 2 (75°55′N to 76°32′N)

The segment 3 basin is delineated by the 3,300 m contour (figures 8 and 9). Its southern and northern boundaries are marked by rift valley volcanoes as well as a change in the strike of the rift valley. The southern discontinuity's volcano shoals to less than 2,900 m while the northern discontinuity volcano shoals to less than 2,800 m. The segment's length is 67.0 km, has an average width of 5.5 km, and a maximum depth greater than

3,500 m. Fault density in this part of the rift valley is 1.3 faults/km and 1.7 faults/km (figure 15); east and west respectively with an average fault length of 6 km (figure 14). The maximum number of faults occurs at mid-segment (5 and 10 at 76°18'N and 76°02'N, east and west respectively). The average fault azimuth in segment 3 is 017° contrasted with the 000° orientation of the long rift valley basin.

In this segment, lava flows are recognizable between 75°55'N and 76°12'N (figure 8). Fresh lava flows can be differentiated by their higher reflectivity (black color) on the imagery. Some of the flows appear to be older and covered by sediment which is suggested by the lighter grayish color on the images. Within the lava flows, only a few faults are observable. This segment is further subdivided by a discontinuity of type 3 at 76°00'N where the rift valley floor narrows creating subsegments 3A and 3B.

3A. Order 3 (75°55'N to 76°00'N)

Segment 3A is an elongate basin outlined by the 3,400 m contour (figure 8). It has a length of 9 km, a maximum depth greater than 3,400 m, and an average width of 3.6 km. The segment is slightly bifurcated by two major axes. The longer axis has an orientation of 045° while the shorter axis has an orientation of 026° resulting in an average overall azimuth of 035°. By comparison, faults within the basin (of which there are 4), trend 023° on average and at its northern boundary, trend 025°. The western boundary of the segment shoals to less than 2,500 m.

3B. Order 3 (76°00'N to 76°32'N)

The segment 3B basin is defined by the 3,400 m contour, has a length of 57.6 km (figures 8 and 9), a maximum depth of greater than 3,500 m, an average width of 6.0 km, and a strike of 000°. In contrast, faults within the segment trend an average of 016°. The segment is bounded in the north by an order 2 discontinuity, where the strike of the rift valley shifts to a more northeasterly trend (020°) and where fault azimuths have an average of 022°. Segment 3B is bounded by an order 3 rift valley discontinuity at its southern terminus where the seafloor shoals to less than 2,800 m. Furthermore, the segment 3B is characterized by a bow-shaped northeastern rift wall (concave towards the axis) (figure 9B). The boundary rift valley faults truncate abruptly at the northern discontinuity where the rift suddenly narrows. Fault density averages 1.3 faults/km and 1.7 faults/km; in the eastern and western rift valley respectively. The mid-section of this segment is most heavily faulted (figure 15), ranging from 0 to 5 (in the eastern rift) and 0 to 10 (in the western rift). Both intermixed fresh and old lava flows cover the mid-segment rift valley.

4. Order 2: 76°38′N to 77°25′N:

The basin comprising segment 4 trends 011° while the average fault azimuth is 012°. In contrast, at its southern and northern boundaries, the rift valley changes strike to 000° and 033° respectively. The segment basin is defined by the 3,100 m contour, has a length of 84.6 km, a maximum depth of greater than 3,700 m, and an average width of 10 km (figures 9 and 10). Fault lengths within this rift valley segment average 4 km compared to 4.5 km and 4.8 km on the adjacent eastern and western flanks (figure 14). Fault density

averages 1.1 faults/km on both sides of the rift floor while fault number varies between 0 and 4 (figure 15). The greatest density of faulting occurs on the southwestern, and northern boundaries; as well as in mid-segment.

The northern boundary is characterized by a large elliptical volcano, extending from 77°24'N to 77°33'N and striking 033° (figure 10). The elongate volcano lies along the eastern side of the rift valley. The base of the elliptical volcano is defined by the 3,100 m contour and it shoals to less than 2,600 m. It has a length of 16.2 km and a width of 3.6 km. Along this boundary, on the eastern and western sides of the rift valley floor, faults and fissures vary in number from 0-4 and 1-3, respectively (figure 15). Fault length within this segment averages 3.8 km compared to 4.6 km and 6.7 km on the adjacent eastern and western flanks (figure 14). Fault azimuth average 001°. Lava flows occur primarily near the western inner rift (figure 10 and 11) and with flow boundaries reminiscent of zigzagging cuspate waves.

The segment is further subdivided into two order 3 segments (4A and 4B) by a discontinuity of type 3 where the rift valley shoals to less than 3,300 m.

4A. Order 3 (76°38'N to 76°48'N)

The segment 4A basin is defined by the 3,300 m contour (figures 9 and 10), has a length of 18 km, a maximum depth greater than 3,600 m, an average width of 6.0 km, and an orientation of 030° (in contrast to an average fault azimuth of 016°). Average fault density is 0.8 faults/km on both sides of the rift. However, on the eastern rift floor, the fault number increases towards the center of the segment. On the western side, the

maximum number of faults (4) occurs at the southern discontinuity and at mid-segment (figure 15). Segment 4A is bounded by a discontinuity at its northern terminus where the rift valley shoals to less than 3,300 m and average fault azimuths change strike to 000°.

4B. Order 3 (76°49'N to 77°25'N)

The segment 4B basin is defined by the 3,300 m contour (figure 10), has a length of 65 km, a maximum depth of greater than 3,700 m, an average width of 10 km, and an orientation of 004° Its northern boundary is characterized by a shift in the strike of the rift valley to 000°. Fault density on the eastern side of the rift floor is 1.4 faults/km (ranging from 0-4 faults) surpassing western side fault density of 0.9 faults/km (ranging from 1 to 3 faults) (figure 15). Fault azimuth in segment 4B is on average 011° which is 7° oblique to the segment's bathymetric trend and the same as the overall trend of the segment 4 basin.

There is a discontinuity of type 4 at 76°59'N where the 3,400 m contour necks at a mid-rift high (possibly a volcano) that shoals to less than 3,300 m. This discontinuity divides the segment further into two type 4 segments (4B1 and 4B2) defined by the 3,500 m contour. From south to north, these two smaller segments have maximum depths of greater than 3,600 m and 3,700 m respectively (figure 10), a length versus width ratio of 8.1 km/1.8 km and 39.6 km/5.6 km respectively, and strikes of 015° and 004° respectively.

The southern segment (4B1) has a maximum of 4 and 3 faults, and a fault density of 1.4 and 0.9 faults/km; east and west of the axis respectively. The fault number on the eastern side increases towards the northern segment boundary while on the western side there is no particular pattern in fault spacing (figure 15).

The northern segment (4B2) has a range of 0-4 and 1-3 faults and a fault density of 1.4 and 1 faults/km, east and west of the axis, respectively. It is not possible to recognize any particular pattern that relates fault number to location within the segment on either side of the rift floor.

5. Order 2 (77°31'N to 77°48'N)

Segment 5 (figure 11) is defined by the 3,300 m contour, trends ~000°, has a length of 31 km, an average width of 7.5 km, a maximum depth of greater than 3,600 m, and a fault density of 0.4 and 0.7 faults/km; east and west, respectively (figure 15). Fault number varies from 0 to 2 on the eastern side of the rift and from 0 to 3 on the western side, slightly increasing in fault number towards mid-segment. Fault length within this segment averages 3.1 km while axial fault azimuth averages 008°, compared to 4.5 km and 7 km on the eastern and western flanks in segment 5A and 5.6 km (eastern flank) to 5.8 km (western flank) in segment 5B (figure 14). Highly reflective fresh lava flows are found at the segment's boundaries while older lava flows of lesser reflectivity are located in the middle of the segment.

Both the southern and northern discontinuities of the order 2 segment are structurally bifurcated creating an "X" shaped rift basin. The northwestern-southeastern axis trends at

350° while the northeastern-southwestern axis trends at 010°. The northern boundary of segment 5 (77°48'N to 77°55'N) (figure 11) is characterized by a large elliptical volcano striking 330° that occupies the eastern and central parts of the rift valley floor. The volcano has long and short axes of 6.4 km and 4.8 km; respectively. There are two circular craters of 1 km width at both its southwestern and northeastern tips. On both the eastern and western side of the volcano, the rift valley deepens to greater than 3,400 m forming narrow elongate basins 2.7 km wide, and 14.4 km long. Between 77°45'N and 77°55'N, the rift valley is dominated by a field of at least thirteen nearly circular volcanoes with average diameters of 0.8 km and less than 100 m relief. Seven of these are arranged in a N-S trending linear belt along longitude 7°25'E from 77°48'N to 77°50'N. On the eastern and western sides of the rift floor, faults and fissures vary in number from 2-3 and 0-1, respectively (figure 15). Fault lengths along this boundary average 2.4 km compared to 4.3 km and 6.2 km on the adjacent eastern and western flanks (figure 14). The average fault azimuth along this discontinuity is 012° (compared to the bathymetric strike of 330°).

Segment 5 is divided into two smaller basins (6A and 6B) where at 77°38'N, the 3,400 m contour necks.

5A. Order 3 (77°31'N to 77°38'N)

Segment 5A is slightly deeper than 3,400 m (figure 11), has an average width of 6.3 km, a length of 13 km and an overall orientation of 000°. Because of its bifurcated shape created by its southern boundary, the length of the segment varies from 9 km along the

north/south axis to 11 km along the northeast/southwest axis. Both eastern and western sides of the rift valley floor have a low fault density; 0.1 faults/km (a total of 0-2 faults) on the eastern side compared to 0.7 faults/km (a total of 1-3) faults on the western side. Maximum fault numbers occur at the segment boundaries (figure 15). The average fault azimuth is 007° which is 7° oblique to the bathymetric trend of the rift basin (5 and 5A). The segment's northern boundary has an average fault azimuth of 352° which is substantially more oblique to fault azimuths described for more southerly second and third order discontinuities.

5B. Order 3 (77°38'N to 77°48'N)

Segment 5B is defined by the 3,500 m contour (figure 11), has a maximum depth of greater than 3,600 m, an average width of 5 km, and an overall strike of 000°. The shape of the segment is also defined by two long axes striking 010° and 348°. In addition, the length of the segment varies from a minimum of 7 km along the northwest/southeast axis to a maximum of 9 km for the northeast/southwest axis. Fault density across the rift valley is 0.7 faults/km (east) and 0.6 faults/km (west). The fault number ranges on both sides of the rift floor from 0 to 2. On the eastern side, fault numbers increase towards both segment boundaries while on the western side, the maximum fault number lies near the southern part of the segment. The average fault azimuth is 005°, 5° oblique to the morphological trend of the rift basin (segments 5 and 5B). The northern terminus of this segment is marked by a large mid-rift volcano which straddles the eastern side of the rift valley between latitudes 77°46'N and 77°55'N. The edifice's four different peaks are

oriented northwest/southeast along a trend of 330° (compared to a trend of 348° for the edifice).

6. Order 2 (77°55'N to 78°33'N)

Segment 6 (figures 11 and 12) strikes 350°, is defined by the 3,200 m contour, has a length of 68.4 km, a maximum depth of greater than 3,600 m, an average width of 10.2 km, and a fault density of 1.3 and 0.9 faults/km; east and west respectively. Fault number varies on the east from 0 to 7 and on the west from 0 to 5 (figure 15). On the western side of the rift floor, fault number increases towards the center of the segment. Segment 6 is broken into subsegments 6A and 6B at 78°13'N to 78°18'N where the rift valley shoals to less than 3,200 m and narrows to a width of 4.5 km creating two subbasins; 6A and 6B. Fault lengths in segment 6A are 3 km while they increase to 3.4 km in segment 6B compared to 3.5 km on the adjacent eastern flank and 5.8-5.6 km on the western flanks adjacent to subsegments 6A and 6B (figure 14). Fault azimuths average 357° which is 7° oblique to the morphological trend of the rift valley. Segment 6's northern discontinuity is the Molloy Transform Fault which is also the northernmost terminus of the Knipovich Ridge.

6A. Order 3 (77°55'N to 78°13'N)

Segment 6A (figure 11) is defined by the 3,300 m contour, has a length of 32.4 km, a maximum depth of greater than 3,600 m, an average width of 11.0 km, an orientation of 349°, and a fault density of 1 and 0.9 faults/km; east and west respectively (figure 15).

Faults appear to be randomly distributed within this segment and their average azimuth is 000° which is 11°oblique to the morphological trend of the segment.

6B. Order 3 (78°18'N to 78°33'N)

Segment 6b (figure 12) is defined by the 3,200 m contour, has a length of 27 km, a maximum depth of greater than 3,300 m, an average width of 11.7 km, an orientation of 002° (despite the overall trend of the rift valley in this area which swings sharply to the northwest at its intersection with the Molloy Transform Fault) and a fault density of 1.6 and 0.8 faults/km; east and west respectively. An examination of the bathymetry reveals a steeply dipping western wall and a gently sloping eastern wall. This can be attributed to a large influx of sediment from turbidity flows, landslides, and debris flows into the eastern rift from the nearby continental shelf and the Svalbard Archipelago. As a result, this part of the rift valley including the eastern inner and outer walls have been inundated by sediment. Fault azimuths average 349° which is 13° oblique to the bathymetric trend of the segment but matches the general trend of the rise axis in this region. Five volcanoes are found on the western side of this segment of which three are aligned along a line trending 340°. Five other volcanoes are located in the central and eastern part of the segment.

Eastern Flank of Knipovich Ridge:

The morphology of the eastern flank of the ridge (figure 8-12) is relatively uniform, shoaling to the continental margin. In some locations, downslope mass wasting from

Svalbard is the most noticeable seafloor process (in particular between 77°30'N and 78°30'N). However, punctuating the continental slope are the following NW-SE trending belts of abyssal hills:

1) Between 76°28'N, 8°00'E and 76°35'N, 7°35'E (figure 9), the SeaMARC II fully or partially imaged three bathymetric highs reaching elevations of 1,200 m, 1,900 m and 2,000 m. The first two highs were not completely mapped and therefore we are unable to determine their true orientation. The third high trends 014°, along its major axis. Faults strike 000° near the southeastern high, 330° on or near the middle high and 014° near the northwestern high. The belt itself trends 325°.

2) Between 76°50'N, 8°45'E and 77°05'N, 7°45'E (figure 10), the SeaMARC II imaged three bathymetric highs which deepen with proximity to the rift valley. The highs (from southeast to northwest) reach elevations of 1,900 m to 2,200 m and trend; 351°, 358°, and 345° respectively. Faults on or near the highs strike 340°, 000°, and 300°; from southeast to northwest, respectively. The belt itself trends 320° (obtained by measuring the average of the trends of lines connecting each pair of peaks.

3) Between 77°02'N, 8°07'E and 77°05'N, 8°00'E (figure 10), the SeaMARC II imaged two bathymetric highs reaching elevations of 2,200 m and 2,600 m. They trend 065° and 330°; from southeast to northwest, respectively and intersect a section of the outer rift valley wall. Fault strikes average 030° on or near both highs while the overall strike of the belt is 305°.

4) Between 77°20′N, 8°45′E and 77°27′N, 7°47′E, the SeaMARC II imaged two bathymetric highs at elevations of 1,500 m and 1,100 m, respectively. The belt of highs intersects the Knipovich Ridge axis (at the major volcanic discontinuity between segments 4 and 5) and crosses onto the western flank of the ridge. Faults immediately to the south of the eastern flank highs strike 320°-350°. In contrast, faults within the rift valley trend 000°-020° while the belt itself trends 295°.

From 5-10 km east of the ridge axis at most latitudes, fault density averages 1.9 faults/km, with fault numbers varying from 0-3. Exceptions occur at 76°54′N-76°55′N, 77°56′N-77°59′N, 78°05′N-78°07′N, 78°12′N-78°18′N where fault numbers are 5-6, 4-5, 4- 6, and 4-7; respectively. Fault azimuths 5-10 km east of the axis, average 004° with most of the faults trending from 350° to 030°. Sharp swings in fault strike occur at 76°28′N-76°31′N, 76°59′N-77°03′N, 77°15′N-77°19′N, 77°43′N-77°46′N, 78°00′N-78°05′N, 78°34′N-78°37′N. The latter is the intersection of the Knipovich Ridge with the Molloy Fracture Zone.

Generally, visible faults on the entire eastern flank trend at a slightly oblique angle (010°) to the axis of the Knipovich Ridge. Locally, faulting is not everywhere linear and there is a clear zigzag pattern dominant on faults longer than 5 km. Long faults can be found at a maximum distance of 19 km (at 76°15′N) and 16 km (at 77°15′N) away from the rift valley, suggesting a northward decreasing fault to rift distance. The maximum observable fault length is 60 km. However, there are 10 faults longer than 5 km with an average

length of 33 km. Short faults tend to lie close to the rift valley except on the shallow bathymetric features.

A high concentration of faults lies to the east and northeast of a large rift valley field of volcanoes between 77°51′N to 78°03′N and 8°00′E to 8°15′E. In contrast to the fault swarms noticed at 76°30′N and 77°22′N, these faults are not associated with any shallow bathymetric features. Here fault density is 0.13 faults/km with fault lengths ranging from 1 km to 19 km and fault spacing less than 2.5 km. While most of these faults are inwardly dipping, there are a few faults where dip cannot be determined.

Western Flank, Boreas Basin, and Hovgård Ridge:

The bathymetry on the western flank of the Knipovich Ridge is more varied than the sediment covered eastern flank (figures 10-13). The axial mountain province (Ohta, 1982) is capped by a plateau with an average width of 20 km between 77°00′N and 78°05′N where it lies parallel to the Knipovich Ridge. The plateau is broken up by widely spaced peaks of different elevations. At 77°43′N, 6°44′E the plateau shoals to 800 m. Between 78°05′N and 78°30′N, the plateau broadens to 47 km in width, 10 km north of the Hovgård Ridge (figures 12 and 13).

To the west of the axial mountains, lies the Boreas Basin and the Hovgård Ridge which trends 290°-300°. The Hovgård Ridge widens from 10 km at its southern tip to 16 km at the western end of the survey area (based on the 2,300 m contour) and is capped by two shallow peaks with elevations of 1,400 m and 1,300 m (figure 13), that trend ~310° There

are 4 faults at the extreme southeastern tip of the Hovgård Ridge that trend approximately 000°. However, all other faults on the Hovgård Ridge trend ~320°.

Only one of the seamount belts on the eastern flank (Belt 4) crosses the rise axis between segments 4 and 5 onto the western flank where it intersects the Hovgård Ridge (figures 10, 11, and 14). Just west of the discontinuity between segments 4-5 at 77°42'N and 6°45'E, lies a noticeable seamount (figure 11), that shoals to less than 900 m. This feature is ellipsoidal in shape with its major axis trending 350°. Long faults (10's of km's) on or near this ellipsoidal high trend 020-030° while short faults (a few km's in length) trend ~320°.

The seamount belt continues to the northwest (figure 13) where several bathymetric highs coalesce to form a shallow elongate ridge (1,900 m at its shallowest peak and 27 km long based on the 2,400 m contour) which trends 325°. At the 2,200 m contour the ridge is divided into two sections whose lengths are 21 km and 5 km respectively from south to north. The southern section has a slightly deformed rectangular shape and is shallowest along its northeastern wall. The northern section has a circular to elliptical shape (a radius of approximately 2.5 km), and strikes 000° (figure 13). The proximity of this ridge to the Hovgård Ridge (the two features are separated by a distance of 6 km) suggests that the two are structurally related. The trend of this ridge is parallel to features within the deeper parts of the Boreas Basin imaged by the SeaMARC II (figure 13). Faults on the ridge trend 020° at its southeast terminus and ~000° at its northwestern terminus.

To the southwest of the Hovgård Ridge, in an area approximately 100 km^2 centered at longitude 0° and latitude 77°45'N, the side-scan imagery detected nearly circular bathymetric highs of approximately 250 m diameter. These features may be volcanic, or intrusive features as has been suggested by K. Hinz (pers. comm., 1990). Whatever their origin, they are found on a seafloor that is otherwise completely covered by sediment. Their height could not determined from the SeaMARC II bathymetry suggesting that they are less than 100 m in elevation (the resolution of the SeaMARC II bathymetry).

Generally, faults on the western flank of the Knipovich Ridge (north of 76°30'N) have strikes of 016°, and are oblique to the strike of the rift valley which trends 002°. Long faults are dominant on the western flank and can be found out to 60 km away from the rift valley. In addition, these faults are non-linear and are concave with respect to the rift valley, and zigzag along their length. In contrast, shorter faults are only slightly curvilinear. As a result of their oblique orientation, some of the long faults lie closer to the rift valley with increasing proximity to the Molloy Fracture Zone.

Molloy Fracture Zone:

The bathymetric data poorly define the exact shape and length of the Molloy Fracture Zone (figure 12) with the exception of a 10 km long elliptical depression (outlined by the 2,900 m contour) that is centered at 78°54'N, 4°30'E. However, the side-scan data reveal a double transform fault trending 305° that is 130 km long (figure 12). In detail, a complex set of 12 anastomosing faults (including the two major faults separated by ~2 km), define the Molloy Fracture Zone. These faults vary in length from 3.6 km to 66 km.

The depth of the transform fault ranges from 2,500 m at 78°26'N, 8°00' to 5,500 m where it terminates in the Molloy Deep (79°05'N, 2°45'E). Just to the south of the transform, faults on the western flank of the Knipovich Ridge curve into the transform changing their orientation by as much as 50° from 000° to 310°. Immediately to the north of the fracture zone, there are numerous faults oriented parallel to both the fracture zone and the rise axis.

Vestnesa Plateau:

Vestnesa is a northwest-westward trending plateau abutting the Spitsbergen continental margin (figure 12), aligned parallel to and north of the Molloy Fracture Zone. The depth of the Vestnesa Plateau ranges from 1,200 m at 79°00'N and 7°15'E to 2,500 m at 79°10'N and 3°45'E. The western tip of the plateau is approximately 5 km distant from the easternmost wall of the Molloy Deep. The SeaMARC II side-looking sonar data reveal that the plateau is completely covered by sediment. In addition, ~50 pockmarks were mapped atop the plateau suggestive of possible methane venting along its crest (Vogt et al., 1994). The nearly circular pockmarks are 200-600 m wide and lie in an elongated field (1-3 km wide and 50 km long). They are not apparent in the SeaMARC II bathymetry, suggesting that they have less than 100 m of vertical relief.

Faults, trending both ridge and transform parallel cut Vestnesa Plateau from south to north along its boundary with the Spitsbergen continental margin. These faults appear to be a northwards extension of the eastern rift valley walls of the Knipovich Ridge to the south. The faults are located in a narrow corridor 5.5 km wide (figure 12) and are oriented

325°. Because of their structural connection with the mid-ocean ridge, they may be evidence of ongoing (or at any rate, recent) northerly rift propagation.

Discussion:

A cross section of the Knipovich Ridge rift valley yields a profile similar to other slow-spreading center (for example as described by Laughton and Searle, 1979). It comprises an inner rift valley graben and a complex outer valley walls consisting of scarps and terraces leading up to the crestal mountains 10-15 km away from the axis. Beyond that, rugged topography can be found, progressively deepening away from the axis. However, the eastern flank does not show surface fault-like structures beyond a maximum distance of 35 km away from the rift valley north of 77°25′. This contrasts with the western flanks, which reveal faults to about 45 km away from the rift valley. Mass wasting and associated sedimentary shelf type features are dominant on the eastern flanks beyond the region of observed faults. The western flank is observed to have an extensive sedimentary cover that is generally smooth and lacking rough topography beyond the region of faults. High sedimentation rates, bottom currents, and mass wasting may have covered or degraded escarpments.

The Knipovich Ridge is easily subdivided into structural and bathymetric segments of different scales (Orders). At the smallest scale, the rift valley of the Knipovich Ridge is segmented into interbasinal fourth order segments. The geometry of the basinal segments is well defined by their bathymetry and their structures. Individual rifted basins have 100-300 m vertical relief, are 1.5-8 km wide and range in length from 2-40 km. Maximum

depths in these basins are greater than 3,700 m. We identified a total of eight fourth order segments along the southern Knipovich Ridge rift valley (73°50′-76°00′), two in the middle part of the rift valley near 76°38′, and none further north. These rifted basins constitute the shortest wavelength undulations evident within the rift valley but are significantly different from fourth order segments described for the Mid-Atlantic Ridge (Macdonald, 1991); and the Reykjanes Ridge (Appelgate et al., 1993). For example, the Reykjanes Ridge fourth order segmentation is characterized by discrete volcanic systems with a vertical relief of 50-200 m (Appelgate, 1993). The Knipovich Ridge's fourth order segments are basins defined by necking bathymetric contours.

Intermediate wavelength (8-60 km in length) third order basinal segments are the most striking feature of the Knipovich Ridge. These rifted basins have 100-500 m of vertical relief, comparable to the southern Reykjanes Ridge (Appelgate et al., 1993) and other segments on parts of the MAR (Sempere, 1990; Sempere et al., 1993). However, in the case of the Knipovich Ridge, predominantly volcanic as well as some non-volcanic structures are distributed along the rift valley, and act as segment boundaries. This is the opposite of what one finds on the Reykjanes Ridge and the MAR where valleys form the discontinuities between segments formed of volcanic ridges (Macdonald, 1986; Sempere et al., 1987; and Appelgate et al., 1993;).

Long wavelength (30-165 km) second order segments are also present along the Knipovich Ridge. These basins exhibit 200-700 m vertical relief and range from 4 to more than 10 km in width, comparable to many sections of the MAR, yet appear to lack

distinctive shallow neovolcanic zones (except for those parts of the Knipovich Ridge which could be buried underneath sediments). Segment 2 (165 km long) is twice as long as the next shorter segment. Excluding segment 2 would yield a second order segment length in the range of 30 to 85 km with an average segment length of about 60 km which is comparable to other parts of the MAR (Macdonald, 1987).

At the largest scale, the ~500 km long Knipovich Ridge may be considered a first order segment with no apparent transform faults between its southern terminus with the Mohns Ridge and its northern intersection with the Molloy Fracture Zone. The rift valley trough is continuous along its entire length. Oblique spreading has been proposed by Vogt (1986) and propagation has been proposed by Crane et al., (1982, 1988). It is likely that the current configuration of the Knipovich Ridge is the result of the two. The SeaMARC II does not provide sufficient evidence to favor one over the other.

Our data show a slight V or U shaped pattern developed on conjugate pairs of faults about the rift valley. The narrower point of the V does not intersect the rift valley (figure 10). While the lack of a stronger V pattern may indicate same age faults developed around an axial magma chamber that narrows to the north, it is unlikely that this case is at work here since fault number and spacing (figure 15) as well as asymmetry in spreading rates (Desimon et al., 1979; Crane et al., 1982, Vogt, 1986; Crane et al., 1988; and Crane et al., 1991) favor addition of crust on the western flanks. Therefore, it is unlikely that equidistant conjugate faults on the flanks of the rift valley have similar age.

Lava flows occur at intervals along the entire length of the Knipovich Ridge rift valley. However, fresh lava flows are concentrated on and near every second order discontinuity, and are especially prominent between segments 3 and 4 as well as 4 and 5. Furthermore, fresh lava flows are located near some third order discontinuities between segments 2A and 2B, 2B and 2C, 2C and 2D, 4A and 4B.

While lava flows are scattered along the entire length of the Knipovich Ridge rift valley, circular volcanoes (cones and craters) are concentrated within only a few fields (figure 17) located near the northwestern boundary of segment 2E, which is also the boundary discontinuity between second order segments 2 and 3. To the east of this discontinuity, a N-S trending field of ~20 volcanoes straddles the base of the eastern inner rift wall bordering segments 3A and 3B. A third volcano field is centered around the discontinuity between segments 5 and 6 and extends to the south and north into the two segments. The last field is found in segment 6B near the intersection of the Knipovich Ridge with the Molloy Fracture Zone. Throughout all these fields the trends of individual volcano belts are nearly parallel to the rift valley, even where the trend of the segment or boundary is oblique to that of the rift valley. In addition, there is a definite correlation between volcanics and the boundaries of second order segments.

The dominant fault type along the rift valley is inward dipping, and linear to curvilinear in shape. This is comparable to other parts of the MAR and slow spreading centers in general (Searle et al., 1977). Fissures are also present and the SeaMARC II imagery suggests that some of these fissures may be evolving into faults since faults were detected inside lava fields. However, the rift valley fault and fissure orientations are often as much

as 30-40° oblique to the rift valley strike. This contrasts with flank faults which follow the trend of the rift valley. Most flank faults are curvilinear and extend for distances longer than most third order segments, and even some second order segments. This suggests that either major faults on the flanks are not inherited from the rift valley or segment lengths have changed throughout the duration of the Knipovich Ridge. If the first concept is correct, then this contradicts the concept that extension within the inner rift valley is the probable origin for major inward dipping faults (Searle, 1984).

If faults are created at some distance off axis, extension may indeed be distributed over a much broader range than previously thought. This is unlikely since the fault trends on the flanks are nearly parallel to the present trend of the outer rift valley walls suggesting that faults form in this location. Also possible is that some of the older Knipovich flank faults formed during the nascent evolution of the Knipovich Ridge while it propagated into the broad Paleo-Spitsbergen Shear Zone. Thus, these flank fault trends may reflect the trend of the paleo shear-zone and the influence of propagation on that trend. By contrast, the inner rift valley faults parallel faults within the Mohns Ridge and thus they indicate that the present regional extensional stress fields for both the Mohns and Knipovich Ridges are roughly equivalent.

A summary of inferred local spreading directions (normals) based on average fault azimuth within second order segments, second order discontinuities, and third order segments can be found in figure 17. Spreading direction appears to be completely independent of the large scale bathymetric trend of the rift valley. In general, a NW-SE

spreading direction is taking place along the entire rift valley with the exception of the northern boundary of segment 6B (adjacent to the Molloy Transform Fault) where the rise axis bends into the transform fault at an orientation of 315°. However, the inferred spreading direction is 30°-50° oblique to the trend of the eastern flank's shallow seamount belts. This suggests that the flanking seamounts might have erupted through regional fracture zones trending in the same direction as the Greenland F. Z. and the Molloy F. Z.; and are not an indication of local spreading direction (unless spreading direction has been altered by 30°-50° during the last 36 MY).

Within second order segments, the presence and trends of faults appear to be related to the location within the segment. At the boundary discontinuities, there are few faults while fault number is maximum within the segment (usually towards the middle). A possible explanation for this relationship is that these segment boundaries are areas where faulting is covered up by excess volcanism emanating from mid-rift highs. Alternatively, the large accumulation of sediment into the rift valley basins may enhance our ability to image faults in these deeper segment centers. The same relationship between fault location and position in the segment appears in third and fourth order segments (to a lesser extent due to volcanic discontinuities separating third order segments).

The above analyses suggest that in the young Knipovich Ridge, rift valley segmentation is bathymetrically similar to segmentation occurring within continental and nascent ocean rifts. Crane (1985) and Schouten et al. (1985) illustrate a spreading rate dependence on segmentation wavelength and rift amplitude while Bonatti (1985) described the evolution

of segmentation for even younger ridges such as the transitional zone of the Red Sea, which is made-up of independent segments that were called "punctiform" shaped axial deeps and troughs. In the Red Sea, four deeps similar to the Knipovich Ridge second order segments, can be found in the transitional zone and they have been interpreted to suggest punctiform initiation of seafloor spreading in the vicinity. Through magnetic anomalies associated with these deeps, the centers were interpreted as the oldest parts of the segments and the most active in terms of generation of lava flows, whereas segment boundaries are the least active.

The close similarity between the morphology of the segmentation on the Knipovich Ridge to the Red Sea transitional zone's deeps suggest that processes active at the time of the initiation of rifting and later production of seafloor may continue for a long time after the evolution of a mid-ocean ridge. However, the volcanic nature and the dominant presence of fresh lava flows at second and third order discontinuities suggest that, unlike the Red Sea deeps, the boundaries of segmentation along the Knipovich Ridge result from preferential asthenospheric upwelling into pre-existing cross-cutting faults. If Crane et al., (1991) are correct about their suggestion that the nascent Knipovich Ridge propagated into the first major fault encountered at its intersection with the multi-fault Paleo-Spitsbergen Shear Zone, then the ridge's overall morphology may be determined by the trend of the ancient shear zone. While fine scale punctiform-like upwelling within and along this fault may have generated the basinal deeps, it is also possible that inherited oblique-splinter faults associated with the Paleo-Spitsbergen Shear Zone may still serve as major thermal boundaries along the length of the present day Knipovich Ridge. In this

case, magma would pond into these thermal boundaries creating chains of seamounts in the process.

It is unlikely that extensional processes are fundamentally different along the Knipovich Ridge from the Reykjanes Ridge and other parts of the MAR. A more viable explanation is that the morphology of the Knipovich Ridge is significantly modified by oblique extension within sets of pre-existing shear zone faults.

A look at the distribution of second order segments suggests that segment 2 (165 km in length) may have evolved to its current length in response to the coalescing of 2 shorter segments. The N-NE orientation of segment 2A is different than the N-NW orientation for all other third order segments within segment 2. If harmonically spaced asthenospheric upwelling is the cause for segment generation, then it is unlikely that there should be such a variation among third order segments. Unfortunately, there was no SeaMARC II coverage on the adjacent flanks to test this idea.

While some of the second order segments are arranged en-echelon with respect to each other, they always lie within conjugate pairs of inner basin boundary faults. The boundaries between segments 3 and 4 and segments 5 and 6 are predominantly volcanic areas (suggested by the shallow bathymetry, high backscatter on the side-scan imagery, and high magnetic anomaly amplitudes and gravity values) (figures 3, 4 and 9). These areas are especially interesting because the rift valley nearly completely disappears between segments 3 and 4 while further north, the rift valley between segments 5 and 6 is partially filled by major volcanoes situated on the eastern and central parts of the rift. This

suggests that this part of the rift valley is presently volcanically active and that with time enough volcanics may erupt to completely fill the rift valley. Alternatively, the presence of long and large offset flanking faults on either side of the rift valley may imply that this region is not volcanically active at present (Sempere et al., 1987). This explanation is unlikely for the boundary between segments 5 and 6 as it actually has the narrowest average width of any second order segment along the Knipovich Ridge, indicating that the magma chamber is not frozen and the rift valley width is not influenced by the long faults on the flanks of the rift valley.

Furthermore, the boundaries between segments 3 and 4 and segment 5 and 6 intersect two of the four shallow seamount belts (Vogt, 1986) that obliquely cross the Knipovich Ridge. This suggests that volcanism has been localized in these regions for millions of years.

Explaining the asymmetry of the outer flank walls posed many problems to Ohta, 1982, and Vogt, 1986. Our data prove that the crests of the western rift mountains are indeed generally shallower than those of the eastern rift mountains by an average of 400-500 m (figure 16). These observations are contrary to previous observations by Desimon et al., (1979) who suggested that there is symmetry between the eastern and western flank walls. An important SeaMARC II observation is the presence of antisymmetrically distributed bathymetric undulations along and across both eastern and western rift valley walls. This antisymmetry could be the result of the oblique spreading that has been proposed by Vogt (1986). However, the fact that the offset is not constant suggests that an additional factor, such as cross-cutting paleo-fracture zones, may constrain the direction of rift's structural

orientation and therefore, affect the shape of the flank walls. North of 76°30′ (where SeaMARC II data are available across both eastern and western flanks), there is only one location where the eastern wall is higher than the western wall by about 400 m (between 77°15′N and 77°20′N) corresponding to the intersection of the rift with a shallow seamount belt which crosses the eastern flank.

We propose that the bathymetrically shallow belts can be explained by either of the following possibilities: 1) They are aligned along a set of non-transform faults related to the Paleo-Spitsbergen Shear Zone (and maintained for unknown reasons), which may have served as thermal boundaries to the evolving Knipovich Ridge. A consequence of these thermal boundaries, could have been the vertical ponding of magma creating large seamounts in the process. Alternatively, 2) the rift valley intersection with these shallow belts maybe ongoing loci for stable magma centers. Seamounts created at these points maybe rafted off the axis with time creating seamount chains in the process. Structures near these shallow belts and within the rift valley support both ideas. Analysis of heat flow data in the Norwegian-Greenland Sea (Okay, 1994) suggest that paleo-shear zones remain "hot" for millions of years and act as heat sources rather than heat sinks. Certainly the volcanic belts which obliquely cross the Knipovich Ridge maybe evidence for the ongoing intrusion of magma into these paleo-fault zones, at least at their intersection with the rise axis.

Our data also indicate a large shift of fault orientations in the area of 77°N from a N-NE strike to a N-NW strike. South of the Hovgård Ridge between 76°50′N 77°00′N, faults in

the rift valley as well as the western and eastern flanks show a sharp swing to the northwest by as much as 60°. North of the Hovgård Ridge, western flank fault orientations parallel the strike of the Hovgård Ridge and the Molloy Fracture Zone. This may be indicative of a Paleo-northern limit to the Knipovich Ridge prior to its most recent northward propagation event. The NW trend of the off-axial faults in this region may also be indicative of a paleo-transform or a zero-offset transform offset associated with the Spitsbergen Fracture Zone. The presently active volcano field located in the southern most part of segment 6 may indicate present leaking and ponding of magma into the same remnant zero-offset transform fault.

Schouten et al., (1982) describe a similar situation along the early MAR where they suggested that normal oceanic crust formed in a string of individual spreading center segments separated by structural anomalies and discontinuities which previously existed in the unrifted basement. Most important is their finding that these boundaries existed even when no offset between cells was apparent.

The Norwegian-Greenland seafloor was dominated by shearing for at least 20 ma (between 56 ma and 36 ma) and later transpression and transtension. Structural evidence suggests that the resulting shear zones are still important structural constraints on the evolution of the spreading center, even if current faulting indicates normal spreading behavior (Bonatti, 1994). A similar ridge-shear zone scenario is located in the Red Sea where the Paleo-Zabargad Fracture zone is the locus for rifting and spreading (Bonatti et al., 1984; Bonatti, 1985, Crane et al., 1986, and Bonatti, 1994).

Explanations regarding the asymmetric evolution and position of the Knipovich Ridge include ridge jumping, ridge propagation into a previous shear zone, asymmetric pure shear spreading, and simple shear spreading. The data presented here strongly suggest that the Knipovich Ridge has not jumped through time. There is no evidence of any prior graben or major sequence of inward dipping faults in the Boreas Basin or north of the Hovgård Ridge. The Knipovich Ridge appears to have always been located within the Spitsbergen Shear Zone. If Crane et al.'s, (1991) suggestion that the Paleo-Spitsbergen Shear Zone is the major fault system along which present day rifting is taking place (and our data strongly support that idea), then their ideas about an asymmetric pure shear evolution are probably valid. Our data suggest that the geographic range of faulting is at least twice as much on the western side of the rift valley as it is on the eastern side (and possibly more since our tracks did not extend to the margin of eastern Greenland). Using Crane et al.'s , (1991) proposed present spreading rates of 0.1 cm/yr. for the eastern flank and 0.7 cm/yr. for the western flank, we can establish ages for the outer faults found in this survey.

The eastern flank's outer faults (near 76°N) observed in this survey should have an age of less than 35 MA. (using 1 mm/yr half spreading rate) We must take into account that these faults are present in oceanic rocks that have been rafted away from the rift valley (Vogt et al., 1982 and Vogt, 1986). It is very likely that none of the initial rift valley faults survived to the present (rift valley faults are much shorter and more oblique to the trend of the rift valley compared to flank faults which tend to be longer and parallel to the rift walls while oblique to the faults in the inner rift valley). In contrast, if the western flank is

spreading 7 times as fast as the east, faults on the western flank located the same distance from the axis as faults on the eastern flank are a factor of 7 younger. Thus, a western fault 45 km from the axis would be only 6.5 MA (using 7 mm/yr half spreading rate). Faults beyond 45 km west of the rise axis are probably present even if they are completely or partially covered by sediment. In any case, this explanation does not attempt to establish the exact age of the initial opening of rifting from the Knipovich Ridge. Rather, we show that similar fault behavior is present on both flanks of the Knipovich Ridge in oceanic crust of probably different age (~29 MA).

Near the intersection of the Knipovich Ridge with the Molloy Fracture Zone, fault orientations in the rift valley and on both flanks swing sharply to the northwest. In the area to the south and along the transform fault, fault orientations on the eastern and western flanks are almost parallel to its strike. Near 78°30'N, eastern flank fault spacing ranges from 0.5-0.7 km compared with the western flank fault spacing of 1 to 2 km (figure 15).

North of the Molloy Fracture Zone, rectilinear faults cut the Vestnesa Ridge. The strike of these faults parallel both the Knipovich Ridge as well as the Molloy Transform Fault and may suggest that the rift is in the process of propagating north of the Molloy Transform Fault; perhaps deactivating the Molloy Ridge and Molloy Transform Fault in the process.

Okay and Crane (1993) suggest that the area between the Knipovich Ridge and Svalbard (including most of Spitsbergen) is structurally complex with a very deep detachment extending from the Knipovich Ridge to Spitsbergen. They also suggest that secondary

faults from Svalbard and the Yermak Plateau dip in the opposite sense and interconnect with the Knipovich detachment fault. Their conclusion is partially based on the presence of Quaternary lava flows along Woodfjord in northwestern Spitsbergen (Prestvik, 1977, Skjelkvale, 1989) and the discovery of acoustically highly reflective seafloor adjacent to seamounts located north of Svalbard in the Arctic Ocean. Ultimately, the degree of northward propagation of the Knipovich Ridge will be determined by the interaction of this ridge, its subjacent asthenosphere and the complex system of paleo-faults cutting through the region.

We mentioned earlier that asymmetric pure shear and simple shear were possible mechanisms to describe the evolution of the Knipovich Ridge. Our data do not show any evidence for a simple shear detachment fault, but evidence would be more likely found by gathering geophysical data at greater depth in the crust. Wernicke (1985) suggests that simple shear rifting is difficult to maintain once a spreading axis has been established. While this is mechanically true, it does not take into account the possibility of the interaction of several detachment faults or even if there are secondary faults that connect these detachments.

Asymmetric pure shear is the rifting model possibly supported by our data. Similar faults are present on both sides of the rift valley. Fault orientations are comparable on both flanks paralleling the overall trend of the Knipovich Ridge. However, they are substantially different from the trends of faults with the rift valley (figures 7-13). Spacing between the eastern flank faults is on average 0.5-1 km less than the spacing between the western flank faults' spacing. Furthermore, there are many more faults on the western

flank compared to the eastern flank. The combination of these two factors suggest more crust is being accreted to the west than to the east.

Conclusions:

1. The Knipovich Ridge rift valley is segmented by basins. However, segment discontinuities are characterized by copious volcanism.

2. Segment discontinuities (as volcanic highs) are rafted off the ridge axis, forming seamount chains.

3. Segment discontinuities appear to coincide with pre-existing zero-offset fault zones which were probably located in the pre-rifted crust.

4. Seamount chains are 30°-50° oblique to the direction of seafloor spreading inferred from inner rift fault orientations.

5. The southern Knipovich Ridge (73°50'N-75°55'N) is morphologically simpler than the northern Knipovich Ridge (75°55'N-78°30'N) with fewer second order discontinuities and more linear and unvarying rift valley topography.

6. The above data suggest that in young and very slow spreading centers, the pre-rift geometry may play a major role in the evolution of the ridge and its surroundings. Major and minor weakness zones act as barriers to the propagation process. Due to the extremely slow spreading rate of less than 1 cm/yr (full spreading rate), the emplacement of oceanic crust at both the onset and later stages of seafloor spreading

may be controlled by the complex geometric memory of pre-rift structures. The ponding of magma into preexisting faults during the transtension of continental crust can create linear chains of seamounts which cross the rise axis onto its flanks. Other bathymetric highs along the same paleo-faults may be continental slivers which were transported and then stranded by shearing and transtension of continental crust.

7. The SeaMARC II's images of the Hovgård Ridge do not resolve whether or not it formed as a slice of uplifted mantle or was transported as a slice of continental crust. However, the Hovgård Ridge appears to be related to the shallow bathymetric seamount belts that are observed on the flanks of the northern Knipovich Ridge. Faults to the northeast of the Hovgård Ridge paralleling the trend of the Molloy Transform are suggestive of a paleotransform fault and may be evidence for past northward propagation of the Knipovich Ridge.

8. Fault traces imaged north of the Molloy Transform Fault suggest that rifting associated with the Knipovich Ridge has propagated north beyond the rift-transform intersection in geologically recent times.

REFERENCES

Appelgate, B., and Shor, A. N., 1993, The Northern Mid-Atlantic and Reykjanes Ridges: Spreading Center Morphology Between 55°50'N and 63°00'N (in press).

Bonatti, E., 1994, The Earth's Mantle below the Oceans, Scientific American, March 1994, 44-51.

Bonatti, E., and Crane, K., 1984, Oceanic Fracture Zones, Scientific American,, Vol. 250, No. 5, 40-51.

Bonatti, E., 1985, Punctiform initiation of seafloor spreading in the Red Sea during transition from a continental to an oceanic rift, Nature, Vol. 316, No. 6023, 33-37.

Cherkis, N. Z. and Vogt, P. R., 1994, Regional Bathymetry of the Norwegian-Greenland Sea, Naval Research Laboratory, Washington, D.C.

Cande, S. C. and Kent, D. V., 1992, A New Geomagnetic Polarity Time Scale for the Late Cretaceous and Cenozoic, Jour. Geophys. Res., 97, 13917-13951.

Chan, W. W., and B. J. Mitchell, 1985, Intraplate Earthquakes in Northern Svalbard, Tectonphysics, 114, 181-191.

Crane, K., Eldholm, O., Myhre, A. M., and Sundvor, E., 1982, Thermal Implications for the Evolution of the Spitsbergen Transform Fault, Tectonophysics, 89, 1-32.

Crane, K. and Bonatti, E., 1987, Fracture Zone Control on the Opening of the Red Sea: SIR A Data, Jour. of the Geological Soc. of London, 144, 407-420.

Crane, K., 1985, The spacing of rift axis highs: dependence upon diapiric processes in the underlying asthenosphere?, Earth and Planetary Science Letters, 72, 405-414.

Crane, K., Sundvor, E., Foucher, J. P., Hobart, M., Myhre, A. M., and LeDouran, S., 1988, Thermal Evolution of the Western Svalbard Margin, Mar. Geophys. Res., 9, 165-194.

Crane, K., Sundvor, E., Buck, R., and Martinez, F., 1991, Rifting in the Northern Norwegian-Greenland Sea: Thermal Tests of Asymmetric Spreading, Jour. Geophys. Res., 96, 14529-14550.

Desimon, A. I., and Karasik, A. M., 1979, Nekotoryye Osobennosti Morfologii I Razrastaiya Okeanicheskogo dna na Khrebte Knipovicha v Severnom Ledovitom Okeane, Dokl. Akad., Nauk SSSR, 247, 1215-1219 (in Russian), Some features of Bottom Relief and Seafloor Spreading on the Knipovich Ridge, Arctic Ocean, Dokl. Earth Science Section, 247, 73-77 (in English).

DeMets, C., Gordon, R. G., Argus, D. F., and Stein, S., 1990, Current Plate Motions, Geophys. J. Int., 101, 425-478

Detrick, R. S. and Humphris, S. E., 1994, Exploration of Global Oceanic Ridge System Unfolds, EOS, 75, 325-326.

Dore. A. G., and Gage, M. S., 1987, Crustal alignments and sedimentary domains in the evolution of the North Sea, North East Atlantic Margin and Barents Shelf. In: J. Brooks and K. Glennie (editors), Petroleum Geology of North West Europe. Graham and Trotman, London, 1131-1148.

Eldholm, O., Vogt, P., and Perry, R., 1978, Plate Tectonic Development of the Mid-Oceanic Ridge System North of the Jan Mayen Fracture Zone, A: Present Plate Boundaries, EOS 59, 371.

Eldholm, O. and Sundvor, E., 1980, The Continental Margins of the Norwegian-Greenland Sea: Recent Results and Outstanding Problems, Royal Society of London Phil. Trans., Ser. A: 294, 77-86.

Eldholm, O., Karasik, A. M., and Reksnes, P. A., 1986, The North American Plate Boundary, DNAG synthesis. Volume Geology of the Arctic Ocean Region Chapter 12.

Harland, W. B., 1969, Contribution of Spitsbergen to understanding of tectonic evolution of North Atlantic Region. In: M. Kay (Editor), North Atlantic: Geology and Continental Drift. American Association of Petroleum Geologists, Memoir 12, 817-851.

Horsfield, W. T. and Maton, P. I., 1970, Transform Faulting along the De Geer Line, Nature 226, 256-257.

Johnson, L. and Heezen, B. C., 1967, Morphology and Evolution of the Norwegian-Greenland Sea, Deep-Sea Research 14, 755-771.

Kovacs, L.C., Johnson, G. L., Srivastava, S. P., Taylor, P. T., and Vogt, P. R., 1987, Residual Magnetic Anomaly Chart of the Arctic Ocean Region (Naval research Laboratory and Naval Ocean research and Development Activity), In: The Arctic Ocean Region, Vol. L., The Geology of North America, edited by Arthur Gantz, L. Johnson, and J. F. Sweeny, 1990, 644p.

Macdonald, K. C., 1986, The Crest of the Mid-Atlantic Ridge: Models for crustal generation processes and tectonics, In: The Geology of North America, Vol. M for the Western north Atlantic Region, Edited by P. R. Vogt and B. E. Tuckolke, Geological Society of America, Boulder, CO.

Macdonald, K. C., Schierer, D. S., and Carbotte, S. M., 1991, Mid-Ocean ridges: Discontinuities, segments, and giant cracks, Science, 253, 986-994.

Minster, W. J., and T. H. Jordan, 1978, Present-Day Plate Motions, Jour. Geophys. Res., 83, 5331-5354.

Morgan, W. J., 1981, Hotspot Tracks and the Opening of the Atlantic and Indian Oceans, in The Sea, 7, edited by C. Emiliani, pp. 443-487, John Wiley, New York.

Okay, N., and Crane, K., 1993, Thermal Rejuvenation of the Yermak Plateau, Marine Geophysical Researches, 15, 243-263.

Okay, N., 1995, Thermal Rejuvenation in the Norwegian-Greenland Sea, Unpublished Ph.D. Thesis.

Ohta, Y., 1982, Morpho-Tectonic Studies Around Svalbard and the Northernmost Atlantic, in Embry, A. F. and Blackwell, H. R., Arctic Geology and Geophysics, Can. Soc. Petroleum Geol., Memoir 8,. 415-431.

Prestvik, T., 1977, Cenozoic plateau lavas of Spitsbergen - a geochemical study, Norsk Polarist, Arbok, 127-143.

Perry, R. K., Fleming, H. S., Weber, J. R., Kristoffersen, Y., Hall, J. K., Grantz, A., Johnson, G. L., Cherkis, N. Z., and Larsen, B., 1985, Bathymetry of the Arctic Ocean, Scale 1:6,000,000, Geol. Soc. Amer. Map Series, MC-56, Naval Research Laboratory, Washington, D.C.

Schouten, H., and Klitgord, K. D., 1982, The memory of the accreting plate boundary and the continuity of fracture zones, Earth Planet. Sci. Lett., 59, 255-266.

Schouten, H., and Klitgord, K. D., and Whitehead, J. A., 1985, Segmentation of mid-ocean ridges, Nature, 317, 225-229.

Searle, R. C., and Laughton, A. S., 1977, Sonar studies of the Mid-Atlantic Ridge and Kurchatov Fracture Zone, Jour. Geophys. Res., 82, 5313-5328.

Searle, R. C., 1984, GLORIA Survey of the East Pacific Rise near 3.5°S: Tectonic and volcanic characteristics of a fast spreading mid-ocean rise, Tectonophysics, 101, 319-344.

Sempere, J. C., and Macdonald, K. C., 1987, Marine Tectonics: Processes at Mid-Ocean Ridges, Reviews of Geophysics, 25, 6, 1313-1347.

Sempere, J. C., Purdy, G. M., and Schouten, H., 1990, Segmentation of the Mid-Atlantic Ridge between 24° N and 30°40N, Mar. Geophys. Res., 15, 153-200.

Sempere, J. C., J. Lin, H. S. Brown, H. Schouten, and G. M. Purdy., 1993, Segmentation and morphotectonic variations along a slow-spreading center: The Mid-Atlantic Ridge (24° N-30°40N, Nature, 344, 427-431.

Shor, A., 1990, SeaMARC II seafloor mapping system: Seven years of Pacific research, Pacific Rim Congress Vol. III; Australian Institute of Mining and Metallogenesis, 49-59.

Skjelkvale, B. L., Amundsen, H. E. F., O'Reilly, S. Y., Griffin, W. L., and Gjelsvik, T., 1989, A primitive alkali basaltic stratovolcano and associated eruptive centers, Northwestern Spitsbergen,: Volcanology and Tectonic Significance, 1989, Journal of Volcanology and Geothermal Research, 37, 1-19.

Sobczak, L. W., and Hearty, D. B., with contributions by R. Forsberg, Y. Kristoffersen, O. Eldholm and S. D. May), 1987, Gravity of the Arctic Ocean, In: The Arctic Ocean Region, Vol. L., The Geology of North America, edited by Arthur Gantz, L. Johnson, and J. F. Sweeny, 1990, 644p.

Stein, S., Melosh, H. J., and Minster, J. B., 1977, Ridge Migration and Asymmetric Sea-floor Spreading, Earth Planet. Sci. Lett., 36, 51-62.

Sundvor, E. and O. Eldholm, 1979, The Western and Northern Margin off Svalbard, Tectonophysics, 59, 239-250.

Talwani, M. and Eldholm, O., 1977, Evolution of the Norwegian-Greenland Sea, Geol. Soc. America Bull. 88, 969-999.

Thiede, J., S. Pfirman, H-W Schenke, and W. Reil, 1990, Bathymetry of the Molloy Deep: Fram Strait between Greenland and Svalbard, Marine Geophysical Researches, 12, 197-214.

Vogt, P. R., and Avery, O. E., 1974, Tectonic History of the Arctic Basins: Partial Solutions and Unsolved Mysteries, in Marine Geology and Oceanography of the Arctic Seas, edited by Herman, Y., 83-117, Springer-Verlag, New York.

Vogt, P. R., R. H. Feden, O. Eldholm, and E. Sundvor, 1978, The Ocean Crust West and North of the Svalbard Archipelago: Synthesis and Review of New Results, Polarforschung, 48, 1-19.

Vogt, P. R., G. L. Johnson, and L. Kristjansson, 1980, Morphology and Magnetic Anomalies North of Iceland, Journal of Geophysics, 47, 67-80

Vogt, P. R., R. K. Perry, R. H. Feden, H. S. Fleming, and N. Z. Cherkis, 1981, The Greenland-Norwegian Sea and Iceland Environment: Geology and Geophysics; In: The Ocean Basins and Margins, Vol. 5, The Arctic Ocean, Edited by A. E. M. Nairn and M. Churkin, pp. 493-598, Plenum, New York, 1981.

Vogt, P. R., L. C. Kovacs, L. C. Bernero, and S. P. Srivastava, 1982, Asymmetric geophysical signatures in the Greenland-Norwegian and southern Labrador Seas and the Eurasia Basin, Tectonophysics, 89, 95-160.

Vogt, P. R., 1986b, Geophysical and Geochemical Signatures and Plate Tectonics, Chapter 11, in The Nordic Seas, edited by B. G. Hurdle, Springer Verlag.

Vogt, P. R., 1986a, Seafloor Topography, Sediments, and Paleoenvironments, Chapter 11, in The Nordic Seas, edited by B. G. Hurdle, Springer Verlag.

Vogt, P. R., K. Crane, E. Sundvor, M. D. Max, and S. L. Pfirman, 1994, Methane-Generated(?) Pockmarks on young thickly sedimented oceanic crust in the Arctic: Vestnesa Ridge, Fram Strait, Geology, 22, 255-258.

Wernicke, B., 1985, Uniform sense normal simple shear of the continental lithosphere, Canadian Journal of Earth Sciences, 22, 108-125.

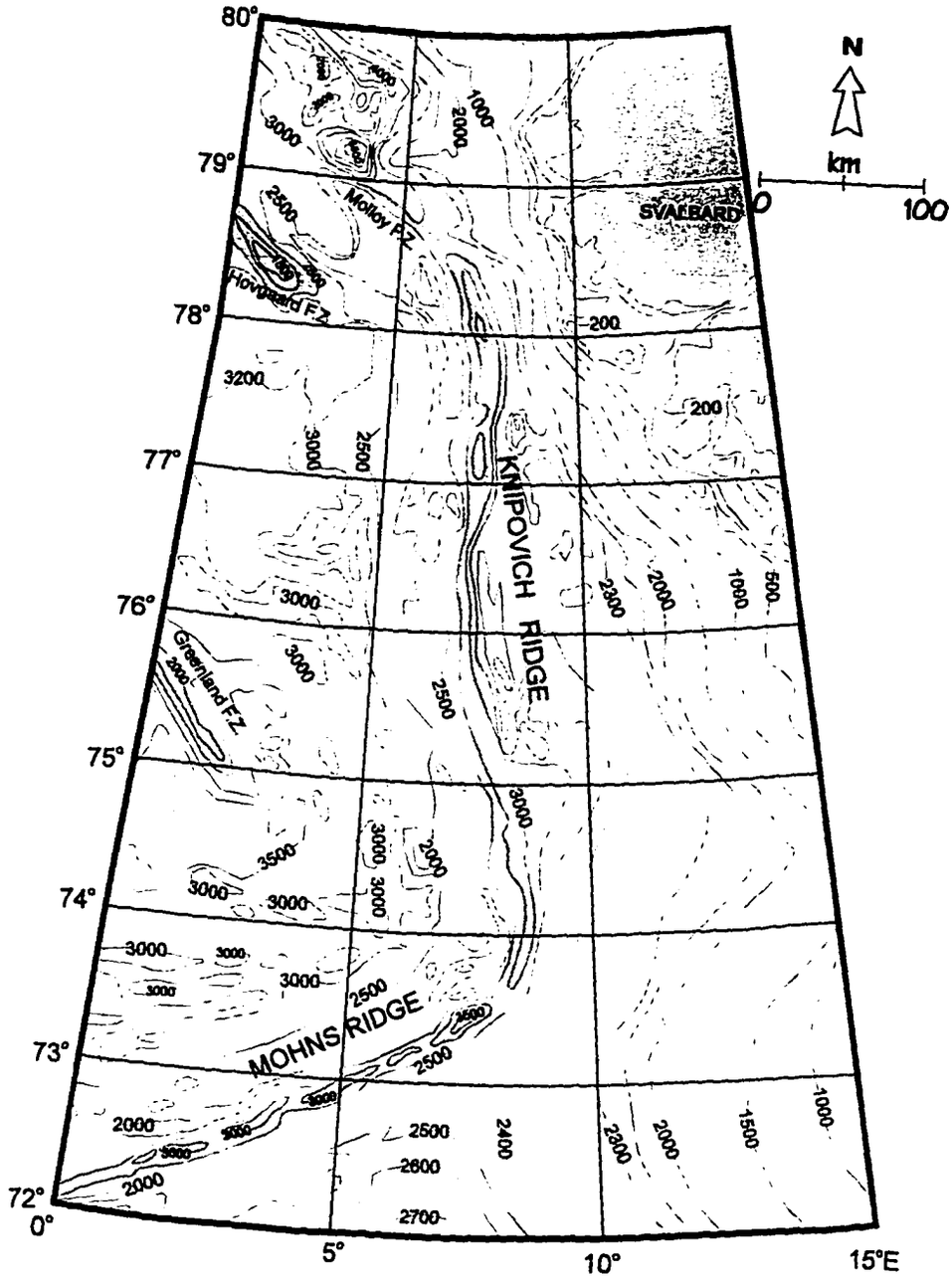

Figure 1: Generalized bathymetry of the surveyed region of the Norwegian-Greenland Sea (after Cherkis and Vogt, 1994).

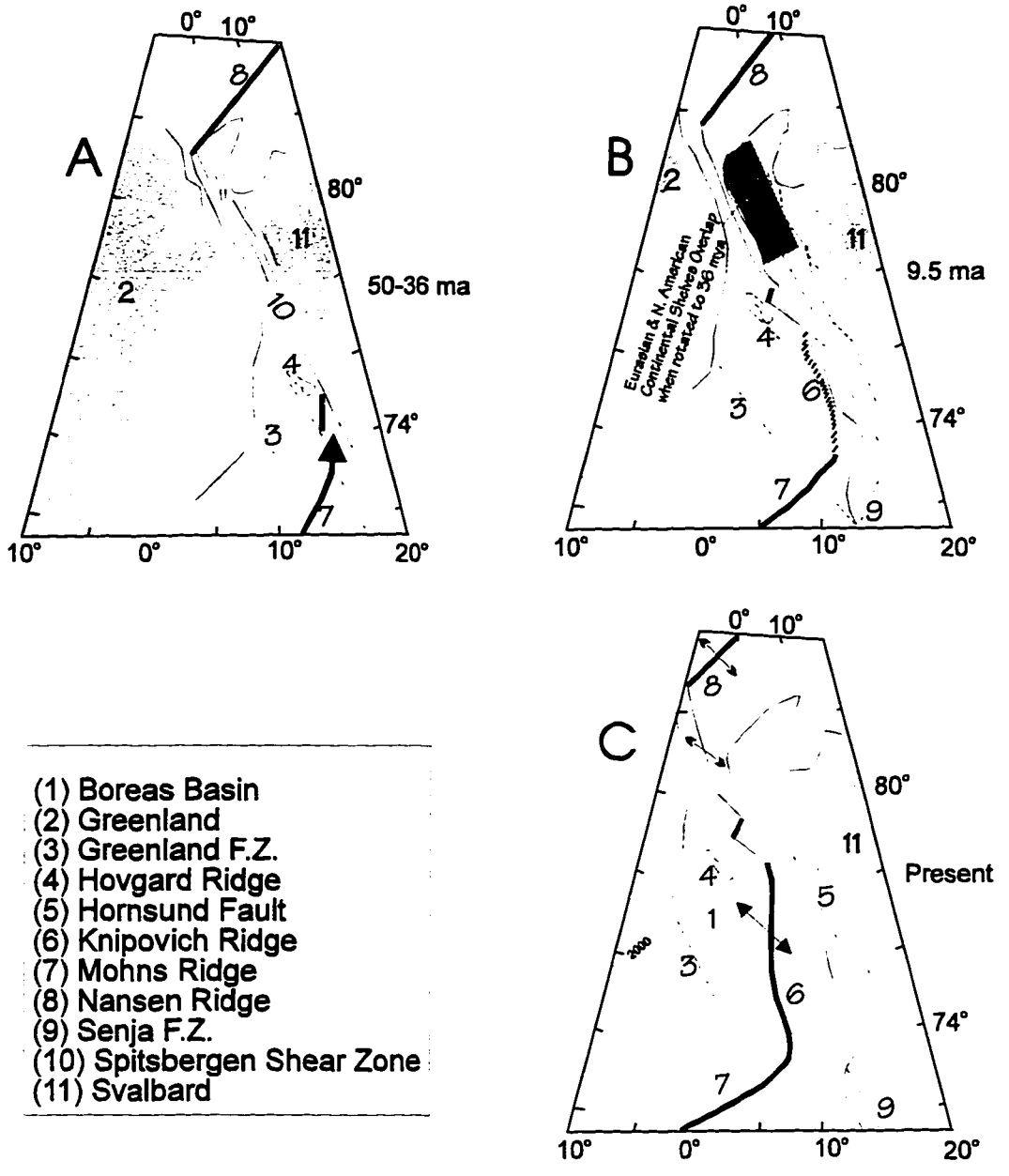

Figure 2: Plate reconstruction at 50-36 MA, 9.5 MA and of the present. The ancient Spitsbergen Shear Zone probably cut through Svalbard (Horsfield and Maton, 1970). As the plate boundary developed, the active spreading center propagated into the continental shear zone from the Norwegian Sea and the Arctic Ocean generating the Knipovich Ridge in the Greenland Sea and the Lena trough (after Crane et al., 1991).

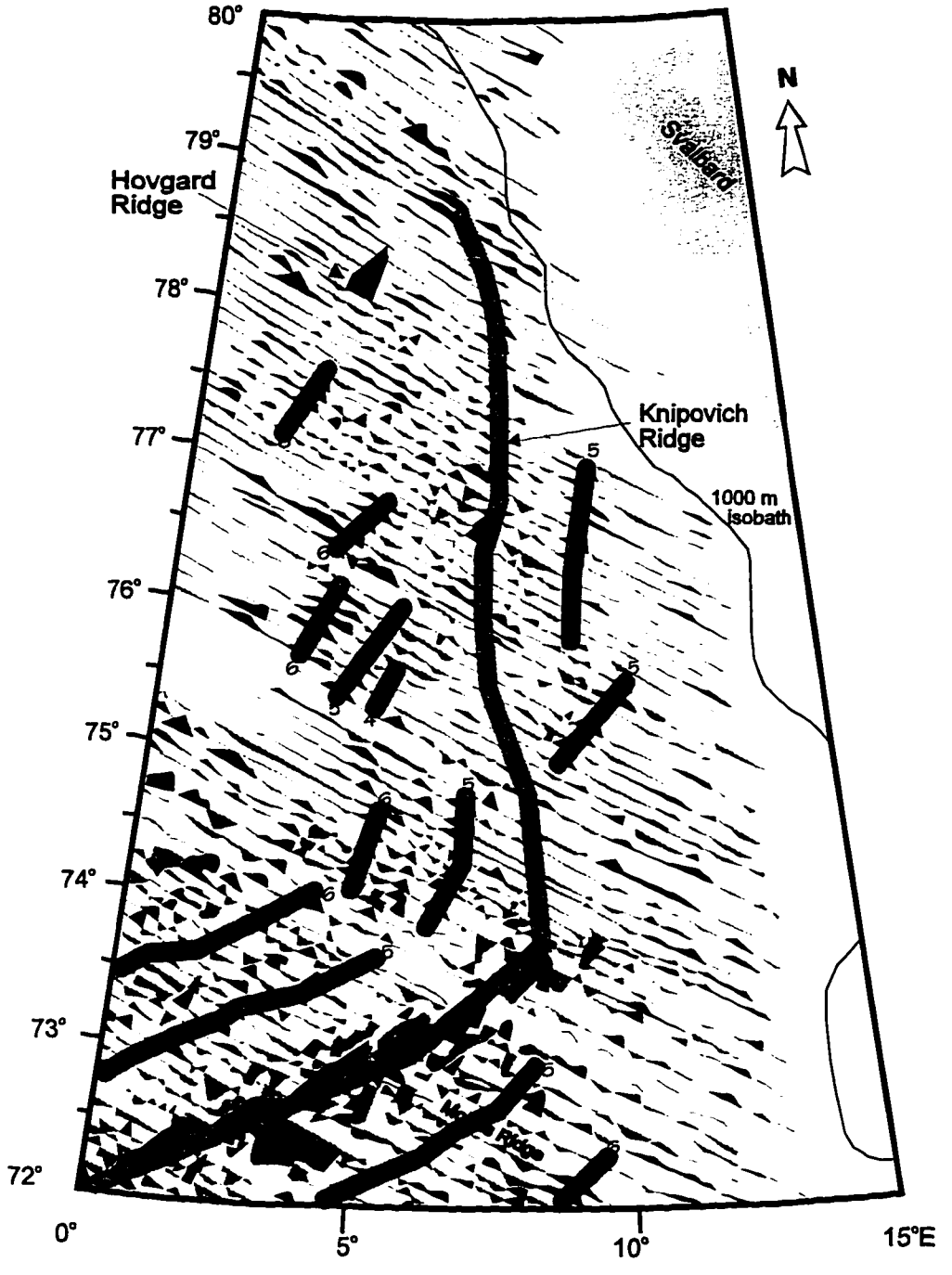

Figure 3: Residual magnetic anomalies within the survey area. All data are shown as fenced anomaly profiles along flight tracks. Positive anomalies are in black while negative anomalies are dotted. Anomaly scale is 4,000 nT per degree of latitude. (After Kovacs et al., 1987). Magnetic anomalies are chaotic or absent in the Greenland Sea compared with more normal anomalies along the northeastern Mohns Ridge. Some anomalies in the Boreas Basin were identified by Vogt (1986) and his interpretations are shown by the darker dotted patterns including the anomaly number.

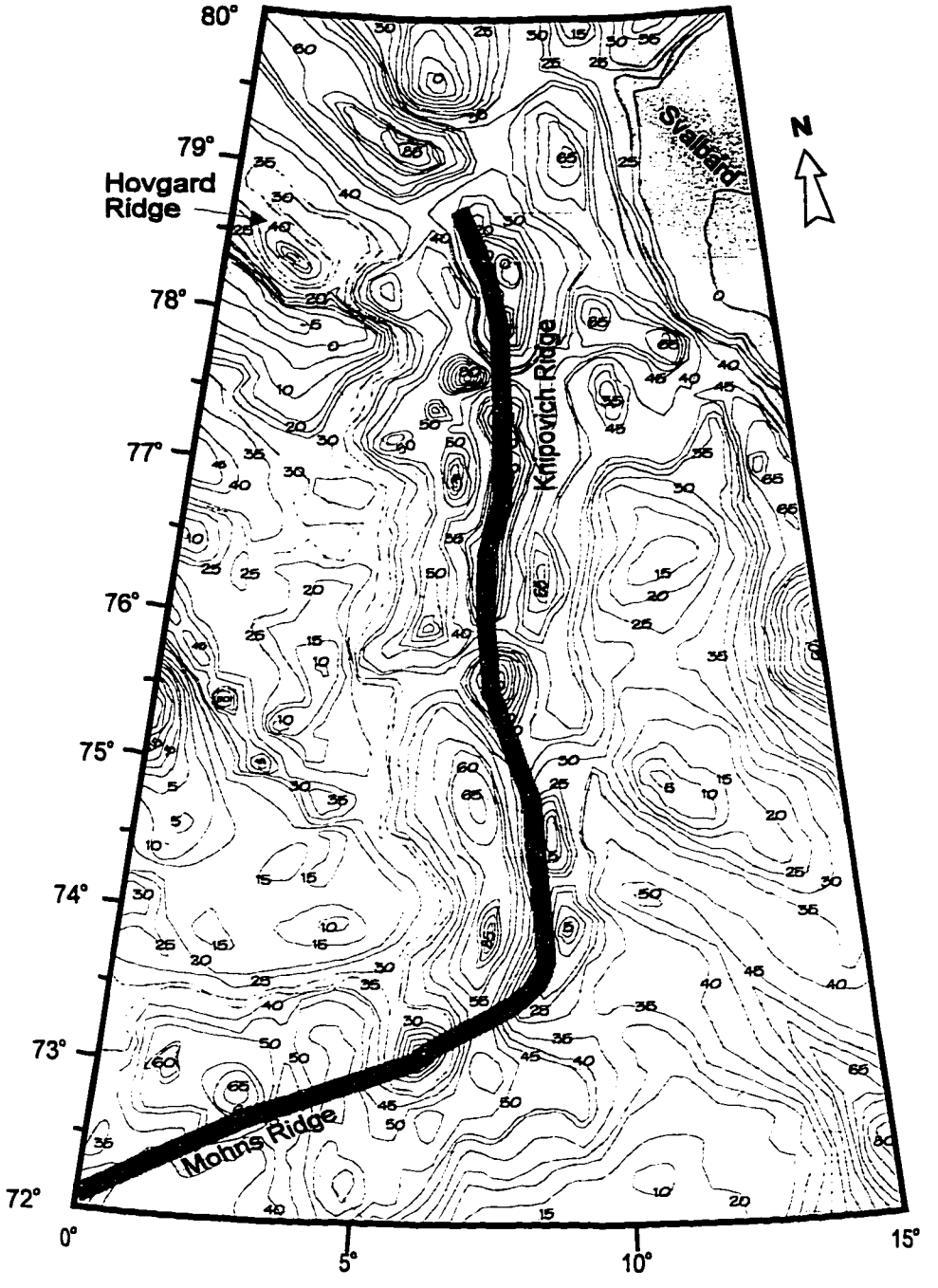

Figure 4: Free-air gravity anomaly map of the survey area. Contour interval is 5 mGal. (After Sobczak et al., 1987). Along the Knipovich Ridge, a belt of well defined gravity minima can be found in the rift valley compared with well defined gravity maxima on the flanks. The dotted lines represent control lines.

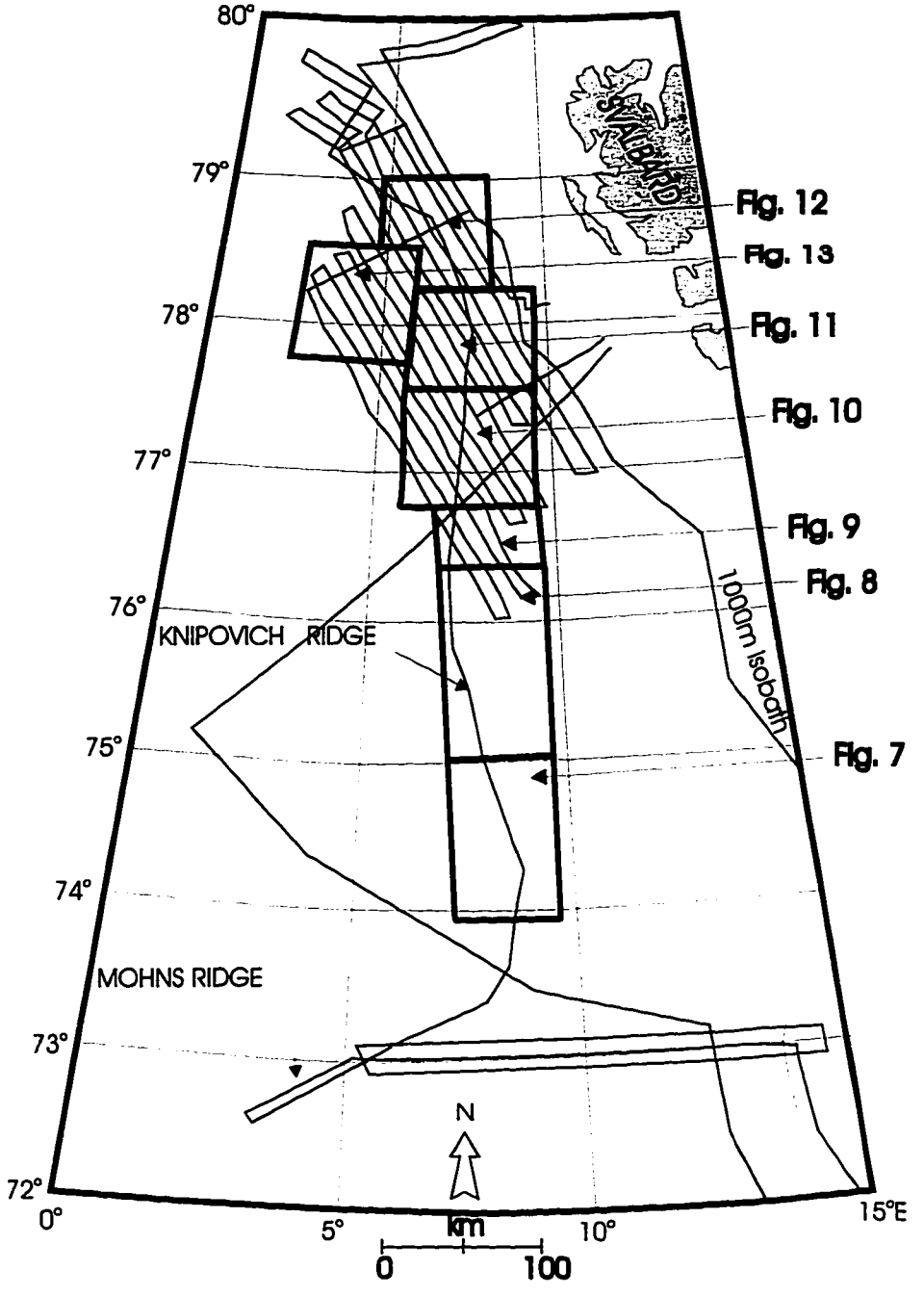

Figure 5: Track map illustrating the SeaMARC II expeditions (1989 and 1990). Regions discussed in this paper are outlined in bold and labeled by the appropriate figure number.

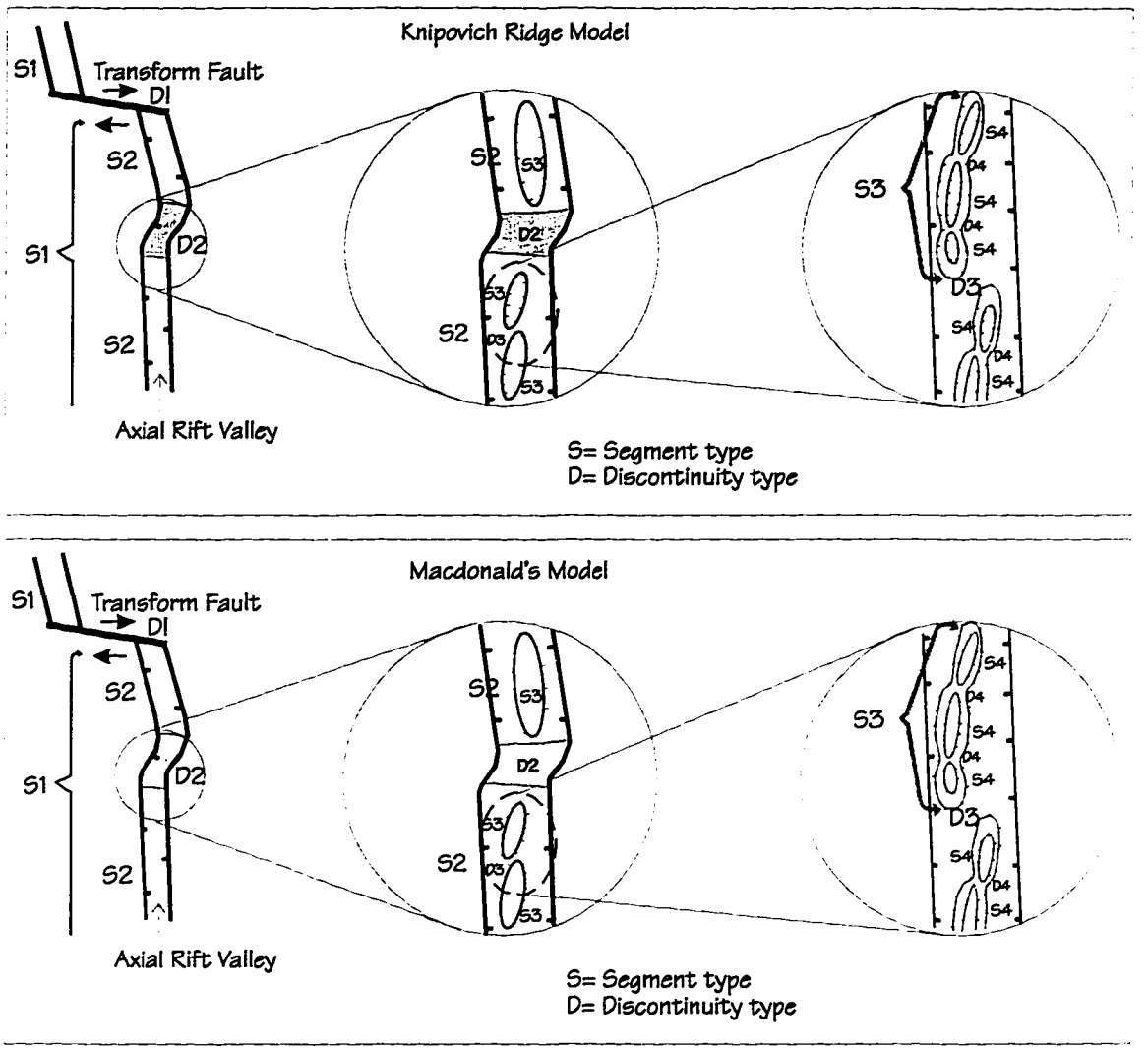

Figure 6: Schematic representation of the segmentation (S1, S2, S3, S4) and discontinuities (D1, D2, D3, D4) proposed for the Knipovich Ridge. Segments are rift valley basins whereas discontinuities are saddles between these basins. For both segments and discontinuities, larger numbers indicate lower order. S1 is the first-order Knipovich Ridge bounded by a D1 discontinuity such as the Molloy transform fault. S2 are second order basinal segments that range from 40 to 80 km in length and are bounded by D2 discontinuity such as rift valley jogs or volcanic highs or a combination of the two. S3 are third order basinal segments bounded by D3 discontinuities such as inter-basinal (S2) highs, which are usually volcanic. S4 are basinal segments that exist within S3 segments and are bounded by D4 discontinuities such as intra-basinal discontinuities which are usually saddles of low relief (top figure). For comparison, Maconald's model is shown in the bottom figure.

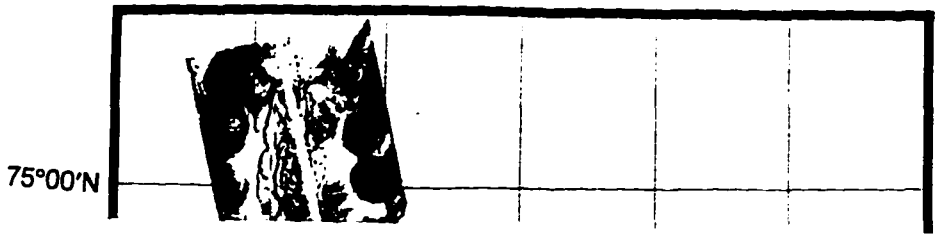

Figure 7A: SeaMARC II side-scan image of the southernmost Knipovich Ridge from 73°50'N to 75°05'N. To the south lies the Mohns-Knipovich transition zone.

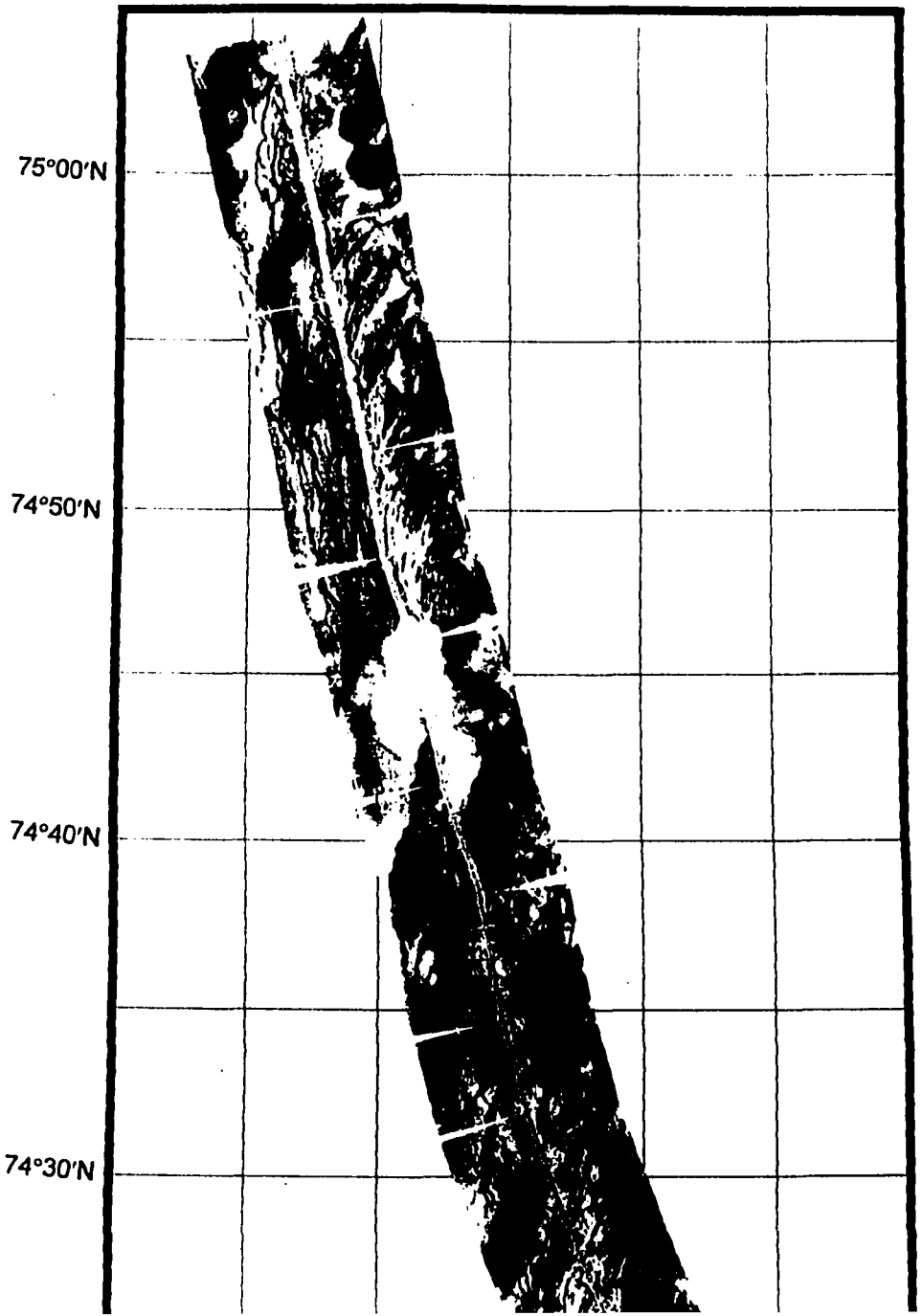

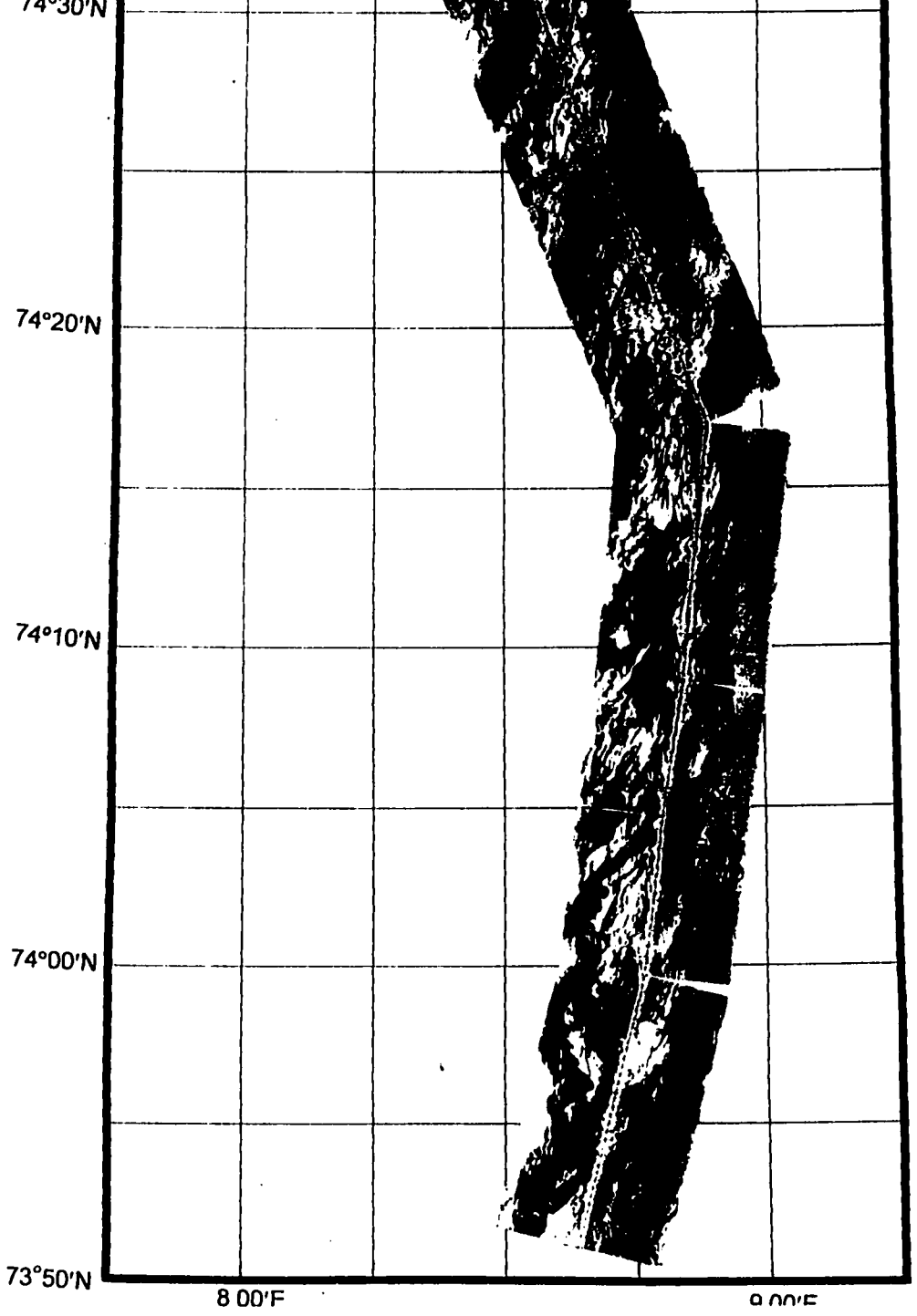

from

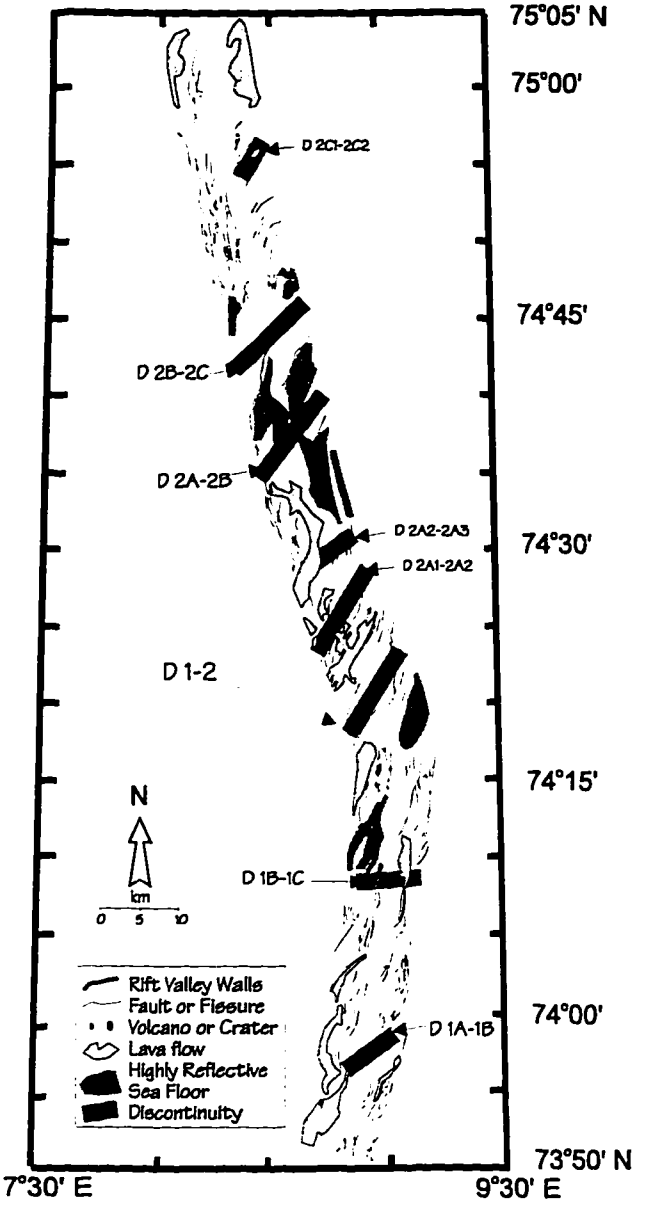

Figure 7B: Structural interpretation of image shown in figure 7A.

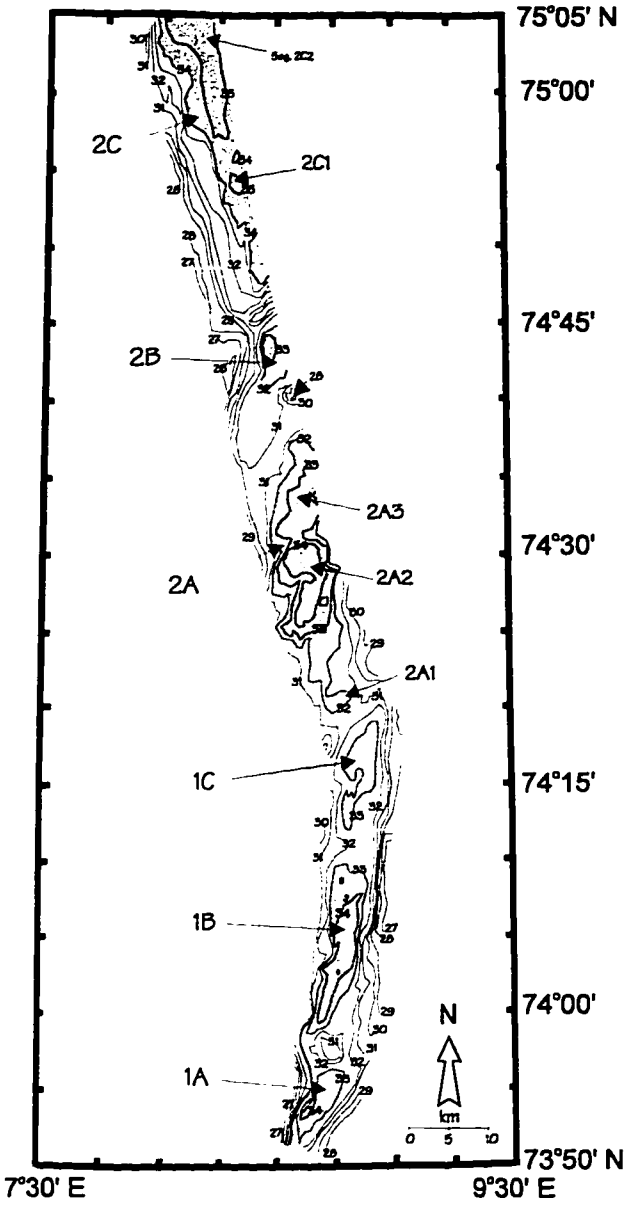

Figure 7C: Bathymetry corresponding to side-scan image shown in figure 7A. Third order segments 1A, 1B, 1C, 2A, 2B, and 2C are shown as well as fourth order segments 2C1 and 2C2. Shaded areas are depressions. Note the change in segment strike along the rift valley between third-order segments of segment 1 (19°-35°) and 2 (0°-340°).

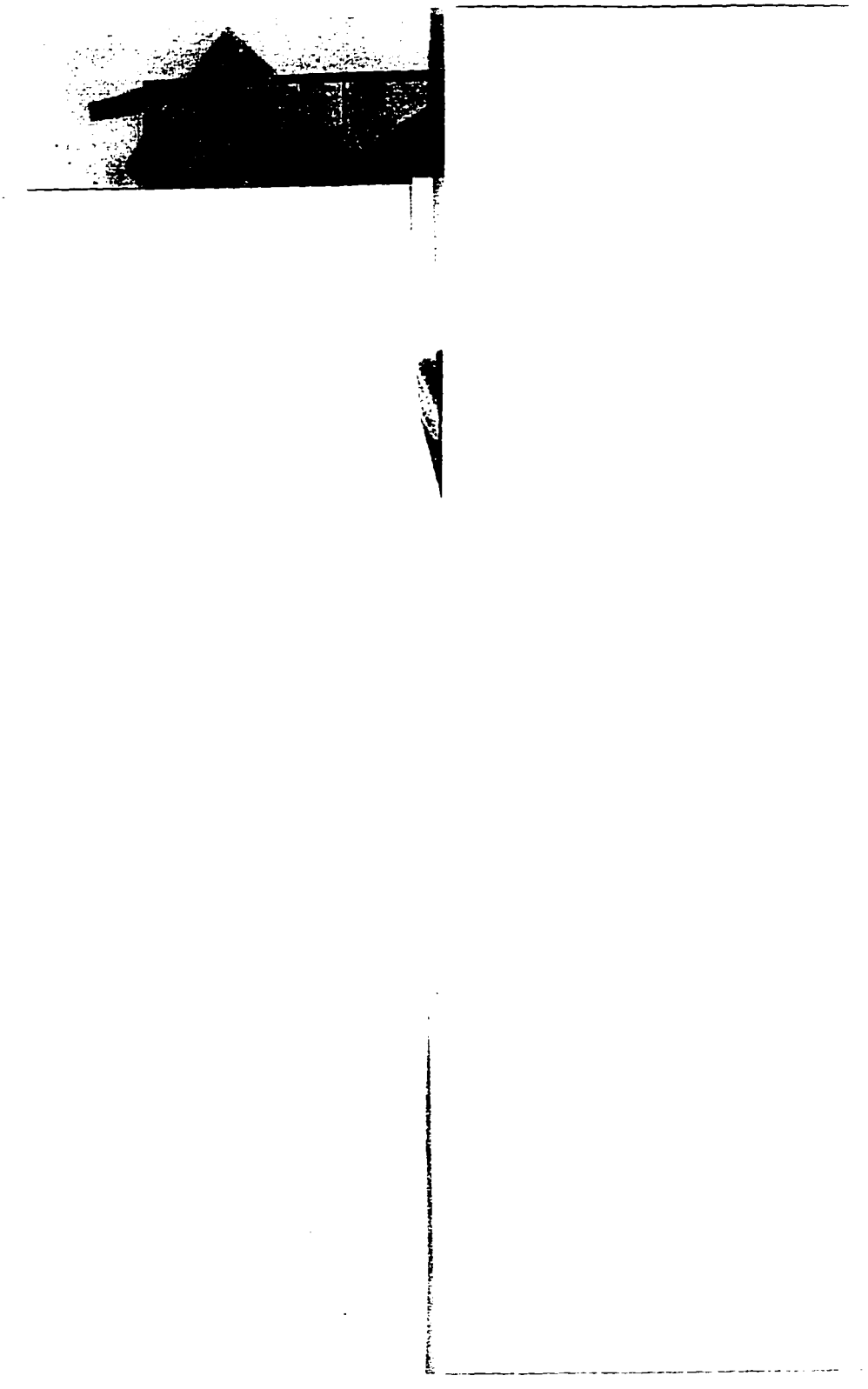

Figure 8A: SeaMARC II side-scan image of the Knipovich Ridge between 75°05'N and 76°25'N.

Fi
76

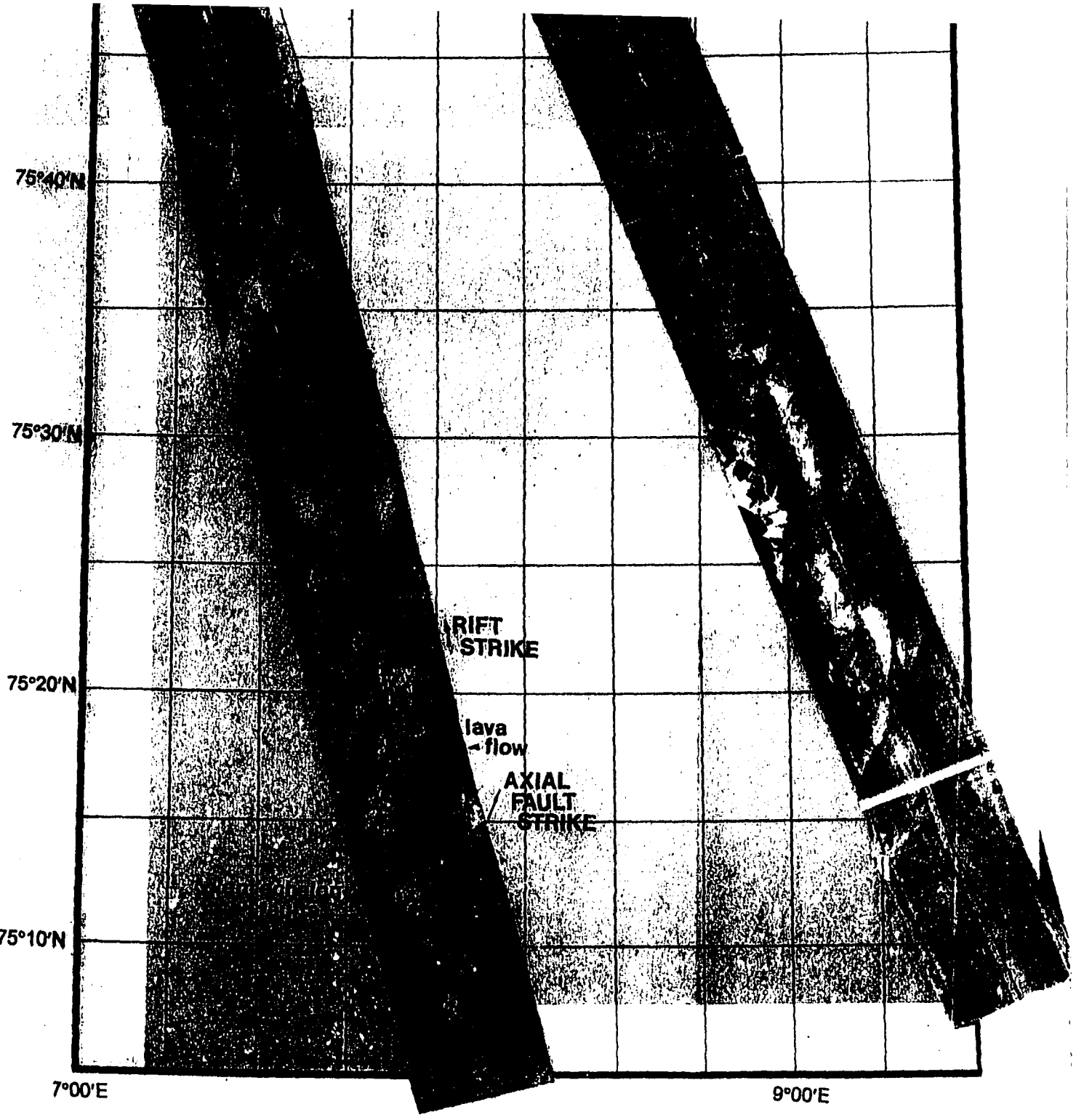

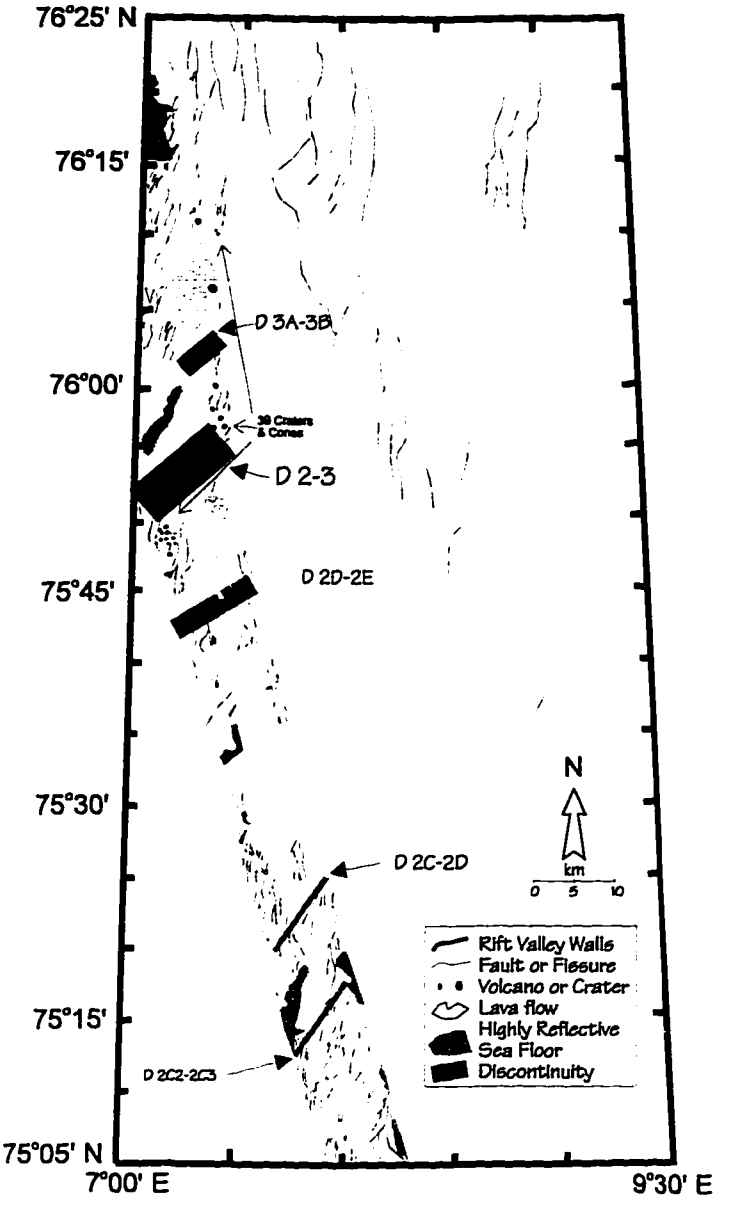

Figure 8B: Structural interpretation of side-scan image shown in figure 8A including the rift valley and a part of the eastern flank. Note the different nature of faults found within the rift valley, which tend to be shorter and oriented to the northeast, and faults found on the eastern flank, which tend to be long and oriented to the north. Between 75°45'N and 76°20'N, there is a rift valley volcano field that consists of approximately 39 craters and cones.

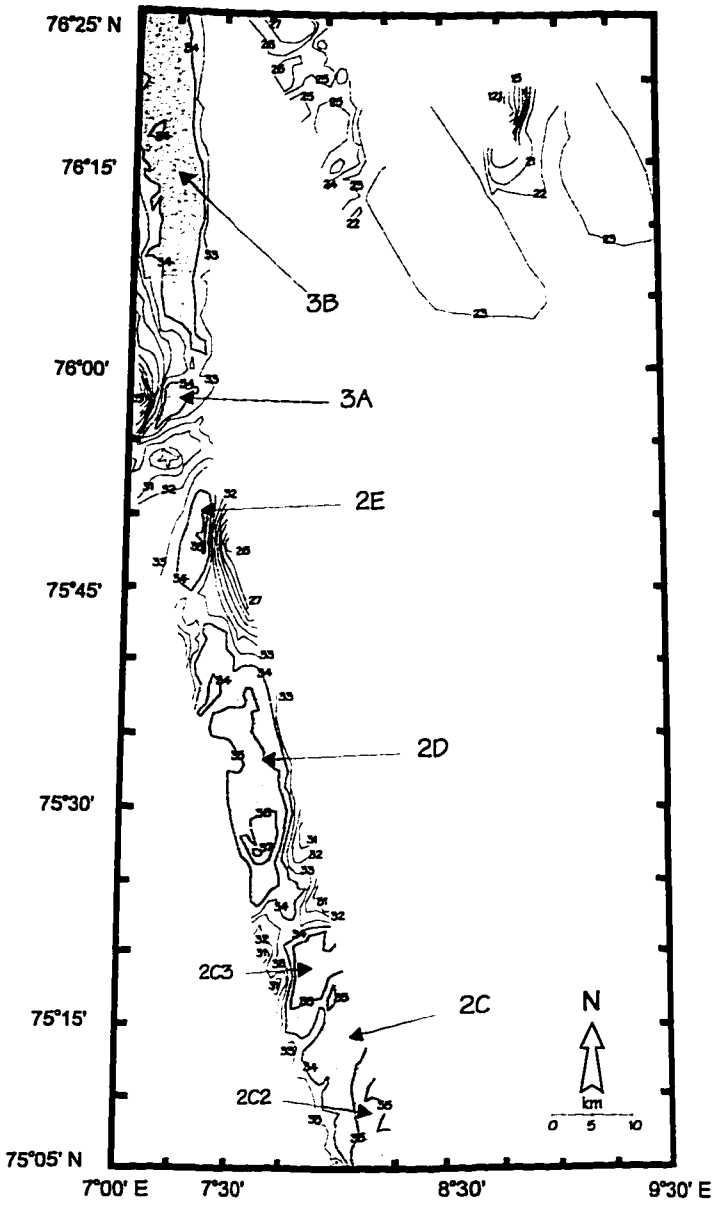

Figure 8C: Bathymetric contours corresponding to side-scan image shown in figure 8A. Third order segments 2C, 2D, 2E, 3A, and 3B and fourth order segments 2C2 and 2C3 are shown. Note the second order discontinuity between segments 2 and 3 (near 74°53'N), which is a change in strike of the rift valley as well as a volcanic high. Third order segment strikes appear to be independent of the rift valley strike.

Figure 9A: SeaMARC II side-scan image of the Knipovich Ridge from 76°15'N to 76°45'N and approximately 40 km of the eastern flank.

le-scan image of the Knipovich Ridge from 76°15'N to
) km of the eastern flank.

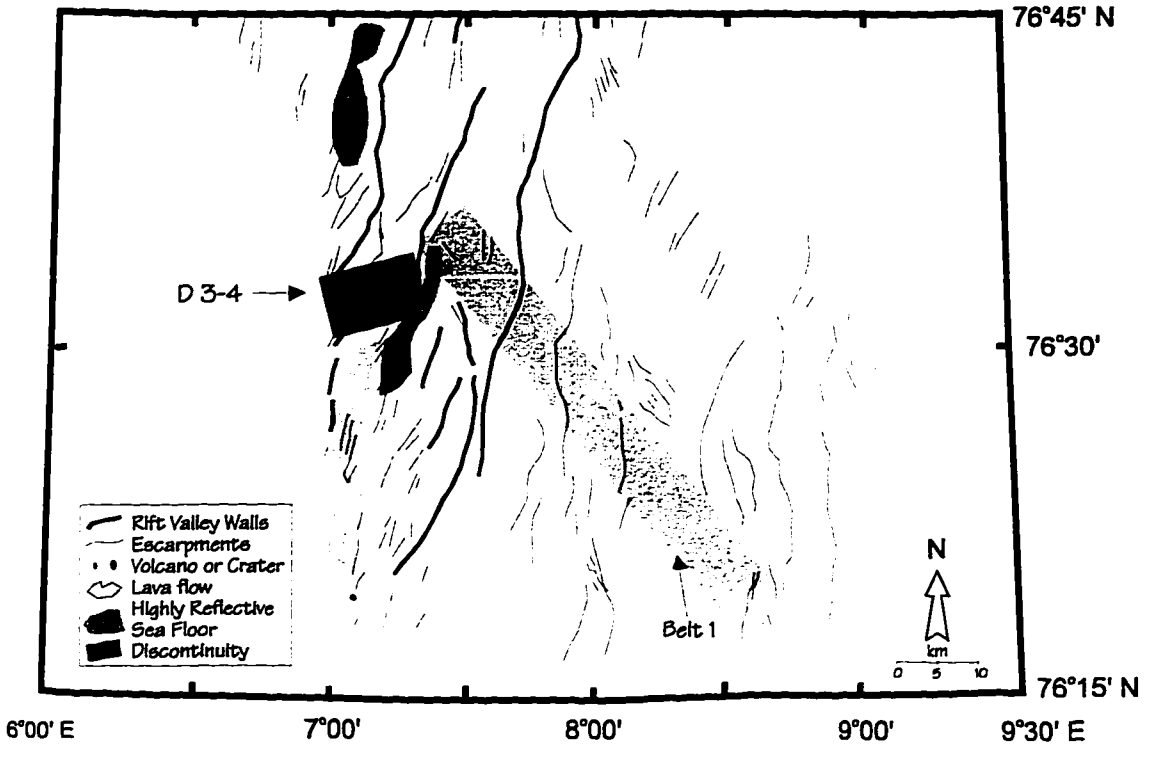

Figure 9B: Structural interpretations of side-scan image shown in figure 9A. Note the second order discontinuity between segments 3 and 4 (near 76°33'N) which is a change in the strike of the rift valley and a volcanic high. Flank faults associated with anomalous bathymetry belt 1 are seen (long gray area) trending an average of 330°.

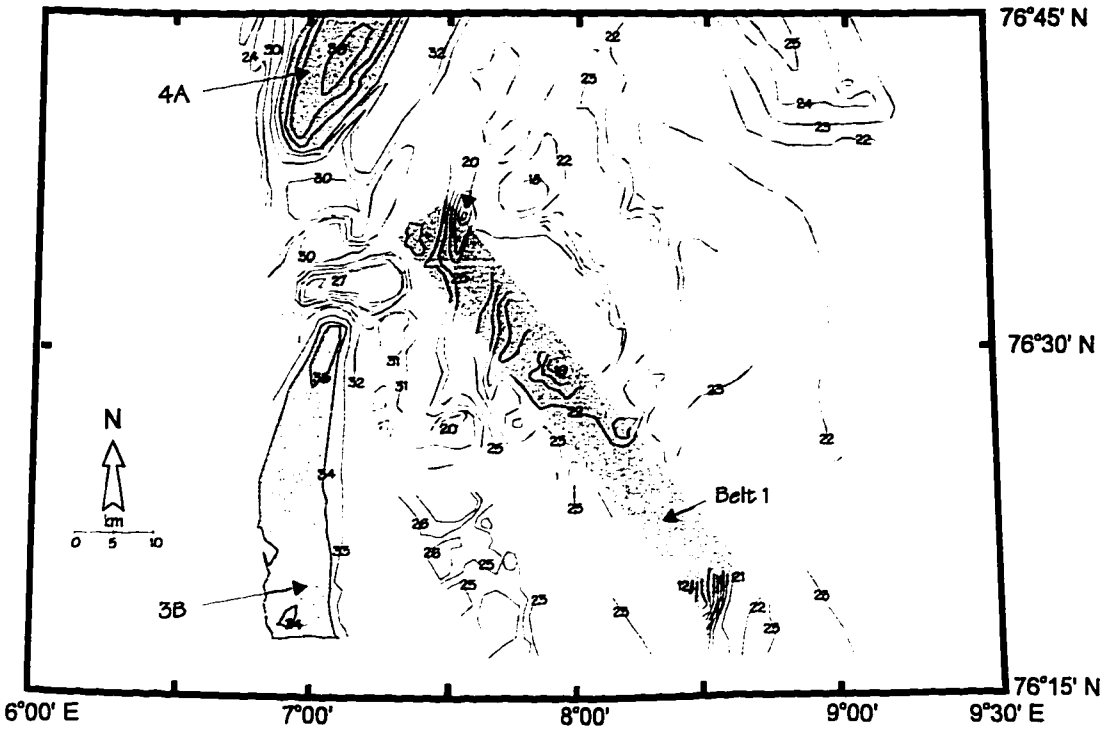

Figure 9C: Bathymetry corresponding to side-scan image shown in figure 9A. Third order segments 3B and 4A are shown. Note the second order discontinuity between segments 3 and 4 (near 76°33'N) which is a change in the strike of the rift valley and a volcanic high. Anomalous bathymetry belt 1 trends 325°, whereas the 3 bathymetric highs trend is less obvious (the first 2 were not completely imaged) and 014° (south to north respectively).

Figure 10A: SeaMARC II side-scan image of the Knipovich Ridge from 76°45'N to 77°30'N as well as the inner flanks.

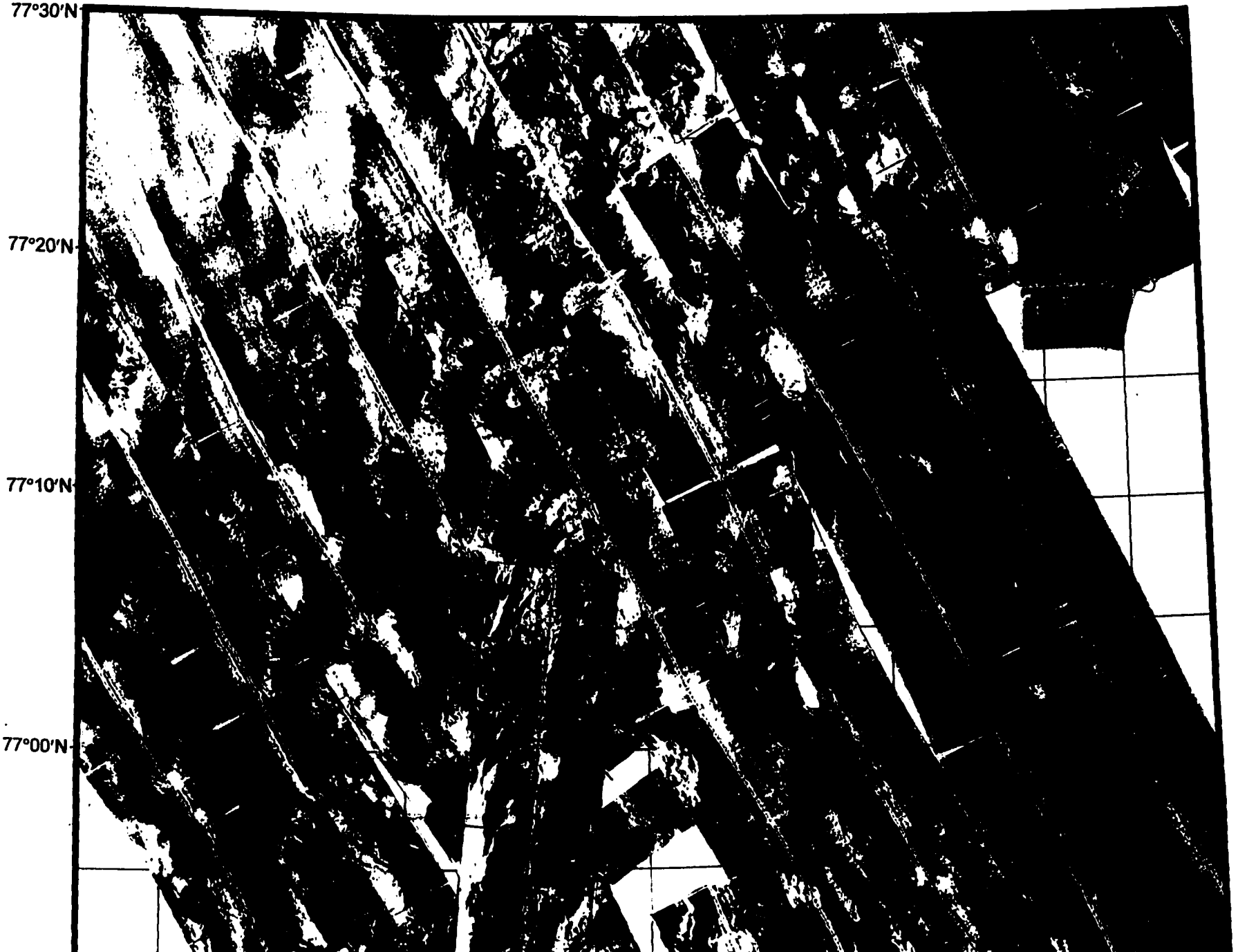

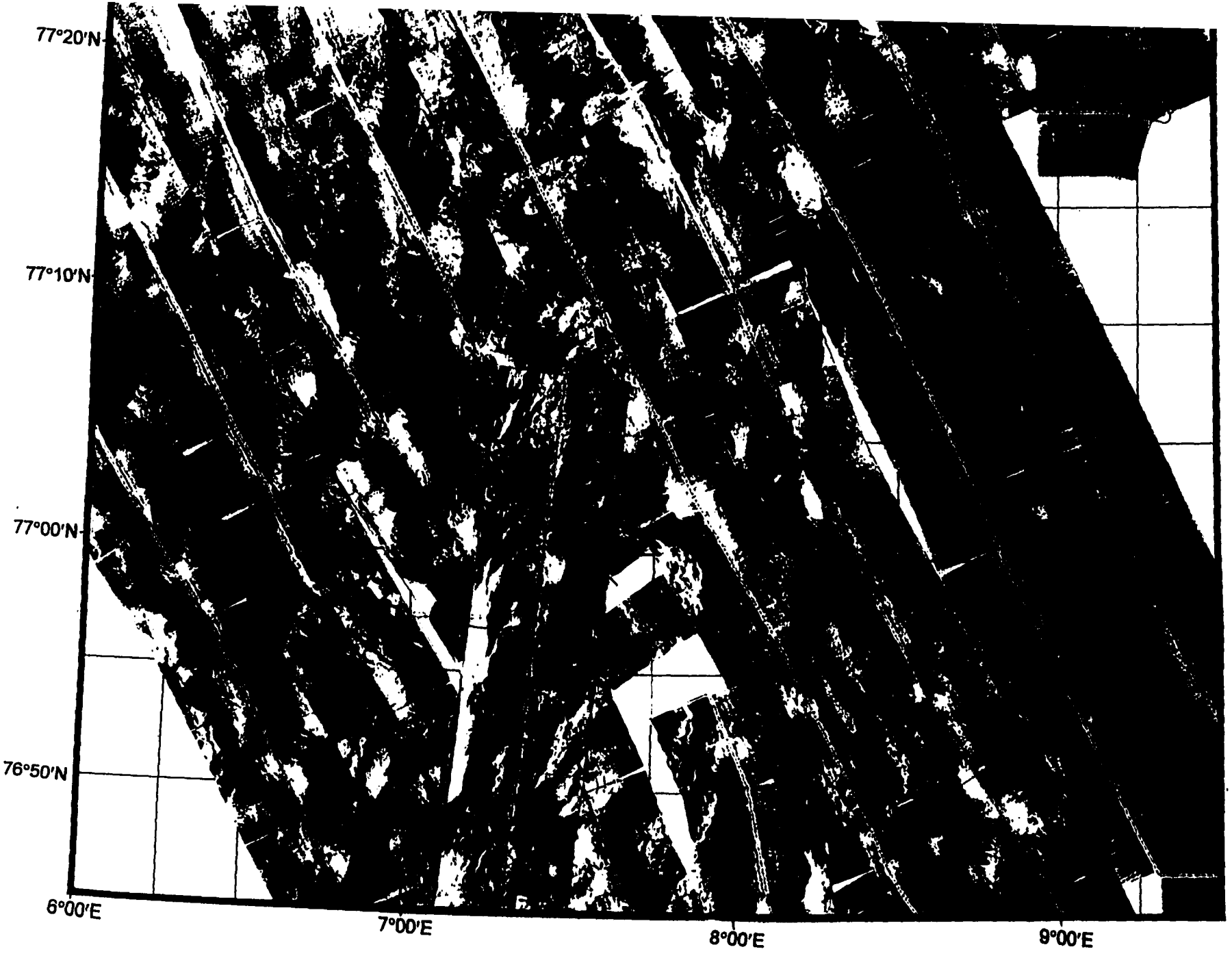

Fig
77'

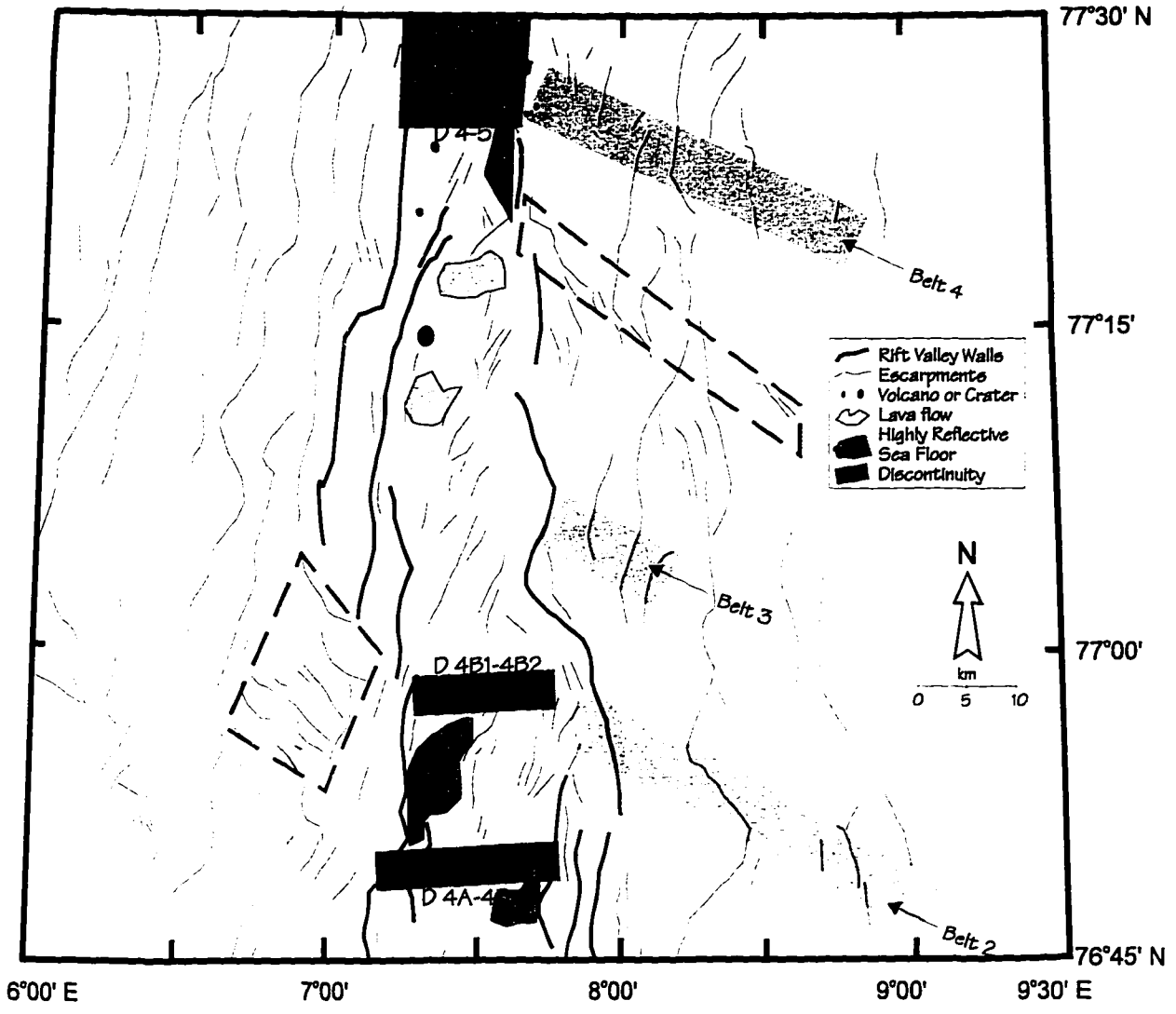

Figure 10B: Structural interpretations of side-scan image shown in figure 10A. Conjugate faults on both flanks tend to converge towards the rift valley from south to north. Shaded boxes (on flanks) show fault trends near the shallow bathymetry belts 2-4 (figure 10C). Dashed empty boxes mark flank locations near the inner rift valley where fault trends are anomalous to local fault trends.

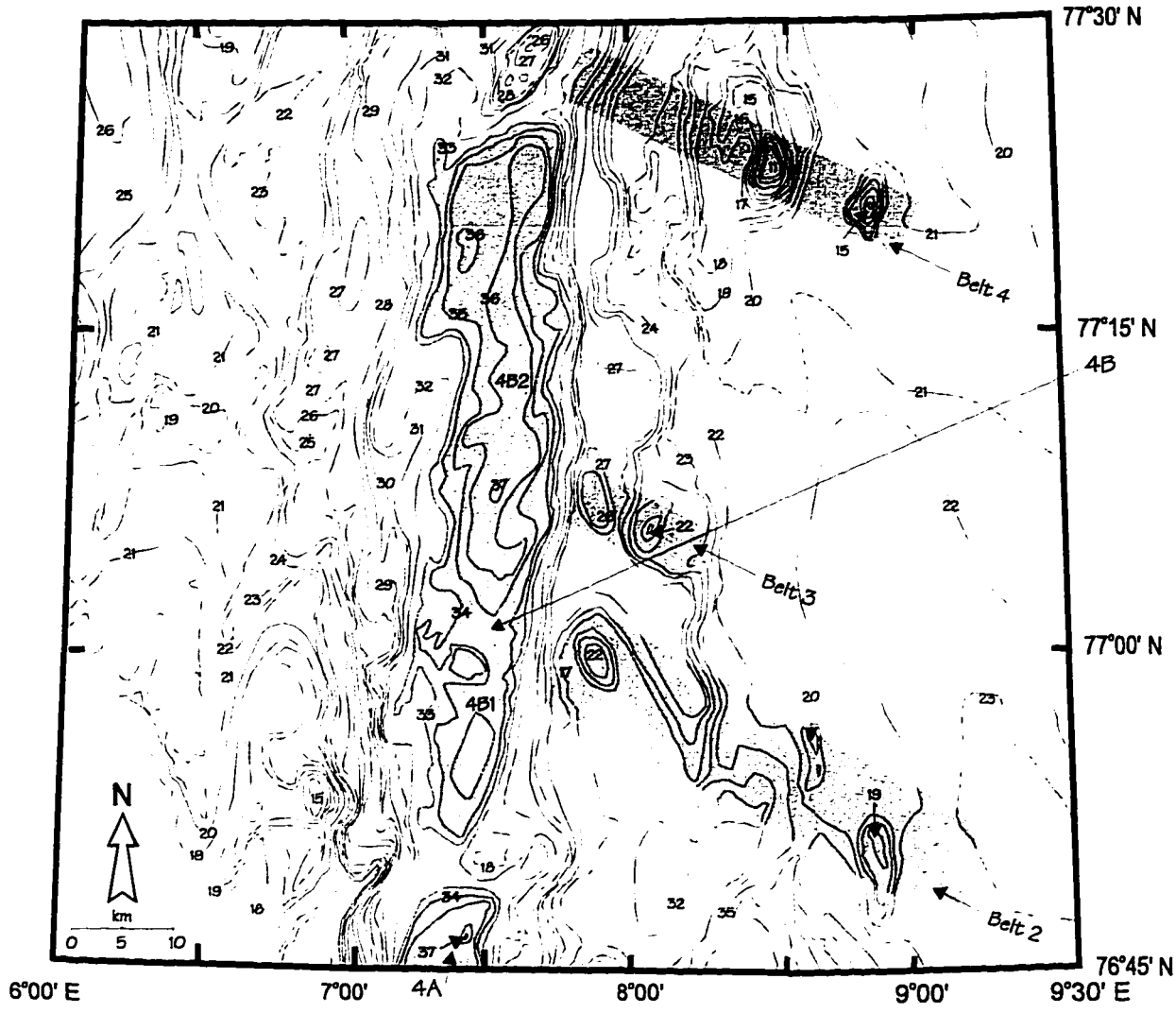

Figure 10C: Bathymetry corresponding to side-scan image shown in 10A. Third order segments 4A and 4B are shown. Note the second order discontinuity between segments 4 and 5 (near 77°24'N) which is a change in the strike of the rift valley. Anomalous bathymetry belts 2, 3, and 4 are seen on the eastern flank trending 320°, 305°, and 295° while the bathymetric highs within them have various trends.

Figure 11A: SeaMARC II side-scan image of the Knipovich Ridge from 77°30'N to 78°15'N and the inner parts of the flanks.

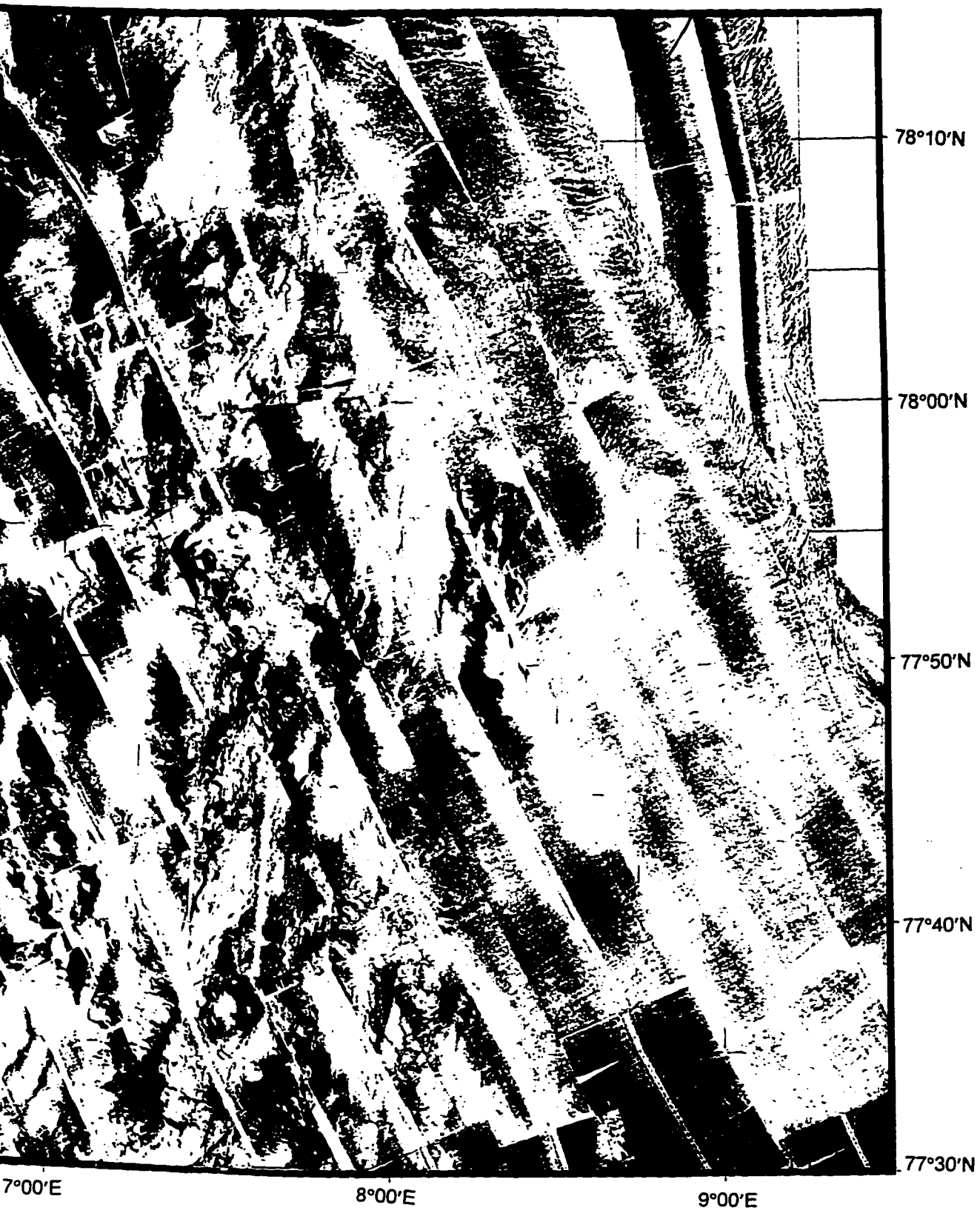

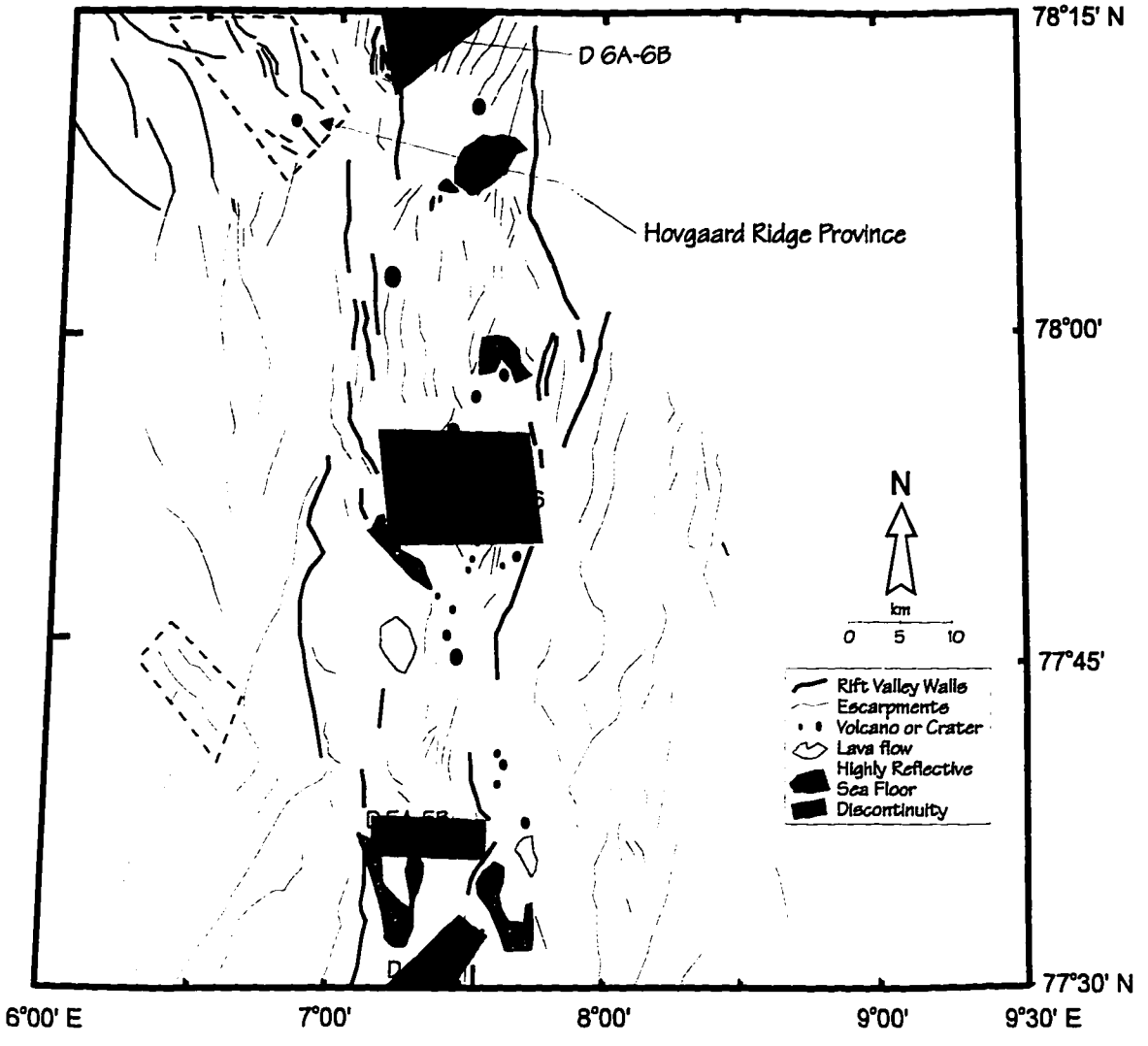

Figure 11B: Structural interpretation of side-scan image shown in figure 11A. Note the presence of many cones (~30) just to the north of segment 2 which may be evidence for the rift valley propagation (or recent leakage) beyond a locked point along the rift valley. Faults in the northwestern corner of the map strike northwesterly suggestive of a paleo-transform fault (associated with the Hovgård Fracture Zone). Dashed empty boxes mark flank locations near the inner rift valley where fault trends are anomalous to local fault trends

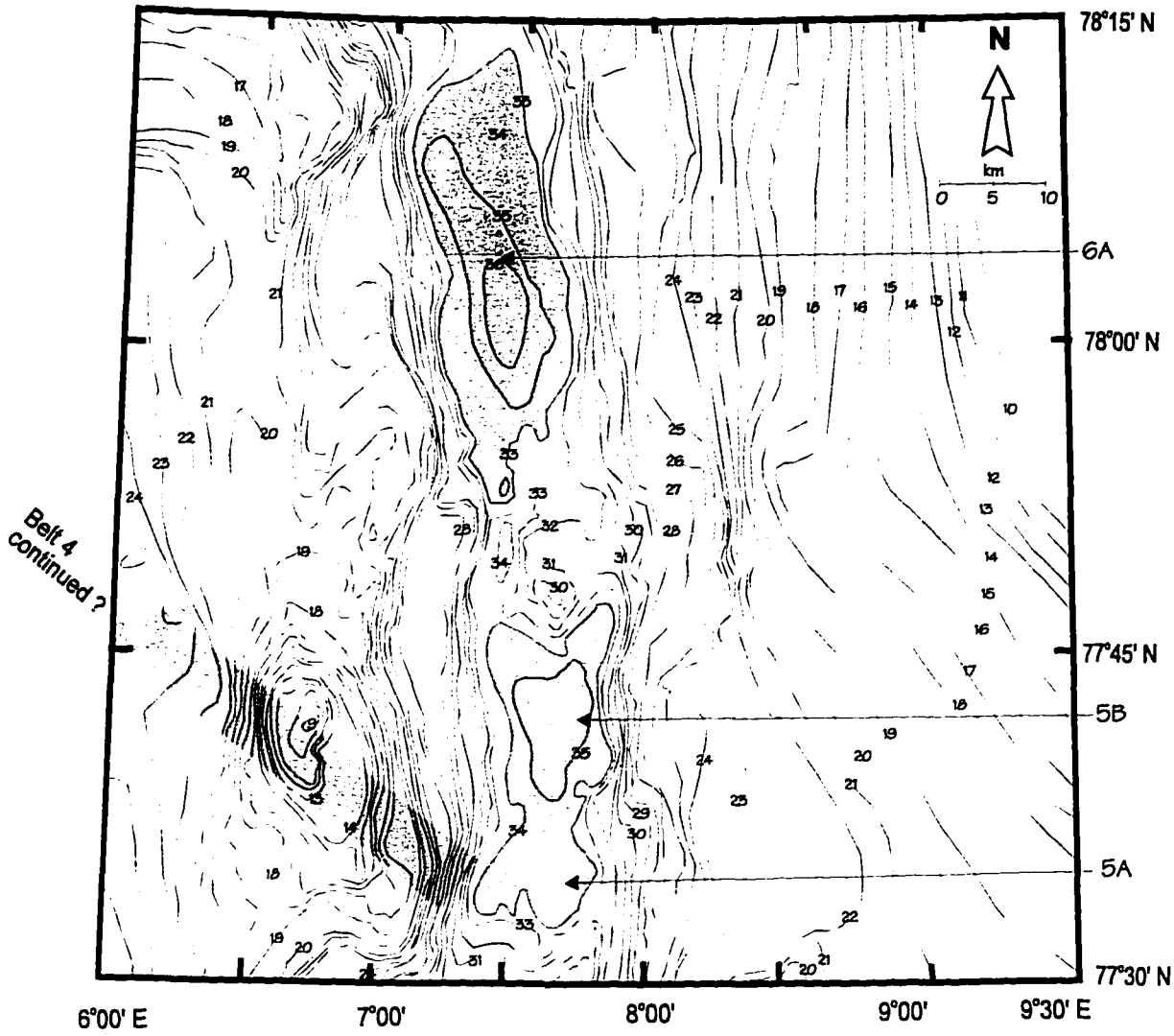

Figure 11C: Bathymetry corresponding to side-scan image in figure 11A. Second order segments 5 and 6 can be seen, as well as third order segment 6A. Note the simple and smooth alignment of contours on the eastern flank, which is attributed to high sedimentation rates.

Figure 12A: SeaMARC II side-scan image of the Knipovich Ridge intersecting the Molloy Transform Fault and the southern part of Vestnesa Plateau (from 78°15'N to 79°00'N).

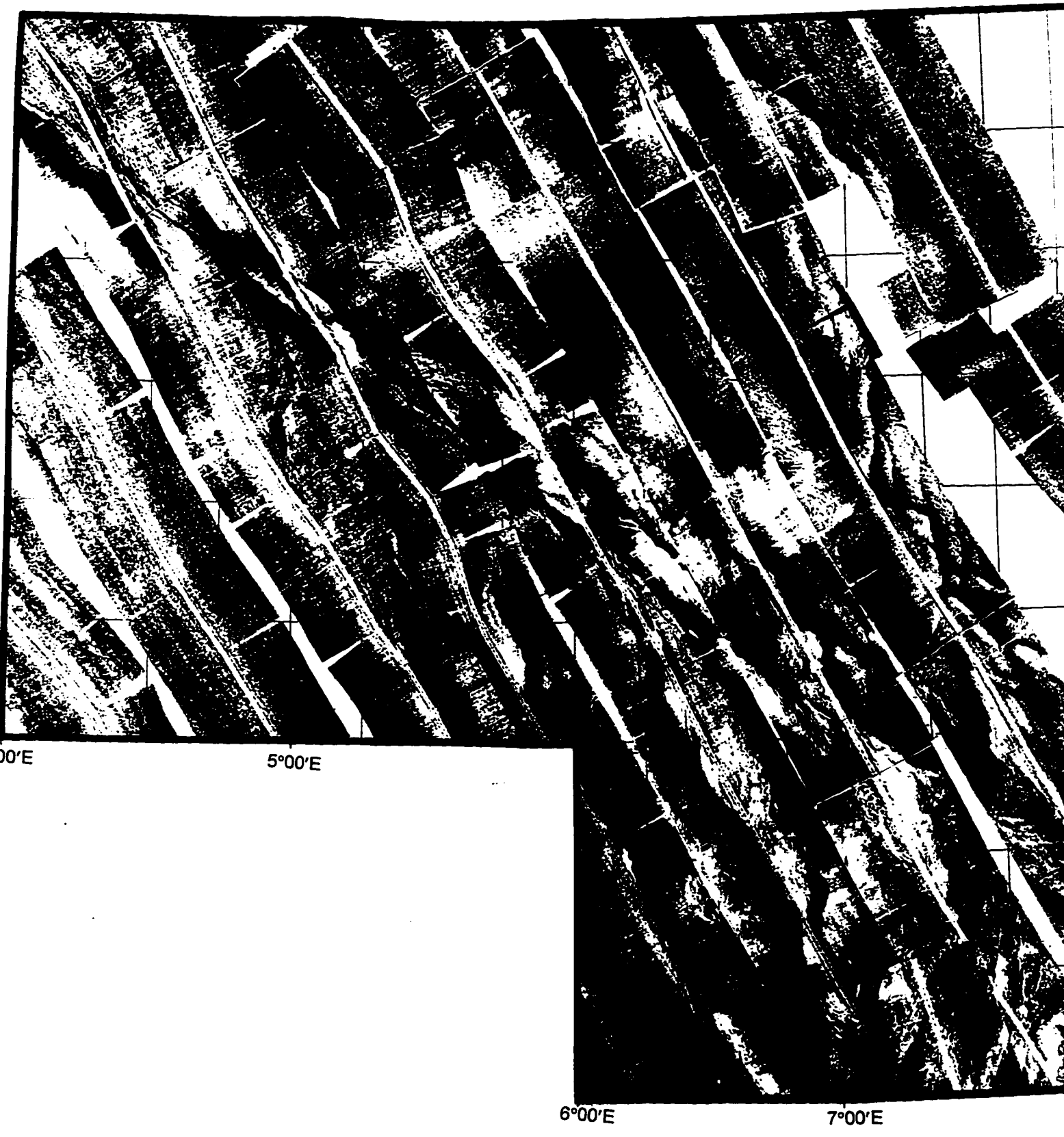

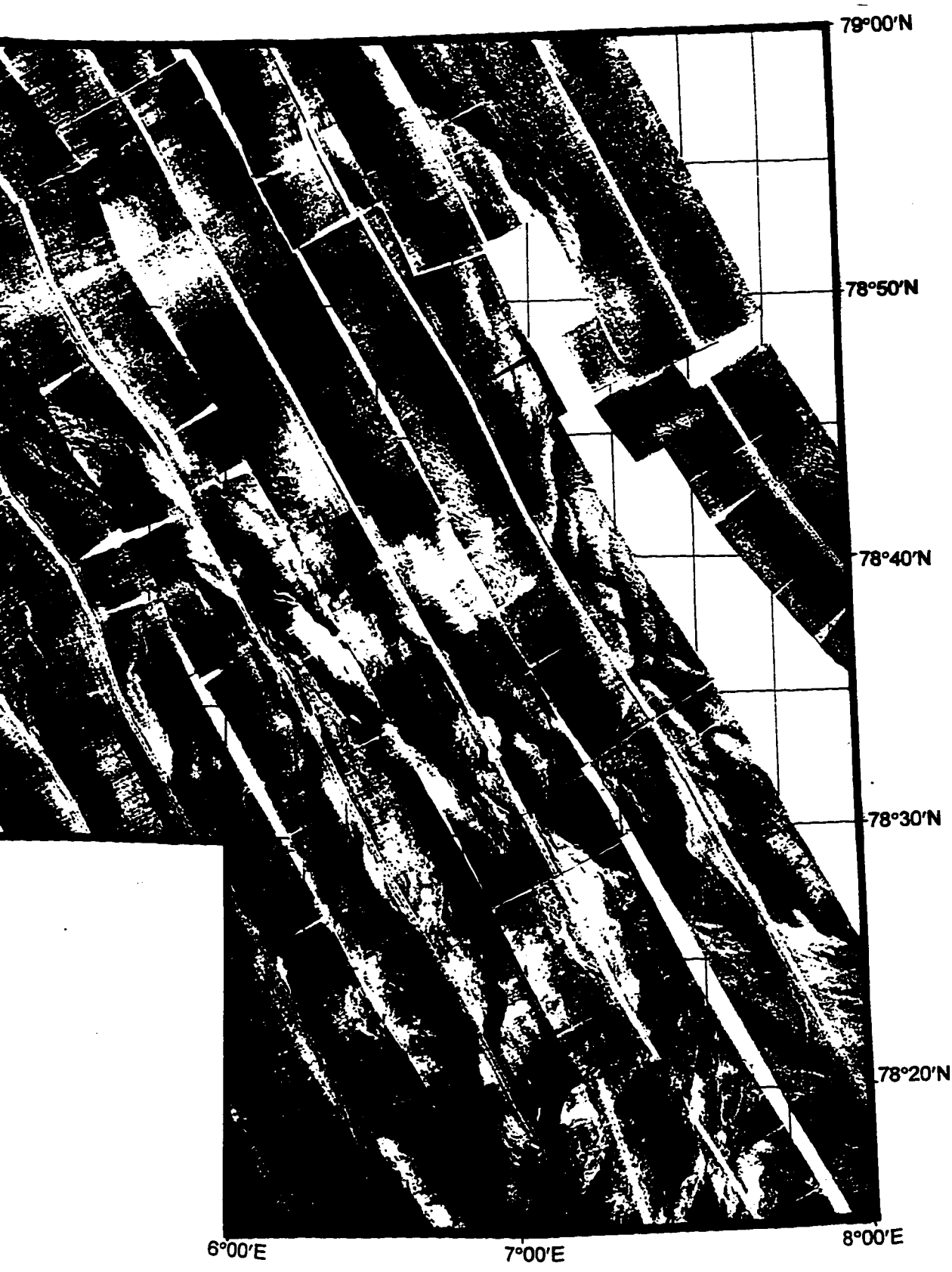

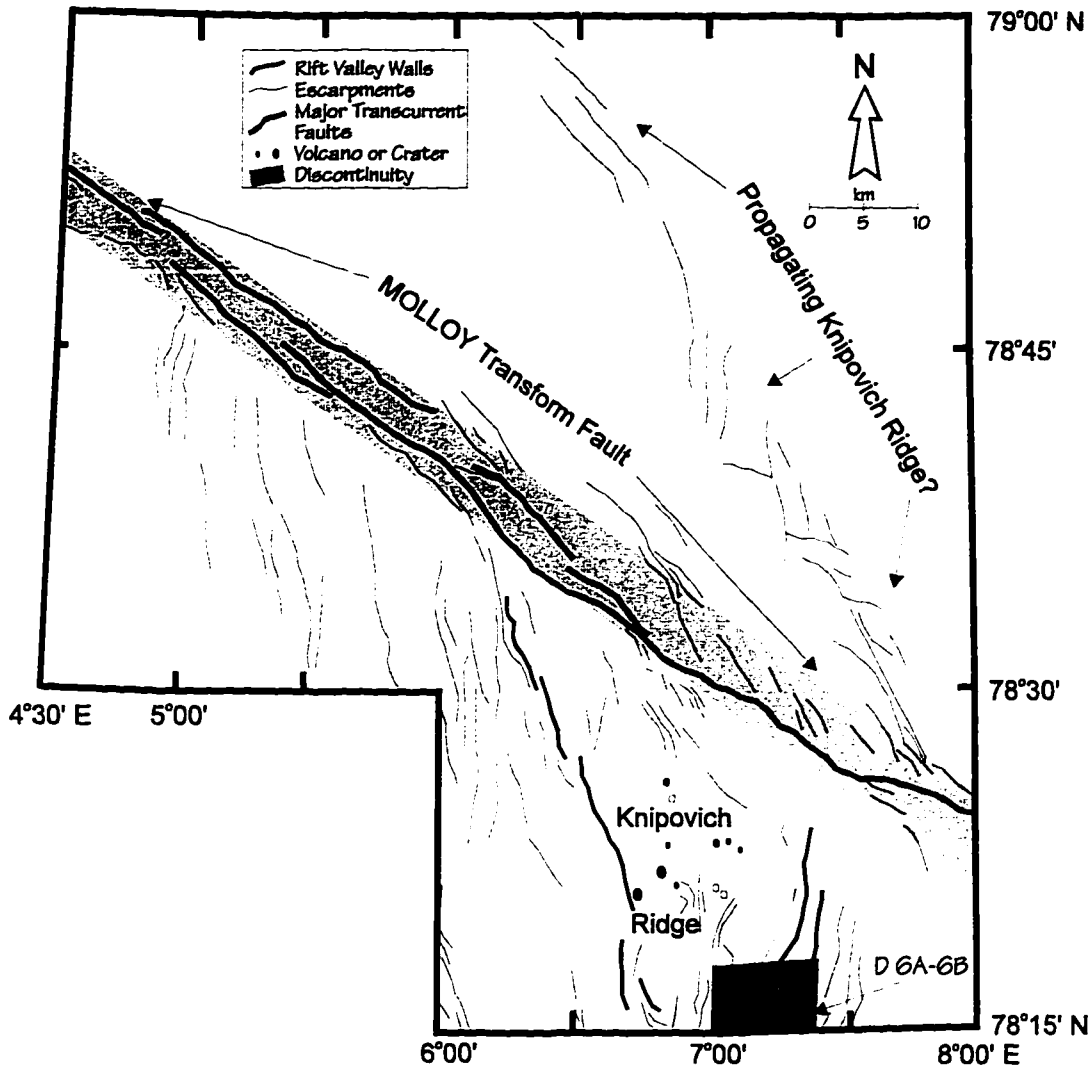

Figure 12B: Structural interpretations of the side-scan image shown in 12A. The Molloy Transform is well defined as a double fault system complicated by smaller anastomosing faults. Note the different trends between faults in the southwest corner of the map (NW due to their connection with the Hovgård Ridge) compared to faults near the Knipovich Ridge (N) and faults at the intersection of the Knipovich Ridge and the Molloy Fracture Zone, which show a change in strike (to NW) along their length. Finally, note the faults to the northeast of the Molloy F.Z. which may indicate recent propagation of the rift valley.

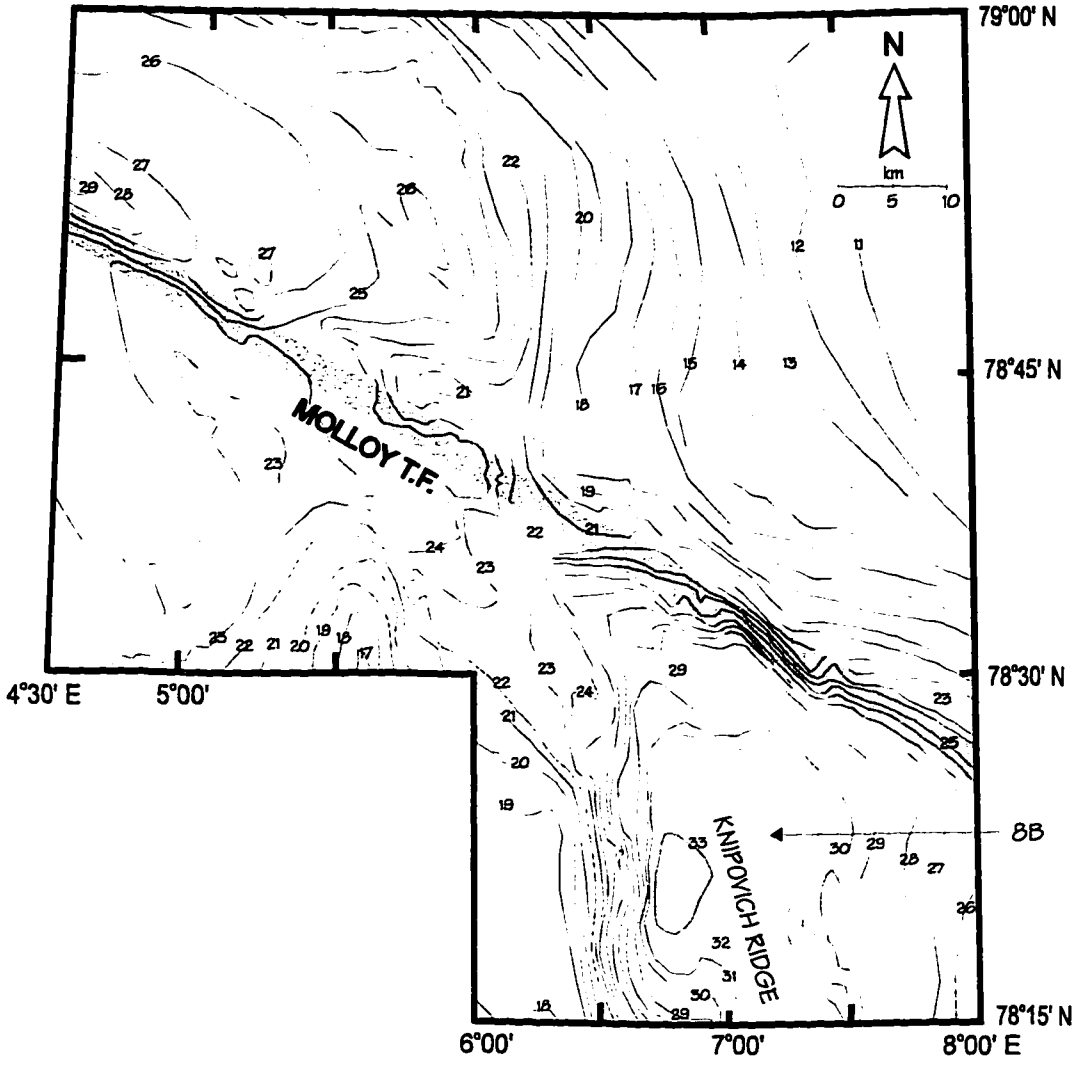

Figure 12C: Bathymetry corresponding to the side-scan image shown in figure 12A.

Figure 13A: SeaMARC II side-scan image of the western flank of the northern Knipovich Ridge near the Hovgård Ridge (from 77°45'N to 78°30'N).

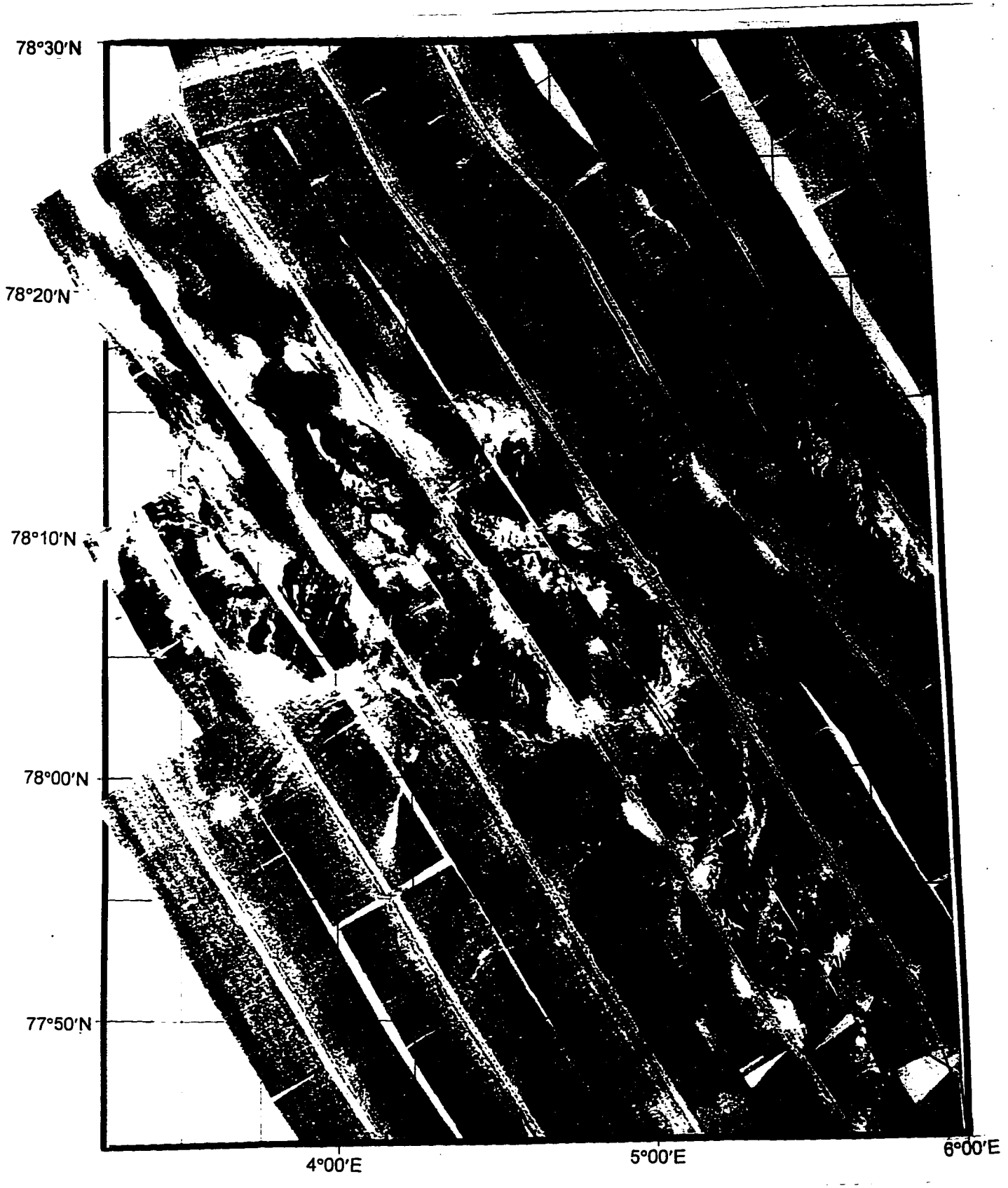

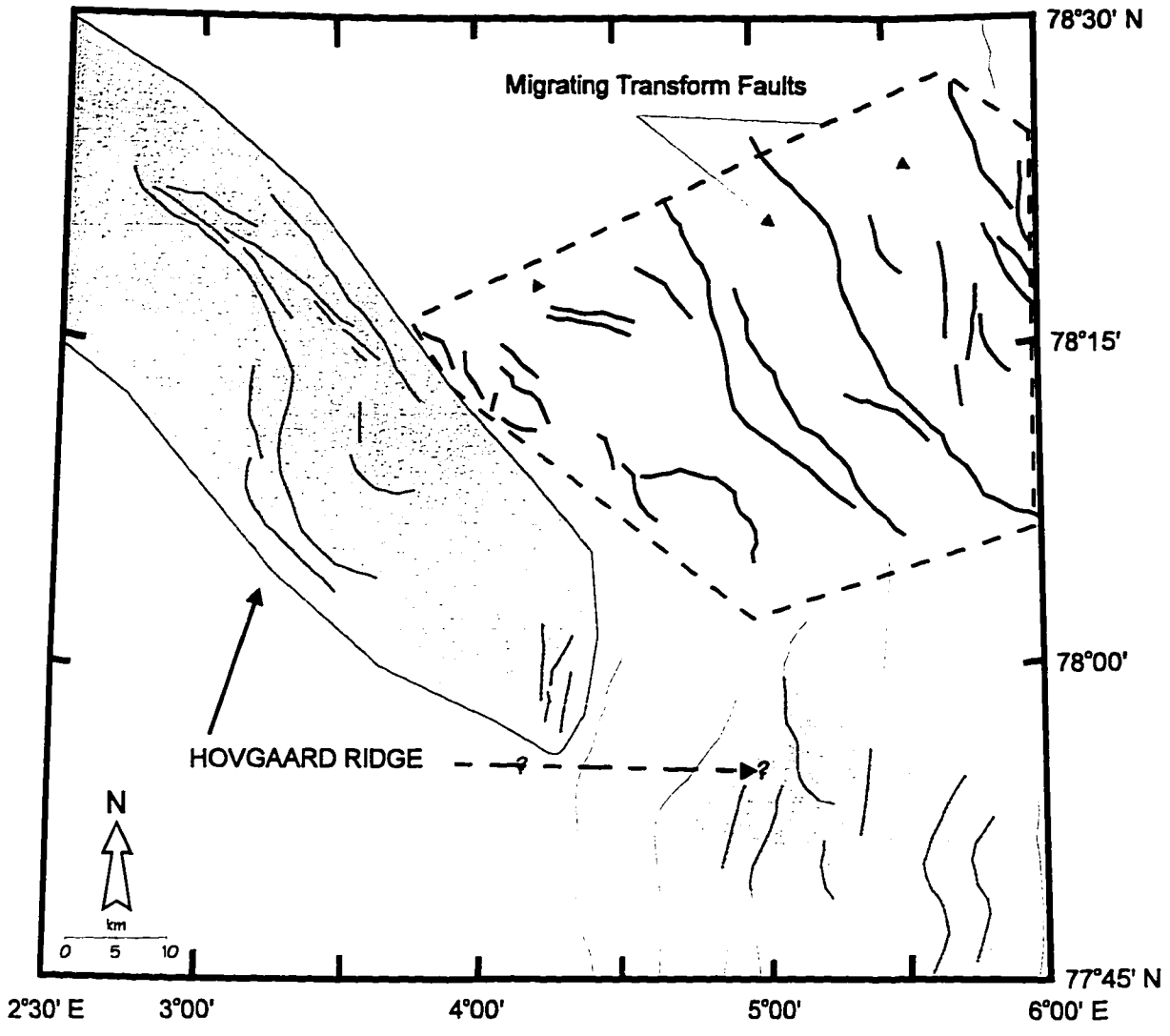

Figure 13B: Structural Interpretations of the side-scan image shown in 13A. Note the northwesterly trend of faults on and northeast of the Hovgård Ridge. The gray shaded area is probably a continuation of the bathymetric Belt 4. The boxed dashed area shows highly anomalous fault trends northeast of the Hovgård Ridge indicative of a paleo-transform fault which was probably deactivated by a propagating Knipovich Ridge.

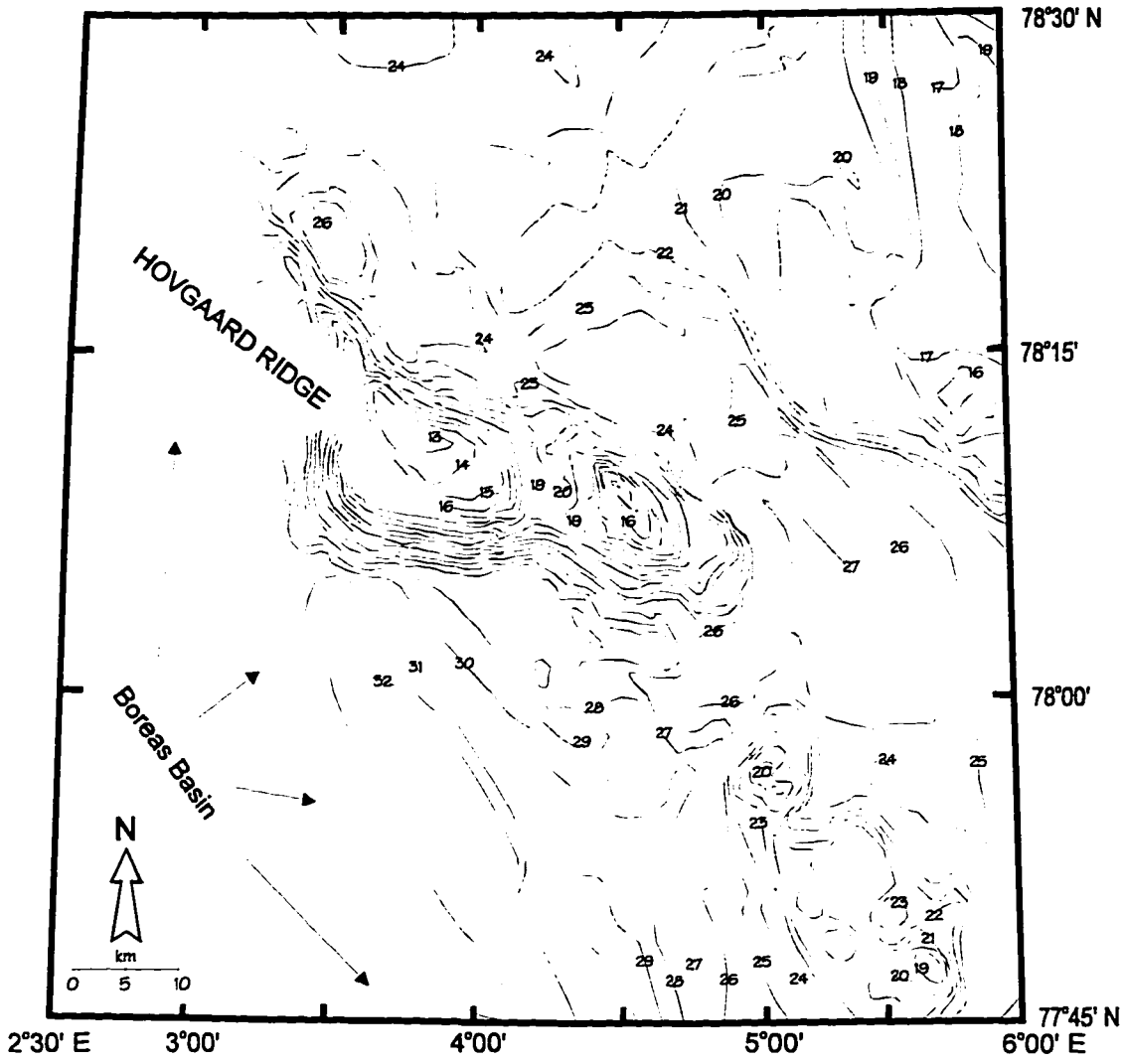

Figure 13C: Bathymetric interpretations of the side-scan image shown in 13A. The Hovgård Ridge and the shallow features to the southeast are easily identifiable.

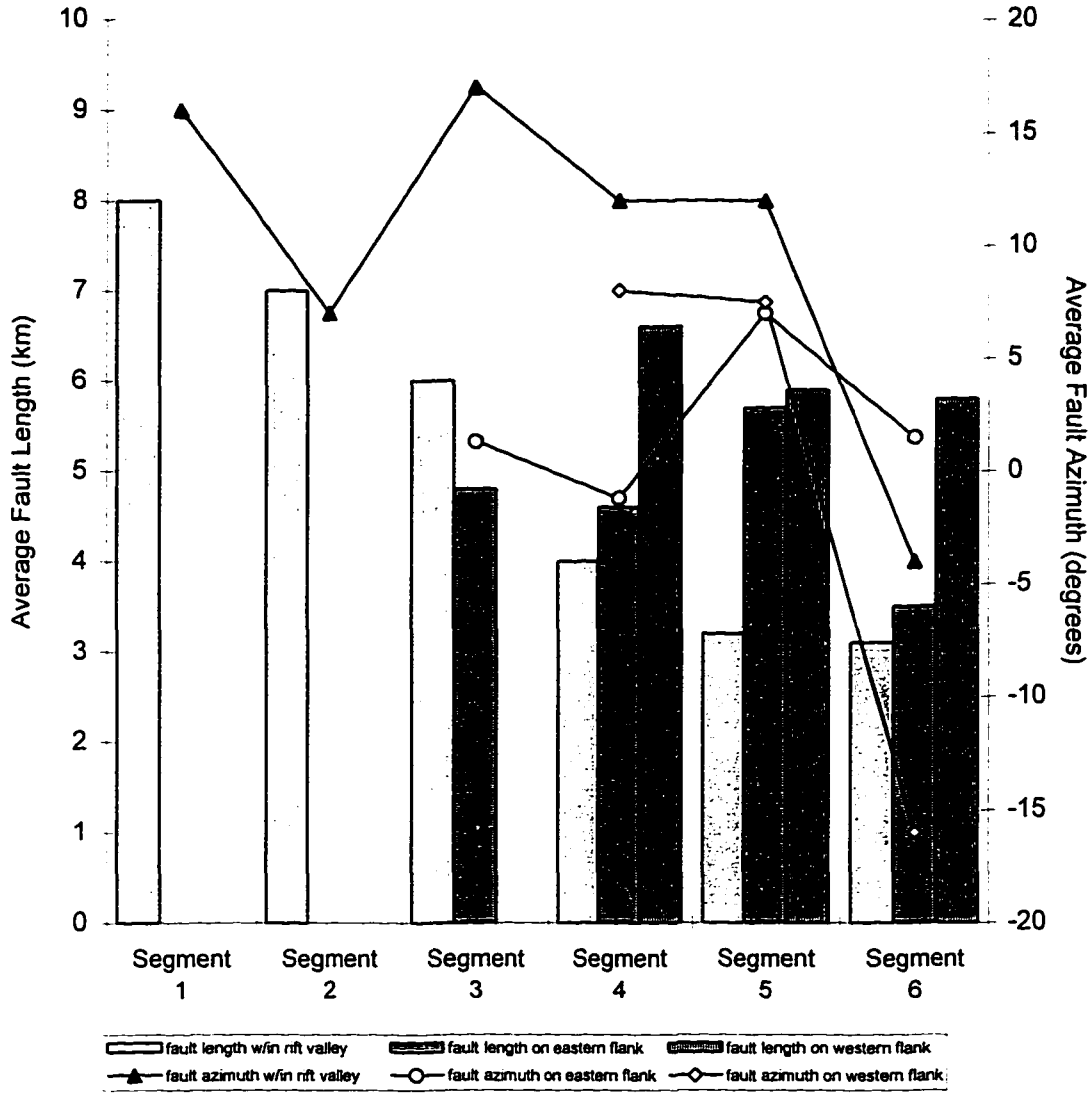

Figure 14A: Average length and azimuth for all second order segments and faults flanking the Knipovich Ridge rift valley. East and west flank information is not available south of segment 3.

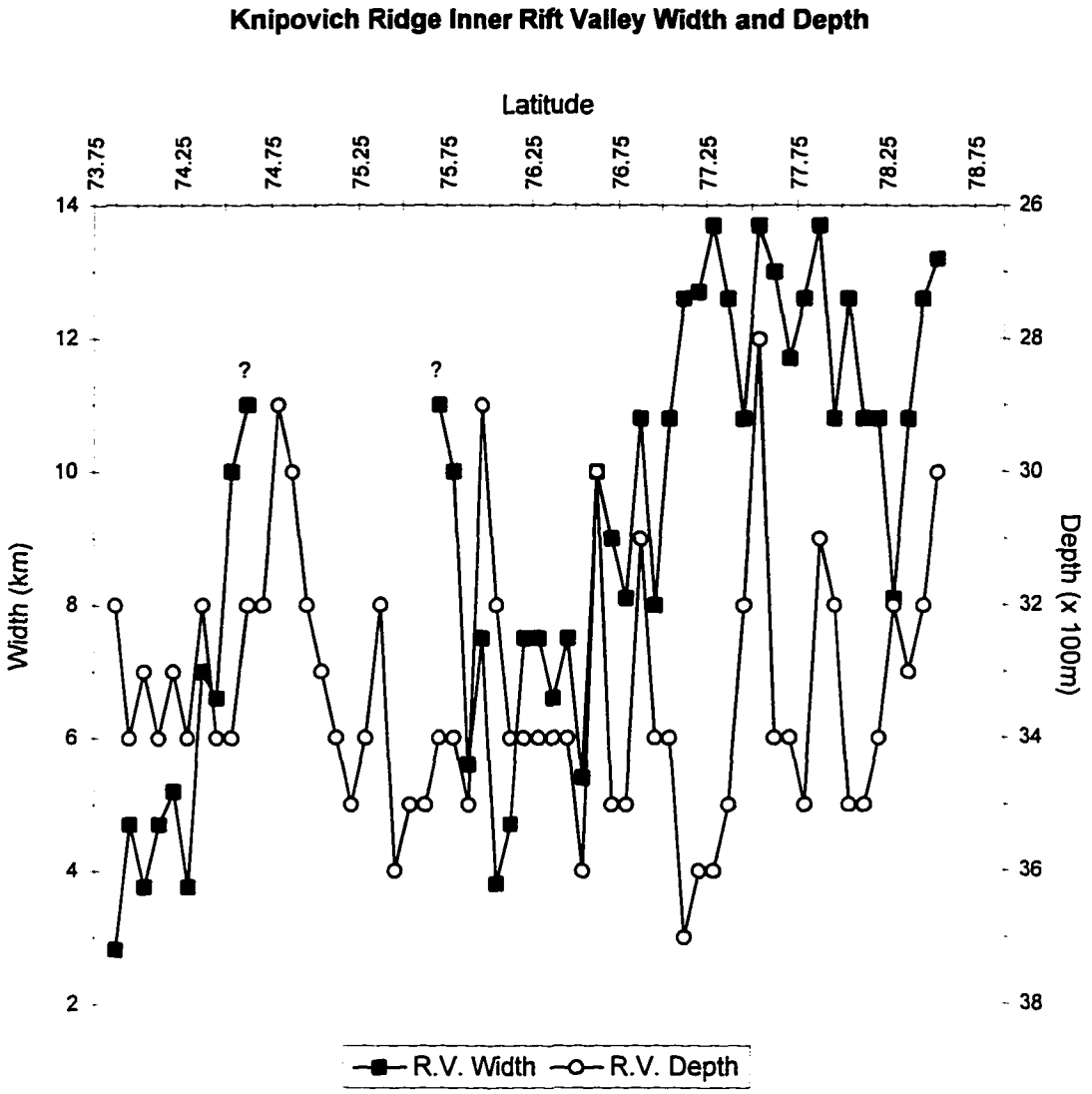

Figure 14B: Comparison of the width vs. depth for the Knipovich Ridge inner rift valley. Where there is no complete SeaMARC II coverage, there is a gap in the graph.

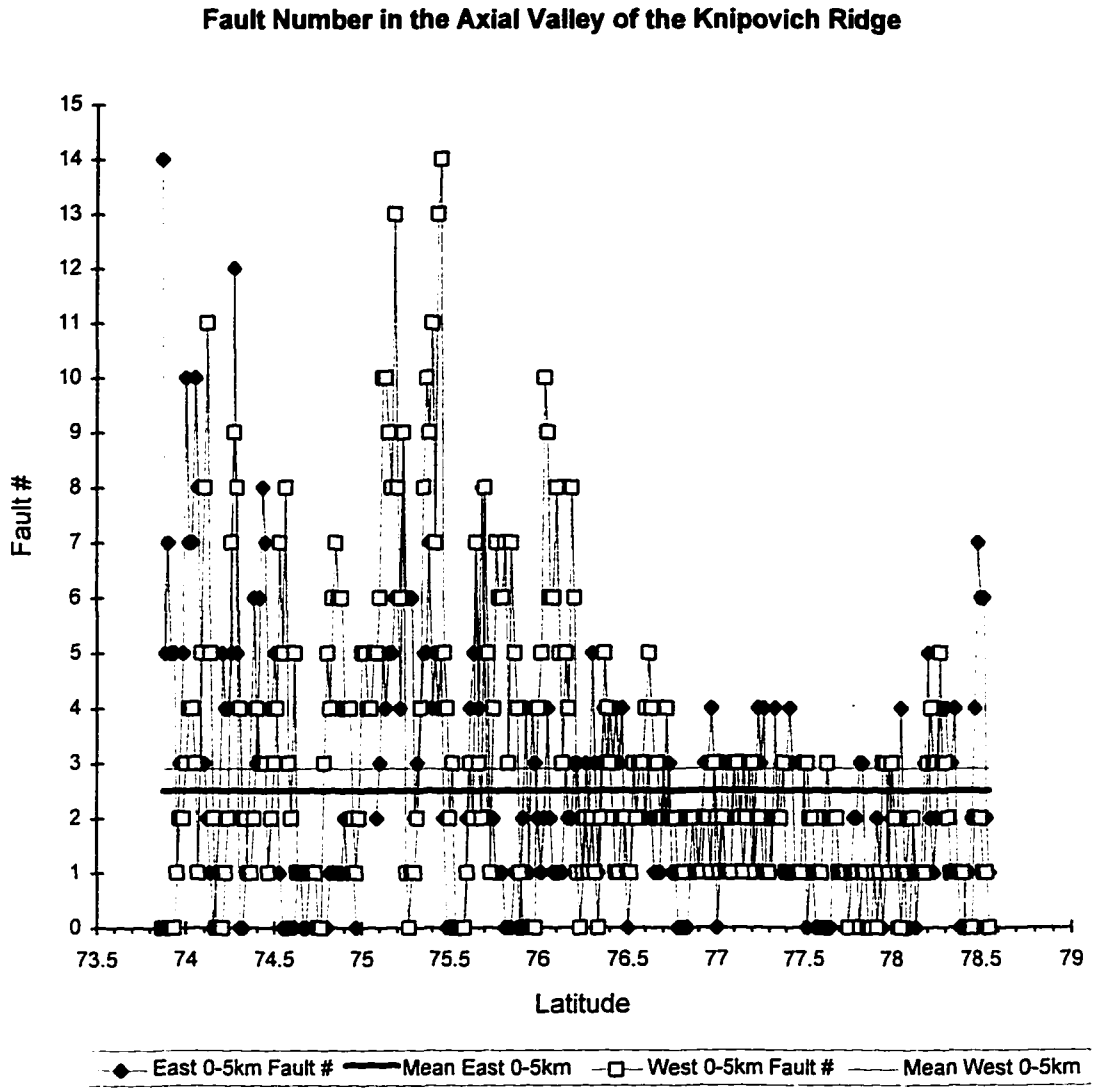

Figure 15A: Fault number variability from south to north within the inner rift valley of the Knipovich Ridge.

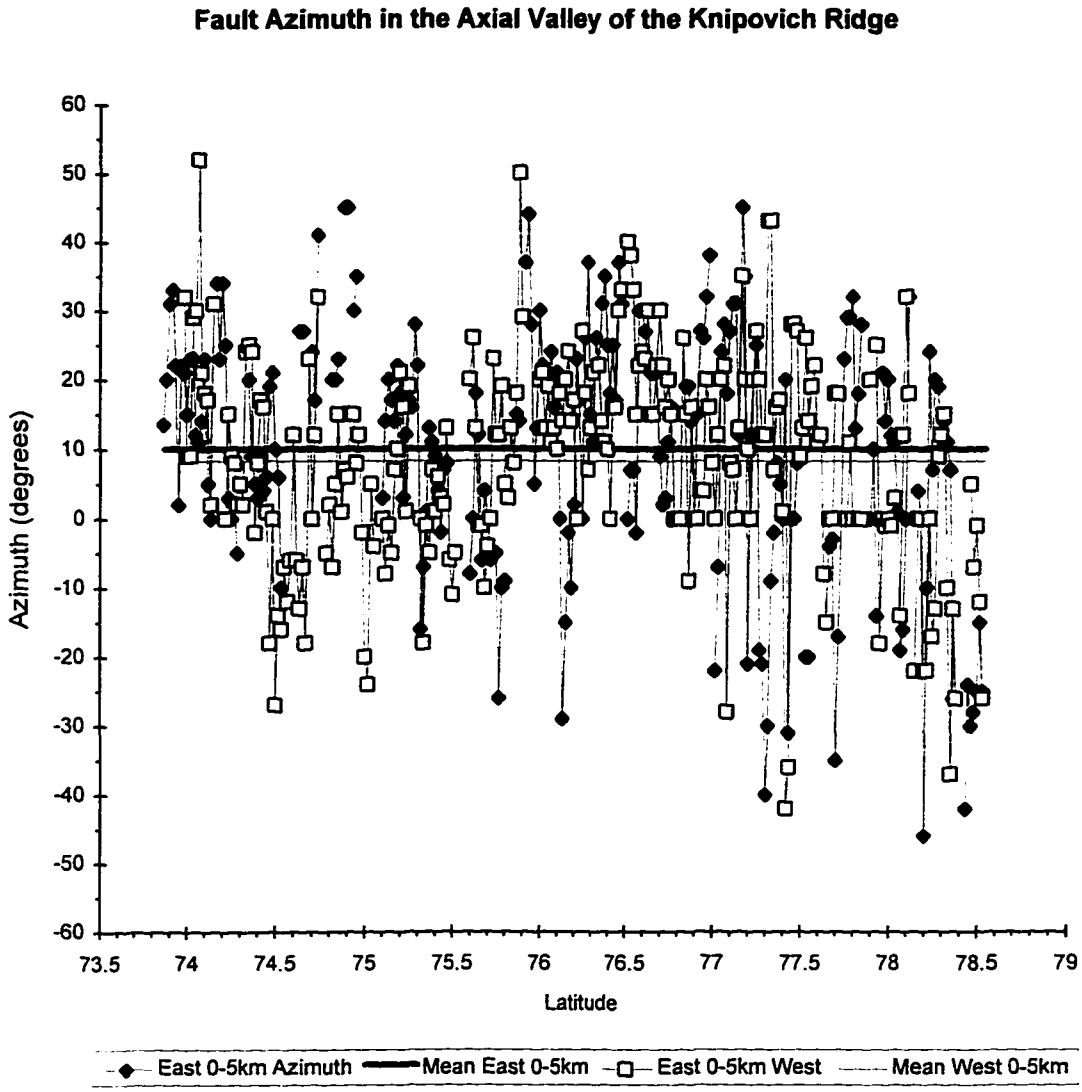

Figure 15B: Fault azimuth variability from south to north within the inner rift valley of the Knipovich Ridge.

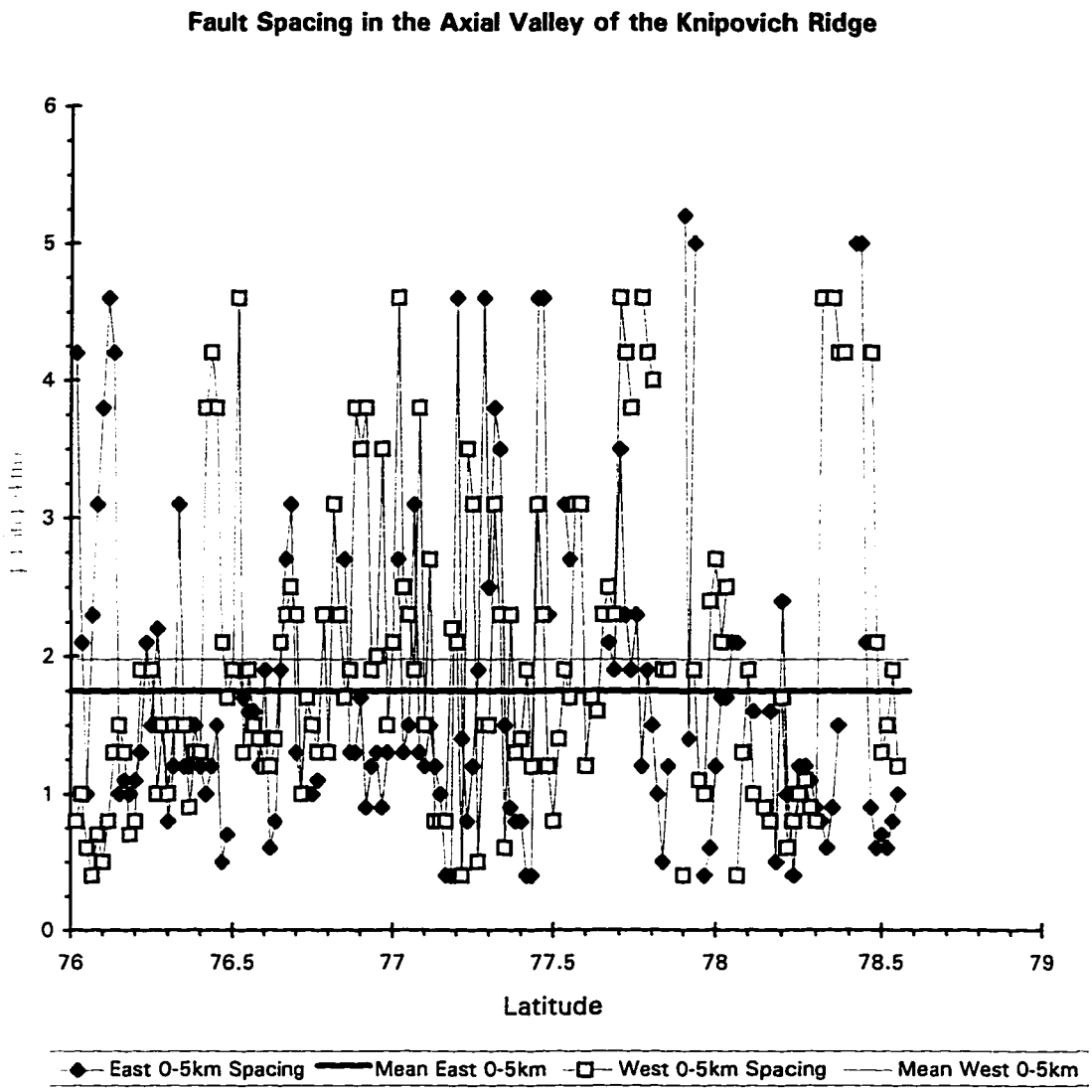

Figure 15C: Fault spacing in the inner rift valley of the Knipovich Ridge. For comparison, typical fault spacing for the Mid-Atlantic Ridge is 2.5-3 km and for the East Pacific Rise (0.5-1 km).

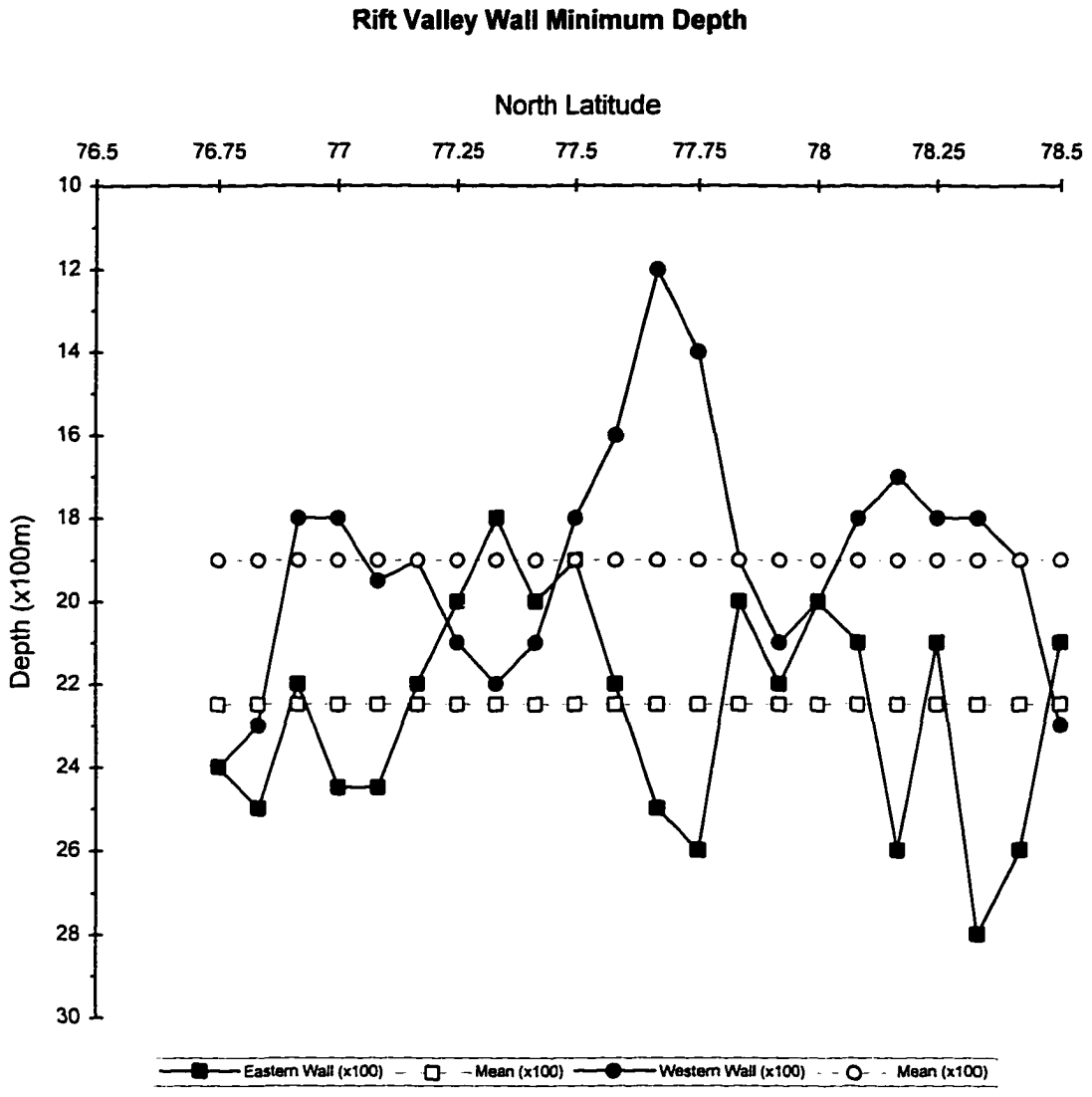

Figure 16: Comparison of minimum depths along the eastern and western flank walls of the Knipovich Ridge. Note that wall depths are anti-correlated across the axis. No data are available south of 76°30'N.

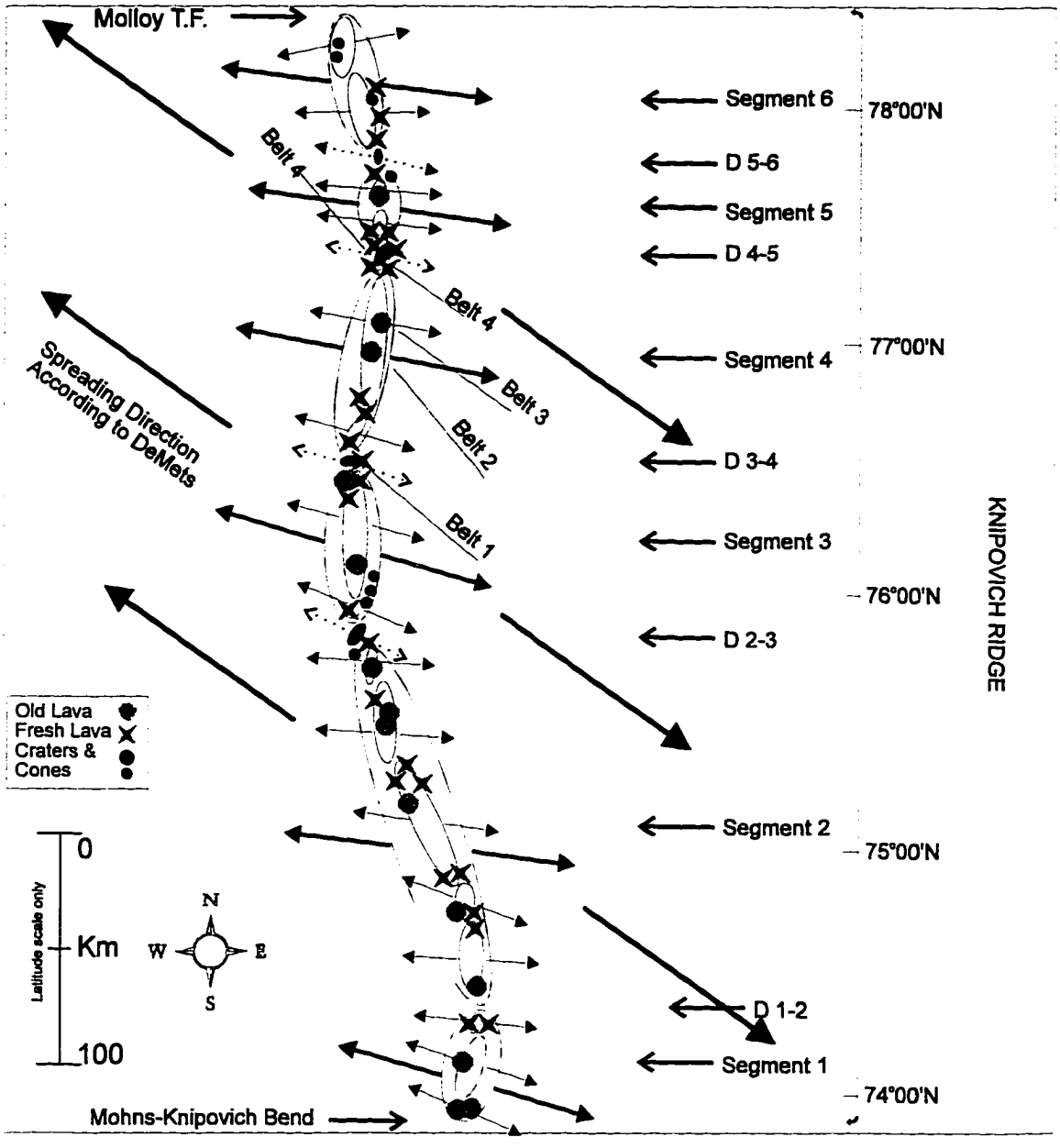

Figure 17: Diagram illustrating the distribution of second and third order segments along the Knipovich Ridge. Along axis segment and discontinuity lengths are to scale while their widths are exaggerated by a factor of three. Bold arrows represent spreading directions inferred from averaging fault azimuths in each second order segment, thin arrows represent inferred spreading directions for third order segments, and dashed arrows represent inferred spreading direction at major volcanic centers associated with a second order discontinuities. The flanks' shallow bathymetry belts are marked. Note that there is ~30°-50° difference between the inferred spreading directions and the trends of these belts. Old and fresh lava flow locations are marked. Fresh lava flows dominate second and third order discontinuities while old lava flows tend to occur at segments centers.

CHAPTER 2

MORPHOLOGY OF THE NORTHEASTERN MOHNS RIDGE: RESULTS FROM SEAMARC II SURVEYS IN THE NORTHEASTERN NORWEGIAN-GREENLAND SEA; PART II: THE ACTIVE PLATE BOUNDARY*

H. Doss[1], K. Crane[1,2,3], P. Vogt[3], and E. Sundvor[4]

(1) Department of Geology and Geography, Hunter College, 695 Park Avenue, NY, NY 10021, USA

(2) Lamont-Doherty Earth Observatory, Palisades, NY 10964, USA

(3) Code 7420, Naval Research Laboratory, Washington, DC 20375, USA

(4) Department of Solid Earth Physics, University of Bergen, Allegaten 41, Bergen, Norway

(*) submitted for publication

Abstract:

In 1989-1990 the SeaMARC II side-scan sonar (11-12 kHz) and swath-bathymetric system imaged more than 80,000 km^2 of the seafloor in the Norwegian-Greenland Sea and southern Arctic Ocean. The data collected encompasses the continental margins along northwestern Norway and western Svalbard, the mid-ocean ridge rift valley along a 150 km long section of the northeastern Mohns Ridge and the entire Knipovich Ridge, the eastern and western flanks of the Knipovich Ridge, the Molloy Transform Fault, the Molloy Deep, and the Molloy Ridge.

Along the relatively young Mohns Ridge, we observe a highly segmented but probably untransformed ridge system that can be divided primarily into basinal segments bounded by rift valley volcanoes. These segments are structurally as well as bathymetrically defined. and are generally aligned en-echelon to each other. Volcanic boundaries are interpreted as sites of recent to present volcanic activity. Notably absent is a well developed neovolcanic system normally associated with other slow-spreading centers such as the Reykjanes ridge and other parts of the Mid-Atlantic Ridge. Instead, the Mohns Ridge is dominated by deep en-echelon fault bounded troughs.

The northwestern flank of the Mohns Ridge is marked by shallow linear ridges. The orientation and geographic position of these ridges suggest that they were formed at the Mohns Ridge and are only slightly deformed, probably by deviatoric stress fields created at the highly oblique Mohns Ridge-Knipovich Ridge bend. Since no transform fault exists between the two ridges and due to the lack of extensive deformation along these off-axial ridges, the Knipovich Ridge must be obliquely spreading to the NW-SE.

Introduction:

The plate boundary in the Norwegian-Greenland Sea reflects a complex rifting and spreading history in this area (figure 1). Seafloor spreading in the Norwegian-Greenland Sea and the Arctic Ocean started at approximately anomaly 24 (approximately 58-57 ma. on the LaBrecque et al., (1977) time scale) (Vogt, 1974; and Talwani et al., 1977). In addition, relative motion between Svalbard and Greenland was oriented northeast to southwest from the Mohns Ridge with no apparent crustal extension to the north. The plate boundary between the incipient Norwegian-Greenland Sea and the Arctic Ocean was instead along the broad regional continental Spitsbergen Shear Zone (also called the de Geer Zone) (Johnson, 1967; Harland, 1969; Horsfield et al., 1970; Eldholm et al., 1978; Talwani, 1977; Eldholm, 1980; Vogt et al., 1981; Dore et al., 1987; Crane et al., 1988)

The area discussed in this manuscript is the northeastern section of the Mohns Ridge (figure 1). A portion of the mid-ocean ridge system that is centrally located in the Norwegian-Greenland Sea between the island of Jan Mayen and approximately 73°30'N (figure 1). The ridge is 575 km long and bounded to the south by the Jan Mayen Fracture Zone and to the north by the Knipovich Ridge (Perry, 1985). The Mohns Ridge is probably the most stable ridge along the mid-ocean ridge north of Iceland and is characterized by an axial rift valley with depth generally between 2.8 and 3.2 km increasing to the northeast (Eldholm et al., 1986). Spreading appears to have initiated from as early as anomaly 24/25 (54-56 MA) (Talwani et al., 1977). Bathymetric and magnetic data led Vogt (1986) to suggest that the Mohns Ridge is continuous along its

entire length. However, the rift valley is thought to consist of short and interconnected spreading axes with varying degrees of obliquity. The flanks of the Mohns Ridge are bathymetrically asymmetric due to the encroachment of the Bear Island Fan on the southeastern flank (Vogt, 1986).

Seismically, the Mohns Ridge is active along its entire axis. Earthquakes are concentrated in the rift valley compared to its northern neighbor; the Knipovich Ridge where seismicity is not prevalent along the rift valley and instead is spread out over 100's of km to the east of the ridge. Vogt (1986) related the high seismicity along the Mohns Ridge to faulting that causes generally higher than expected topography along the entire ridge. Based on earthquake epicenter data by Nishenko (1986), Vogt (1986) suggested that the northeastern Mohns Ridge is divided into en-echelon and slightly overlapping segments.

From an analyses of well developed magnetic anomalies across the Mohns Ridge (figure 3), Talwani and Eldholm, (1977) calculated a half-spreading rate of 0.45 cm/yr. for this plate boundary. However, the magnetic field is generally quiet over most of the entire Boreas Basin adjacent to the Knipovich Ridge (Sundvor and Eldholm, 1979) making it difficult to determine spreading rates from the magnetic anomaly time scale. Vogt et al., (1982) and Vogt (1986) have proposed tentative anomalies 5 and 6 in the southern Boreas Basin on the western flanks of the Knipovich Ridge and near the Mohns Ridge. Magnetic anomalies are chaotic in the northern Norwegian-Greenland Sea compared with more normal anomalies along the northeastern section of the Mohns Ridge where the rift valley is characterized by a positive anomaly of 200-1300 nT (figure 4; after Kovacks et al., 1987).

In contrast to the Knipovich Ridge, the northeastern Mohns Ridge rift valley lacks a well defined belt of gravity minima surrounded by flanks with gravity maxima. As figure 4 indicates, the NE Mohns Ridge is almost unidentifiable gravimetrically except for a well developed circular feature with a gravity low of 10 mGals. According to Vogt (1986), the average gravity anomaly was found to be 0-10 mGals higher on the northwestern flank than on the southeastern flank (for crust younger than 10 MA). Furthermore, crestal mountains and older basement topography as well as the associated gravity anomalies appear to be asymmetrically higher on the western flanks of the Mohns Ridge (Vogt et al., 1982). The Greenland Fracture Zone (also on the northwestern flank of the Mohns Ridge, figure 1) is demarcated by a prominent ridge where an elongated gravity high reaching 117 mGals is found. Immediately to the southwest of the Greenland Fracture Zone, a sediment-filled trough is characterized by a -16 mGal gravity low (figure 3).

During the falls of 1989 and 1990, mapping expeditions were carried out along the Mohns and Knipovich Ridges, northern Svalbard-Nordaustlandet margin, and along the southeastern tip of the Greenland Fracture Zone. The goals were to resolve the fine scale structures and morphology of the plate boundary and to investigate the sedimentary environments along the Barents Sea- Svalbard escarpments. Data from these surveys are used to constrain the models for the evolution of the region.

Instrumentation:

The primary tool used for these surveys was the SeaMARC II which was outfitted on the Norwegian research ship "R/V Haakon Mosby". The SeaMARC II is a shallow tow, long

range, high resolution seafloor mapping system with the capability of simultaneous recording of digital side-scan sonar images as well as bathymetry across a swath of ensonified seafloor. Bathymetry is determined by measuring phase differences of acoustic arrivals on a pair of transducer arrays on each side of the tow vehicle. For deep ocean surveys, it is towed at a depth of approximately 100 m below the surface which allows it to avoid the high sound velocity gradients near sea surface (Shor, 1990). The system operates at 11 kHz on the port side and 12 kHz on the starboard side. A drogue is attached to the slightly positively buoyant sonar vehicle provides stability of about 1° in roll and 2-3° for pitch and yaw.

During our 1989 survey, speed was mostly in the 7-10 knots range when we were surveying in the vicinity of the Mohns Ridge. In contrast, the 1990 survey encountered very rough weather (high sea-state) and system problems occurred. There were several days when speed averaged less than 1 knot, and the fish had to be recovered for repair.

For seafloor depths greater than 1.0 km, the side-scan sonar subsystem is configured to produce a swath of data 10 km wide. Bathymetric data are recorded from nadir to a maximum angle of 60° (a maximum bathymetric swath equal to 3.4 times water depth). The bathymetric swath width is independent of the side-scan swath setting.

The SeaMARC II side-scan images contain 1024 pixels of digital data on either side of the swath with the inner 40 pixels not logged. The individually logged reflectivity values are equally spaced horizontally across the track (assuming a depth of the first arrival). Pixel spacing was 5 m for the 10 km swath width configured for this survey. Along-track

resolution is a function of the beam width of the system, which is nominally 2° (about 3% of slant range) and therefore widens towards the outer edge of the swath. Side-scan data are slant-range corrected to water depth below the vehicle at the time of collection.

Recognition of seafloor patterns is a function of the type of feature causing the echo. Linear to semi-linear features (such as faults) are recognized if they have dimensions of only a few to several tens of meters. Since fault escarpments are much easier to identify if they are young, not yet degraded, and offset a uniformly sedimented seafloor, areas of thin, disturbed, or non-existent sediment are more likely not to show faults. Within the survey area, this does not appear to be a problem for detecting faults since sediment thickness varies from as little as 100 m to a few hundred meters (Vogt, 1986) and faults are present through most of the tracks. In other words, within the survey area fault detection is not a problem near the rift valley. As sediment thickens increases on either of the rift valley, only faults with the largest offset (hundreds of meters) will be recognized on the sonar imagery. This possibly contributes to lower fault distribution statistics towards the outer sections of the survey. In contrast, three dimensional features (such as sediment waves) must have dimensions on the order of a few hundred meters to display a recognizable shape.

Additionally, the ship was outfitted with a gravimeter, magnetometer, and a 3.5 kHz plus 38 kHz echo-sounders. The gravimeter measured the total gravity field below the ship while the magnetometer measured the total magnetic field below the ship. Sea-floor topography profiles were obtained using the echo-sounders. Unfortunately, the data quality from these instruments was poor during high sea states and therefore will not be

used in this paper.

The area covered by the SeaMARC II survey over or near the Mohns Ridge (figure 5) encompasses 230 km along the northeastern Mohns Ridge (from 72°30'N to 73°50'N) extending beyond the transition to the Knipovich Ridge, the eastern flank extending to the Bear Island Fan, and one track near the bend between the two spreading ridges and westwards along the Greenland Fracture Zone. Bathymetric contours at 100 m intervals were traced (by hand) from the SeaMARC II bathymetry images and then digitized using ARC/INFO software to insure accurate positioning and further subdivision of data into different maps. Where there was a gap in the data, some interpolation was required in between closely spaced tracks. Interpolations were limited to gaps between swaths inside the total area mapped by this cruise.

Nature of Segmentation:

Macdonald et al. (1991) suggest that segmentation for slow spreading centers can be broken into four orders: Order 1 has a segment length of as much as 400 km and is bounded by a transform fault or rift valley propagator tip. Order 2 has a segment length of 50 km (+/- 30 km) and is bounded by oblique shear zones or rift valley jogs. Order 3 has a segment length of 15 km (+/- 10 km) and is bounded by inter-volcanic lows. Finally, order 4, with a segment length of 7 km (+/- 5 km), is bounded by intra-volcanic lows.

The nature of segmentation of nascent mid-ocean ridges has been studied along the rifted margins of the central Red Sea (Bonatti, 1985; Crane et al, 1987). From these observations, Bonatti (1985) suggested that segmentation of incipient mid-ocean ridges is

determined by the spacing between "punctiform" nucleation points where basinal segments form above upwelling asthenosphere. On well developed mid-ocean ridges, axial segmentation has been attributed to a similar Rayleigh-Taylor type of gravitational instability in a partially molten mantle beneath spreading centers creating volcanic domes on the rise axis (Crane, 1985; and Schouten et al., 1985). In these two gravitational instability models, first and second order segments are thought to mark the locus of rising and melting mantle diapirs. However in the nascent spreading center case, eruption of harmonically spaced magmatic centers creates crust more dense than its surrounding (Crane, 1985), thus creating volcanic basins; the bathymetric inverse to the harmonically spaced volcanic domes located on a well developed mid-ocean ridge.

Along the Mohns Ridge, this paper will attempt to show that the above models are generally adequate to describe its segmentation. However, the distribution of axial depth maxima and minima (figure 14) suggests that harmonically spaced magmatic centers are not as obvious on the Mohns Ridge (partially the result of only 240 km with the SeaMARC II vehicle) as proposed by Crane (1985) and Schouten (1985) for other midocean ridges. Furthermore, the ridge is dominated by basins (figure 14) rather than rift valley volcanic highs as described by Macdonald (1991).

In this paper, the rift valley is divided into basins bounded by axial depth minima of dominantly volcanic nature. Segments are described from one crest to the next. Axial depth variation between successive crests of more than 500 m are considered as second order discontinuities while those of 200 m or less are considered third order discontinuities.

Detailed Along Axis Segmentation:

In the following descriptions of the Mohns Ridge segmentation, we will use a starting point of latitude 72°32'N and longitude 3°10'E (kilometer 1). From southwest to northeast, the Mohns Ridge is segmented as follows:

1. Order 2: 72°32'N to 72°46'N (1-40 km along SeaMARC II tracks)

This >40 km long segment (figure 6) is bounded to the north by a volcanic axial depth minimum of 1,900 m and an unknown minimum to the south (not imaged by SeaMARC II). The segment is on average 6 km wide, greater than 3,400 m in depth, and is oriented 055°. Fault azimuths within the segment trend from 079° to 012° (figure 16) and average 040°. Lava flows are observed towards the southern part of the segment as well as its northern discontinuity.

The northern volcanic discontinuity (figures 6 and 13) has an average width of 9 km at the 2,600 m contour interval, a length of 20 km (encompassing two segments) and trends 025°, (obliquely oriented to the rift valley axis (055°). Faults cut its eastern margin in close proximity to the rift valley walls while strong backscatter on its northern and western flanks point to recent lava flows in very close proximity to the volcano's crater. Faults on the northwestern flank are on average 3-8 km in contrast to the southeastern flank where fault length ranges from 0.5-3 km. This volcanic discontinuity is also characterized by a "relatively well defined magnetic anomaly" (> 500 nT compared to local magnetic signature) (Vogt, 1986).

Segment 1 is further subdivided into three smaller subsegments; 1A, 1B and 1C.

1A. Order 3: (1-8 km along SeaMARC II tracks)

Segment 1A (figure 6) is 8 km long and is defined by an axial depth minima of 3,000 m to the north and an unknown depth minimum to the south (not imaged by SeaMARC II). This segment is on average 6.0 km wide and is oriented 054° while faults within the segment trend on average 046°. Fault density across the rift valley is 3.1 faults/km to the east and 1.2 faults/km to the west of the axis while fault lengths average 1.4 km for the majority of faults. At the inner rift valley walls, fault lengths increase to 3.2 km. A large lava flow (17 km^2) covers the southernmost section of this segment.

1B. Order 3 (9-19 km along SeaMARC II tracks)

The third order segment 1B (figure 6) is 11 km long and is defined by axial depth minima of 3,000 m at its southern boundary and 2,900 m at its northern boundary. This segment is on average 7.0 km wide and is oriented 052° while faults within the segment trend on average 037°. Fault density across the rift valley is 1.6 fault/km to the east and 0.9 fault/km to the west of the axis. Fault lengths in the valley of this segment average 1.8 km and increase to 2.5 km except for near the base of the inner rift walls.

1C. Order 3 (20-40 km along SeaMARC II tracks)

Segment 1C (figure 6) is defined by axial depth minima of 2,900 m at its southern boundary and 1,900 m at its northern boundary. It is 21 km long, has an average width of 7.3 km, and an orientation of 055°. By comparison, faults within this segment trend on

average 040°. Fault density in this segment averages 1.6 faults/km to the east and 1.1 fault/km to the west of the axis. Fault length for most faults averages 1.9 km within the rift valley and increase in length to 4.5 km near the base of the inner rift walls. The segment's northern boundary is cut by two short faults (< 1.0 km) and is marked by very low backscatter on the SeaMARC II imagery. In contrast, between kilometers 36 and 39 (figure 7), a large lava flow covers the eastern side of the rift valley extending to the northwest.

2. Order 2: 72°46'N to 73°04'N (41-101 km along SeaMARC II tracks)

Segment 2 (figures 6 and 7) is bounded to the south and north by two axial depth minima; 1,900 m and 2,800 m, respectively (figure 14). This segment is on average 11 km wide, 61 km long, deeper than 3,500 m, and trends 047°. Fault azimuths range from 019° to 068 ° (figure 16) and average 044° to the east and 041° to the west.

The segment's volcanic northern boundary (figures 6 and 13) is defined by the 2,900 m contour and shoals to less than 2,800 m. It is 2 km wide, 6 km long and is oriented 030°; en-echelon to the segments that it separates. Lava flows completely dominate the rift valley north of this volcano (figure 15). The only faults observed lie on the northwestern side of the volcano along the base of the inner wall. These faults are oriented 030-040° (figure 16) parallel to the trend of the axial volcano.

Segment 2 is further subdivided into three subsegments; 2A, 2B, and 2C.

2A Order 3 (41-71 km along SeaMARC II tracks)

Segment 2A (figure 6) is an elongate basin that is 31 km long. It has a maximum depth greater than 3,500 m, an average width of 9.8 km and a trend of 045°. Faults within the basin trend 041°. The segment's southern and northern boundaries are characterized by axial depth minima of 1,900 m and 3,200 m; respectively (figure 14). Fault density averages 1.0 fault/km to the east and 0.53 fault/km to the west of the axis (figure 17). Most faults are located near the central part of the basin and are nearly absent near the northern boundary (figure 15). On the western part of the basin, a large (~ 15 km^2) lava flow is observed.

2B. Order 3 (72-85 km along the SeaMARC II tracks)

The segment 2B (figures 6 and 8) is defined by axial depth minima of 3,200 m on its southern and northern boundaries (figure 14). It has an average width of 6.2 km, a length of 14 km, and trends 037° (in contrast to average fault azimuths of 043°). Fault density is 1.1 faults/km to the east and 1.3 faults/km to the west of the axis (figure 17) while fault length averages 0.7 km. Near the segment's northern boundary (at approximately kilometer 80), the basin is nearly flat and is characterized by medium strength backscatter on the SeaMARC II imagery typical of sediment outpouring from the eastern flanks. While the imagery may suggest that a rift valley jug occurs at this site, it is more likely that sediment from the outer fringes of the nearby Bear Island Fan (figure 7) have breached the rift valley, resulting in the peculiar shape of the bathymetric contours.

2C. Order 3 (86-101 km along the SeaMARC II tracks)

The segment 2C (figure 8) is defined by axial depth minima of 3,200 m on its southern

boundary and 2,600 m on its northern boundary (figure 14). It has an average width of 8.1 km, a length of 16 km, and trends 050°. Fault density is 0.7 faults/km to the east and 1.5 faults/km to the west of the rift valley (figure 17) while fault length averages 1.6 km. Strong to moderate backscatter on the eastern part of the basin may indicate a large partially covered lava flow.

3. Order 2: 73°04'N to 73°24'N (102-168 km along SeaMARC II tracks)

Segment 3 (figures 8 and 9) is a basin bounded by axial depth minima of 2,800 m on the south and 2,600 m on the north (figure 14). It is 67 km long, has an average width of greater than 8 km (the western side of basin was not completely imaged by the SeaMARC II), exceeds 3,400 m in depth, and trends 054°. Fault azimuths deviate from segment's trend by 5°-15° (figure 16). The rift valley is characterized by strong backscatter on the SeaMARC II imagery. However, on the eastern side, medium to dark backscatter returns were observed to be uniform and uninterrupted; characteristic of a lava flow that is partially being covered by sediment. In contrast, on the western side of the valley, strong linear to curvi-linear backscatter returns characteristic of faults were observed. It is possible that some of these faults are also sites of fissure eruptions.

The volcanic discontinuity at the segment's northern boundary (figure 10) is defined by the 2,900 m contour and shoals to less than 2,600m (figure 14). It is approximately 2 km wide, 6 km long and is oriented 030°, en-echelon to both its southern and northern neighboring segments. While numerous faults are found on this discontinuity, lava flows are not present.

Segment 3 is subdivided into four subsegments; 3A, 3B, 3C, and 3D.

3A. Order 3 (102-120 km along the SeaMARC II tracks)

Segment 3A (figure 8) is a well defined elongate basin that is 19 km long. It is greater than 8 km wide, deeper than 3,400 m, and trends 053° along its axis (nearly identical to the average fault azimuth of 052°). It is bounded by axial depth minima of 2,800 m to the south and 3,300 m to the north (figure 14). Fault density is 1.1 faults/km to the east and greater than 1.9 faults/km to the west of the axis (figure 17) while fault length averages 2.3 km. The western side of the rift valley is characterized by approximately 9 semi-circular to circular structures. These structures are most likely small volcanic cones that are less than 100 m in height as they do not appear on the bathymetric maps. In contrast, the eastern side of the basin is characterized by strong backscatter indicative of a flat lying lava flow.

3B. Order 3 (121-131 km along the SeaMARC II tracks)

The segment 3B (figure 8) is bounded by axial depth minima of 3,300 m on the south and 3,000 m on the north (figure 14). It is 11 km long, deeper than 3,400 m, has an average width of greater than 7 km, and trends 050° (compared to an average fault azimuth of 040 °). Fault density is 1.5 faults/km to the east and approximately 5.1 faults/km to the west of the axis (figure 17) while fault length averages 0.9 km.

3C. Order 3 (132-155 km along the SeaMARC II tracks)

The segment 3C (figure 8) is bounded by axial depth minima of 3,000 m on the south and

north (figure 14). It is 33 km long, deeper than 3,300 m, and has an average width of greater than 6 km. The segment trends 052° compared to an average fault azimuth of 047° . Fault density averages 0.6 fault/km to the east and greater than 0.7 faults/km to the west of the axis, while fault lengths average 2.3 km in the southern part of the segment (from southern boundary to 20 km away within the basin) compared to 1.2 km in the northern part of the segment.

3D. Order 3 (155-168 km along the SeaMARC II tracks)

The partially imaged segment 3D (figures 9 and 10) is bounded by axial depth minima of 3,000 m in the south and 2,600 m in the north (figure 14). This segment is 14 km long, deeper than 3,200 m, trends 045°, and greater than 5 km in width. Fault density averages 0.3 faults/km to the east and approximately 2.9 faults/km to the west of the axis (figure 17). Sediment encroachment from the eastern flank appears to cover most of this basin's eastern faults (figure 7).

4. Order 2: 73°24'N to 73°35'N (169-201 km along SeaMARC II tracks)

Segment 4 (figure 10) is oriented en-echelon to segment 5, with more than 3.0 km of overlap. It is bounded by axial depth minima of 2,600 m to the south and 2,200 m to the north (figure 14), is 32 km long, deeper than 3,200 m, and approximately 10 km wide. The general orientation of the segment is 040°; parallel to average fault azimuths within its rift valley. The eastern floor of segment 4's rift valley is covered by sediment that has spilled into the rift basin from the Bear Island Fan (figure 7), and is acoustically characterized by strong yet variable return on the side-scan imagery. In contrast, the

western rift valley is heavily faulted.

The volcanic discontinuity that is this segment's northern boundary (figure 10) is defined by the 2,500 m contour which shoals to less than 2,200 m (figure 14). It is 15 km long, ~3 km wide, and oriented 036°. The southern part of the discontinuity (where the volcano is shallowest) is oriented 050°. It appears that the active craters atop the volcano are located at its geographic center, while faults are dominant on the western side of the volcano and nearly absent on the east perhaps because they are buried by sediment (figure 15).

Segment 4 is further subdivided into subsegments 4A and 4B.

4A. Order 3 (169-190 km along the SeaMARC II tracks)

Segment 4A (figure 10) is bounded by axial depth minima of 2,600 m to the south and 2,900 m to the north (figure 14). This segment is 21 km long, deeper than 3,200 m, and wider than 9 km. This sub-segment trends 019° along its southern terminus shifting to 053° in the north. Average fault azimuths within the rift basin trend 043° (highly oblique to the trends of the rift basin). Fault density averages 0.3 faults/km to the east and 1.5 faults/km to the west of the axis (figure 17) while fault length averages 1.3 km. The eastern side of this segment appears to be nearly covered by sediment spilling into the rift basin from its eastern flanks.

4B. Order 3 (191-201 km along the SeaMARC II tracks)

Segment 4B (figure 10) is bounded by axial depth minima of 2,900 m to the south and 2,200 m to the north (figure 14). The basin is deeper than 3,000 m, 11 km long, ~5 km

wide, and oriented 050°. Average fault azimuths of 036° parallel the local rift valley's trend, but not the trend of the segment. Fault density averages 1.1 fault/km to the east and 2.1 faults/km to the west of the axis (figure 17) while fault length averages 1.9 km.

This sub-segment lies at the geographic center of the bend between the Mohns and Knipovich Ridge (Perry, 1980; Vogt, 1986; and many others).

5. Order 2: 73°37'N to 73°41'N (202-240 km along SeaMARC II tracks):

Segment 5 (figure 10) is bounded by axial depth minima of 2,700 m to the south and 2,900 m to the north (figure 14). The basin changes orientation from 040° in the south to 025° in the center to 010° in the north, close to the average trend of the Knipovich Ridge to the north. In comparison, fault azimuths change from an average of 023° in the south to 003° in the north (figure 16). For this reason, we believe that within segment 5, lies the structural intersection of the Mohns and Knipovich Ridges. Segment 5 is 39 km long and more than 8 km wide (the western boundary was not imaged by the SeaMARC II). Fault density is 0.9 faults/km to the east and approximately 1.5 faults/km to the west of the axis (figure 17) while fault lengths average 3 km. The western part of the rift valley is marked by strong acoustic backscatter characteristic of a lava flow.

Mohns Ridge - Greenland Fracture Zone Track:

Because the Mohns and Knipovich Ridges intersect one another at a highly oblique angle and are separated by the once active Greenland Fracture Zone, we attempted to image a swath of seafloor extending from the bend between the Mohns and Knipovich Ridges

westward along the Greenland Fracture Zone to reveal any complex stress field changes in the region indicative of complex plate boundary evolution in this region. We expected that this corridor would be dominated by compressional and shear structures created in response to spreading within the acute angle side of the 070°-080° bend in the ridge intersection (figure 1). Indeed, prior to our survey, Vogt (1986) (based on Perry et al., 1985) suggested that northeast trending features are prominent in the region and they probably reflect northeastward propagation of rifts or flow of asthenosphere materials away from the Jan Mayen Hotspot.

As figures 9 and 10 show, the most predominant structures are oriented 030°-035°; nearly parallel to the transition zone between the Mohns and Knipovich Ridges. Fault bounded ridges are ~0.7-2.5 km wide and at times capped by several volcanic cones (for example: between. 74°02′N, 5°50′E and 74°06′N, 5°10′E, figure 11), suggesting that the ridges formed on the mid-ocean ridge and were rafted off-axis over time. Furthermore, off-axial ridges occur in clusters. From southeast to northwest, we mapped the following five clusters of fault bounded ridges from the rise axis to the ancient Greenland Fracture Zone:

1. 30 km west of the central rift valley lies a cluster of three ridges distributed over ~9 km of seafloor, with an average depth of 1500 m (figure 10).

2. 46 km west of the rift valley lies a cluster of five ridges (figure 11) distributed over ~19 km of seafloor with average depths of 2,500 m

3. 53 km west of the rift valley lies a cluster of eight ridges (figure 11) scattered over ~36 km of seafloor with average depths of 2,700 m.

4. 71 km west of the rift valley lies a cluster of four ridges scattered over 22 km of seafloor with average depths of 2,650 m (figure 12).

5. 125 km west of the rift valley (on crust 20-30 MA Palmer, 1983; Kent at al., 1986; and Vogt, 1986) lie two ridges just to the southeast of the Greenland Fracture Zone (figure 12). They trend 015° and 002°, respectively, and may be evidence for the propagation of the paleo-Mohns Ridge into the Greenland Fracture Zone (figure 13). The ridges are closely spaced (4.5 km apart) and average 2,850 m depth.

In general, individual ridges are linear to curvilinear features longer than 10 km with varying depth along their strike. Closer to the Greenland Fracture Zone, a few ridges appear to occur or terminate abruptly (figure 12). It is likely that higher sediment cover buries some of the deeper parts of these ridges. Alternatively, the ridges are not continuous features along the northwestern flank of the Mohns Ridge and may correspond to a reorientation of different spreading segments that have changed shape and boundaries through time.

In contrast to the ridges on the western flank of the Mohns-Knipovich Bend, off axial ridges on the southeastern flank are narrower (1.5-2 km) and are more randomly distributed (figures 8 and 9). With a high influx of sediment from the Bear Island Fan (figure 7), partial to full burial of the southeastern ridges masks their true shape and distribution.

The Greenland Fracture Zone (figure 13) is a prominent bathymetric feature that shoals to less than 1,700 m. Structurally, with the exception of a N-S trending fault, the seafloor on

and near the fracture zone is covered by sediment with limited faulting. IN contrast, elongated ridges are observed to the northeast in the Boreas Basin at 75°30'N, 2°30'E; 75 °50'N, 3°45'E; and 76°00'N, 4°00'E (figure 13). The first two of these ridges trend parallel to the fracture zone (300°-320°), while being cut by faults which trend 030°-035° parallel to the trend of the Mohns Ridge. The third ridge shoals to 2600 m where a remnant volcanic cone is observed, trends 356° (Knipovich Ridge parallel) while faults observed just to the northeast of the ridge trend ~035°. Magnetic amplitude data (figure 3) show the latter two ridges coinciding with a positive anomaly of more than 60 nT. However, the free air gravity field (figure 4) along the entire Greenland Fracture Zone track reveals a 10-15 mGal anomaly in this region.

Discussion:

Topographically, this northernmost section of the Mohns Ridge consists of second order basinal segments oriented 045°-055° to the rift valley and are bounded by second order volcanic discontinuities trending 025°-035°. These basins are further broken into third order subsegments which tend to slightly deviate from the rift valley orientation. Twelve third order basinal subsegments were identified along the Mohns Ridge up to its intersection with the Knipovich Ridge

The volcanic discontinuity between segments 1 and 2, shoals to less than 1,900 m and appears to be a currently active volcanic system (Vogt, 1986). It is characterized by the highest magnetic anomaly along the northeastern Mohns Ridge; 1300 nT (figure 3) (Kovacks et al, 1987) and a narrow and flat free air gravity anomaly of 55 mGal (Sobczak

et al, 1987). The volcanic discontinuity between segments 2 and 3 is 900 m deeper than the volcanic discontinuity between segments 1 and 2, yet is well defined on the free air gravity map (figure 4) by a circular anomaly of 10 mGal. The side-scan sonar data do not reveal major differences between the two discontinuities with the exception that volcanic discontinuity 2-3 is characterized by darker backscatter than volcanic discontinuity 1-2 suggesting that the associated lava flows of the former are newer and less covered by sediment than the latter. Both rift valley volcanoes are neighbored by long basinal segments that are further subdivided into smaller segments suggesting that the volcanoes are sites where magma has been erupting for long periods of time and may be representative of punctiform shaped stable magma centers on the crest of harmonically spaced asthenospheric upwellings as was implied by Crane (1985), Schouten et al. (1985), and Bonatti (1986).

Vogt, (1986) suggested that there are only occasional true transform faults present along the southwestern Mohns Ridge. In our survey along the northeastern Mohns Ridge, we detected the presence of five possible locations where fault trends simulate those of transforms. However, no clear offsets in the Mohns Ridge magnetic anomaly patterns may be more characteristic of a rise axis free of classic transform faults.

While oblique spreading along the volcanic segments has been suggested (Geli, 1993; and Vogt, 1986), our data only partially support this idea. We are limited in our analysis by the extent of SeaMARC II coverage on the northwestern flank which primarily consisted of one track from the Mohns-Knipovich Ridge to the Greenland Fracture Zone (figures 9-11). However, on the southeastern flank, our data show extensive faulting that is oriented

nearly parallel to the rift valley (040° average for all faults). Histograms for fault trends within the inner rift (figure 18) and the flanks (figure 19) suggest that the preferred fault trend is 036°-045° which is only slightly oblique to the dominant rift valley orientation (045°).

En-echelon faulting (which occurs in the rift valley) does not extend onto the imaged southeastern flank. However, as figure 18 demonstrates, fault orientations within the inner rift valley have a general preference for the range of 000°-044° compared to 045°-050° (trend of the Mohns Ridge rift valley) and 050°-065° suggesting that oblique spreading may be occurring presently at least within the axial rift valley. Indeed, volcanic discontinuities are oriented nearly 20° oblique to the rift valley.

The Nishenko (1986) compilation of epicenters along the northeastern Mohns Ridge suggests that the entire section of the Mohns Ridge is seismiclly active. However, similar to the midocean ridge in general north of Iceland, the Mohns Ridge is in many ways atypical of slow-spreading centers (Vogt, et al., 1982; and Vogt, 1986). For example, the Reykjanes Ridge is segmented into fourth and third order segments that are entirely axial volcanic systems (Appelgate et al., 1993). In contrast, the Mohns Ridge, which is a mix of distinctive basinal segments bounded by occasionally very shallow volcanoes, is the bathymetric inverse to the Reykjanes Ridge. Volcanic discontinuities along the northeastern Mohns Ridge have vertical relief of more than 1.5 km compared to adjacent basinal depth maxima which is nearly 3-4 times as much as other volcanic parts of the Mid-Atlantic Ridge in the North Atlantic Ocean (Sempere et al., 1990; and Appelgate,

1993). Some volcanic discontinuities completely occupy the inner rift valley (such as the volcanic discontinuity between segments 1 and 2).

The Mohns Ridge segmentation is more representative of the segmentation style of the Knipovich Ridge (Doss et al, in prep) than any other section of the Mid-Atlantic Ridge. However, unlike the Knipovich Ridge where segmentation is thought to be controlled by ancient faults cutting across rift valley, the Mohns Ridge appears to be evolving from a very slow-spreading harmonically distributed punctiform centers of magma upwelling. The five segments along this section of the Mohns Ridge are second order and are 32-67 km in length (similar to segment length along the northern Knipovich Ridge).

The 030° orientation of the flank ridges in the Greenland Basin is a confirmation of the detailed SEABEAM and magnetic survey data near 72°30'N (approximately mid point of the Mohns Ridge) presented by Geli (1993) He suggested that these ridges and the topographic troughs in between them represent periods of intense volcanic activity where accelerated accretion took place (resulting in higher topography) followed by times of limited to no volcanic activity (resulting in deeper topography). The ridges we observed occurred more frequently, and closer to the transition zone averaging a spacing of ~2 km. Using Vogt's (1986) suggested full spreading rate for crust younger than 10 MA, this suggests a periodicity of ~450,000 years for relaxation of the volcanic events that construct these ridges. Thus, periods based on our data of intense volcanic activity should have a periodicity of 160,000-550,000 yr. (this range is possibly misleading since times of intense volcanic activity would mean massive vertical and horizontal buildup of these

ridges). A look at both the magnetic anomaly and gravity maps (figures 3 and 4) shows no correlation between the ridges observed here and these geophysical signatures. However, if we compared groups of ridges to the magnetic anomaly map, we see some correlation. A positive magnetic anomaly of 400 nT corresponds to the large five closely spaced ridges (group 3) between latitudes 74°03'N and 74°13'N; and longitudes 6°00'E and 5°15 'E (figure 11). Further northwest, a positive magnetic anomaly of 500 nT corresponds to the next set of ridges (group 4) between latitudes 74°15'N and 74°40'N; and longitudes 5° 00'E and 4°00'E. This suggests that (at least along the Mohns Ridge) we can correlate times of volcanic buildup with positive and high amplitude magnetic anomalies.

That the off-axial ridge orientations of ~030° appear uniform on our SeaMARC II track between the Greenland Fracture Zone and the transitional zone of the Mohns-Knipovich system suggests that the ridges were formed under the stress of the Mohns and not the Knipovich Ridge. If Geli's suggestion that the off-axial ridges can be found along the entire northwestern flank of the Mohns Ridge up to the transition zone (Mohns-Knipovich bend), then oblique spreading may not only be occurring across the Mohns Ridge, but additionally, substantial oblique spreading may also be occurring along the Knipovich Ridge. Otherwise, a region of significant compression would deform on the western side of the Mohns Ridge-Knipovich Ridge transition zone (which is not supported by the SeaMARC II data presented in this paper).

In the case of the Mohns Ridge, there is evidence that axial cones are preserved intact on the off-axial ridges; e.g., the northwesternmost volcanic ridge with preserved cones near

74°30'N, 4°00'E, (figure 12) (Palmer, 1983; Kent et al., 1986; and Vogt, 1986). In contrast, the Reykjanes Ridge, for example does not show any evidence of preserved volcanic edifices beyond its neovolcanic zone (Appelgate, 1993).

A simple explanation for this geometry may lie in the obliquely spreading Knipovich Ridge (Vogt, 1986). Two possibilities exist: firstly, the stress field related to both the Mohns and Knipovich Ridges does influence these ridges creating structures resulting from the intersection of two different spreading vectors; or secondly, the Knipovich Ridge does not affect these Mohns Ridge parallel ridges. The second possibility agrees with Doss et al. (in prep.) and Vogt (1986) who suggested that the Knipovich Ridge is an atypical mid-ocean ridge and that its oblique spreading is actually constrained by major fracture zones such as the Greenland Fracture Zone.

The Mohns-Knipovich Bend is characterized by a continuous rift valley segment with well defined inner-facing boundary faults. There is no offset between the 2 mid-ocean ridges. Instead, second order segment 5 is curves towards the southern tip of the Knipovich Ridge trending 019° near 73°30'N. While the Knipovich Ridge rift valley maintains a dominantly north-northeast trend, the individual segments within the rift valley are oriented 035°-050°. This suggests that the true spreading direction of the Knipovich Ridge is parallel to the spreading direction of the Mohns Ridge.

The absence of a transform offset in the transition zone between the two ridges coupled with the structural fabric of the northwestern flank of the transition zone, suggests that the Mohns Ridge simply propagated into and was thus trapped by the Paleo-Spitsbergen

Shear Zone (Crane et al., 1988; Crane et al., 1991; Okay et al., 1993; and Doss et al, in prep) creating the Knipovich Ridge in the process.

However, geophysical evidence suggests that in addition to surficial entrapment within the Spitsbergen Shear Zone, the deep seated asthenosphere associated with the Mohns Ridge most likely continued to propagate in a northeasterly direction underplating the Barents Sea in the process (Okay et al., 1993 and Crane et al. 1991).

The SeaMARC II track located between the Greenland Fracture Zone and the Knipovich Ridge revealed three prominent ridge like features trending 300°, 320° and 356°, southwest to northeast respectively. The change in orientation of these ridges may provide clues about the way in which the Mohns Ridge propagated beyond the Greenland Fracture Zone. Bathymetric evidence suggests that the Greenland Fracture Zone acted as a barrier to the northeasterly propagating Mohns Ridge, causing magma to leak and vertically pond into the barrier. As time progressed, the Mohns Ridge moved beyond the fracture zone into the fault which at present defined the position of the Knipovich Ridge.

Conclusions:

1. The Mohns Ridge is segmented into second and third order basinal segments bounded by volcanic discontinuities aligned along faults which are highly oblique to the rise axis and appear to be points of recent to present extrusive volcanic activity.

2. Although the Mohns Ridge is segmented, it is atypical of other mid-ocean ridges because the most volcanically active regions lie not in the centers but at the

boundaries of the segments.

3. Fault trends within and on the flanks of the Mohns Ridge axis suggest that subtle oblique spreading (010°-020°) is taking place.

4. On the northwestern flank, dominantly volcanic and undeformed ridges lie parallel to the Mohns-Knipovich Ridge transitional zone. These linear ridges were probably formed at the Mohns Ridge and are not being subjected to compressive stress from the Knipovich Ridge.

5. The absence of compressive structures on the northwestern side of the Mohns-Knipovich Bend suggests that the Knipovich ridge is likely to be spreading obliquely

6. The SeaMARC II imagery demonstrated that the transition from the Mohns Ridge to the Knipovich Ridge occurs without any transform fault activity.

7. The Knipovich Ridge has probably formed as a result of north-northeasterly propagation of the Mohns Ridge into the ancient Spitsbergen Shear Zone.

References:

Appelgate, B., and Shor, A. N., 1993, The Northern Mid-Atlantic and Reykjanes Ridges: Spreading Center Morphology Between 55°50'N and 63°00'N, in press.

Bonatti, E., 1985, Punctiform initiation of seafloor spreading in the Red Sea during transition from a continental to an oceanic rift, Nature, Vol. 316, No. 6023, 33-37.

Bonatti, E., G. Ottonello, and P. R. Hamlyn, 1986, Peridotites from the island of Zabargad (St. John) Red Sea: Petrology and Geochemistry, Jour. Geophys. Res., 91, 599-631.

Cherkis, N. Z. and Vogt, P. R., 1994, Regional Bathymetry of the Norwegian-Greenland Sea, Naval Research Laboratory, Washington, D.C.

Courtillot, V., 1982, Propagating Rifts and Continental Breakup, Tectonics, 1, 239-250.

Crane, K., 1985, The spacing of rift axis highs: dependence upon diapiric processes in the underlying asthenosphere?, Earth and Planetary Science Letters, 72, 405-414.

Crane, K., and E. Bonatti, 1987, The role of fracture zones during early Red Sea rifting: structural analysis using Space Shuttle radar and LANDSAT imagery, Jour. Geol. Soc., 144, 407-420.

Crane, K., Sundvor, E., Foucher, J. P., Hobart, M., Myhre, A. M., and LeDouran, S., 1988, Thermal Evolution of the Western Svalbard Margin, Mar. Geophys. Res., 9, 165-194.

Crane, K., Sundvor, E., Buck, R., and Martinez, F., 1991, Rifting in the Northern Norwegian-Greenland Sea: Thermal Tests of Asymmetric Spreading, Jour. Geophysical. Res., 96, 14529-14550.

Dore. A. G., and Gage, M. S., 1987, Crustal alignments and sedimentary domains in the evolution of the North Sea, North East Atlantic Margin and Barents Shelf. In: J. Brooks and K. Glennie (editors), Petroleum Geology of North West Europe. Graham and Trotman, London, 1131-1148.

Eldholm, O., Vogt, P., and Perry, R., 1978, Plate Tectonic Development of the Mid-Oceanic Ridge System North of the Jan Mayen Fracture Zone, A: Present Plate Boundaries, EOS 59, 371.

Eldholm, O. and Sundvor, E., 1980, The Continental Margins of the Norwegian-Greenland Sea: Recent Results and Outstanding Problems, Royal Society of London Phil. Trans., Ser. A: 294, 77-86.

Eldholm, O., Karasik, A. M., and Reksnes, P. A., 1986, The North American Plate

Boundary, DNAG synthesis. Volume Geology of the Arctic Ocean Region Chapter 12.

Geli, L., 1993, "Volcano-tectonic breathing" and Sedimentation since late Miocene times at the Mohns Ridge in the Norwegian-Greenland Sea, unpublished work.

Harland, W. B., 1969, Contribution of Spitsbergen to understanding of tectonic evolution of North Atlantic Region. In: M. Kay (Editor), North Atlantic: Geology and Continental Drift. American Association of Petroleum Geologists, Memoir 12, 817-851

Horsfield, W. T. and Maton, P. I., 1970, Transform Faulting along the De Geer Line, Nature 226, 256-257

Johnson, L. and Heezen, B. C., 1967, Morphology and Evolution of the Norwegian-Greenland Sea, Deep-Sea Research 14, 755-771.

Kent, D. V., and Gradstein, F. M., 1986, A Jurassic to recent Chronology, In P. Vogt and B. Tucholke (editors), 1986, The Western North Atlantic Region, Vol. M, Decade of North American Geology (DNAG) series, Geological Society of America, Boulder.

Kovacs, L.C., Johnson, G. L., Srivastava, S. P., Taylor, P. T., and Vogt, P. R., 1987, Residual Magnetic Anomaly Chart of the Arctic Ocean Region (Naval research Laboratory and Naval Ocean research and Development Activity), In: The Arctic Ocean Region, Vol. L., The Geology of North America, edited by Arthur Gantz, L. Johnson, and J. F. Sweeny, 1990, 644p.

LaBrecque, J. L., Kent D. V., and Cande S. C., 1977, Revised Magnetic Polarity Time Scale for Late Cretaceous and Cenozoic Time, Geology, 5, 330-335.

Macdonald, K. C., Scheirer, D. S., and Carbotte, S. M., 1991, Mid-Ocean ridges: Discontinuities, segments, and giant cracks, Science, 253, 986-994,

Nishenko, S., 1986, Compilation (digital file) of earthquake epicenters etc. In the North Atlantic area prepared for Zoback et al. (1986) and Einarrson (1986).

Okay, N., and Crane, K., 1993, Thermal Rejuvenation of the Yermak Plateau, Marine Geophysical Researches, 15, 243-263.

Palmer, A. R., 1983, The Decade of North American Geology 1983 Geologic Time Scale, Geological Society of America, Boulder

Perry, R. K., Fleming, H. S., Weber, J. R., Kristoffersen, Y., Hall, J. K., Grantz, A., Johnson, G. L., Cherkis, N. Z., and Larsen, B., 1985, Bathymetry of the Arctic Ocean, Scale 1:6,000,000, Geol. Soc. Amer. Map Series, MC-56, Naval Research Laboratory, Washington, D.C.

Schouten, H., and Klitgord, K. D., and Whitehead, J. A., 1985, Segmentation of mid-

ocean ridges, Nature, 317, 225-229.

Sempere, J. C., Purdy, G. M., and Schouten, H., 1990, Segmentation of the Mid-Atlantic Ridge between 24° N and 30°40N, Nature, 344, 427-431.

Shor, A., 1990, SeaMARC II seafloor mapping system: Seven years of Pacific research, Pacific Rim Congress Vol. III; Australian Institute of Mining and Metallogenesis, 49-59.

Sobczak, L. W., and Hearty, D. B., with contributions by R. Forsberg, Y. Kristoffersen, O. Eldholm and S. D. May), 1987, Gravity of the Arctic Ocean, In: The Arctic Ocean Region, Vol. L., The Geology of North America, edited by Arthur Gantz, L. Johnson, and J. F. Sweeny, 1990, 644p.

Sundvor, E. and O. Eldholm, 1979, The Western and Northern Margin off Svalbard, Tectonophysics, 59, 239-250.

Sundvor, E., and Austegard, A., 1990, The Evolution of the Svalbard Margins: Synthesis and new results, In: Geological History of the Polar Oceans: Arctic Versus Antarctic, U. Bleil and J. Thiede (editors), Kluwer Academic Publishing, 77-94.

Talwani, M. and Eldholm, O., 1977, Evolution of the Norwegian-Greenland Sea, Geol. Soc. America Bull. 88, 969-999.

Vogt, P. R., and Avery, O. E., 1974, Tectonic History of the Arctic Basins: Partial Solutions and Unsolved Mysteries, in Marine Geology and Oceanography of the Arctic Seas, edited by Herman, Y., 83-117, Springer-Verlag, New York.

Vogt, P. R., Perry R. K., Feden R. H., Fleming H. S., and Cherkis N. Z., 1981, 'The Greenland-Norwegian Sea and Iceland Environment: Geology and Geophysics, in: The Ocean Basins and Margins, 5, Nairn, A. E. M. and Churkin, M. (editors), pp. 493-598.

Vogt, P. R., L. C. Kovacs, L. C. Bornero, and S. P. Srivastava, 1982, Asymmetric geophysical signatures in the Greenland-Norwegian and southern Labrador Seas and the Eurasia Basin, Tectonophysics, 89, 95-160.

Vogt, P. R., 1986, Geophysical and Geochemical Signatures and Plate Tectonics, Chapter 11, in The Nordic Seas, edited by B. G. Hurdle, Springer Verlag.

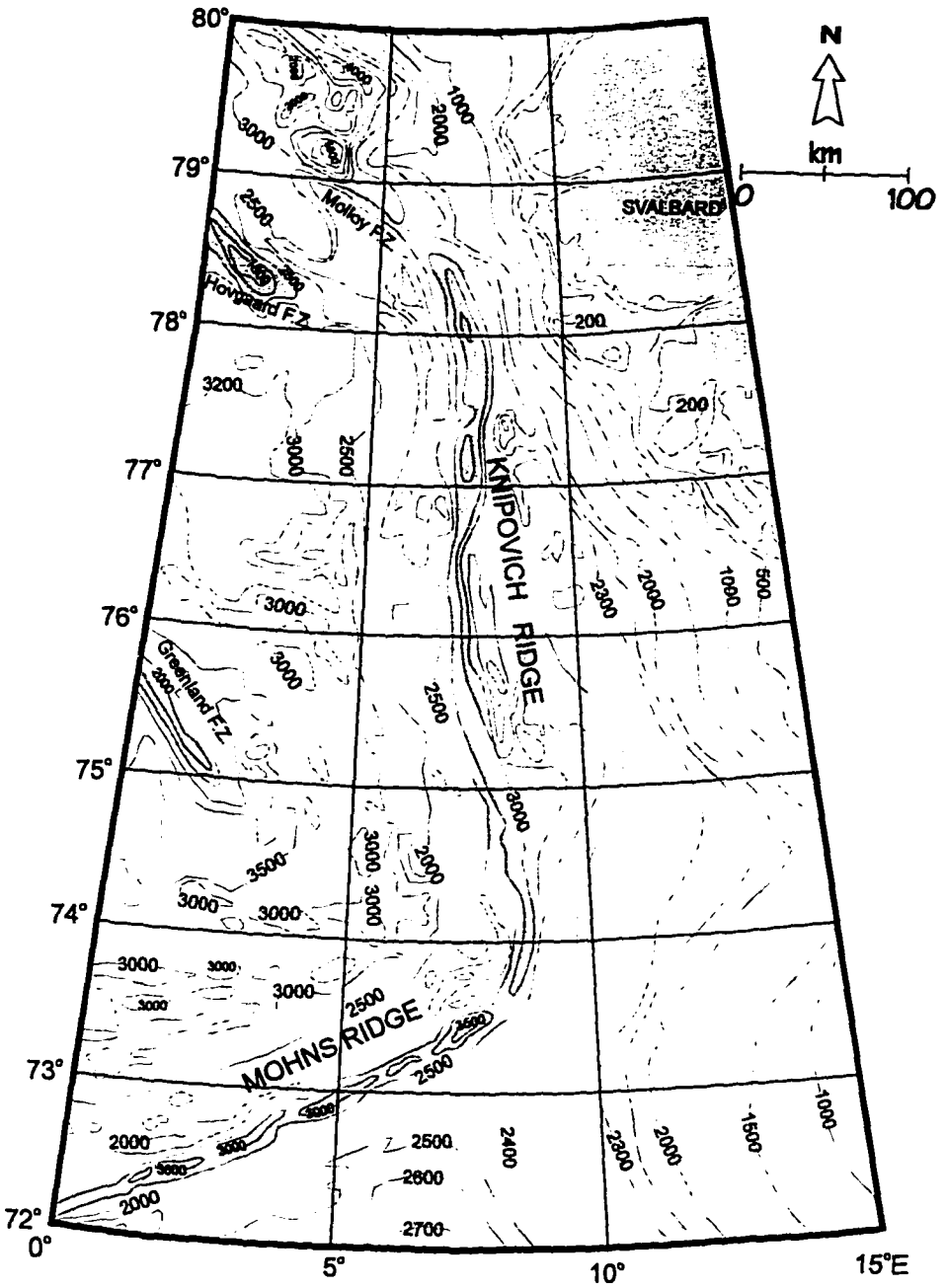

Figure 1: Regional bathymetry (m) of the surveyed region within the Norwegian-Greenland Sea (after Cherkis and Vogt, 1994).

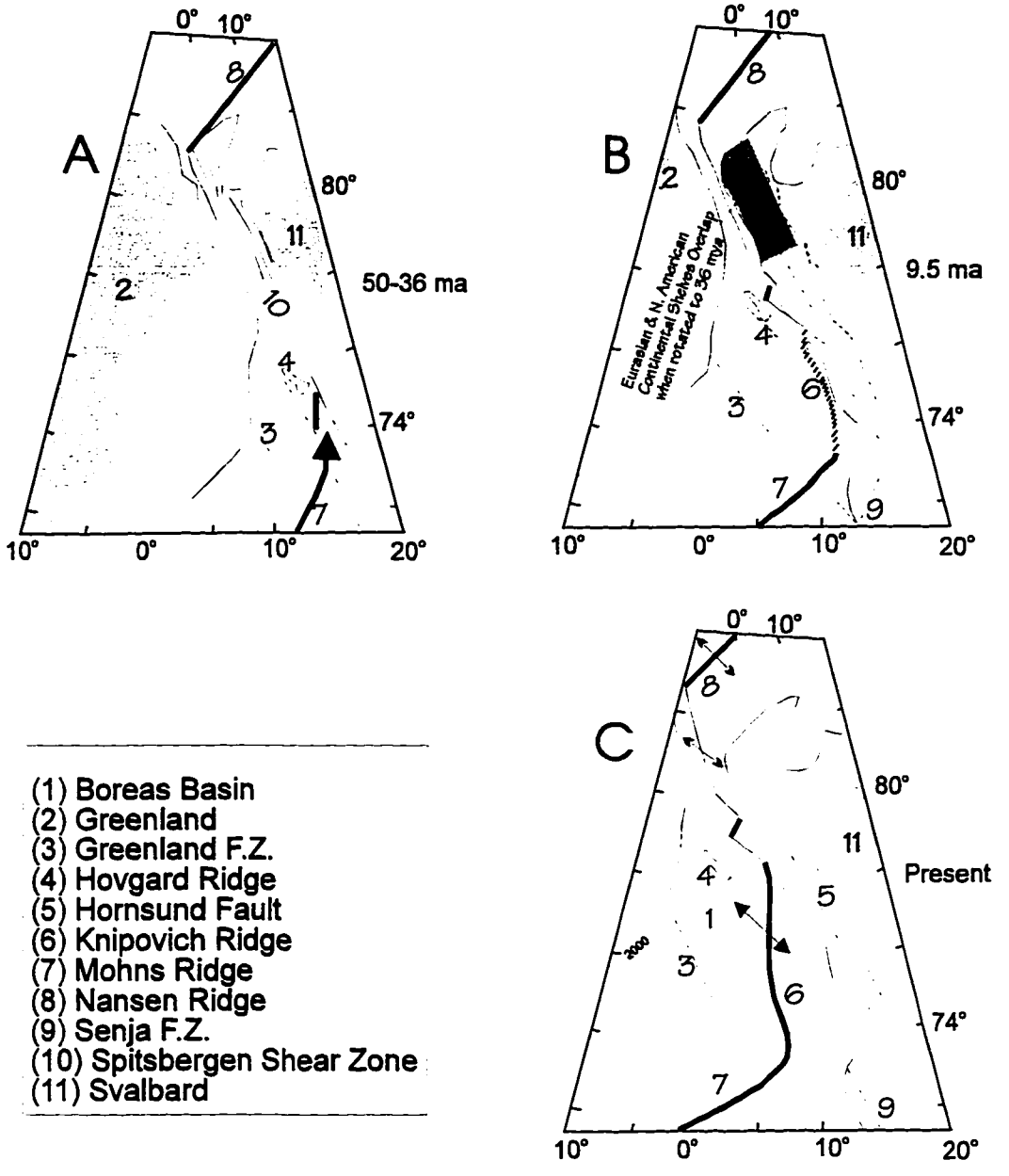

Figure 2: Plate reconstruction at A) 50-36 MA, B) 9.5 MA and C) of the present. A)The ancient Spitsbergen Shear Zone probably cut through Svalbard (Horsfield and Maton, 1970). As the plate boundary developed, the active spreading center propagated into the continental shear zone from the Norwegian Sea and the Arctic Ocean generating the Knipovich Ridge (B) in the Greenland Sea and the Lena trough (C) (after Crane et al., 1991).

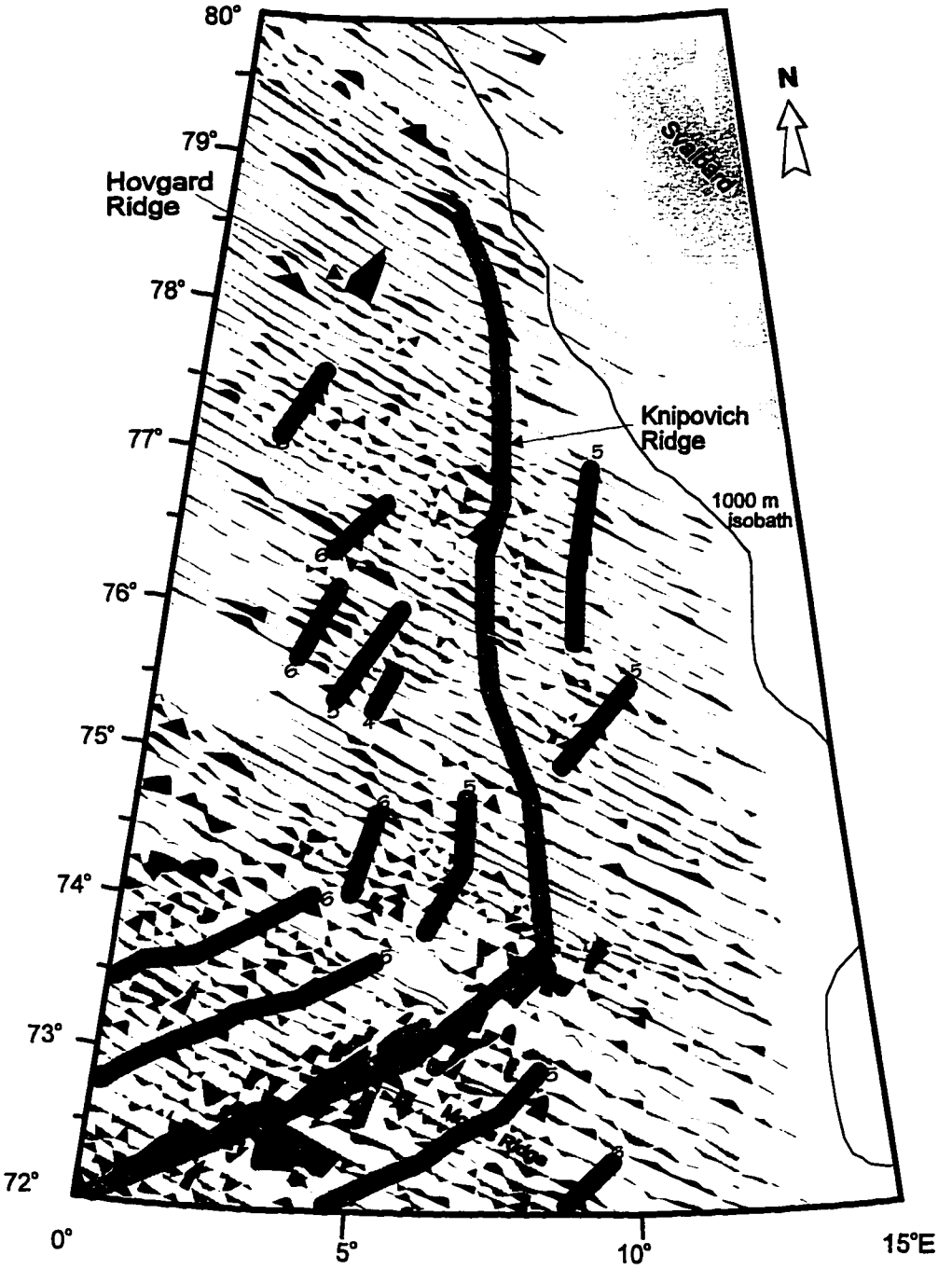

Figure 3: Residual magnetic anomalies within the survey area. All data are shown as fenced anomaly profiles along flight tracks. Positive anomalies are in black while negative anomalies are dotted. Anomaly scale is 4,000 nT per degree of latitude. (After Kovacs et al., 1987). Magnetic anomalies are chaotic or absent in the Greenland Sea compared with more normal anomalies along the northeastern Mohns Ridge. Some anomalies in the Boreas Basin were identified by Vogt (1986) and his interpretations are shown by the darker dotted patterns including the anomaly number.

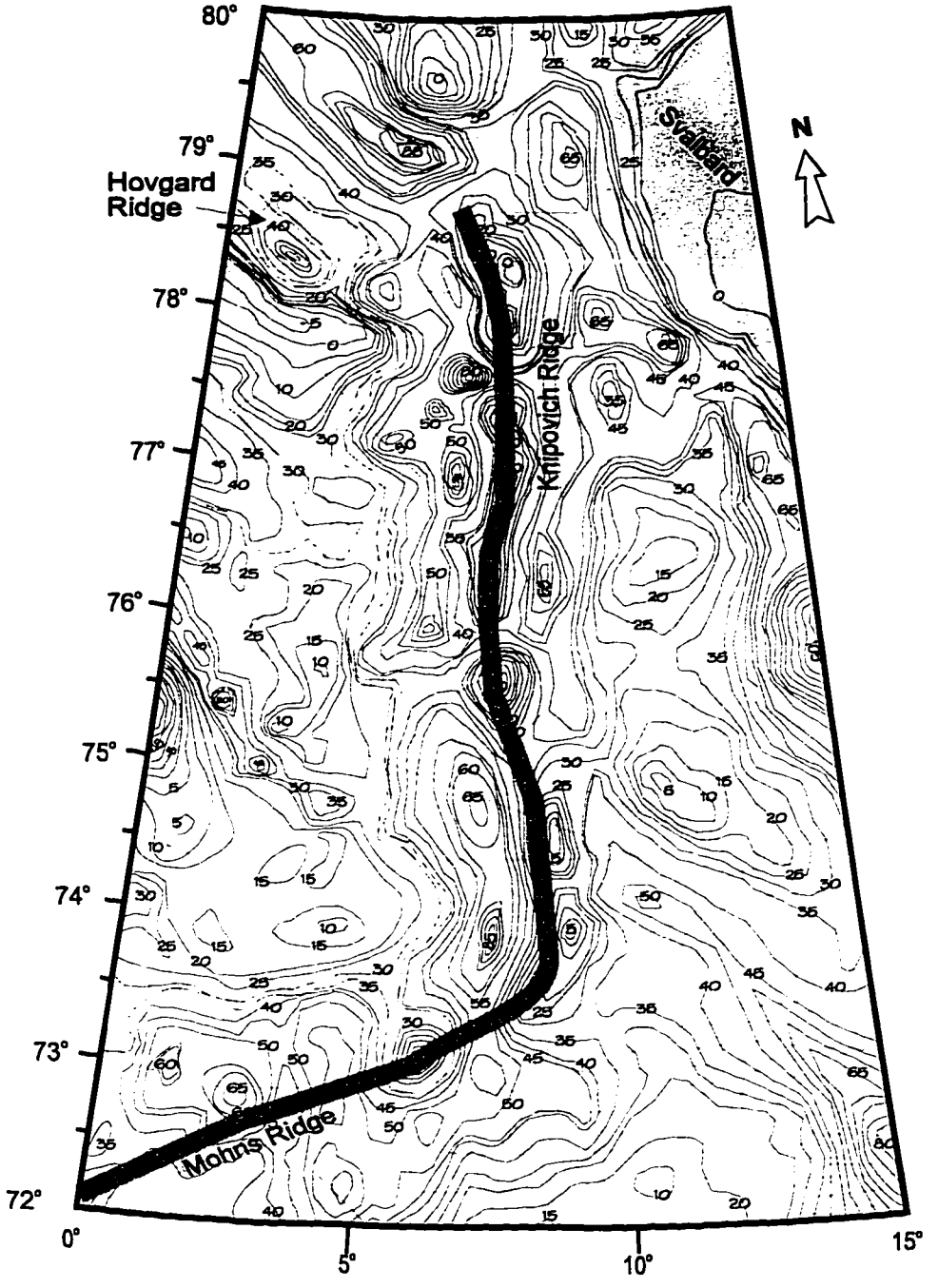

Figure 4: Free-air gravity anomaly map of the survey area. Contour interval is 5 mGal. (After Sobczak et al., 1987). Dotted lines represent control lines

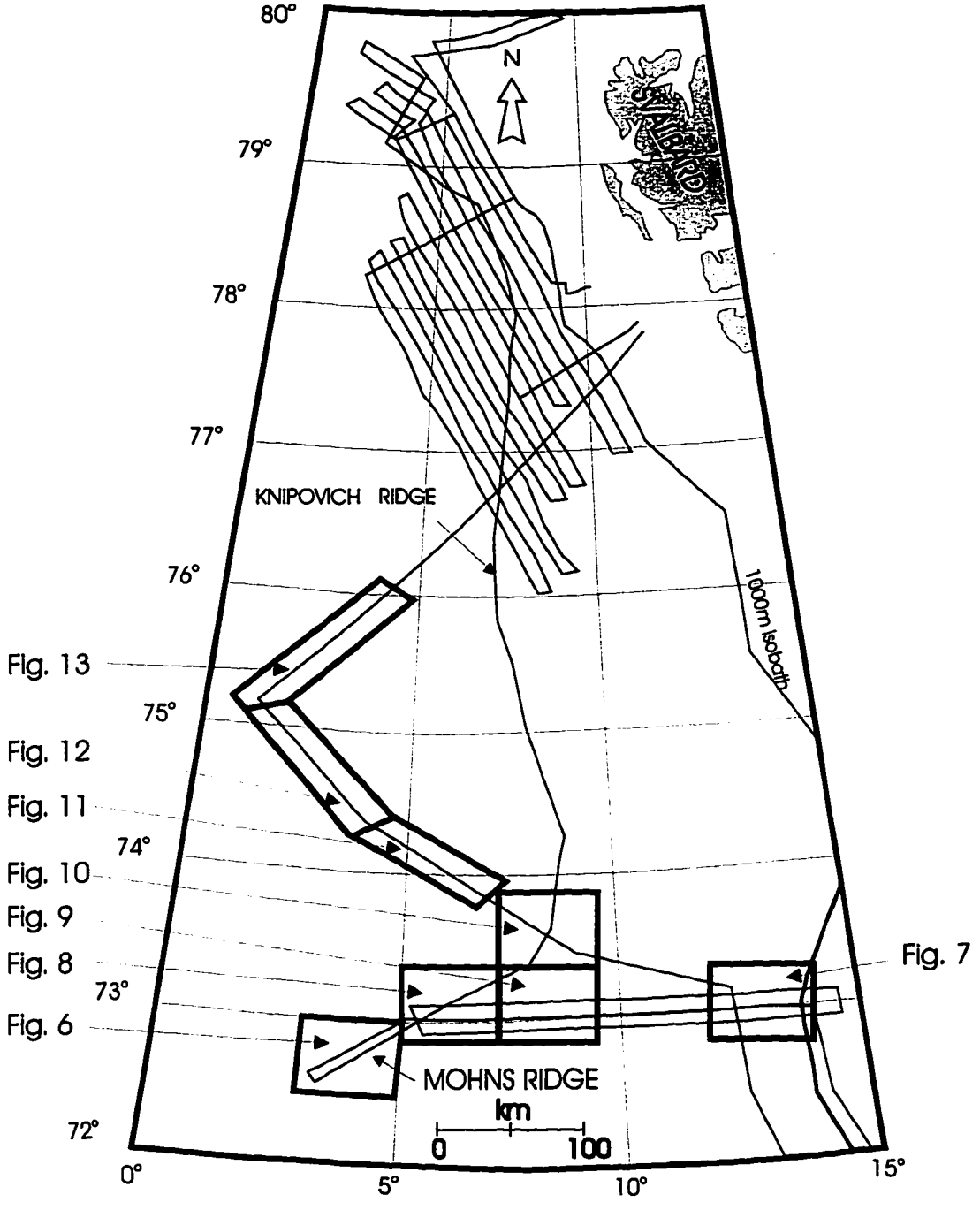

Figure 5: Track map illustrating the SeaMARC II tracks (1989 and 1990). All tracks referred to in this paper are outlined and labeled by the appropriate figure number.

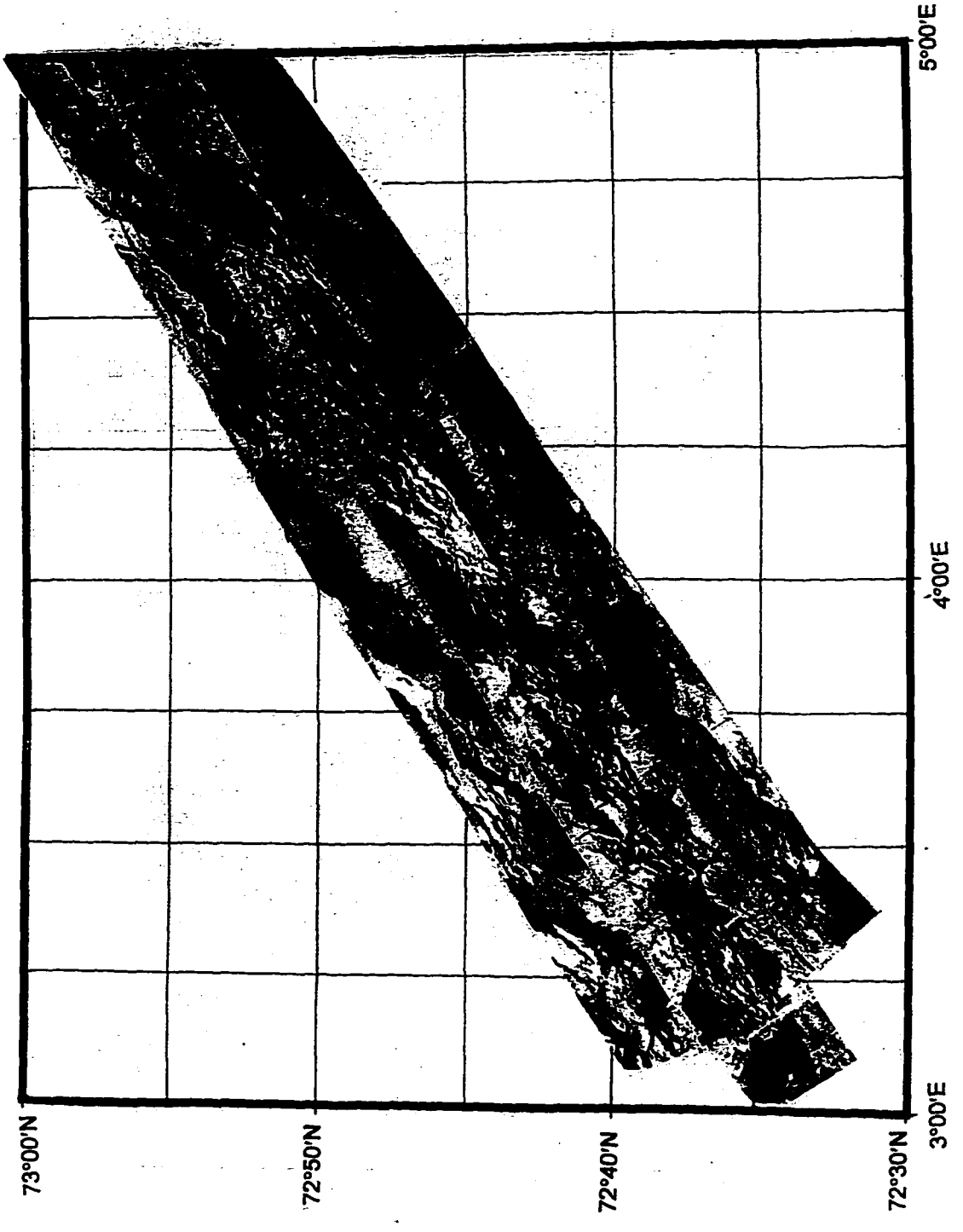

Figure 6A: SeaMARC II side-scan image of the Mohns Ridge between 72°30'N and 73°00'N.

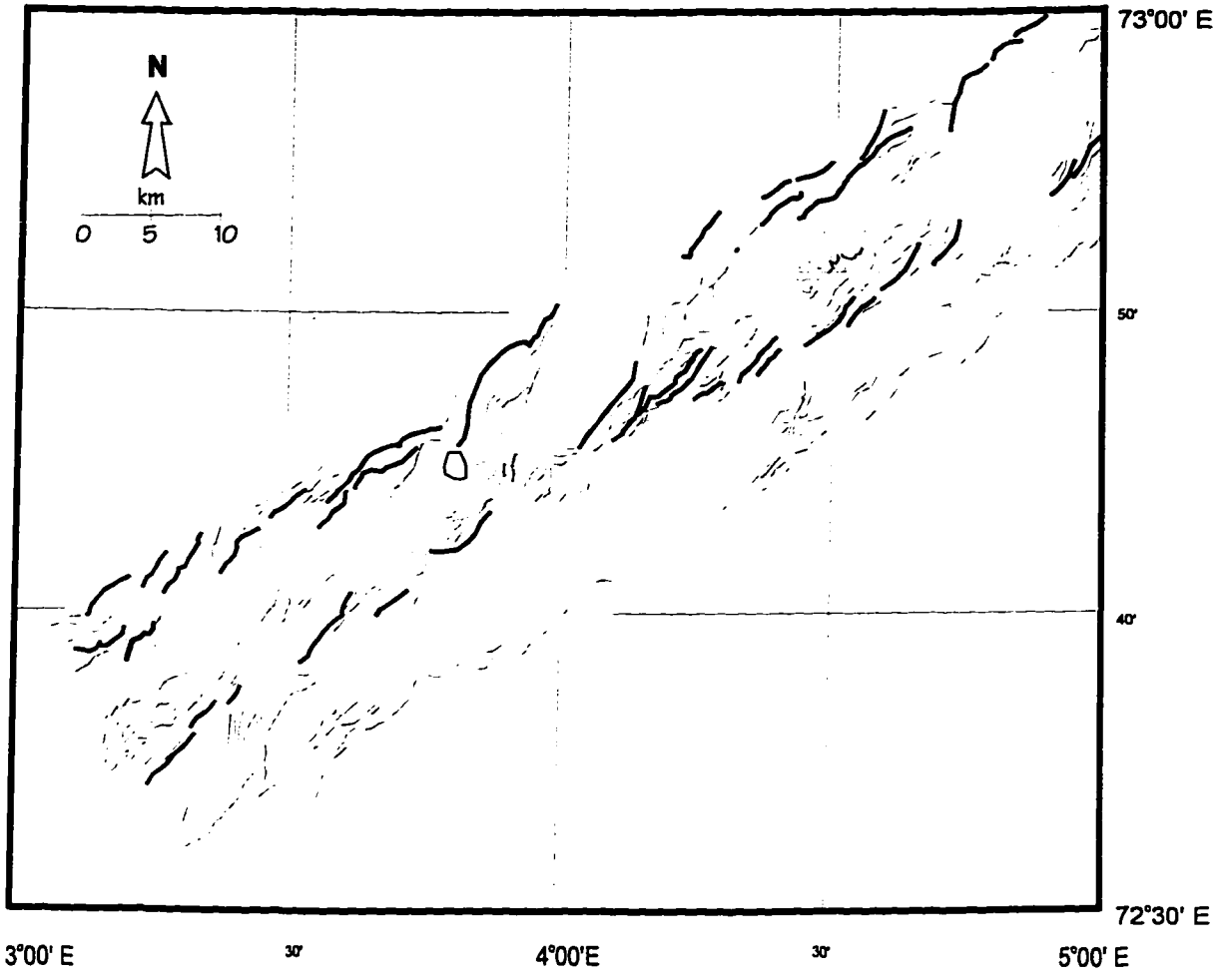

Figure 6B: Structural interpretation of side-scan image shown in figure 6A including the rift valley and a part of the eastern flank. Bold features are interpreted to be major faults bounding the inner rift valley.

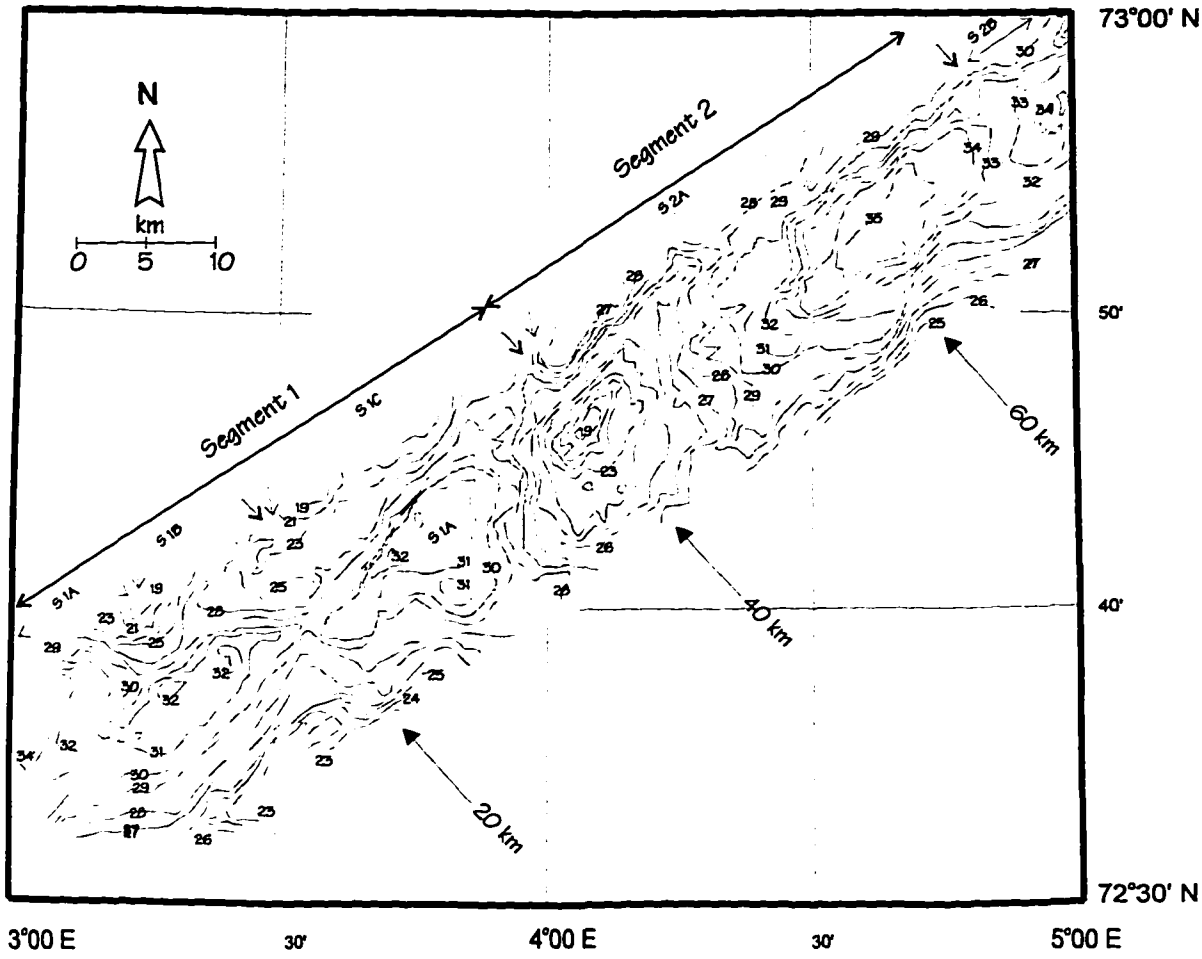

Figure 6C: Bathymetry contours in hundreds of m in the region of the side-scan image shown in figure 6A. Third order segments 1A, 1B, 1C, 2A, and 2B are shown. Note the second order discontinuity between segments 2 and 3 (near 72°45'N), which is a major volcanic high.

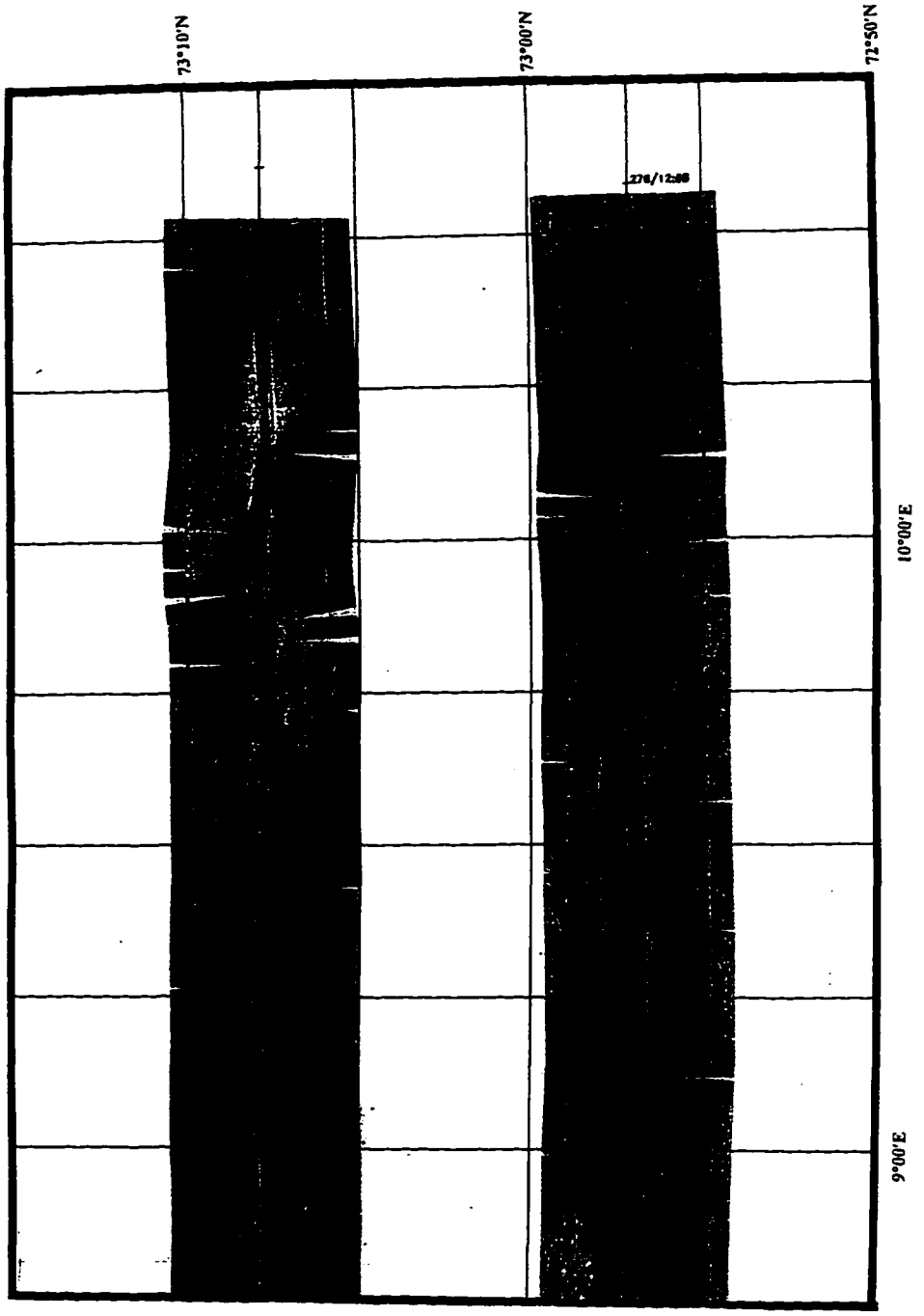

Figure 7: SeaMARC II side-scan image of a section of the Bear Island Fan which contributes large quantities of sediment to the eastern flanks of the Mohns Ridge.

Figure 8A: SeaMARC II side-scan image of the Mohns Ridge from 72°50'N to 73°20'N and a section of the eastern flank.

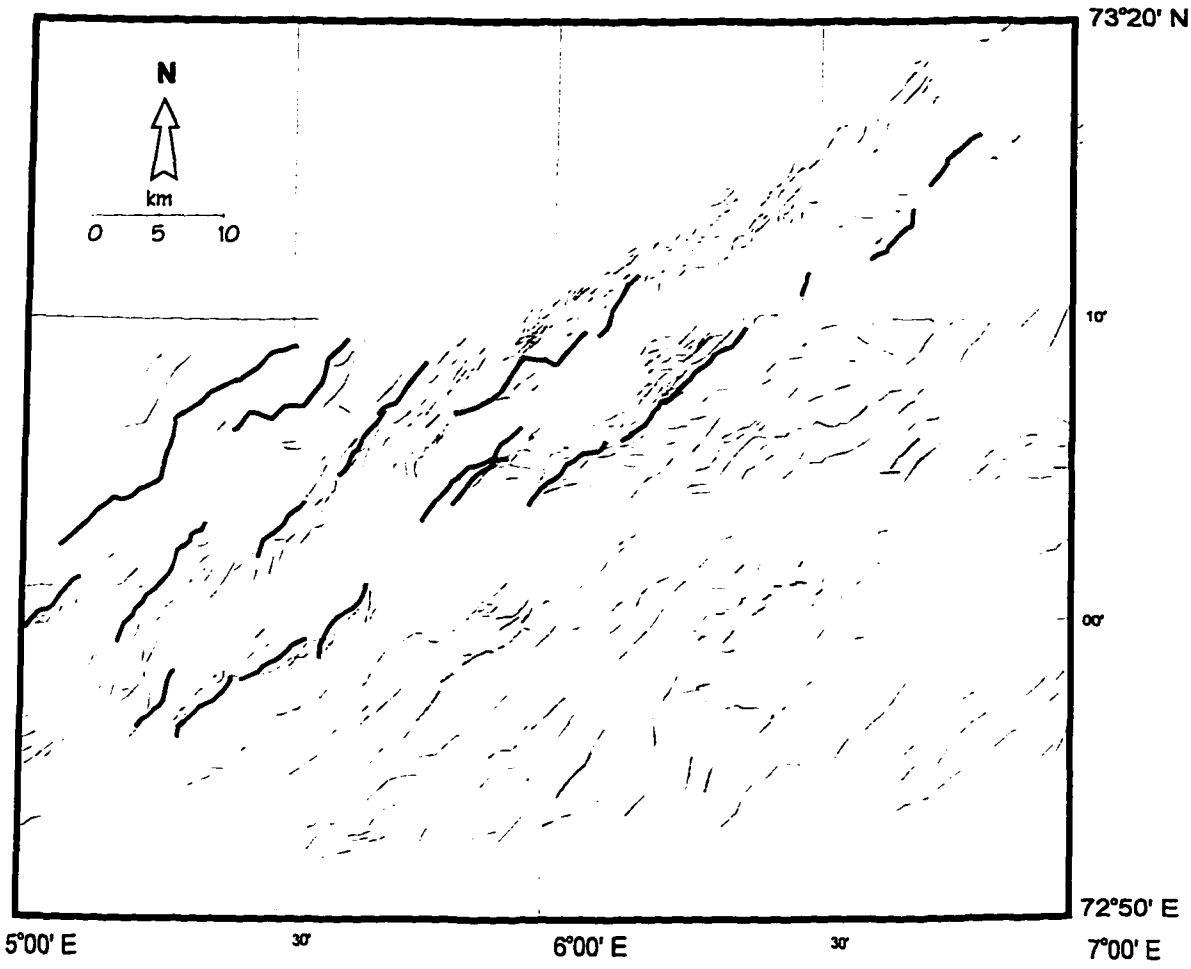

Figure 8B: Structural interpretation of image shown in figure 8A. Bold features represent faults bounding the rift valley. Regions highlighted in light gray represent off axial ridges.

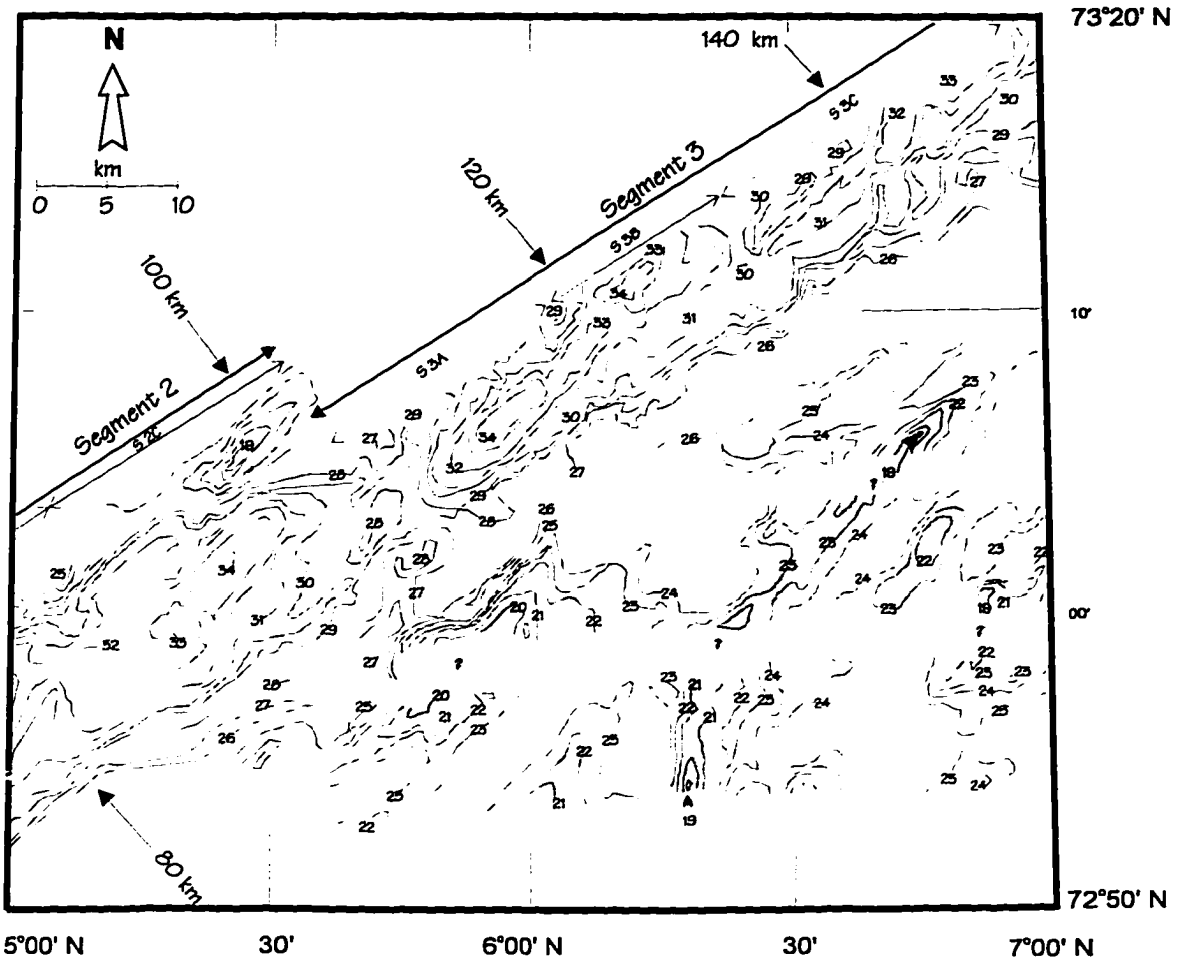

Figure 8C: Bathymetry corresponding to side-scan image shown in figure 8A. Contour lines are in hundreds of meters. Third order segments 2B, 2C, 3A, 3B, and 3C are observed.

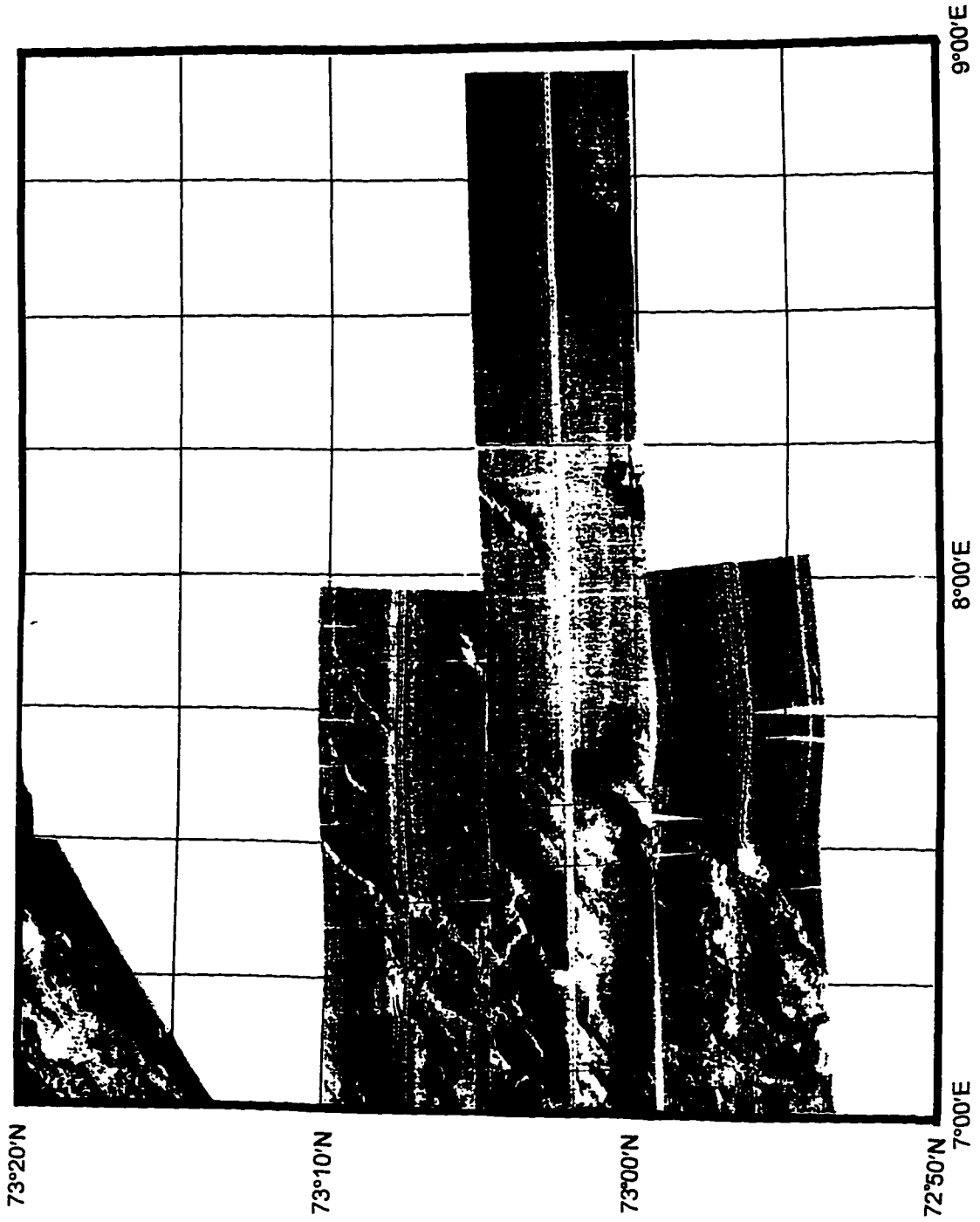

Figure 9A: SeaMARC II side-scan image of a section of the eastern flank of the Mohns Ridge between 72°50'N and 73°20'N. A small section of the eastern outer rift valley can be seen in the northwest corner of the image.

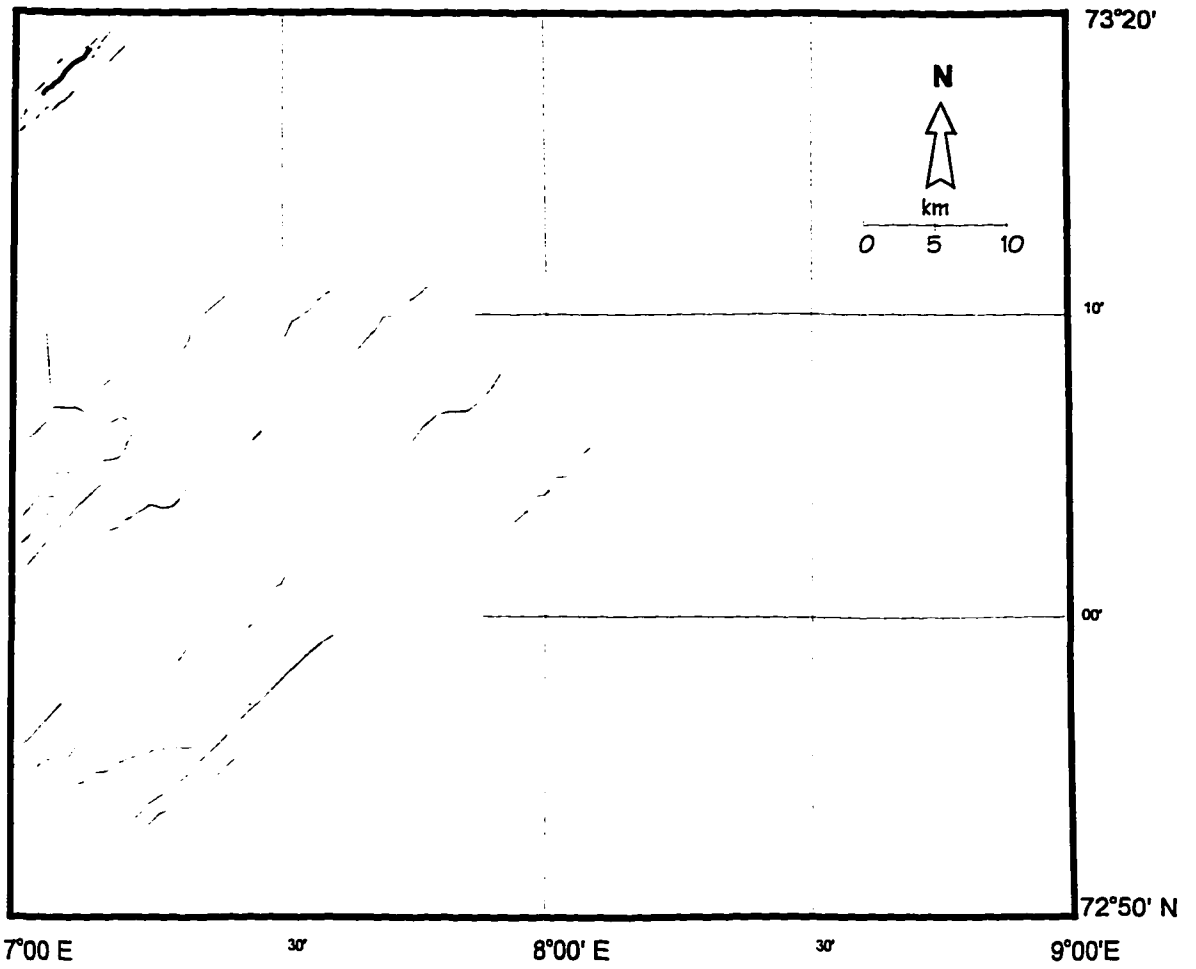

Figure 9B: Structural interpretation of faults and fissures from the side-scan image shown in figure 9A

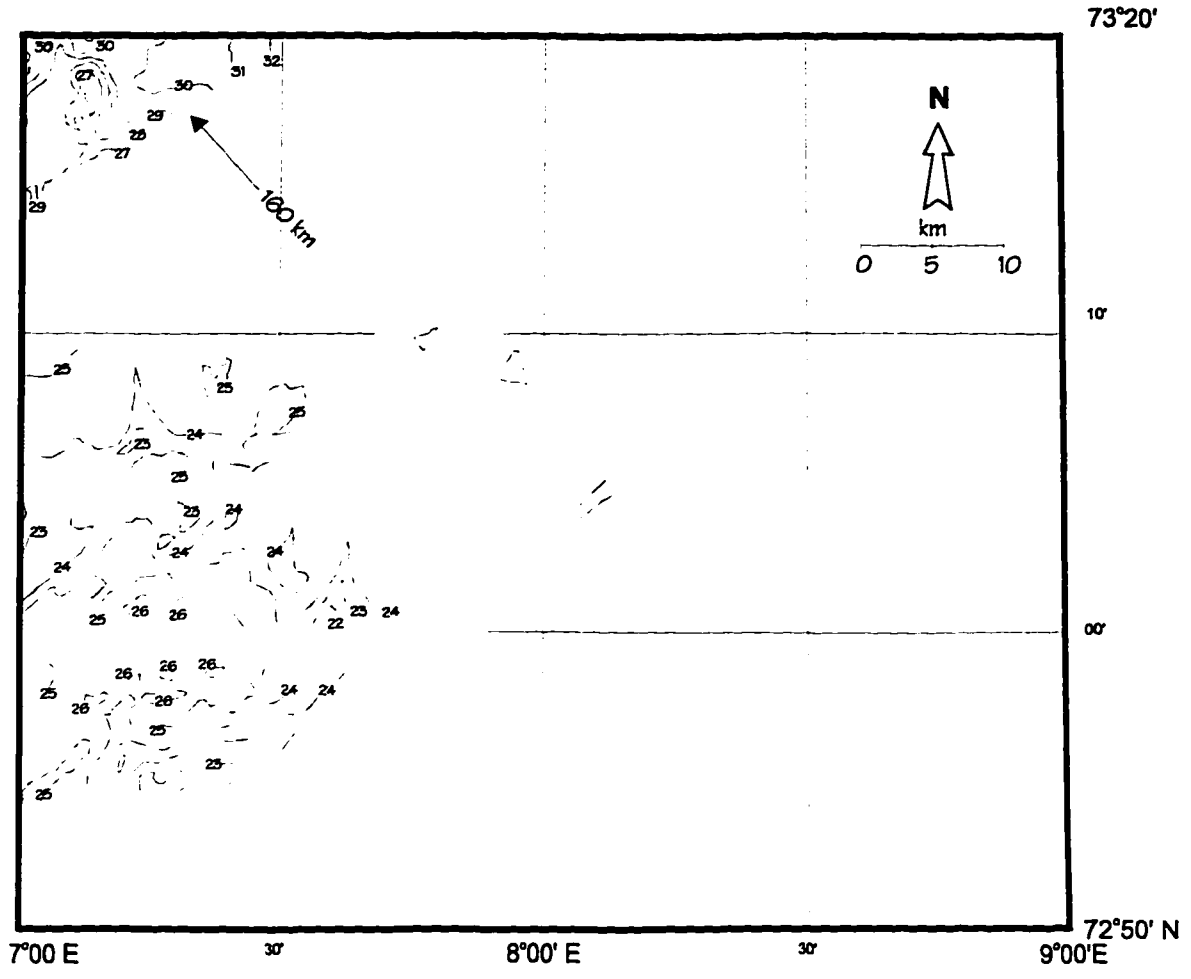

Figure 9C: Bathymetric contours in hundreds of meters corresponding to side-scan image shown in figure 9A.

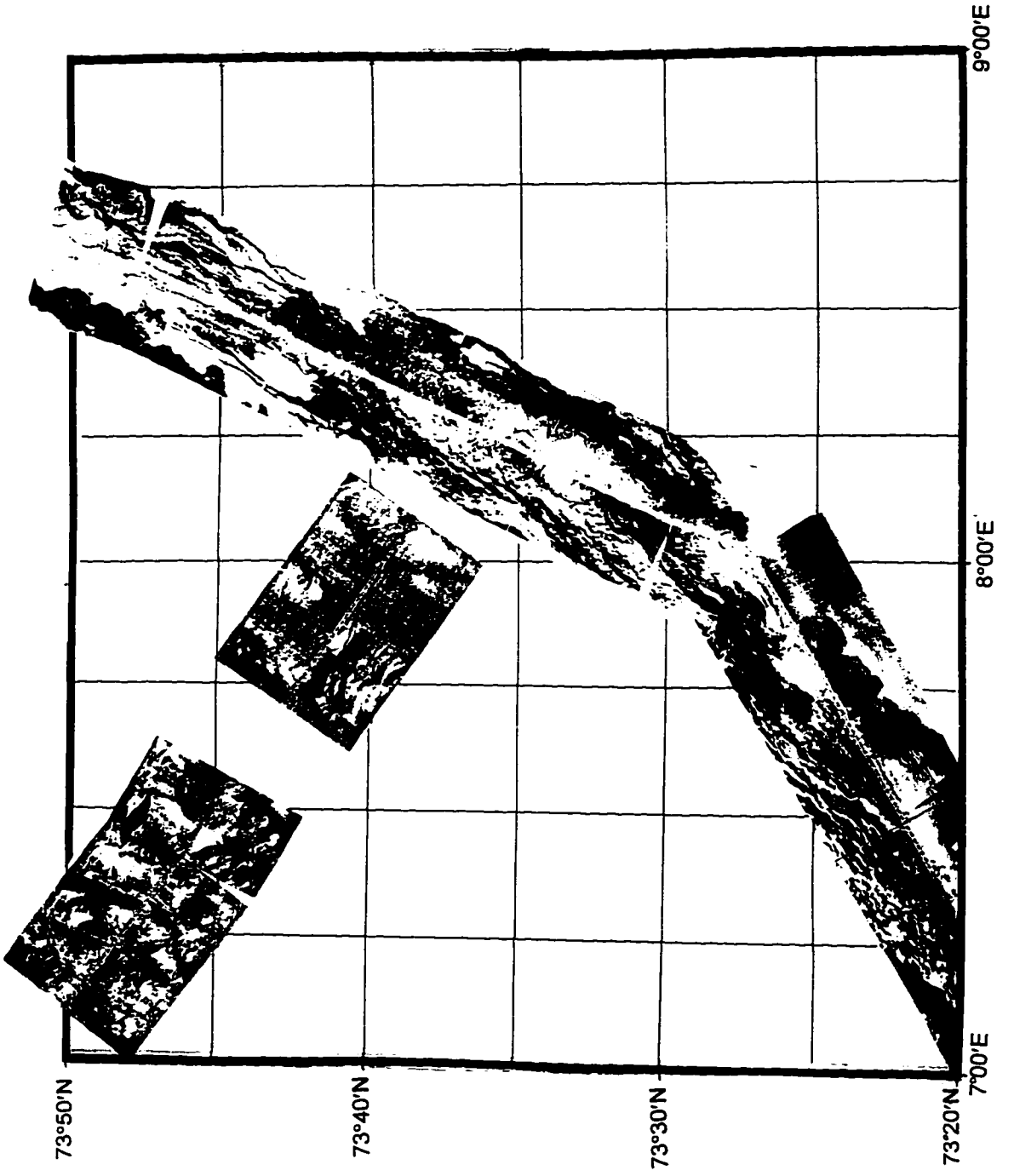

Figure 10A: SeaMARC II side-scan image of the Mohns Ridge from 73°20'N to 73°51'N. including the Mohns-Knipovich transition zone. A section of the western flank can be seen in the northwest part of the image.

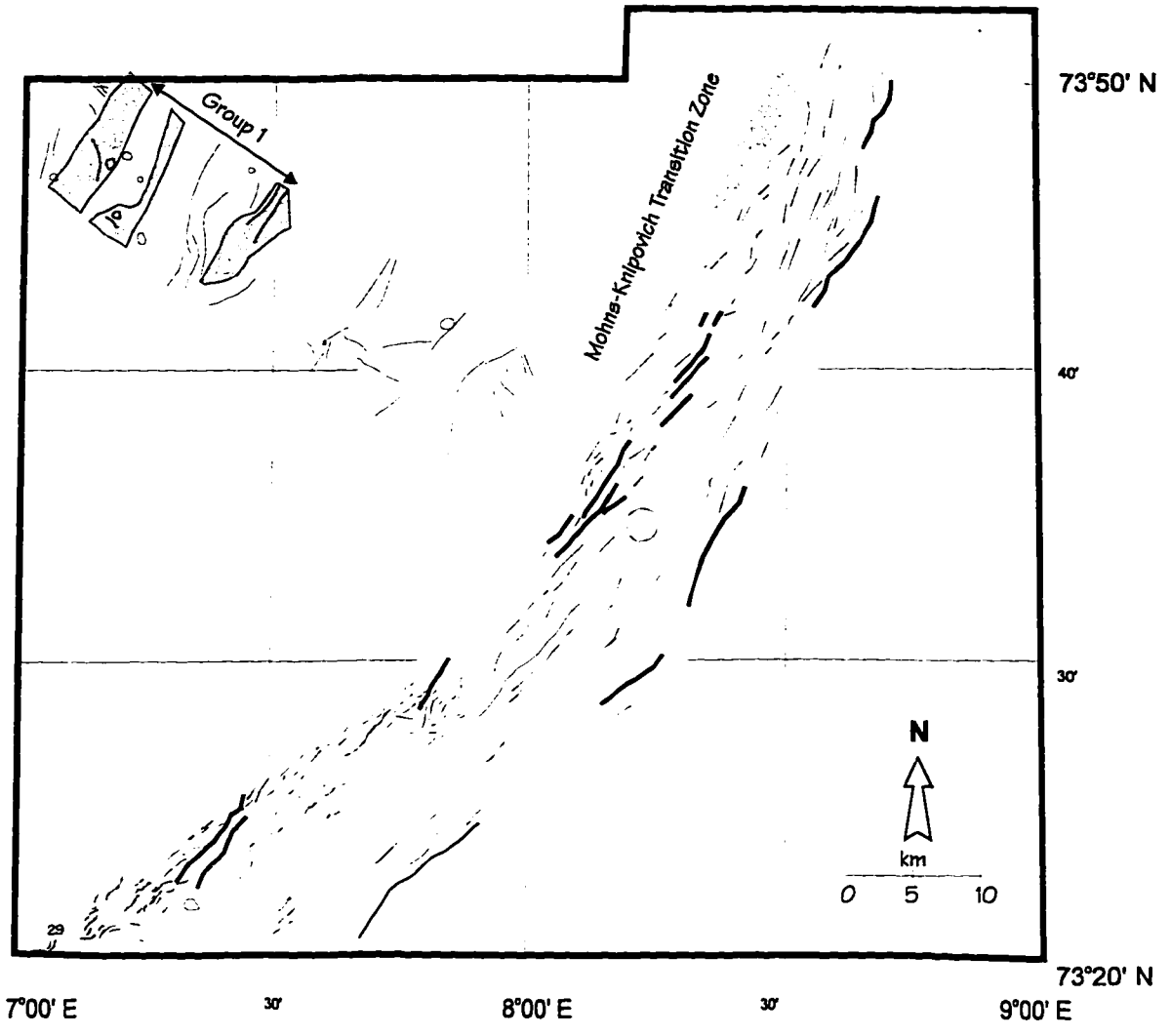

Figure 10B: Structural interpretations of side-scan image shown in figure 10A. Note the absence of any evidence of transform fault activity between the Mohns Ridge and Knipovich Ridge. Rift valley faults are nearly parallel to the rift valley in the transition zone. In the northwestern part of the map (in bold), Group 1 of the off-axial ridges is included. Note their orientation parallel to the rift valley.

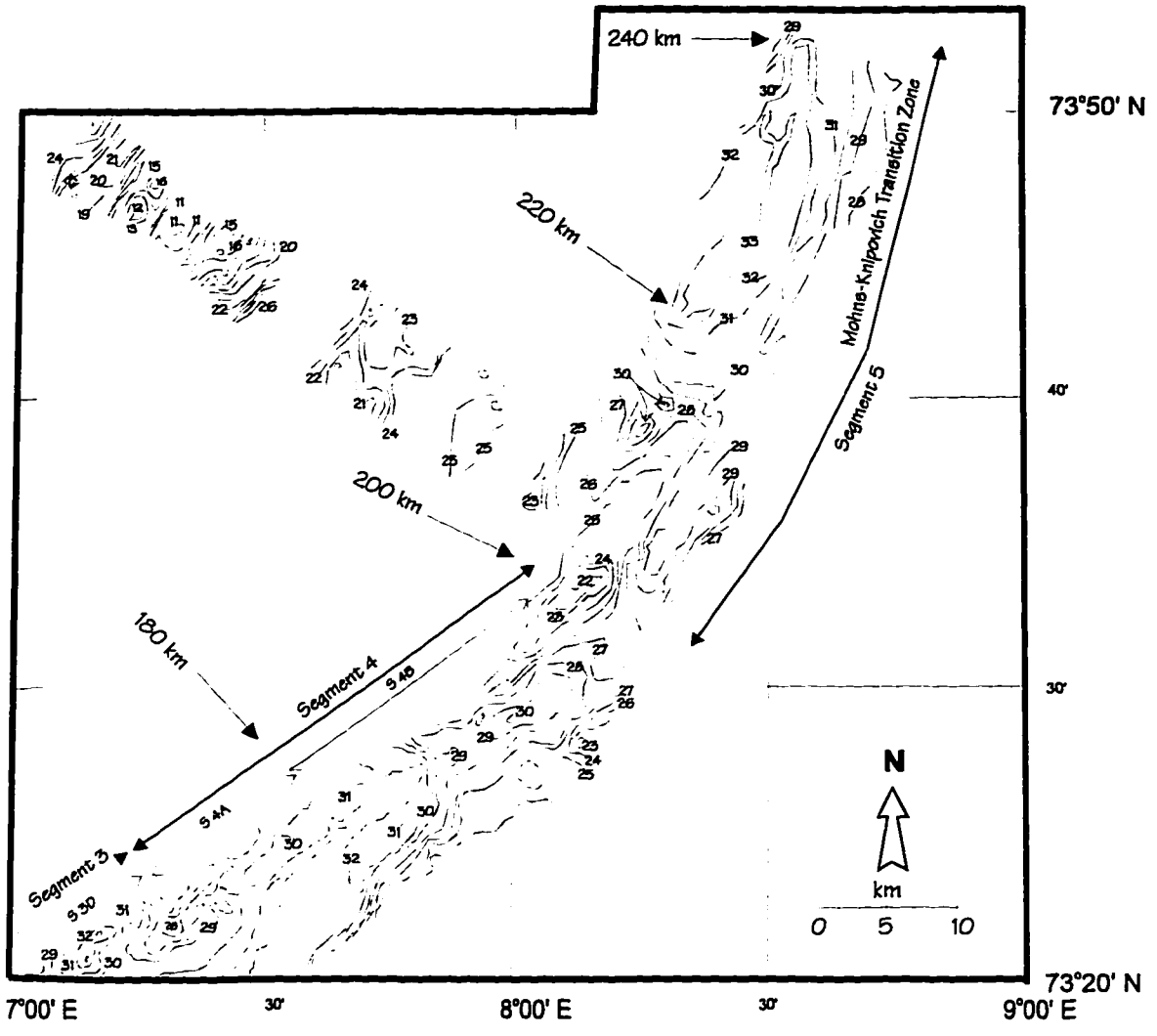

Figure 10C: Bathymetry corresponding to side-scan image shown in figure 10A. Note the continuity of the rift valley from the Mohns Ridge to the Mohns-Knipovich transition zone into the Knipovich Ridge. Third order segments 3D, 4A, and 4B, and second order segment 5 are shown.

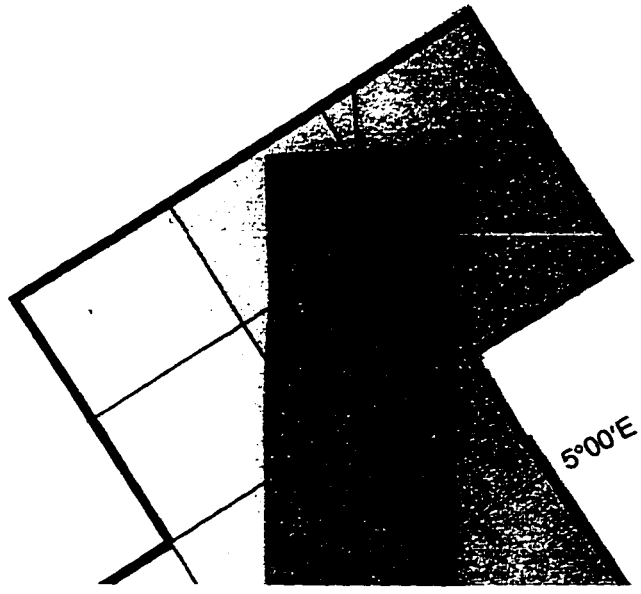

Figure 11A: SeaMARC II side-scan image of the western flank of the Mohns Ridge from 73°50'N to 74°25'N.

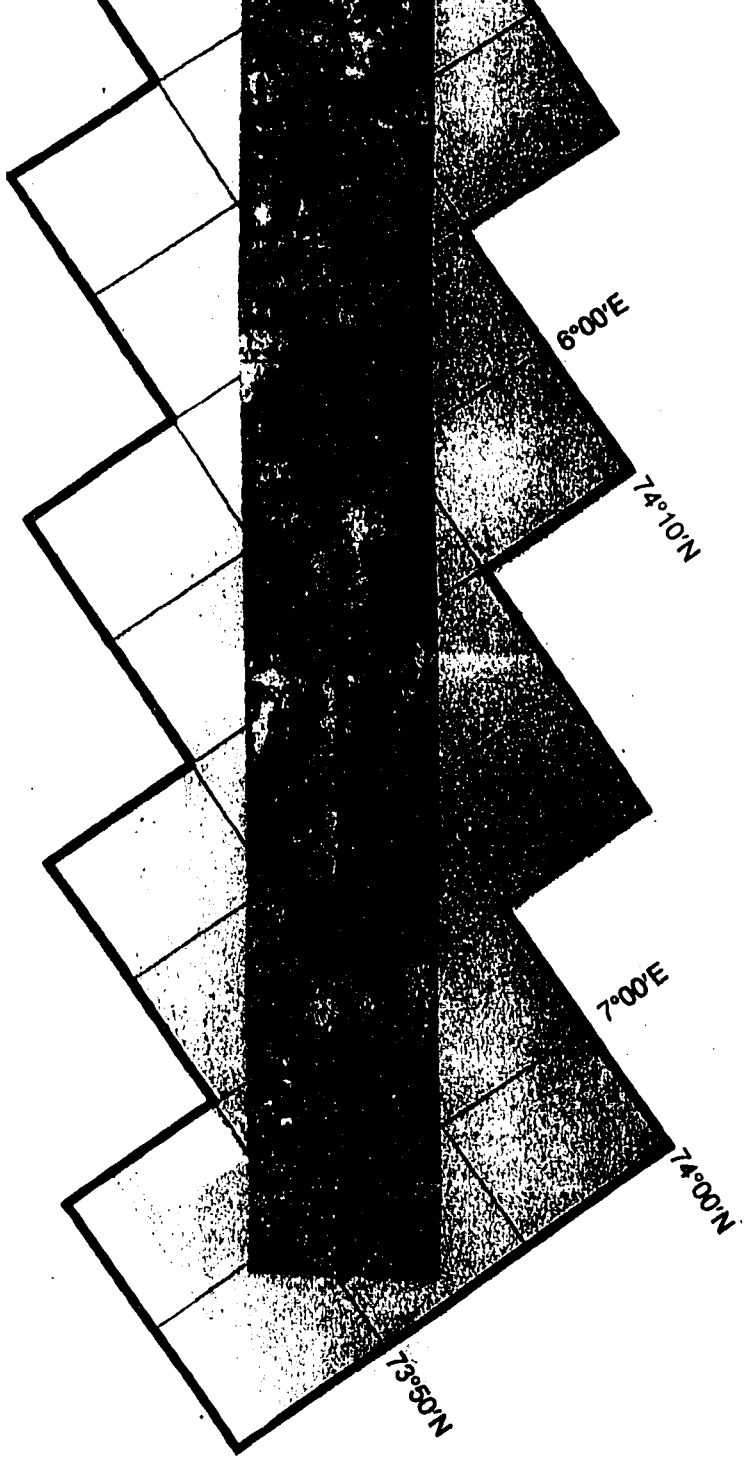

Figure 11A hns Ridge from 73°50'N to

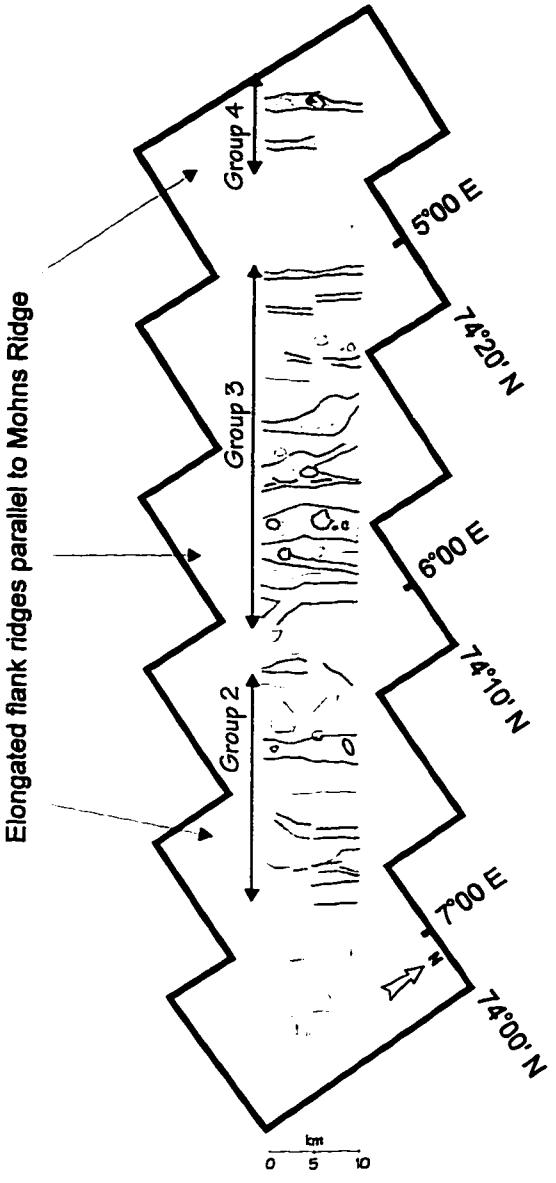

Figure 11B: Structural interpretations of the western ridge flank side-scan image shown in figure 11A. Note the off axial Mohns Ridge parallel fault block groups (2, 3, and 4)

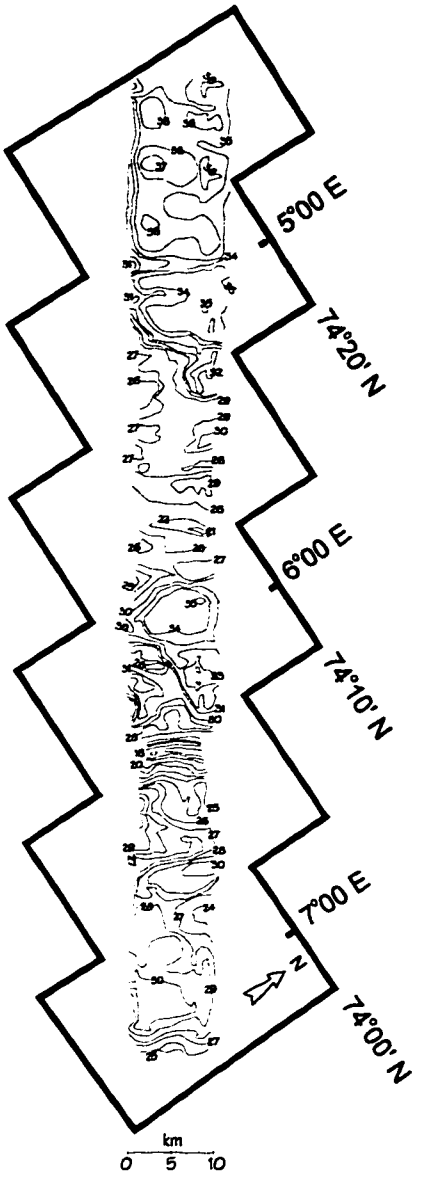

Figure 11C: Bathymetry corresponding to side-scan image shown in figure 11A. Contours in hundreds of meters.

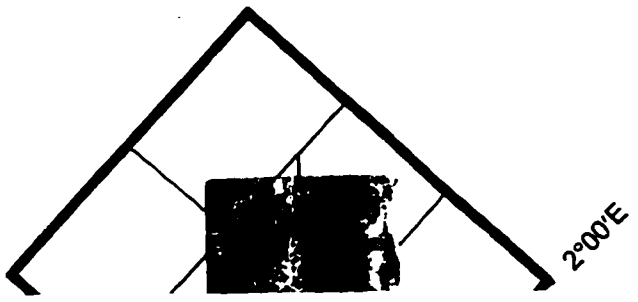

Figure 12A: SeaMARC II side-scan image of a section of the western flank of the Mohns Ridge from 74°15'N to 75°10'N.

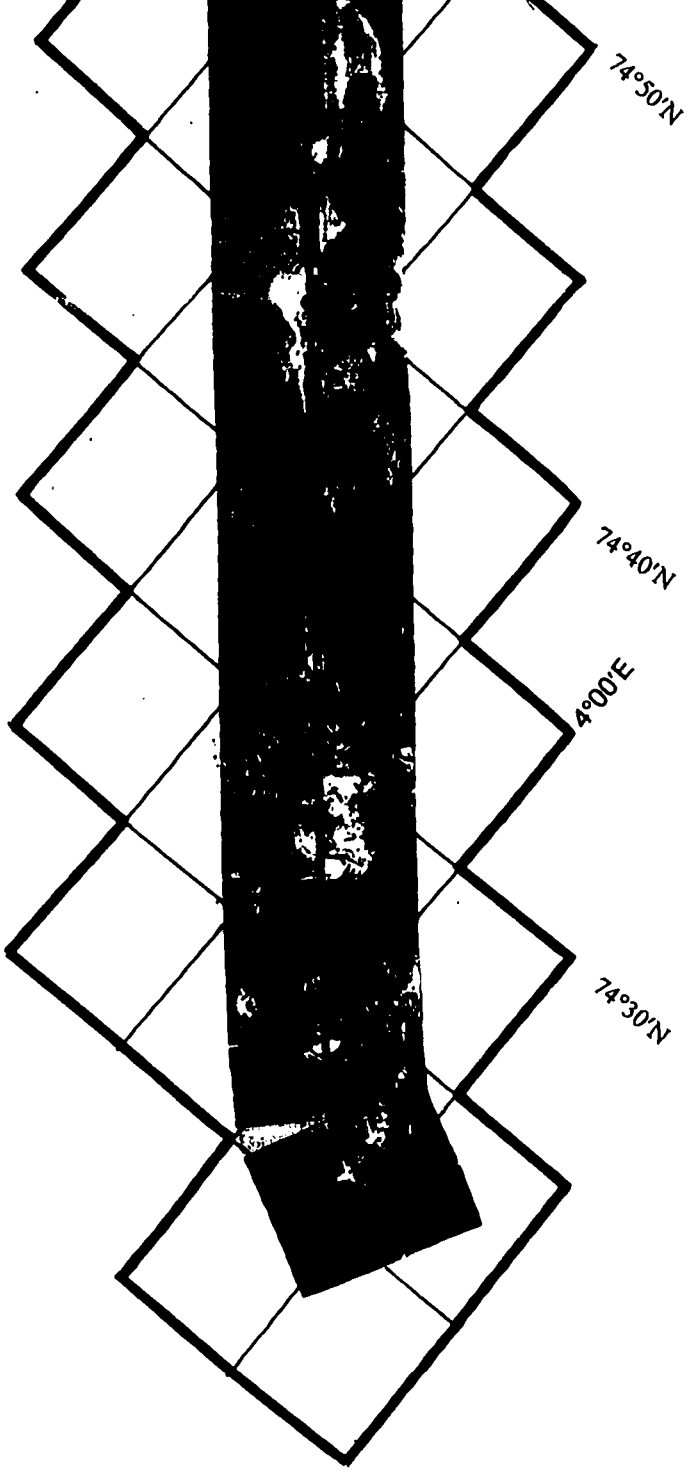

Figure 12A: Se f the Mohns Ridge from 74°

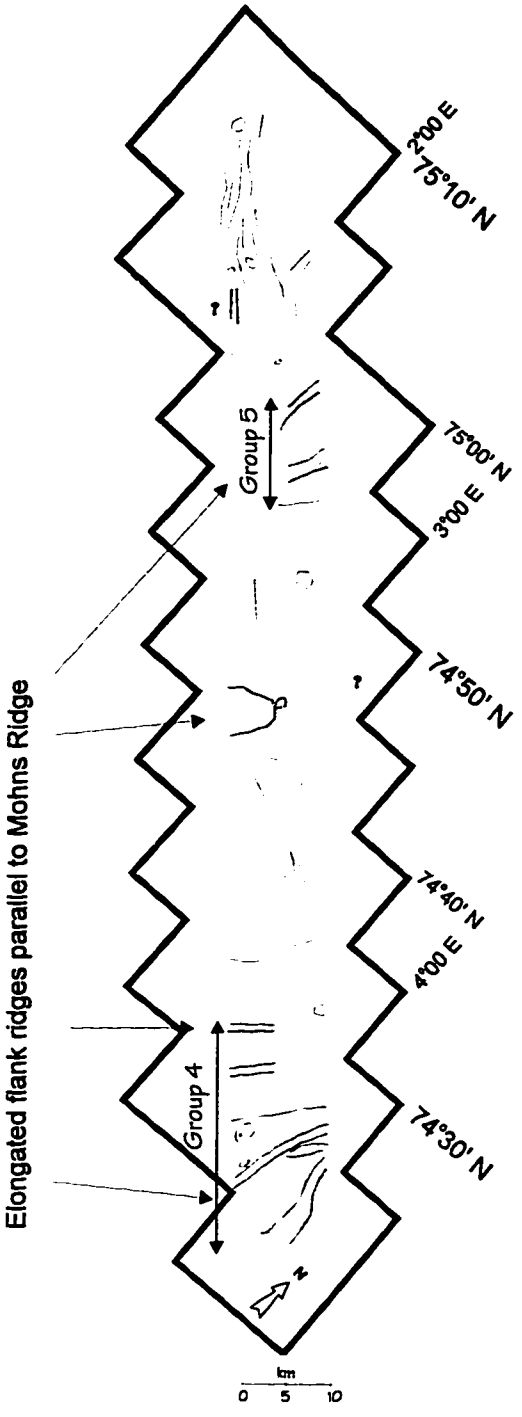

Figure 12B: Structural interpretation of side-scan image shown in figure 12A. Note the Mohns Ridge parallel fault block groups (4 and 5).

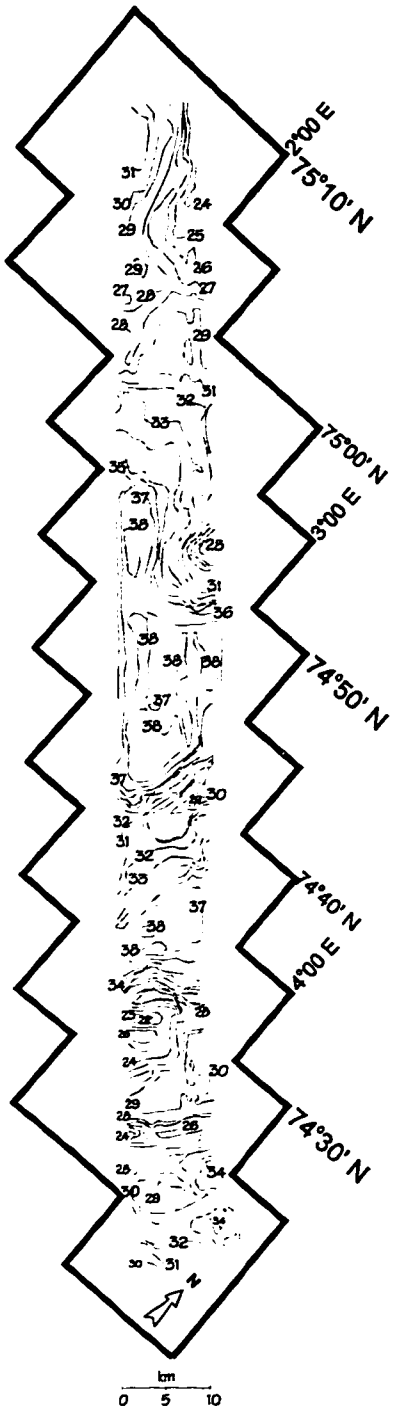

Figure 12C: Bathymetry corresponding to side-scan image in figure 12A. Contours in hundreds of meters.

Figure 13A: SeaMARC II side-scan image of the western flank of the Mohns Ridge from 75°05'N to 76°05'N). The western terminus of the Greenland Fracture Zone can be observed in the bottom of the image.

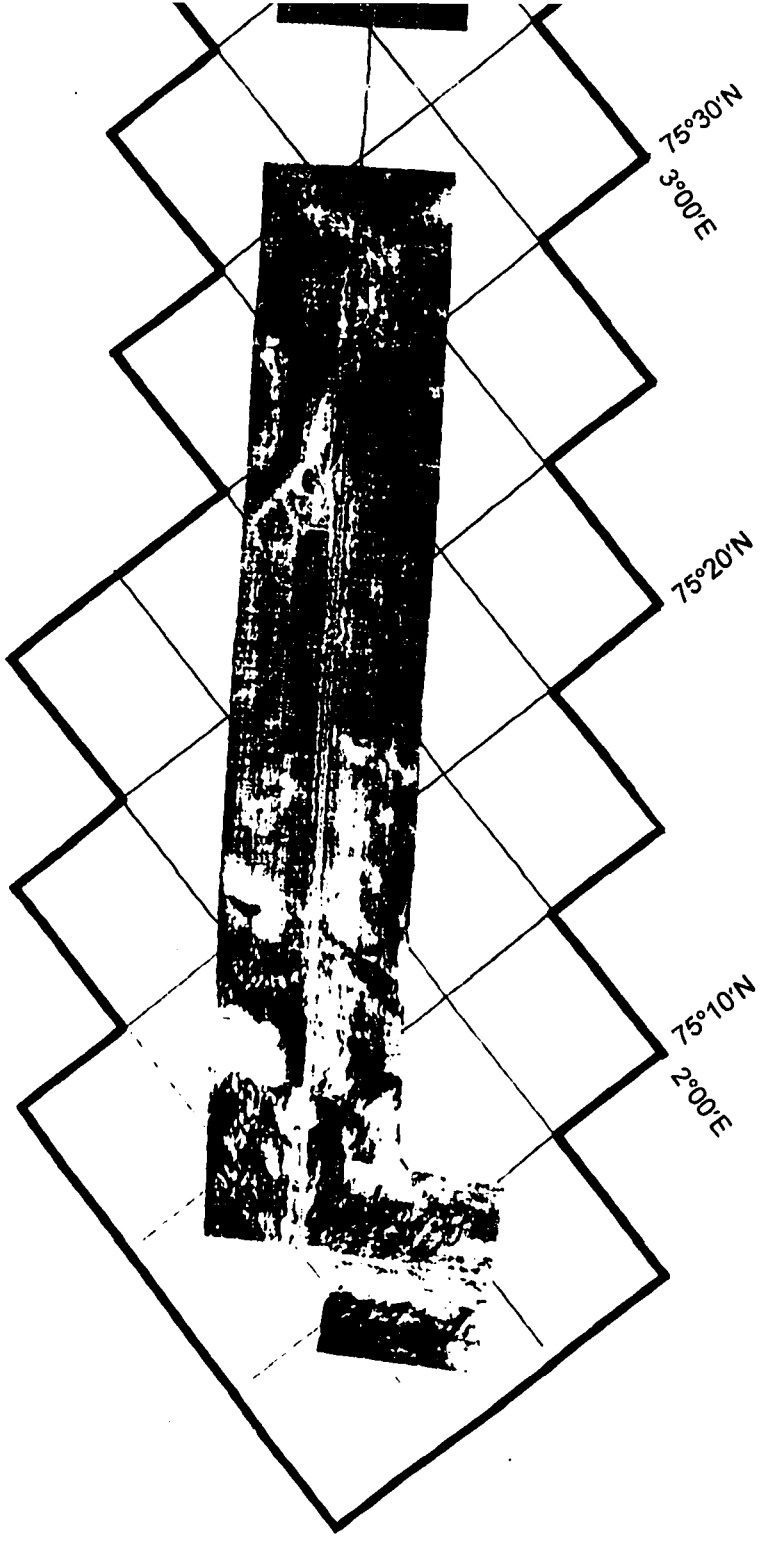

Figure 13/
75°05'N t
observed i

idge from
ıe can be

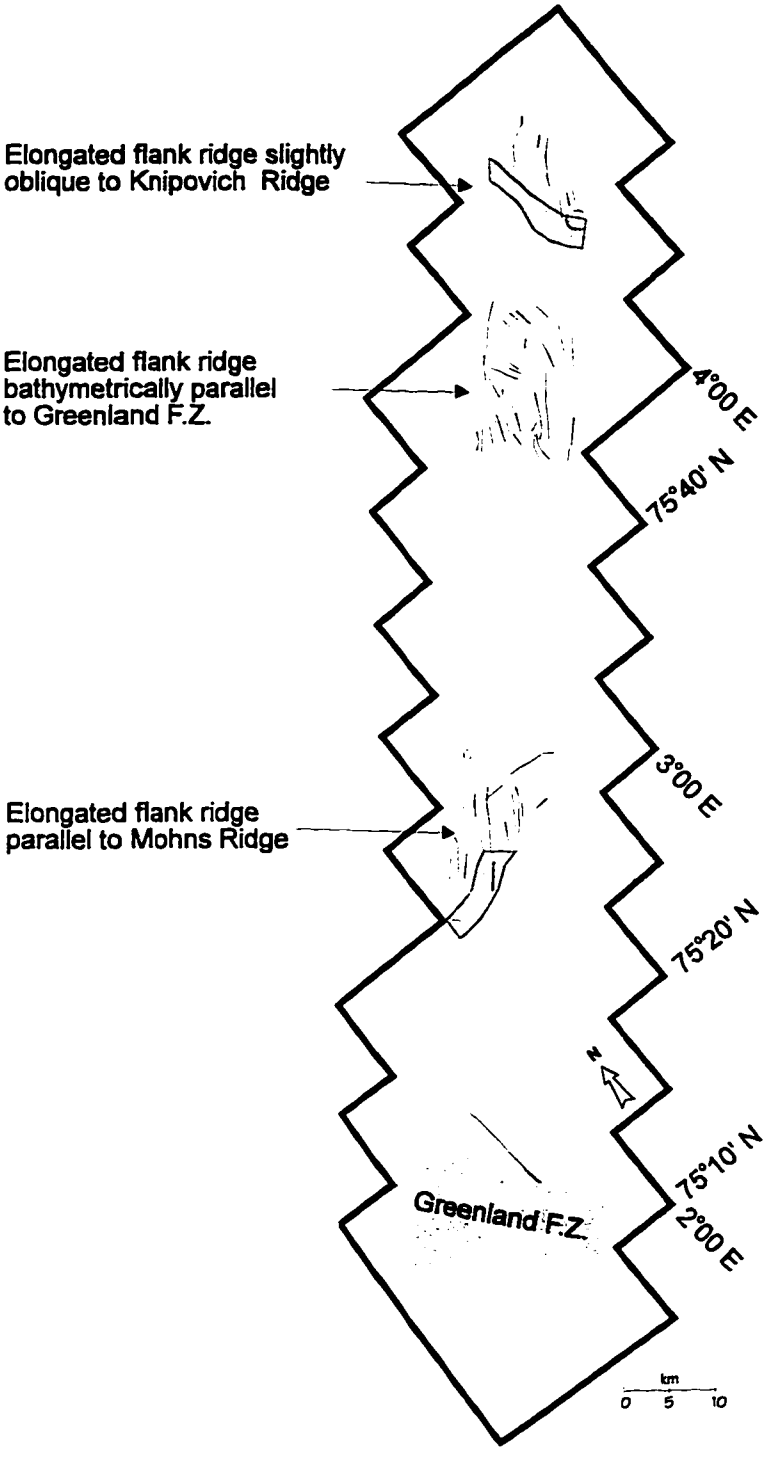

Figure 13B: Structural interpretation of the side-scan image shown in figure 13A. Contours in hundreds of meters.

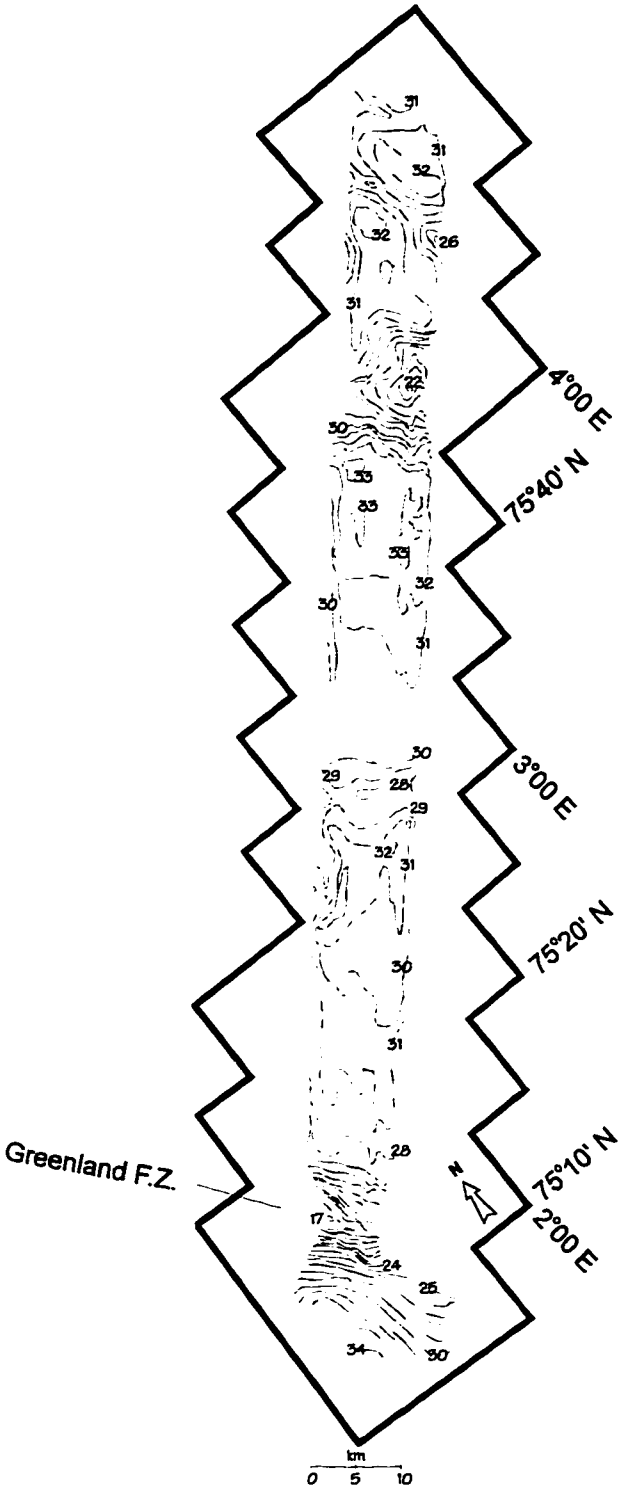

Figure 13C: Bathymetry corresponding to the side-scan image shown in figure 13A. Note the Greenland F. Z. and other the three smaller ridges that punctuate an otherwise flat seafloor of the Boreas Basin

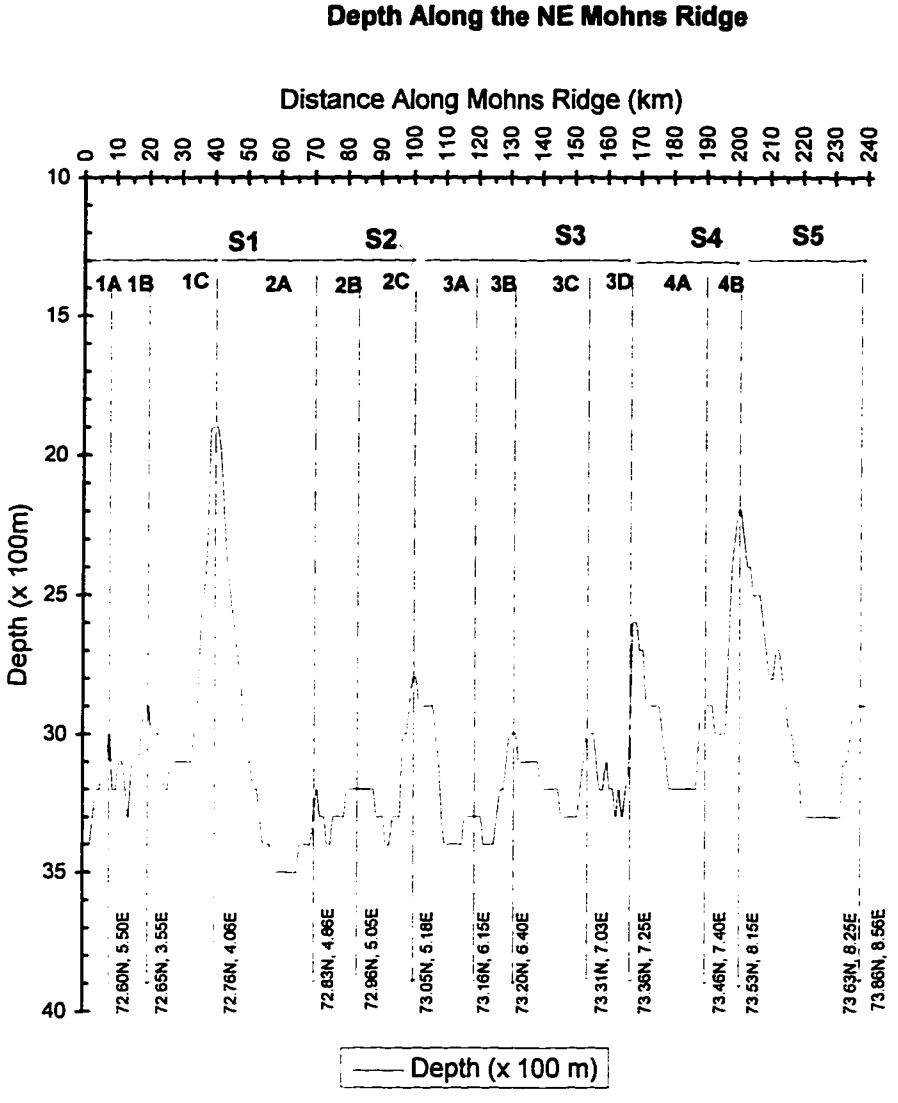

Figure 14: Chart showing depth along the inner rift valley of the Mohns Ridge. Second and third order segments are marked along the chart. Note the two volcanic discontinuities D 1-2 and D 4-5

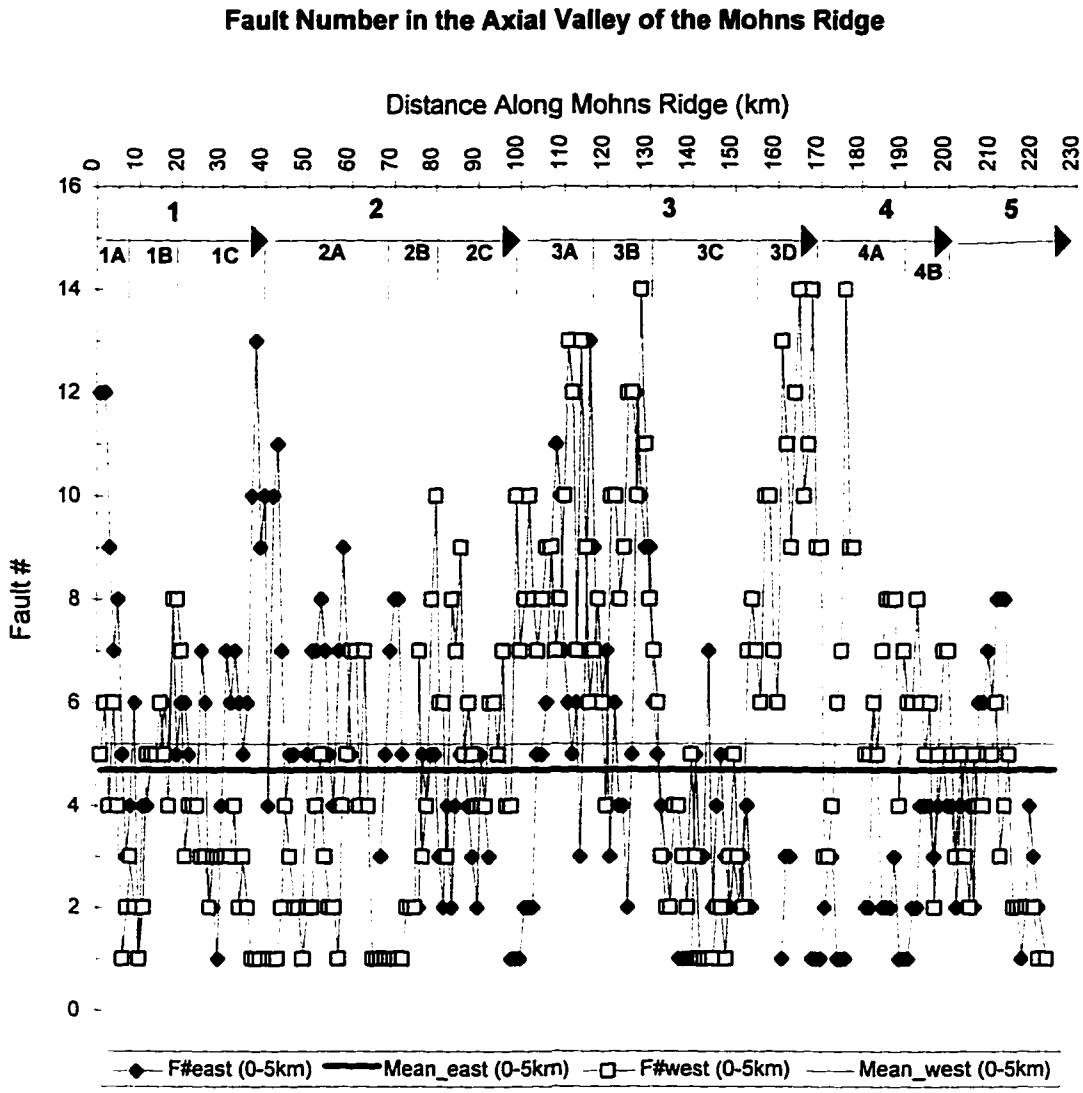

Figure 15: Fault number variability from south to north within the inner rift valley of the Mohns Ridge.

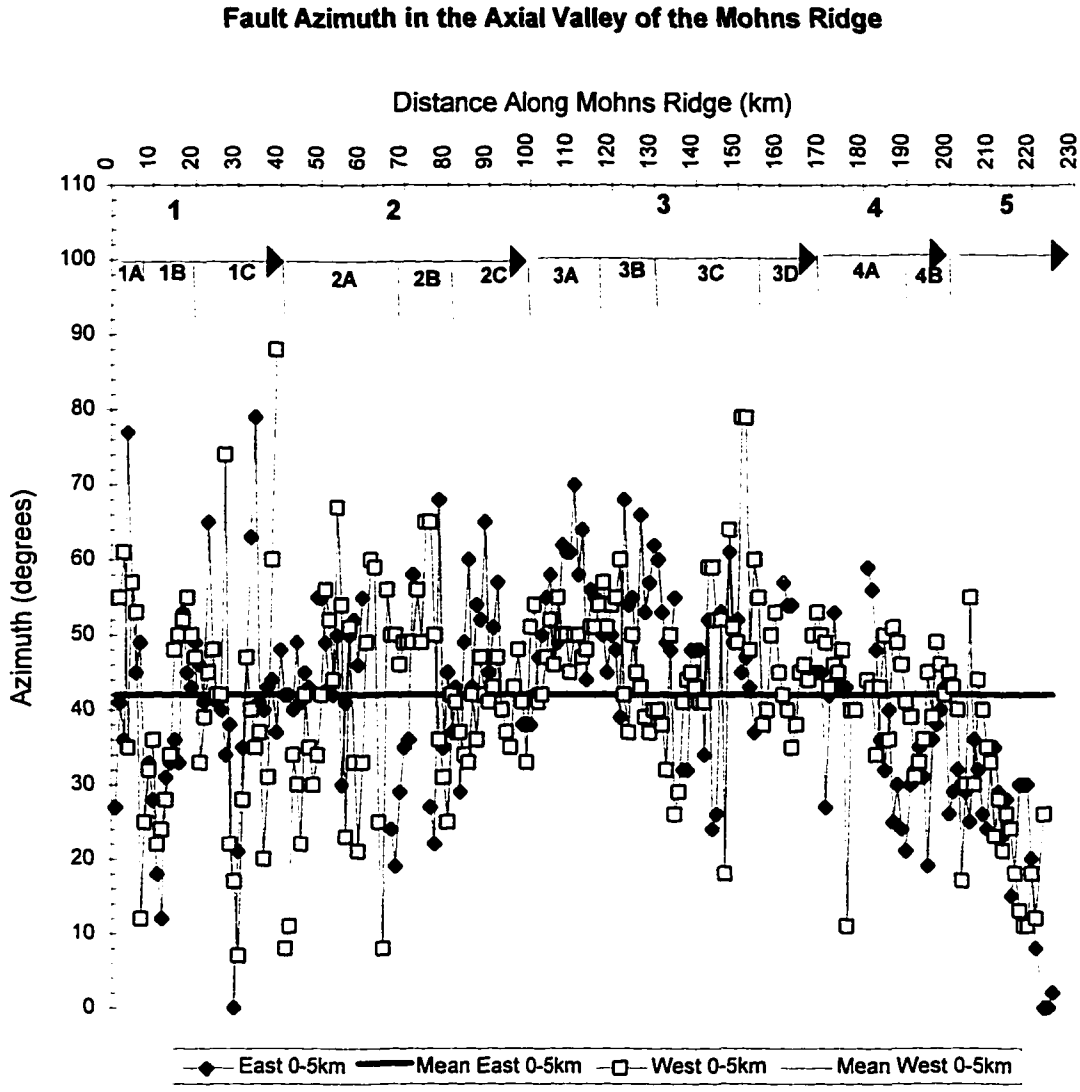

Figure 16: Fault azimuth variability from south to north within the inner rift valley of the Mohns Ridge.

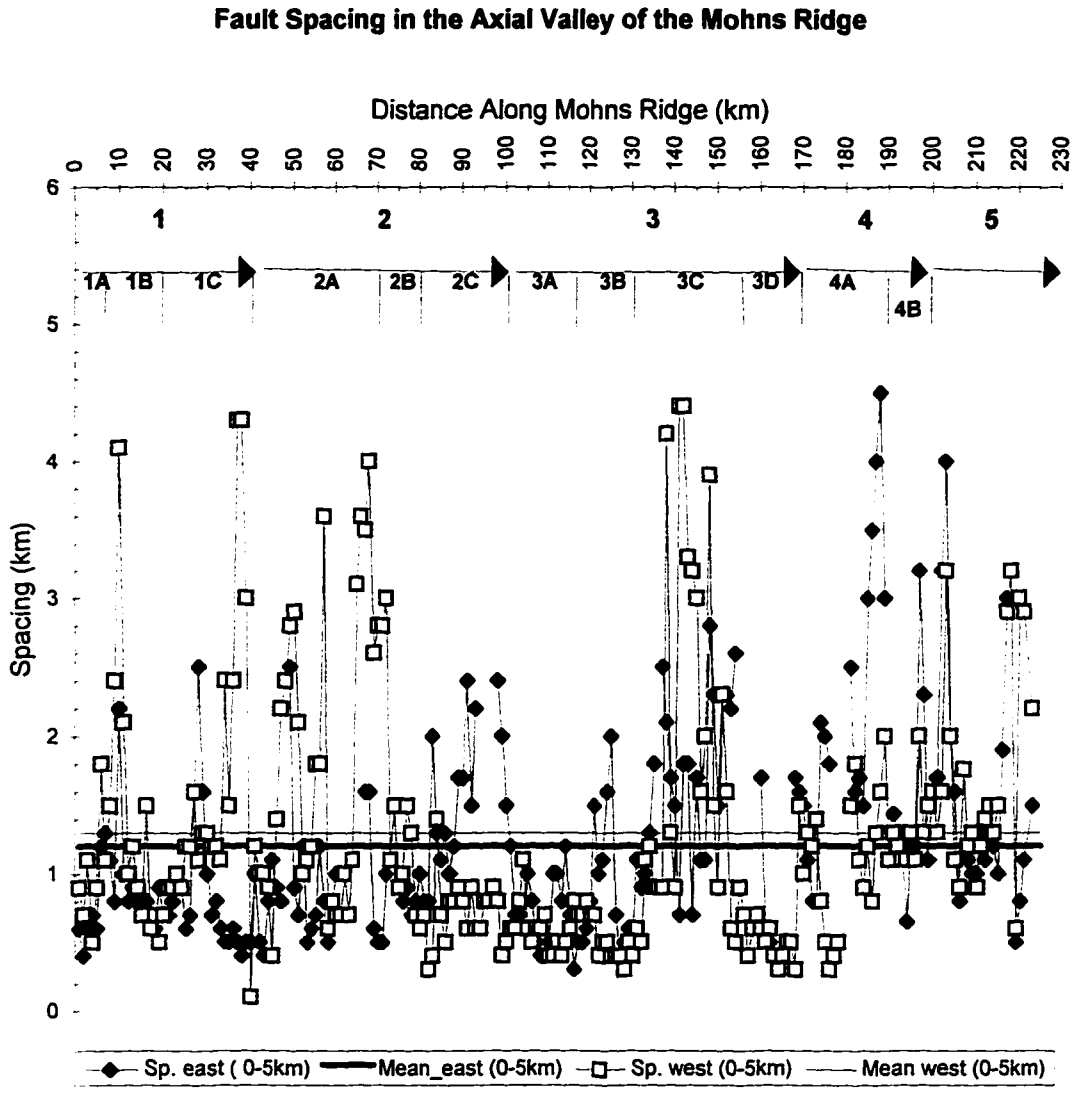

Figure 17: Fault spacing in the inner rift valley of the Mohns Ridge. By comparison, typical fault spacing for the Mid-Atlantic Ridge is 2.5-3 km and for the East Pacific Rise (0.5-1 km).

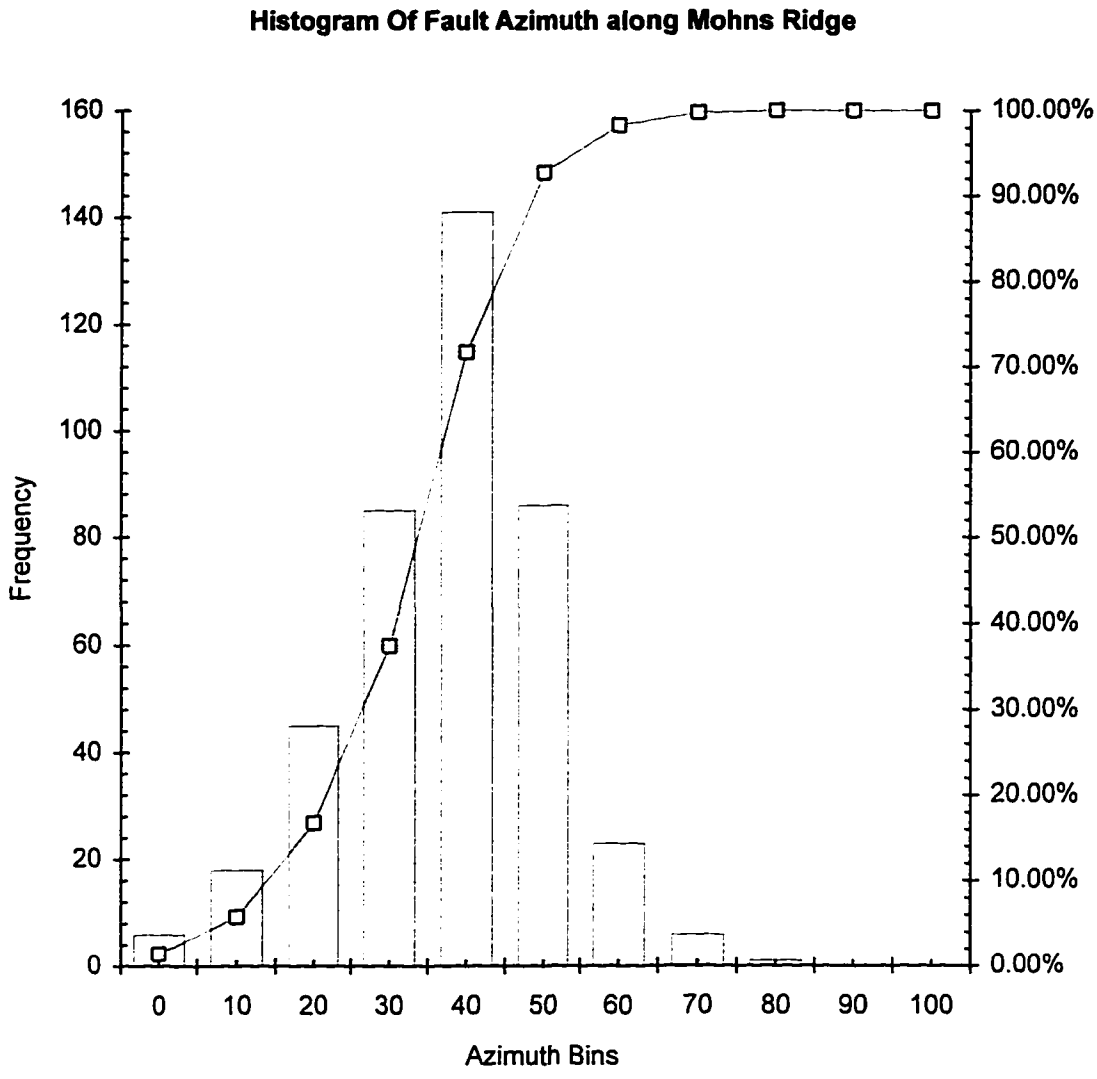

Figure 18: Histogram for all fault azimuths within the inner rift valley. Note the northwesterly (relative to the rift valley) trend of faults (72% of all faults are oriented 000 °-040°).

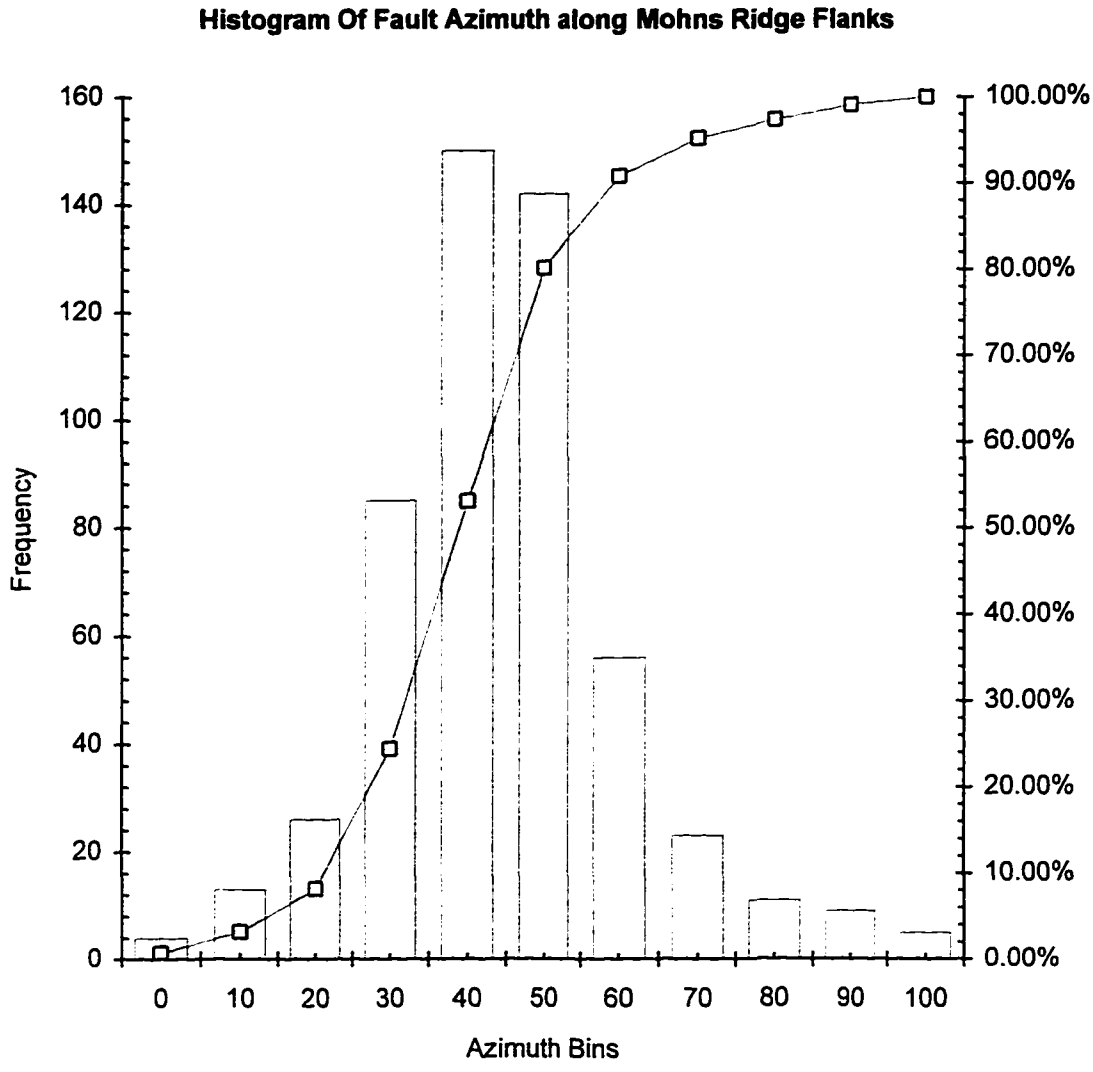

Figure 19: Histogram for all fault azimuths along the flanks of the Mohns Ridge. Note the northwesterly (relative to the rift valley) trend of faults (83% of all faults are oriented 000 °-050°).

CHAPTER 3

STRUCTURAL CONSTRAINTS IMPOSED BY THE PALEO-SPITSBERGEN SHEAR ZONE ON THE EVOLUTION OF THE KNIPOVICH RIDGE: A MODEL BASED ON SeaMARC II SIDE-SCAN SURVEY RESULTS FROM THE NORWEGIAN-GREENLAND SEA

H. Doss[1], K. Crane[1,2,3], P. Vogt[3], and E. Sundvor[4]

(1) Department of Geology and Geography, Hunter College, 695 Park Avenue, NY, NY 10021, USA

(2) Lamont-Doherty Earth Observatory, Palisades, NY 10964, USA

(3) Code 7420, Naval Research Laboratory, Washington, DC 20375, USA

(4) Department of Solid Earth Physics, University of Bergen, Allegaten 41, Bergen, Norway

(*) submitted for publication

Abstract:

Geophysical signatures in the Norwegian-Greenland Sea have long been a puzzle when compared to other ocean basins. Along most mid-ocean ridges such as the Mid-Atlantic Ridge, seismic activity is concentrated in a narrow continuous belt coinciding with the rift valley axis. In contrast, seismic activity in the northern Norwegian-Greenland Sea Basin is diffuse, with the majority of events located on the eastern flank of the Knipovich Ridge extending onto Svalbard. Zebra-style magnetic anomalies which are common in most ocean basins are remarkably lacking in the northern Norwegian-Greenland Sea. Heat flow is noticeably higher in the eastern Norwegian-Greenland Sea compared to the western side of the basin. Using data obtained from the SeaMARC II side-scan sonar system, we present a model that may help explain these anomalies. Numerous seamount chains which obliquely cross the Knipovich Ridge and lie nearly parallel to its spreading direction are interpreted to be the result of magma upwelling into an ancient splinter faults associated with the Paleo-Spitsbergen Shear Zone. This model suggests that the Knipovich Ridge evolved through time by propagating from the south into the ancient Spitsbergen Shear Zone and was trapped in one or more of the complex fault systems associated with the paleo-shear zone. Later evolution of the midocean ridge was constrained by secondary faulting oblique to the ancient shear zone. The model presented here suggests that paleo fracture-shear zones may control the opening geometry of mid-ocean ridges for tens of millions of years after initial rifting occurs.

Introduction:

The Mid-Atlantic Ridge can be traced through Iceland into the Norwegian-Greenland Sea as the Mohns and Knipovich Ridges of which the latter is oriented 70° oblique to the axis of the former (figure 1). The northern Knipovich Ridge lies in close proximity to the continental margin of the Svalbard Archipelago (figure 1), thereby unequally dividing the northern Norwegian-Greenland seafloor into the eastern Svalbard margin and the western Boreas Basin. At approximately 78°30'N, the Knipovich Ridge rift valley terminates against the Molloy Fracture Zone underneath thick layers of terrestrially and in part biologically derived sediment.

The Knipovich Ridge is thought to be connected to the slow-spreading Nansen Ridge in the Arctic Ocean by a remnant of the Paleo-Spitsbergen Shear Zone (figure 1). It is believed that transtension across this shear zone has led to the creation of several short spreading centers (pull-apart basins) (Crane et al., 1982; Thiede et al., 1990 and Crane et al., 1991) of which the Molloy Deep-Rift is an example. In addition, the more northwesterly section of the Spitsbergen Shear Zone is thought to be undergoing leaky transtensional opening, creating the Lena Trough in the process (figure 1) (Talwani and Eldholm, 1977; Sundvor and Eldholm, 1979; Crane et al., 1982; Eldholm et al., 1986; and Vogt, 1986).

The intricate geometry of the plate boundary, probably dominated by transtension and transpression, is accompanied by an array of off-axial structures that are non-linear and do not trend either orthogonal or parallel to the present day plate motion. These fault blocks and abyssal hills are thought to have been deformed by the substantial deviatoric stress

generated across this young plate boundary which was constrained in its early history by inherited structural zones of weakness cutting across former continental crust (Crane et al., 1988 and Crane et al., 1991). Some of these off-axial features are thought to represent: (1) slivers of continental crust separated from the margin by transtension or, (2) fossil transform ridges and troughs which became deactivated as the spreading center propagated northward and the stress field changed from transpression to transtension while the crust underwent rotation, tilting, and bending. Finally, volcanic seamounts were created by ponding and leaking of magma into formally active shear zones leaving linear and oblate hills strewn across the abyssal plain (Crane et al., 1991).

The complexity of the plate boundary in the Norwegian-Greenland Sea reflects the complex opening history in this area. Seafloor spreading in the Norwegian-Greenland Sea and the Arctic Ocean started at approximately anomaly 24 (approximately 54-56 ma. on the Cande et al., (1992) time scale) (Vogt et al., 1974, and Talwani et al., 1977). In addition, relative motion between Svalbard and Greenland during the early period was oriented northeast to southwest, with no apparent crustal extension to the north. The plate boundary between the incipient Norwegian-Greenland Sea and the Arctic Ocean was located instead along the broad regional continental Spitsbergen Shear Zone (also called the de Geer Zone) (Johnson et al., 1967; Harland, 1969; Horsfield et al., 1970; Eldholm et al., 1978; Talwani, 1977; Eldholm, 1980; Vogt et al., 1981; Crane et al., 1982; Dore et al., 1987; Crane et al., 1988)

A change in plate motion is thought to have occurred at about anomaly 13 (34 ma.) as a result of a change in the pole of rotation that increased the east-west component of

opening. This marked the beginning of seafloor spreading in the northern Norwegian-Greenland Sea forming the Knipovich Ridge in the process (Talwani et al., 1977) (figure 2). Crane et al. (1988 and 1991) and Okay et al. (1993) proposed that the Knipovich Ridge propagated to the north along one of the major faults which comprised the Paleo-Spitsbergen Shear Zone.

Geophysical Signatures of the northern Norwegian-Greenland Seafloor:

From an analyses of well developed magnetic anomalies across the Mohns Ridge, Talwani and Eldholm (1977) calculated an average half-spreading rate of 0.45 cm/yr (28 to 20 mybp) for this plate boundary. In contrast, the magnetic field is generally quiet over most of the entire Boreas Basin adjacent to the Knipovich Ridge (figure 3) (Sundvor and Eldholm, 1979) making it difficult to determine spreading rates from the magnetic anomaly time scale. Vogt et al., (1982 and 1986) have tentatively identified anomalies 5 and 6 on the western flanks of the Knipovich Ridge (concluding a half-spreading rate of 0.32 cm/yr for the period 36 to 13 mybp). They also suggested that additional anomalies may be identifiable. As figure 3 illustrates, magnetic anomalies are chaotic adjacent to the Knipovich Ridge compared with more normal anomalies along the northeastern section of the Mohns Ridge (Kovacs et al., 1987). Further north, the Nansen Ridge in the Arctic Ocean is characterized by predictable magnetic anomalies as well. Possible mechanisms to explain the chaotic magnetic signatures in the Norwegian-Greenland Sea include thermal blanketing by sediments in the rift valley combined with a wide diffuse zone of injection (Eldholm et al., 1978; and Vogt, 1986), fragmentation due to excessive axial shifting and short lived transforms, and slow oblique spreading (Vogt et al., 1981).

Using heat flow data, Crane et al., (1988) determined a half-spreading rate of 0.45 cm/yr. at 75°N and 0.15 -0.31 cm/yr. at 78°N. However, if these spreading rates are correct, they would violate rigid plate tectonics of the area. Crane et al., (1991) revised these spreading rates for the northern Knipovich Ridge after analyzing more than 100 heat flow stations. They determined that spreading was very asymmetric at a rate of approximately 0.7 cm/yr. to the northwest and 0.1 cm/yr. to the southeast.

Stein et al., (1977) proposed that spreading rate asymmetry could develop when one of the two diverging plates travels faster with respect to the deeper mantle. Thus more crust will be accreted to the slower plate. Minster and Jordan (1978) and Morgan (1981) have suggested that the North American plate has moved much more rapidly than the quasi-stationary Eurasian plate. This would seem to refute the Stein et al. (1977) hypothesis, because crust is apparently accreting more rapidly on the faster North American side (Vogt et al., 1982 and Crane et al, 1991).

Seismic asymmetry is also very pronounced across the Knipovich Ridge, with a region of anomalous seismic activity extending from Nordaustlandet west to the Knipovich Ridge. In contrast, the western Boreas Basin is nearly aseismic. Unfortunately, to date, very few focal depths have been established. However, first motions have been determined for several earthquakes on Svalbard (Chan and Mitchell, 1985). They indicate sinistral strike-slip motion on E-SE striking faults which are fairly oblique to all of the known major faults in the region. This seismic asymmetry across the Knipovich Ridge suggests widespread tectonic intraplate deformation on the Eurasian plate.

Along the Knipovich Ridge a belt of well defined gravity minima can be found in the rift

valley (figure 4) (after Sobczak et al., 1990). The axial gravity anomaly is semi-continuous from the Mohns Ridge to about 76°N where it is right-laterally offset. The continuity of the anomaly suggests a regionally continuous ridge without major offsets. Along the Knipovich Ridge, the western flank has free air gravity values of 10 to 20 mGal higher than the eastern flank (Vogt, et. al., 1982). However, adjacent to the southern Knipovich Ridge, the free air gravity field of the western flank is as much as 60 mGal higher than the eastern flank (figure 4).

Doss et al. (in preparation) suggest that the Mohns-Knipovich transition occurs without any transform faults or rift valley adjustment. Furthermore, large scale oblique compression which was thought to occur on the western side of the transition zone (Crane et al., 1988 and 1991) was lacking or not present. They explained the lack of compressional structures on the inside part of the Mohns-Knipovich bend as an indication that the Knipovich Ridge is obliquely spreading. Their conclusion agrees with Vogt (1986) who used tentative magnetic anomalies (figure 5) and bathymetric flowlines (figure 1) to suggest that the Knipovich Ridge is spreading obliquely.

Instrumentation and Data:

The primary tool used for the surveys was the SeaMARC II which was outfitted on the Norwegian research ship "R/V Haakon Mosby". The SeaMARC II is a shallow tow, long range, high resolution seafloor mapping system with the capability of simultaneous recording of digital side-scan sonar images as well as bathymetry across a swath of ensonified seafloor. Bathymetry is determined by measuring phase differences of acoustic arrivals on each of two pairs of transducer arrays, one on each side within the tow vehicle.

For deep ocean surveys, it is towed at a depth of approximately 100 m below the surface, which allows it to avoid the high sound velocity gradients near sea surface (Shor, 1990). The system operates at 11 kHz on the port side and 12 kHz on the starboard side. A drogue is attached to the slightly positively buoyant sonar vehicle, providing stability of about 1° in roll and 2-3° for pitch and yaw.

For seafloor depths greater than 1.0 km, the side-scan sonar subsystem is configured to produce a swath of data 10 km wide. Bathymetric data are recorded from nadir to a maximum angle of 60° (a maximum bathymetric swath equal to 3.4 times water depth). The bathymetric swath width is independent of the side-scan swath setting.

The SeaMARC II side-scan images contain 1024 pixels of digital data on either side of the swath with the inner 40 pixels not logged (to avoid interference from multiple sound signals). The individually logged reflectivity values are placed at even spacing across the track, the bottom being assumed planar and equal to the depth directly below the towfish. Pixel spacing was 5 m for the 10 km swath width configured for these surveys. Along-track resolution is a function of the beam width of the system, which is nominally 2° (about 3% of slant range) and therefore widens towards the outer edge of the swath. Side-scan data are slant-range corrected to water depths below the vehicle at the time of collection.

During our 1989 survey, the speed was mostly in the 7-10 knots range, with slower speeds used when maneuvering around or avoiding ice floes (north of latitude 78°30'N). In contrast, the 1990 survey encountered several periods of very rough weather (high sea-

state) and system problems occurred. There were several days when the speed averaged less than 1 knot, and the tow vehicle had to be recovered for repairs.

The area covered by the SeaMARC II survey encompasses the entire Knipovich Ridge rift valley, the western ridge flank of the Knipovich Ridge from 76°45'N to the Molloy Transform Fault (extending west and away from the rift valley to a maximum distance of approximately 45 km), the eastern ridge flank of the Knipovich Ridge from 76°15'N to the Molloy Transform Fault (extending east and away from the rift valley to a minimum depth of approximately 1000 m near the continental margin, the Molloy Transform Fault, the Hovgård Ridge, and the eastern part of the Boreas Basin (figure 6).

Data Interpretation:

The emphasis of this study is on fault azimuth variation on the eastern and western flanks of the Knipovich Ridge. Using increments of 5 km, east and west of the rift valley axis and north of 76°00'N (where there is flank coverage), we recorded fault azimuth variation of all faults along each latitude. We make one important assumption in this study that applies to long faults (several kilometers to greater than 20 km). Changes in a given long fault orientation are the result of a pre-existing stress field and not the result of more popular hypotheses that attempt to relate them to rift valley processes. This assumption is based on two factors; firstly, Doss et al. (in preparation) conclude that present-day rift valley segmentation along the Knipovich Ridge does not appear to influence faulting on its flanks. Secondly, clusters of short faults are most often oriented oblique to the rift valley and located on the near-axial flanks.

Figures 6-10 illustrate that faults on the Knipovich Ridge and along its flanks vary widely in orientation. In conducting our analyses, we used the DeMets et al. (1990) oblique spreading direction of ~305° as a benchmark for the Knipovich Ridge. In addition, when multiple faults were found in a 5 km section, the average fault azimuth was calculated.

Fault Azimuth Analysis:

Based on the above criteria, we can now present faults in the northeastern Greenland Sea with major orientation changes between 76°00'N and 78°35'N. This data is summarized in tables 1-9 and is based on the charts in figures 11-19.

Table 1: Section 0-5 km east and west of the inner rift valley (figure 11A):

Section 0-5 km East of Rift Valley	Fault Azimuth		Section 0-5 km West of Rift Valley	Fault Azimuth
76°08'N	331°		76°52'N	351°
77°01'N	338°		77°05'N	332°
77°12'N	339°		77°25'N-77°26'N	318°-324°
77°16'N-77°19'N	341°-320°		77°39'N	345°
77°26'N	329°		77°57'N	342°
77°32'N-77°33'N	340°		78°04'N	344°
77°42'N	325°		78°09'N	338°
77°56'N	346°		78°21'N	323°
78°04'N	341°		78°32'N	334°
78°12'N	314°			
78°22'N	334°			
78°26'N-78°32'N	318°.			

Table 2: Section 5-10 km east and west of the inner rift valley (figure 11B):

Section 5-10 km East of Rift Valley	Fault Azimuth		Section 5-10 km West of Rift Valley	Fault Azimuth
76°30′N	351°		76°59′N-77°00′N	311°-333°
77°01′N-77°03′N	313°-319°		77°02′N	328°
77°09′N-77°12′N	340°		77°38′N-77°39′N	302°-311°
77°16′N	328°		77°53′N-77°55′N	330°-346°
77°18′N	340°		78°09′N-78°11′N	306°-317°
77°48′N	335°		78°13′N-78°17′N	326°-348°
78°01-78°04′N	330°-342°		78°21′N-78°25′N	330°-346°
78°25′N-78°26′N	295°-316°		78°29′N-78°33′N	320°-348°
78°29′N	320°			

Table 3: Section 10-15 km east and west of the inner rift valley (figure 11C):

Section 10-15 km East of Rift Valley	Fault Azimuth		Section 10-15 km West of Rift Valley	Fault Azimuth
76°24′N-76°25′N	333°-337°		76°52′N	333°
77°01′N	332°		76°55′N-77°05′N	307°-345°
77°15′N	318°		77°44′N	319°
77°21′N-77°22′N	331°-333°		78°13′N-78°14′N	311°-325°
77°48′N	342°		78°22′N-78°23′N	323°-325°

Table 4: Section 15-20 km east and west of the inner rift valley (figure 11D):

Section 15-20 km East of Rift Valley	Fault Azimuth		Section 15-20 km West of Rift Valley	Fault Azimuth
76°15′N-76°18′N	341°-345°		76°56′N-76°57′N	336°-345°
76°25′N	342°		77°09′N	340°
76°34′N	337°		77°41′N-77°45′N	340°-350°
76°39′N	325°		78°06′N-78°07′N	329°-344°
76°42′N-76°43′N	330°-345°		78°13′N-78°16′N	290°-332°
76°58′N	322°		78°26′N	340°
77°22′N-77°24′N	316°-342°		78°29′N-78°31′N	334°-342°
77°48′N	328°			
78°22′N-78°25′N	(294°-333°			

Table 5: Section 20-25 km east and west of the inner rift valley (figure 11E):

Section 20-25 km East of Rift Valley	Fault Azimuth		Section 20-25 km West of Rift Valley	Fault Azimuth
76°15'N-76°18'N	340°-343°		76°52'N-76°54'N	318°-345°
76°25'N-76°28'N	328°-347°		77°41'N	328°
76°52'N-76°55'N	321°		77°49'N-77°51'N	322°-341°
76°57'N	342°		78°01'N	335°
77°00'N	338°		78°06'N-78°27'N	304°-351°
77°22'N	305°			
77°26'N-77°27'N	338°			

Table 6: Section 25-30 km east and west of the inner rift valley (figure 11F):

Section 25-30 km East of Rift Valley	Fault Azimuth		Section 25-30 km West of Rift Valley	Fault Azimuth
76°24'N	344°		76°53'N-76°54'N	296°-307°
76°26'N	330°		76°57'N	337°
77°11'N-77°12'N	325°		77°44'N-77°45'N	317°-326°
			77°54'N-77°55'N	331°-336°
			78°06'N-78°10'N	283°-327°
			78°23'N	333°

Table 7: Section 30-35 km east and west of the inner rift valley (figure 11G):

Section 30-35 km East of Rift Valley	Fault Azimuth		Section 30-35 km West of Rift Valley	Fault Azimuth
76°17'N	343°		76°58'N-76°59'N	330°-345°
76°22'N-76°23'N	341°		77°02'N	323°
76°56'N-76°58'N	332°		77°32'N-77°33'N	332°
			78°07'N-78°12'N	294°-329°
			78°18'N-78°19'N	313°-328°

Table 8: Section 35-40 km east and west of the inner rift valley (figure 11H):

Section 35-40 km East of Rift Valley	Fault Azimuth		Section 35-40 km West of Rift Valley	Fault Azimuth
76°08'N-76°10'N	341°		77°06'N-77°08'N	320°
76°50'N-76°53'N	340°		78°12'N-78°15'N	307°-334°
			78°21'N-78°24'N	320°-330°

Table 9: Section 40-45 km east and west of the inner rift valley (figure 11I):

Section 40-45 km East of Rift Valley	Fault Azimuth		Section 40-45 km West of Rift Valley	Fault Azimuth
76°27'N	341°		77°14'N-77°15'N	326°-328°
			77°49'N	341°
			78°08'N-78°13'N	311°-331°
			78°15'N	332°
			78°17'N-78°22'N	315°-339°
			78°24'N	330°

Obliquely Oriented Fault Clusters:

Six obliquely oriented fault clusters were observed along the flanks of the Knipovich Ridge (tables 1-9). From south to north, these clusters can be described as follows:

1) Between latitudes 76°19'N to 76°37'N and longitudes 7°35'N to 8°40'N (figure 6) on the eastern flank of the Knipovich Ridge. This cluster is characterized by short to medium length faults (1-5 km) that are oriented 312° on average (nearly parallel to the spreading direction and adjacent to seamount Belt 1 (Doss et al., in preparation). Several long faults (>20 km) parallel to the rift valley cut through this cluster.

2) Between latitudes 76°50'N to 76°56'N and longitudes 6°17'N to 6°28'N (figure 7) on the western flank of the Knipovich Ridge. This cluster is characterized by short faults (0.5-3 km) that are oriented 325° on average, and are on line with the eastern flank cluster 1.

3) Between latitudes 76°57'N to 77°06'N and longitudes 6°37'N to 7°12'N (figure 7) on the western flank of the Knipovich Ridge. This cluster is characterized by medium to long faults (3-8 km) that are oriented 322° on average, and lies adjacent to subsegment 4A (Doss et al., in preparation). However, at present, in the rift valley, fault azimuths average

016° compared to the western flank's cluster trending 322°.

4) Between latitudes 77°10′N to 77°21′N and longitudes 7°40′N to 8°46′N (figure 7) on the eastern flank of the Knipovich Ridge. This cluster is characterized by medium to long faults (2.5-8 km) that are oriented 320° on average. and are adjacent to seamount Belt 4 (Doss et al., in preparation) and to fresh lava flows within the rift axis.

5) Between latitudes 77°41′N to 77°45′N and longitudes 6°26′N to 6°45′N (figure 8) on the western flank of the Knipovich Ridge. This cluster consists of three faults oriented 335° that appear to cut two long faults (>30 km) parallel to the rift valley, and adjacent to the rise axis' subsegment 5A (Doss et al., in preparation).

and 6) Between latitudes 78°07′N to 78°15′N and longitudes 6°18′N to 7°00′N (figure 8) on the western flank of the Knipovich Ridge, east of the Hovgård Ridge. With an average fault azimuth of 335°, this cluster is dominated by short to medium length faults (1-7 km), and lies adjacent to subsegment 6B (Doss et al., in preparation).

Discussion:

While faults oblique to the rise axis appear dispersed in both location and orientation, figure 13 reveals that they are organized into bands that are nearly parallel to the suggested spreading direction of DeMets (1991). Furthermore, these bands lie adjacent to regions of recent volcanism in the inner rift valley.

Doss et al. (in preparation) suggest that structural weakness zones associated with the Paleo-Spitsbergen Shear Zone may have played a major role in the evolution of oceanic crust on the flanks of the Knipovich Ridge. Our data suggest that both clusters of faults as well as seamount chains located on the flanks of the rise axis and parallel to the spreading

direction are further evidence of this possibility.

While faults discussed in this paper range in orientation from 284°-350° near the axis, at a distance of 15 km away from the center of the rift valley, fault azimuths range from 284°-320°. A 40° range of orientations is significant, and most likely represents a changing state of stress created during northwards rift propagation into one of the main faults associated with the Spitsbergen Shear Zone.

Courtillot et al., 1974; Crane, 1976; Lonsdale, 1978; Searle, 1979; Macdonald et al., 1979; Gallo et al., 1980, Fox and Gallo, 1982; 1983; and Gallo et al., 1984 suggested that structures oblique to both transform faults as well as mid-ocean ridges may be created by the influence of a transform generated shear couple. If these structures are Riedels, anti-Riedels, secondary shear faults that accommodate strike-slip displacement, thrust faults or if they are just obliquely trending normal faults is not known.

However, a comparison of an ideal shear couple oriented along the trend of the Paleo-Spitsbergen Shear Zone, with present day on and off-axial fault trends reveals the following similarities. It the Paleo-Spitsbergen Shear Zone was oriented 335°, then ideally Riedel shears trending 350°, normal extensional faults trending 022° and thrust faults trending 290° would have been likewise associated with the shear zone. The vast majority of present day Knipovich Ridge inner rift faults lie en-echelon to one another and trend 024° (in the middle of segments).

In general, the overall trend of the Knipovich Ridge ranges from 345°-005°, while off-axial seamount chains and ridges trend 290°-340° and offaxial oblique faults trend 283°-351°. We believe that the present day trend of the Knipovich Ridge is controlled by

preexisting riedel shears associated with the paleo shear zone. Furthermore, inner rift faults have evolved superimposed upon normal extensional faults associated with the preexisting shear couple (figure 12). In addition, we propose that paleo thrust zones and major oblique shear zone faults remained structural zones of weakness in the proto-oceanic crust evolving into locations where excess magma erupted along the Knipovich Ridge axis creating seamount chains in the process. Figure 12 illustrates the range of present-day oblique off-axial lineaments. It is clear that these features overlap with the distribution of ancient shear-couple related thrust and shear faults.

The dominance of shear-couple related trends in the present-day oceanic crust in the northern Norwegian-Greenland Sea also could explain the extreme obliquity of spreading across the Knipovich Ridge, the en-echelon nature of obliquely oriented inner rift faults, and the absence of any transform faults, and the chaotic crustal signature across the Boreas Basin.

Conclusions:

1. Numerous faults on oceanic crust off-axis from the Knipovich Ridge are obliquely oriented to the rift valley at an azimuth that is nearly parallel to the suggested spreading direction of the Knipovich Ridge.
2. These faults are oriented parallel to ancient shear and thrust faults created by the shear couple about the immense Paleo-Spitsbergen Shear Zone.
3. The rifting and spreading of the Knipovich Ridge axis is likely to be constrained by the pre-rifting trend of riedel shears and normal extensional faults oriented obliquely to and created by the state of stress associated with the Paleo-Spitsbergen Shear Zone.

4. If our model is correct, many young mid-ocean ridges may evolve obliquely to their spreading direction if they propagate into pre-existing shear zones.

REFERENCES

Chan, W. W., and B. J. Mitchell, 1985, Intraplate Earthquakes in Northern Svalbard, Tectonphysics, 114, 181-191.

Cande, S. C. and Kent, D. V., 1992, A New Geomagnetic Polarity Time Scale for the Late Cretaceous and Cenozoic, Jour. Geophys. Res., 97, 13917-13951.

Crane, K., Eldholm, O., Myhre, A. M., and Sundvor, E., 1982, Thermal Implications for the Evolution of the Spitsbergen Transform Fault, Tectonophysics, 89, 1-32.

Crane, K. and Bonatti, E., 1986, Fracture Zone Control on the Opening of the Red Sea: SIR A Data, Jour. of the Geological Soc. of London, 144, 407-420.

Crane, K., 1985, The spacing of rift axis highs: dependence upon diapiric processes in the underlying asthenosphere?, Earth and Planetary Science Letters, 72, 405-414.

Crane, K., Sundvor, E., Foucher, J. P., Hobart, M., Myhre, A. M., and LeDouran, S., 1988, Thermal Evolution of the Western Svalbard Margin, Mar. Geophys. Res., 9, 165-194.

Crane, K., Sundvor, E., Buck, R., and Martinez, F., 1991, Rifting in the Northern Norwegian-Greenland Sea: Thermal Tests of Asymmetric Spreading, Jour. Geophys. Res., 96, 14529-14550.

DeMets, C., Gordon, R. G., Argus, D. F., and Stein, S., 1990, Current Plate Motions, Geophys. J. Int., 101, 425-478

Dore. A. G., and Gage, M. S., 1987, Crustal alignments and sedimentary domains in the evolution of the North Sea, North East Atlantic Margin and Barents Shelf. In: J. Brooks and K. Glennie (editors), Petroleum Geology of North West Europe. Graham and Trotman, London, 1131-1148.

Eldholm, O., Vogt, P., and Perry, R., 1978, Plate Tectonic Development of the Mid-Oceanic Ridge System North of the Jan Mayen Fracture Zone, A: Present Plate Boundaries, EOS 59, 371.

Eldholm, O. and Sundvor, E., 1980, The Continental Margins of the Norwegian-Greenland Sea: Recent Results and Outstanding Problems, Royal Society of London Phil. Trans., Ser. A: 294, 77-86.

Eldholm, O., Karasik, A. M., and Reksnes, P. A., 1986, The North American Plate Boundary, DNAG synthesis. Volume Geology of the Arctic Ocean Region Chapter 12.

Harland, W. B., 1969, Contribution of Spitsbergen to understanding of tectonic evolution of North Atlantic Region. In: M. Kay (Editor), North Atlantic: Geology and Continental Drift. American Association of Petroleum Geologists, Memoir 12, 817-851.

Horsfield, W. T. and Maton, P. I., 1970, Transform Faulting along the De Geer Line, Nature 226, 256-257.

Johnson, L. and Heezen, B. C., 1967, Morphology and Evolution of the Norwegian-Greenland Sea, Deep-Sea Research 14, 755-771.

Kovacs, L.C., Johnson, G. L., Srivastava, S. P., Taylor, P. T., and Vogt, P. R., 1987, Residual Magnetic Anomaly Chart of the Arctic Ocean Region (Naval research Laboratory and Naval Ocean research and Development Activity), In: The Arctic Ocean Region, Vol. L., The Geology of North America, edited by Arthur Gantz, L. Johnson, and J. F. Sweeny, 1990, 644p.

Minster, W. J., and T. H. Jordan, 1978, Present-Day Plate Motions, Jour. Geophys. Res., 83, 5331-5354.

Morgan, W. J., 1981, Hotspot Tracks and the Opening of the Atlantic and Indian Oceans, in The Sea, 7, edited by C. Emiliani, pp. 443-487, John Wiley, New York.

Okay, N., and Crane, K., 1993, Thermal Rejuvenation of the Yermak Plateau, Marine Geophysical Researches, 15, 243-263.

Shor, A., 1990, SeaMARC II seafloor mapping system: Seven years of Pacific research, Pacific Rim Congress Vol. III; Australian Institute of Mining and Metallogenesis, 49-59.

Sobczak, L. W., and Hearty, D. B., with contributions by R. Forsberg, Y. Kristoffersen, O. Eldholm and S. D. May), 1987, Gravity of the Arctic Ocean, In: The Arctic Ocean Region, Vol. L., The Geology of North America, edited by Arthur Gantz, L. Johnson, and J. F. Sweeny, 1990, 644p.

Stein, S., Melosh, H. J., and Minster, J. B., 1977, Ridge Migration and Asymmetric Sea-floor Spreading, Earth Planet. Sci. Lett., 36, 51-62.

Sundvor, E. and O. Eldholm, 1979, The Western and Northern Margin off Svalbard, Tectonophysics, 59, 239-250.

Talwani, M. and Eldholm, O., 1977, Evolution of the Norwegian-Greenland Sea, Geol. Soc. America Bull. 88, 969-999.

Thiede, J., S. Pfirman, H-W Schenke, and W. Reil, 1990, Bathymetry of the Molloy Deep: Fram Strait between Greenland and Svalbard, Marine Geophysical Researches, 12, 197-214.

Vogt, P. R., 1986b, Geophysical and Geochemical Signatures and Plate Tectonics, Chapter 11, in The Nordic Seas, edited by B. G. Hurdle, Springer Verlag.

Vogt, P. R., 1986a, Seafloor Topography, Sediments, and Paleoenvironments, Chapter 11, in The Nordic Seas, edited by B. G. Hurdle, Springer Verlag.

Vogt, P. R., and Avery, O. E., 1974, Tectonic History of the Arctic Basins: Partial Solutions and Unsolved Mysteries, in Marine Geology and Oceanography of the Arctic Seas, edited by Herman, Y., 83-117, Springer-Verlag, New York.

Vogt, P. R., R. K. Perry, R. H. Feden, H. S. Fleming, and N. Z. Cherkis, 1981, The Greenland-Norwegian Sea and Iceland Environment: Geology and Geophysics; In: The Ocean Basins and Margins, Vol. 5, The Arctic Ocean, Edited by A. E. M. Nairn and M. Churkin, pp. 493-598, Plenum, New York, 1981.

Vogt, P. R., L. C. Kovacs, L. C. Bernero, and S. P. Srivastava, 1982, Asymmetric geophysical signatures in the Greenland-Norwegian and southern Labrador Seas and the Eurasia Basin, Tectonophysics, 89, 95-160.

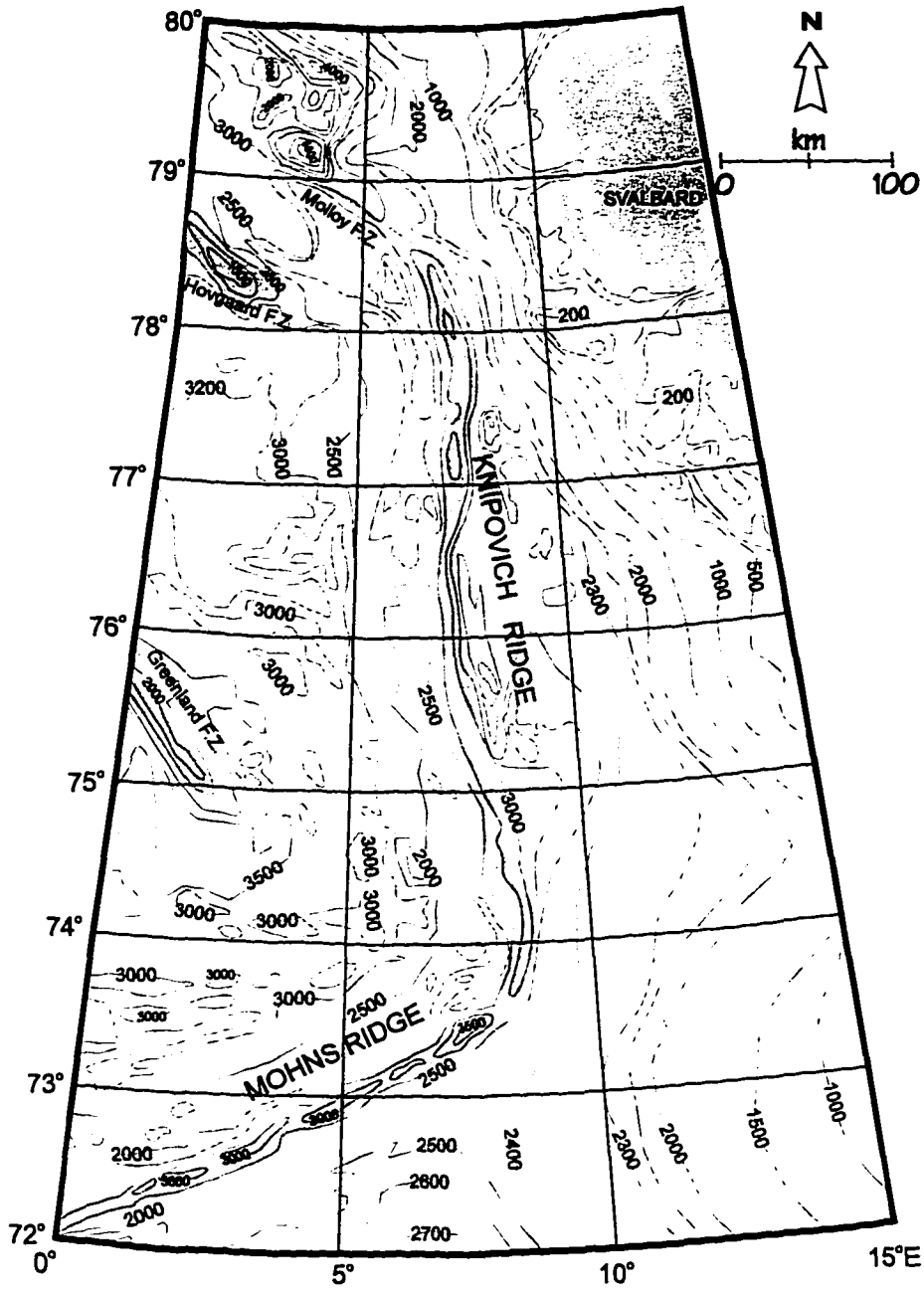

Figure 1: Bathymetry of the northern the Norwegian-Greenland Sea (after Cherkis and Vogt, 1994).

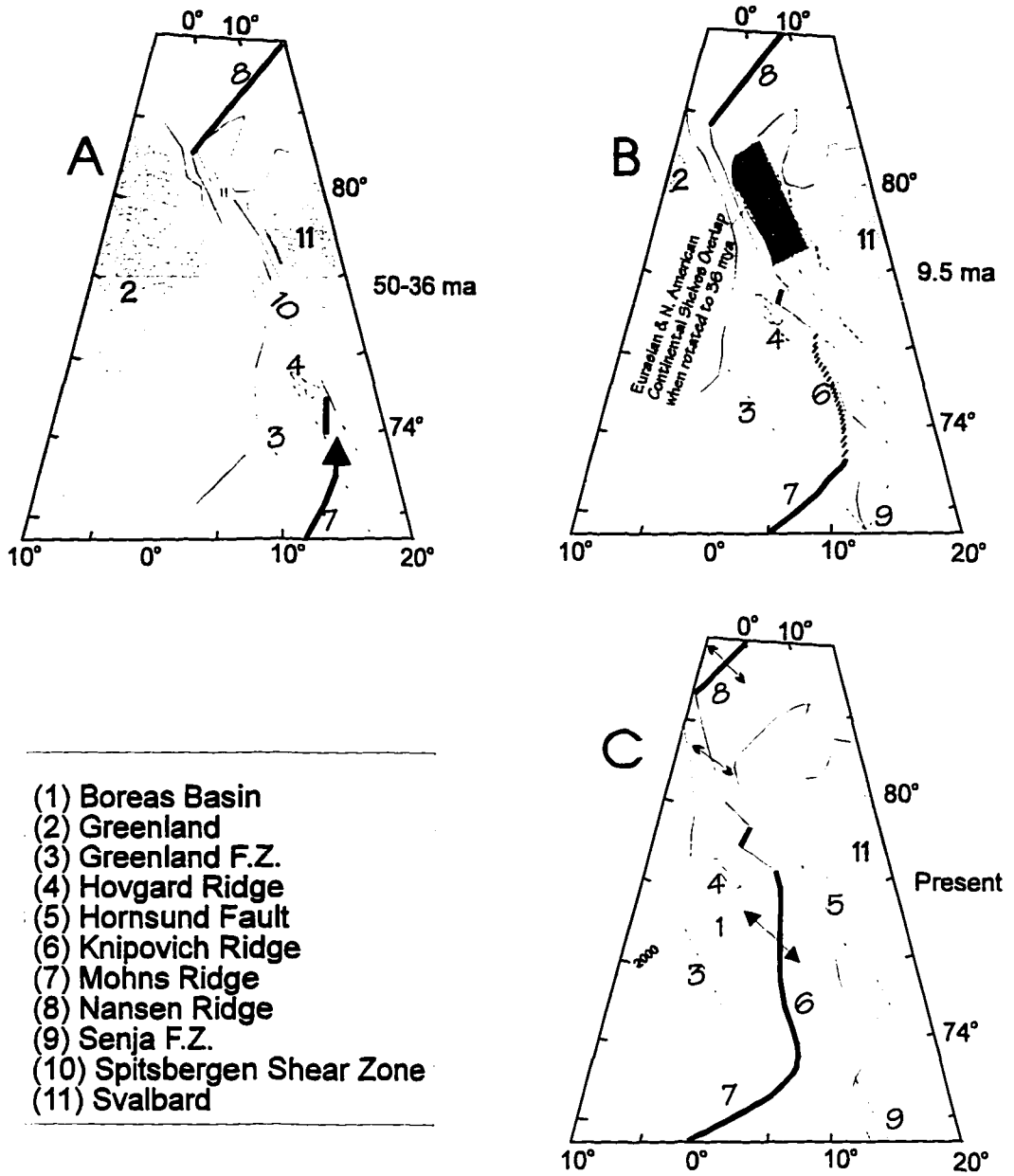

Figure 2: Plate reconstruction at 50-36 MA, 9.5 MA and of the present. The ancient Spitsbergen Shear Zone probably cut through Svalbard (Horsfield and Maton, 1970). As the plate boundary developed, the active spreading center propagated into the continental shear zone from the Norwegian Sea and the Arctic Ocean generating the Knipovich Ridge in the Greenland Sea and the Lena trough (after Crane et al., 1991).

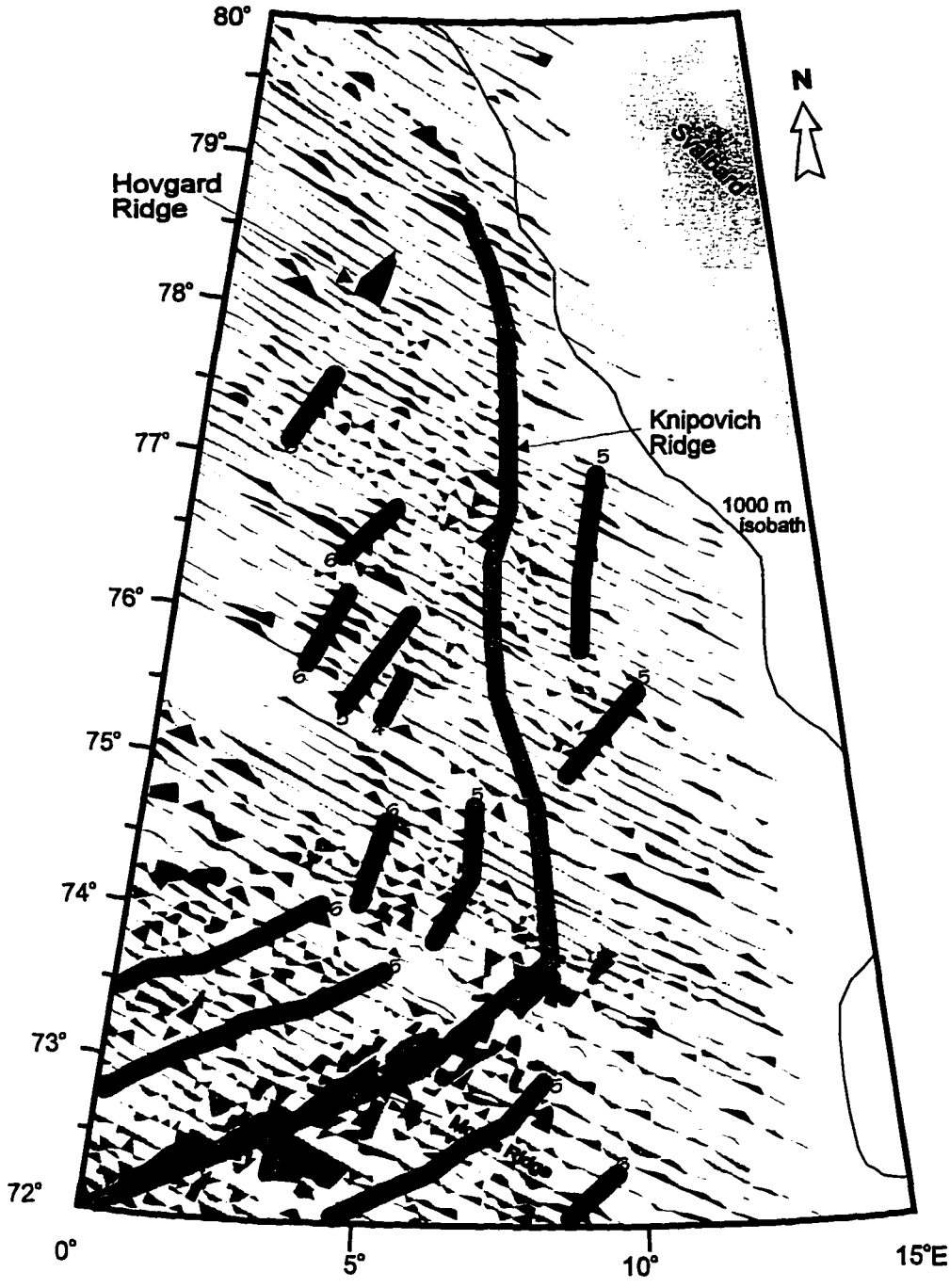

Figure 3: Residual magnetic anomalies within the survey area. All data are shown as fenced anomaly profiles along flight tracks. Positive anomalies are in black while negative anomalies are dotted. Anomaly scale is 4,000 nT per degree of latitude. (After Kovacs et al., 1987). Magnetic anomalies are chaotic or absent in the northern Norwegian-Greenland Sea compared with more normal anomalies adjacent to the northeastern Mohns Ridge. Some anomalies in the Boreas Basin were identified by Vogt (1986) and his interpretations are shown by the darker dotted patterns including the anomaly number.

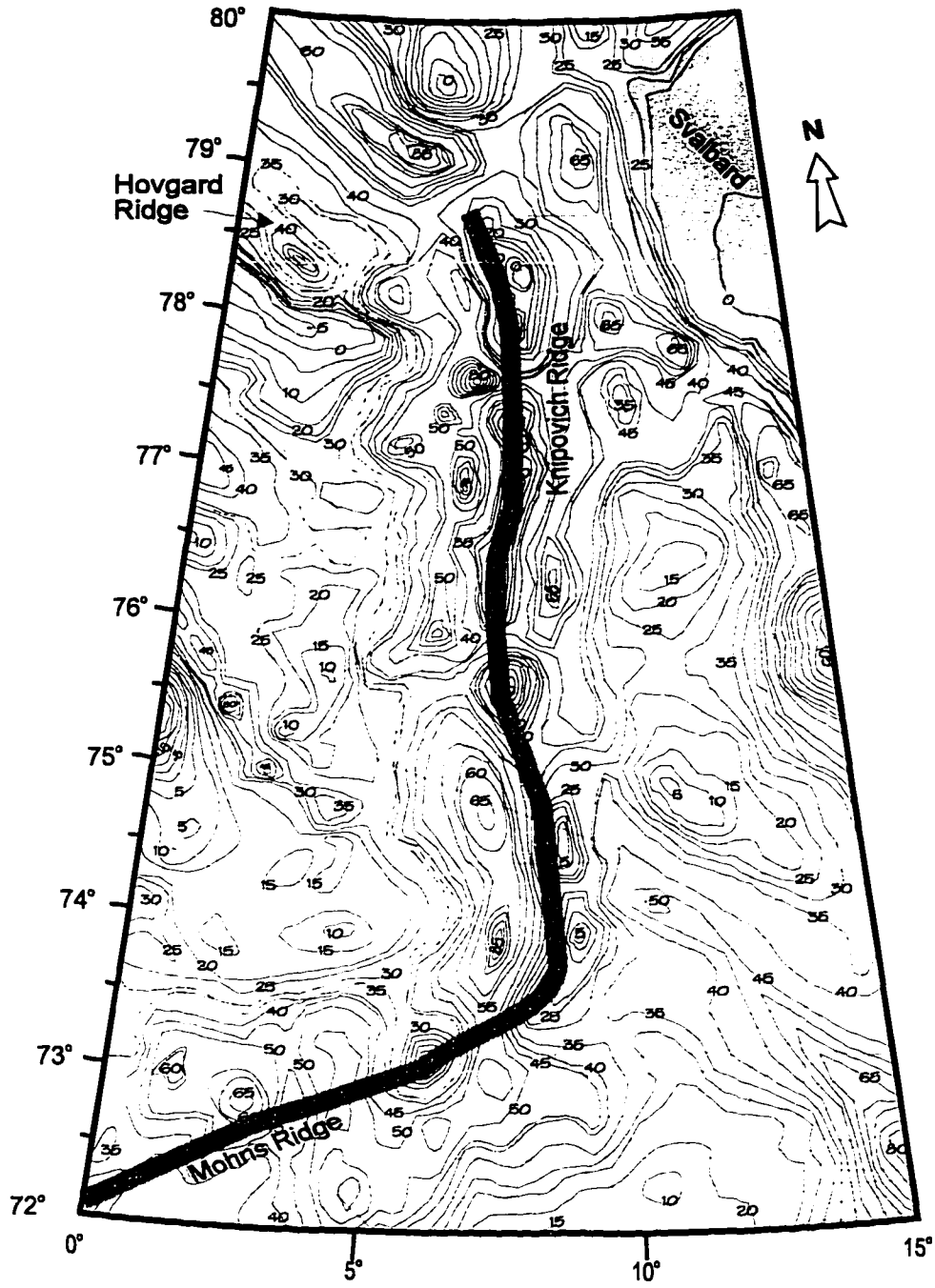

Figure 4: Free-air gravity anomalies within the survey area. Contour interval is 5 mGal. (After Sobczak et al., 1987). Along the Knipovich Ridge a belt of well defined gravity minima can be found in the rift valley compared with well defined gravity maxima on the flanks. Along the northeastern Mohns Ridge and the Mohns-Knipovich Ridge transition zone, there is no coherent pattern to the distribution of anomalies across the rift valley and the flanks. The dotted lines represent control lines.

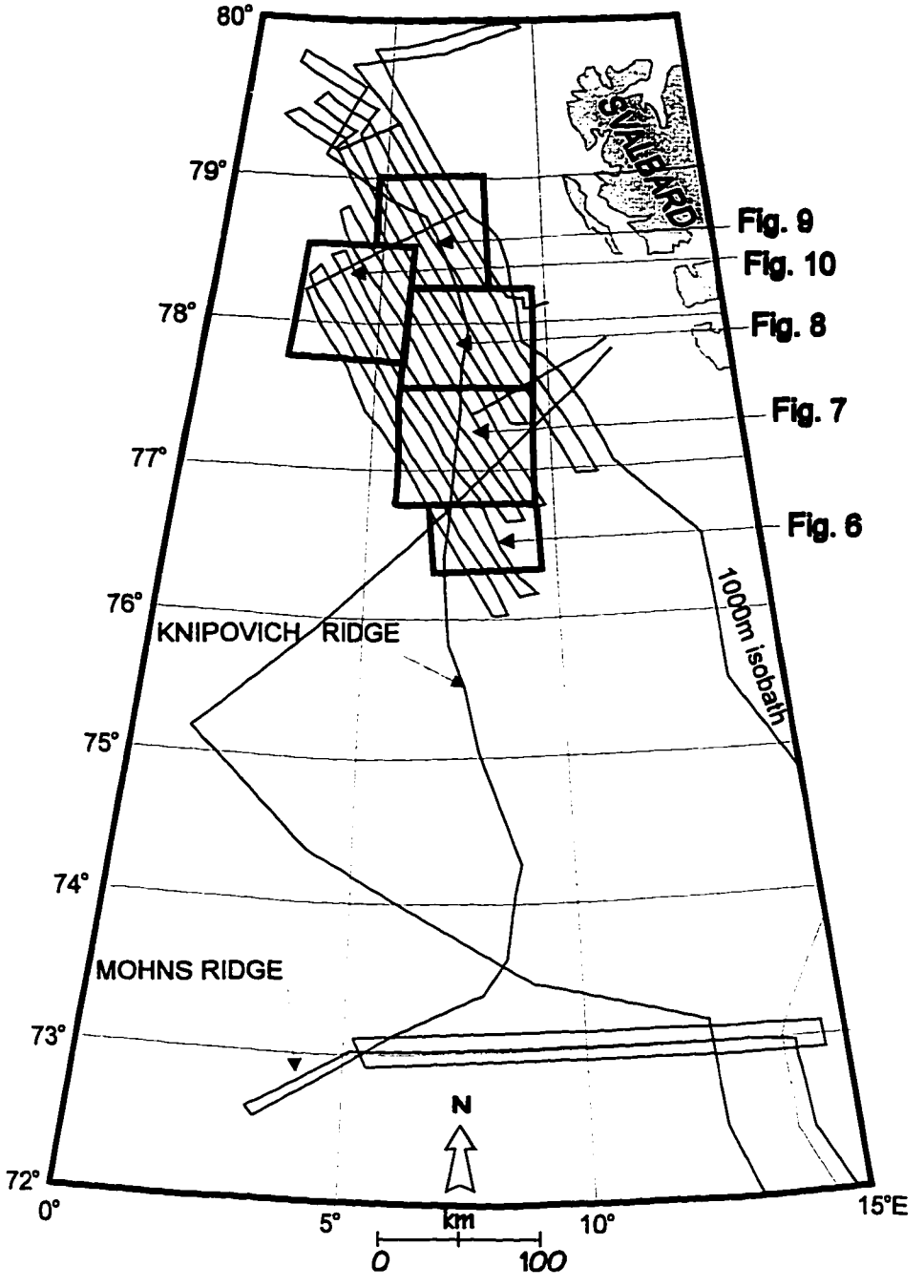

Figure 5: Map illustrating the SeaMARC II tracks (1989 and 1990. Regions outlined in bold are illustrated in following figures.

Figure 6A: SeaMARC II side-scan image of the Knipovich Ridge from 76°15'N to 76°45'N and approximately 40 km of the eastern flank.

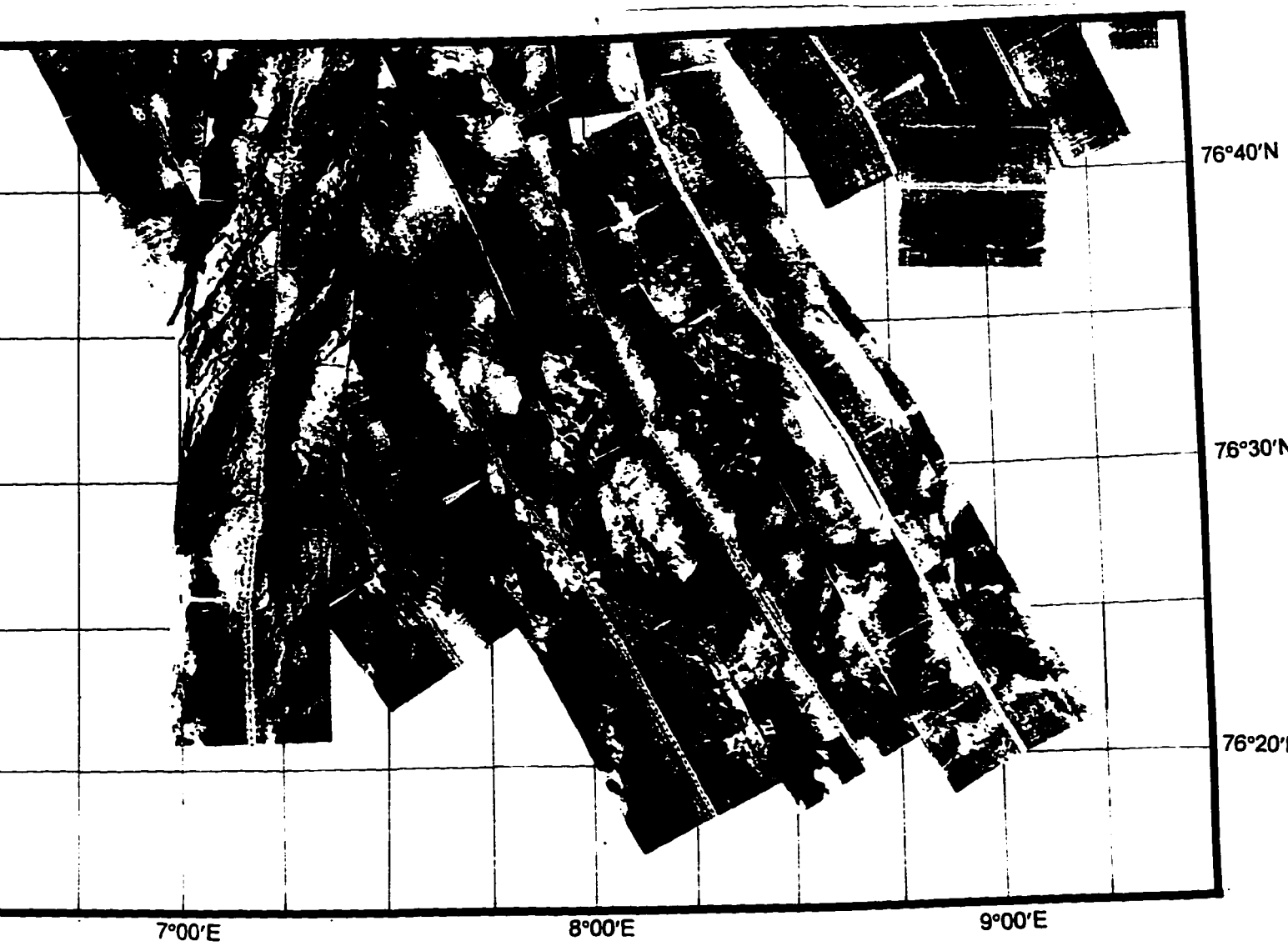

MARC II side-scan image of the Knipovich Ridge from 76°15'N to
roximately 40 km of the eastern flank.

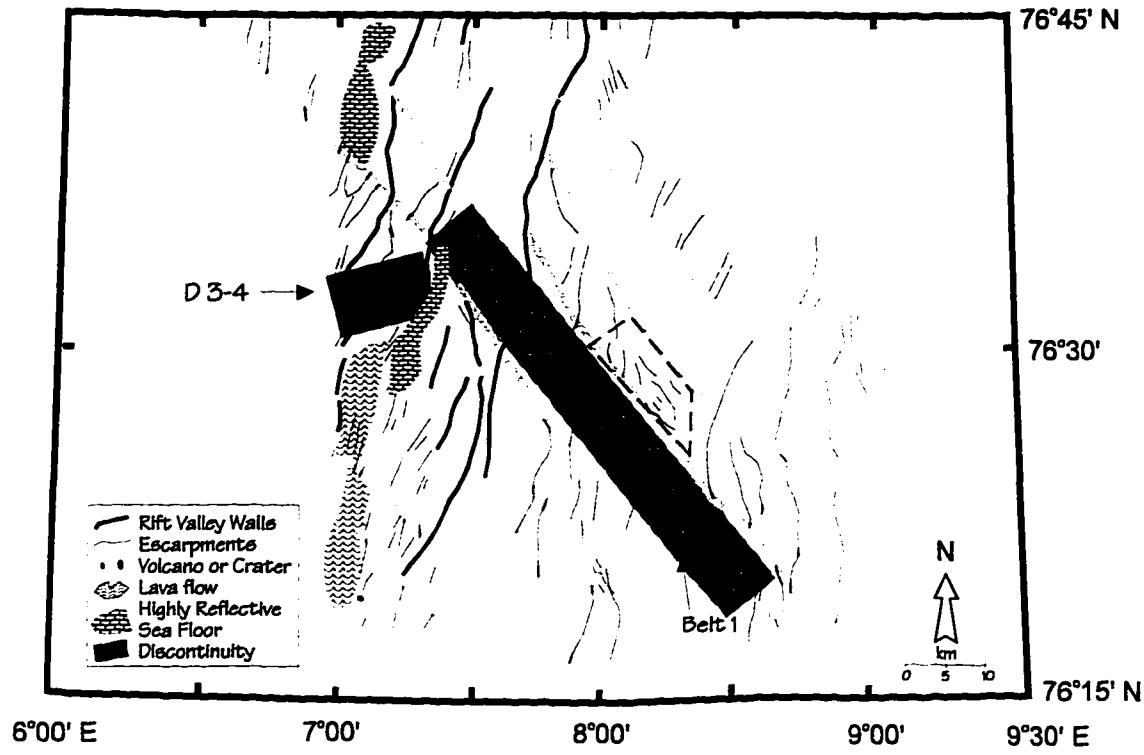

Figure 6B: Structural interpretation of side-scan image shown in figure 6A. Note the second order discontinuity between segments 3 and 4 (near 76°33'N) which is characterized by a change in the strike of the rift valley and a volcanic high. Flank faults associated with Seamount Belt 1 are seen (long gray area) trending an average of 330°. Light gray lines cutting across faults are suggested traces of seafloor spreading based on disruptions in the off-axial fault patterns.

Figure 7A: SeaMARC II side-scan image of the Knipovich Ridge from 76°45'N to 77°30'N as well as the inner flanks.

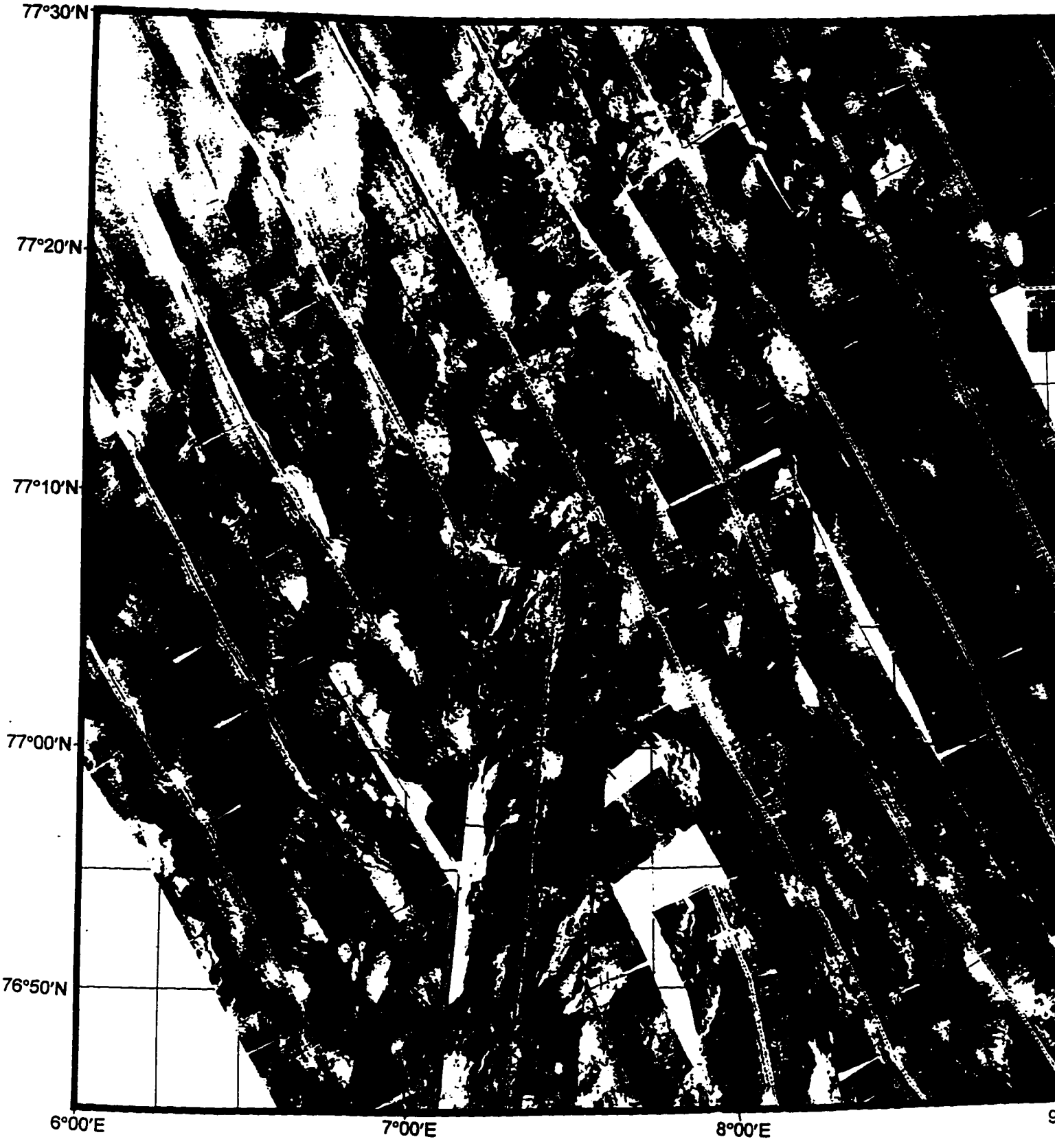

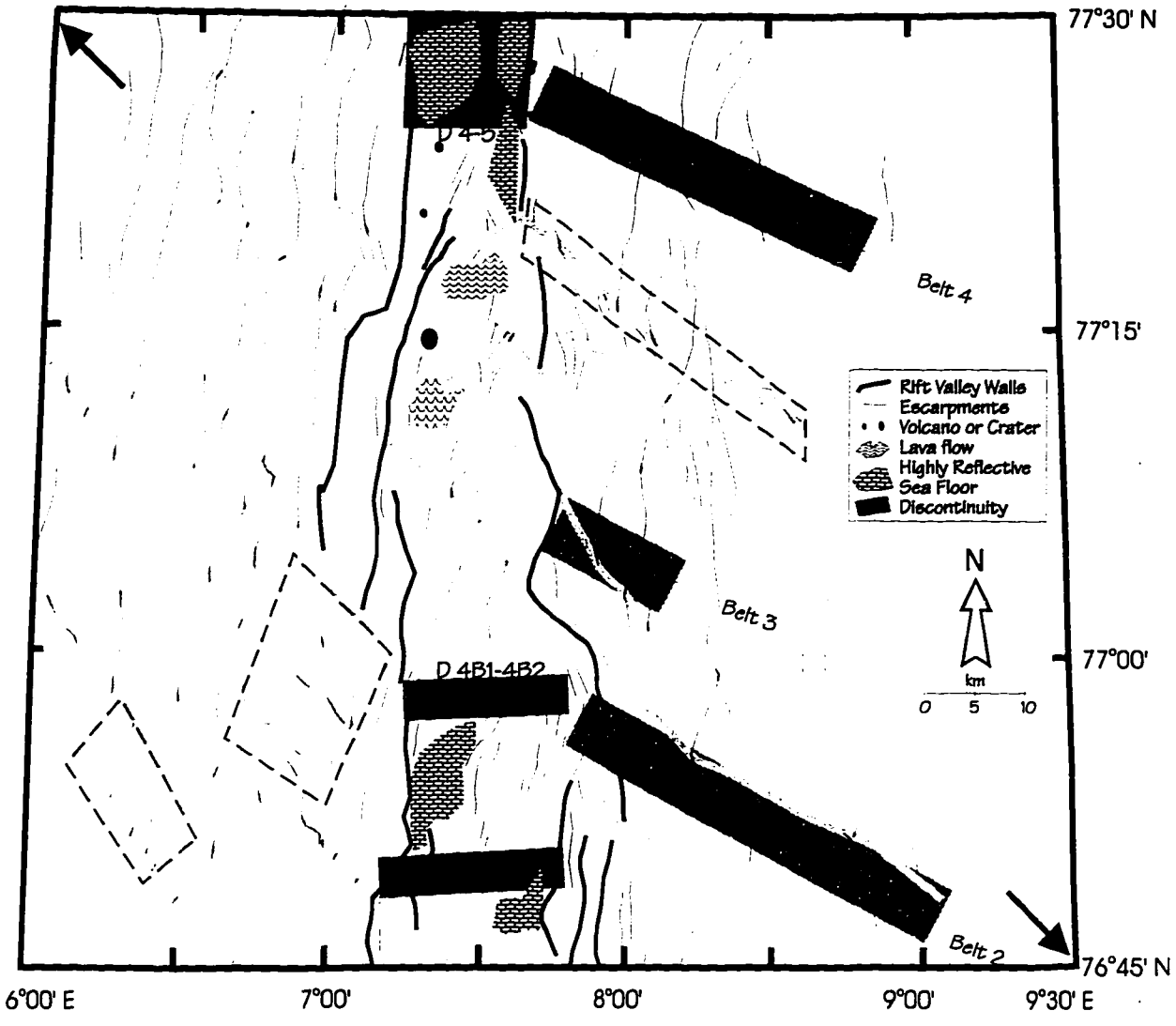

Figure 7B: Structural interpretation of side-scan image shown in figure 7A. Conjugate faults on both flanks tend to converge towards the rift valley from south to north. Shaded boxes (on flanks) show fault trends near Seamount Belts 2-4 (figure 10C). Dashed empty boxes mark flank locations near the inner rift valley where fault trends are oblique to local fault trends. Light gray lines cutting across faults are suggested traces of seafloor spreading based on disruptions in the off-axial fault patterns.

Figure 8A: SeaMARC II side-scan image of the Knipovich Ridge from 77°30'N to 78°15'N and the inner parts of the flanks.

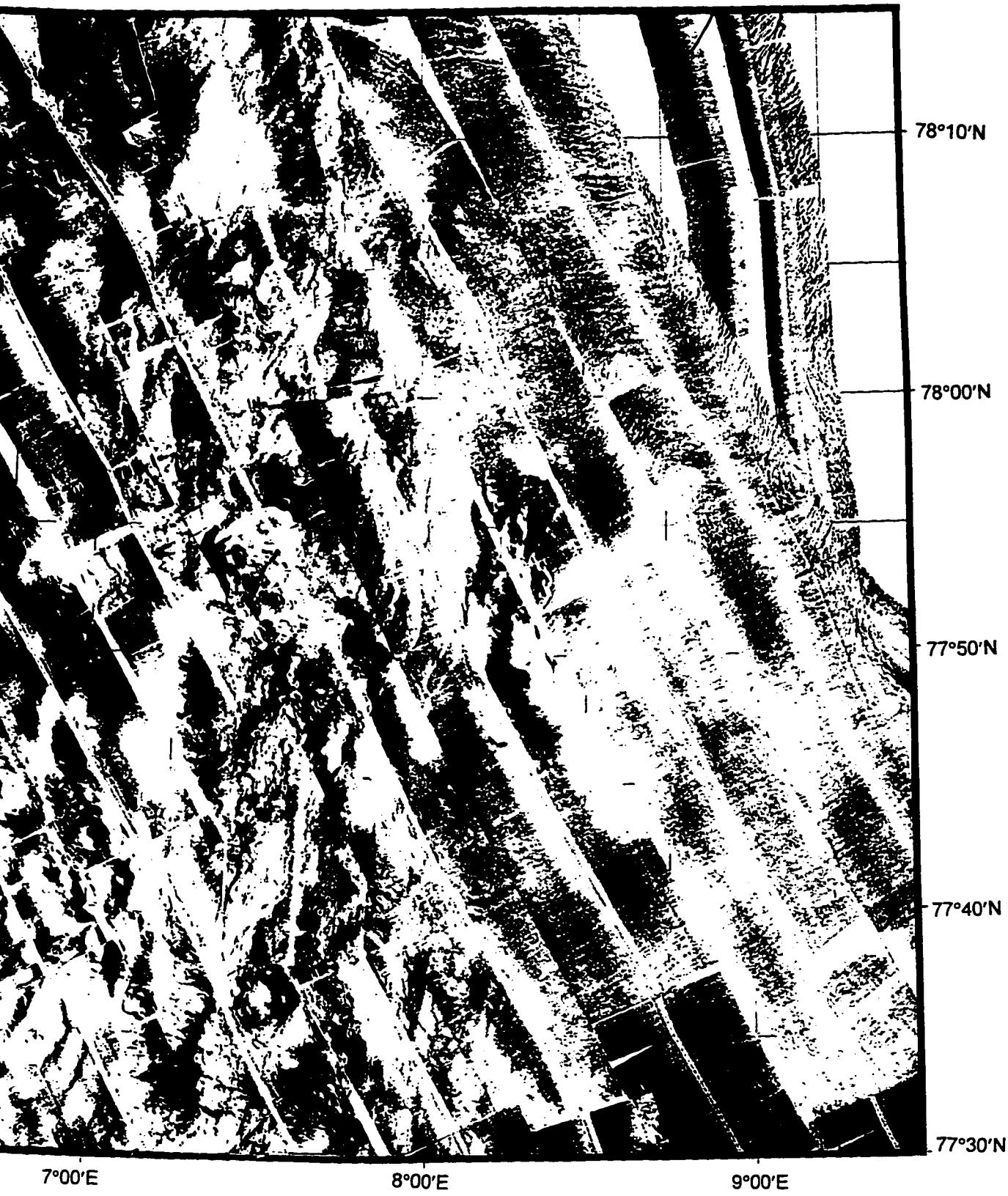

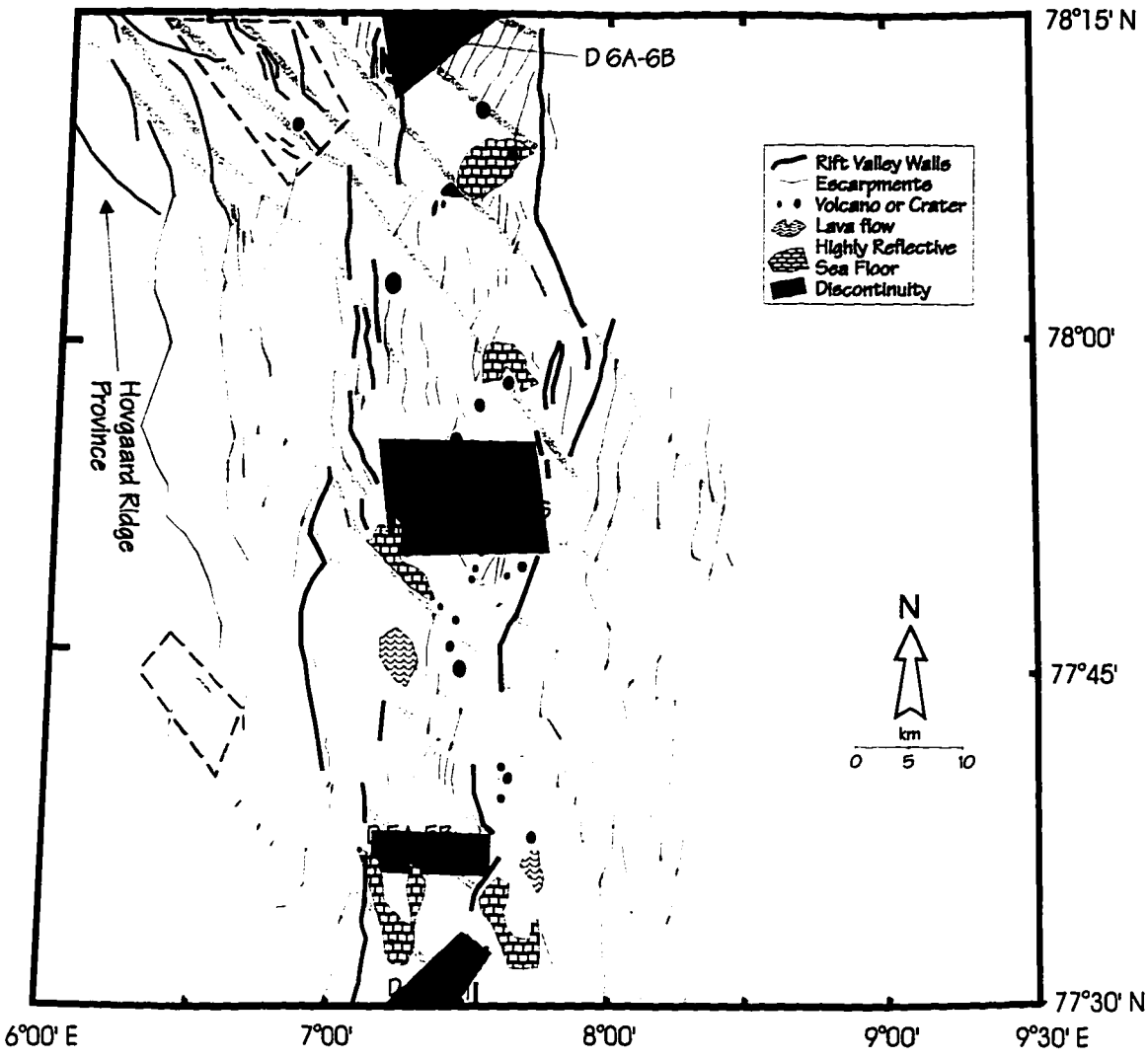

Figure 8B: Structural interpretation of side-scan image shown in figure 8A. Note the presence of many volcanic cones (~30) just to the north of segment 4 which may be evidence for recent volcanic activity. Faults in the northwestern corner of the map strike northwesterly suggestive of a paleo-transform fault (associated with the Hovgård Fracture Zone). Dashed empty boxes mark flank locations near the inner rift valley where fault trends are oblique to local fault trends. Light gray lines cutting across faults are suggested traces of seafloor spreading based on disruptions in the off-axial fault patterns.

Figure 9A: SeaMARC II side-scan image of the Knipovich Ridge at its intersection with the Molloy Transform Fault and the southern part of Vestnesa Plateau (from 78°15'N to 79°00'N).

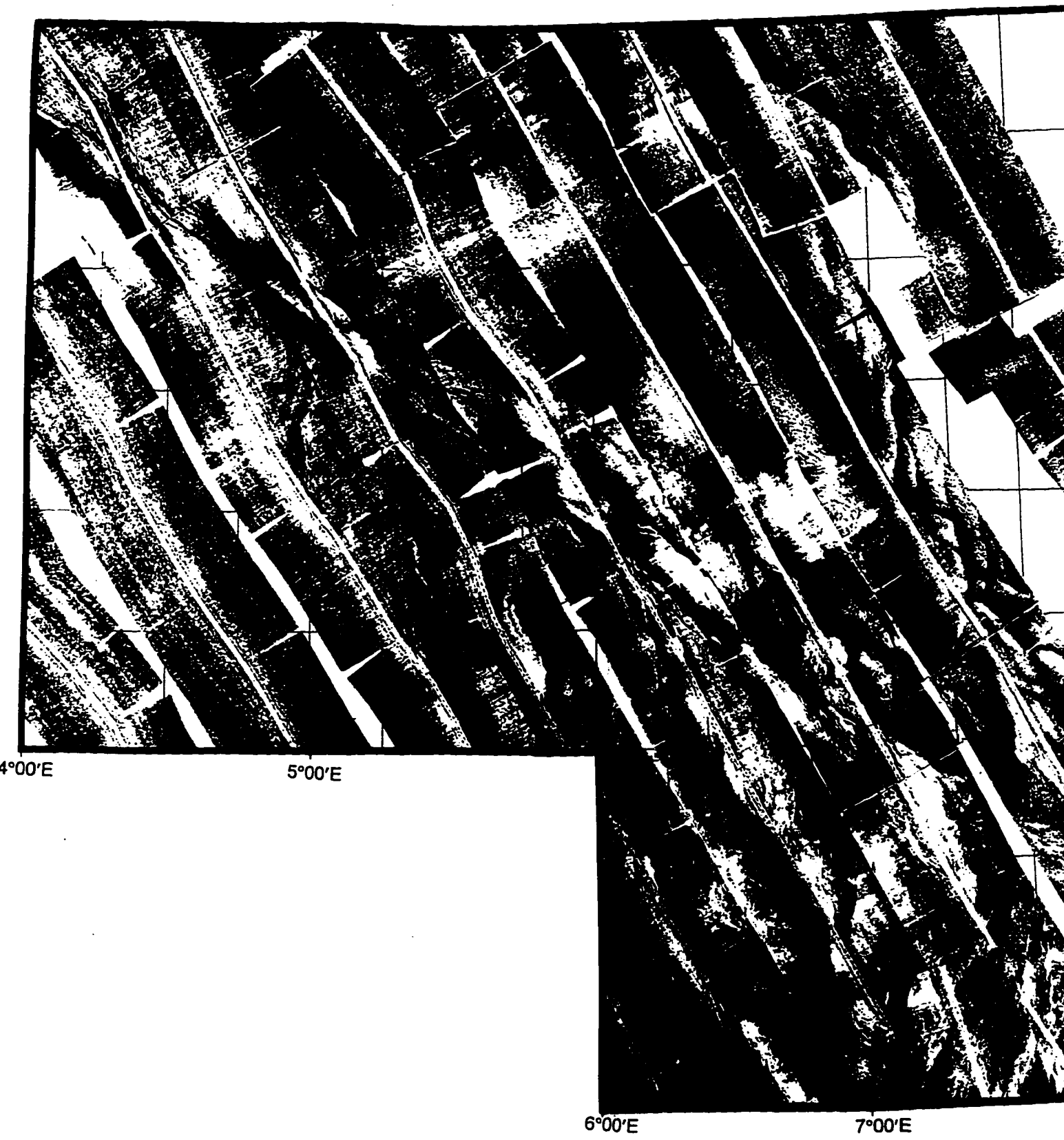

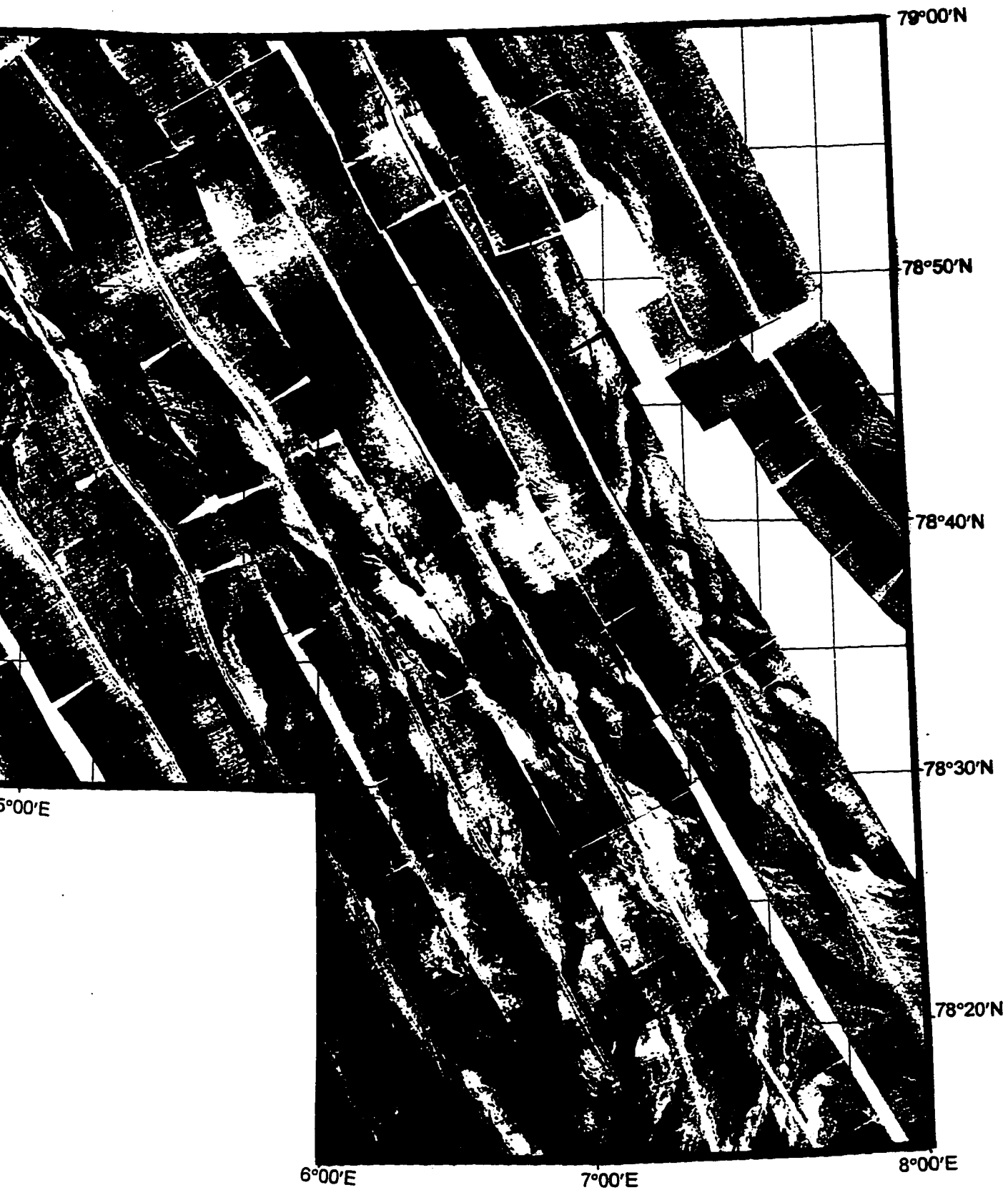

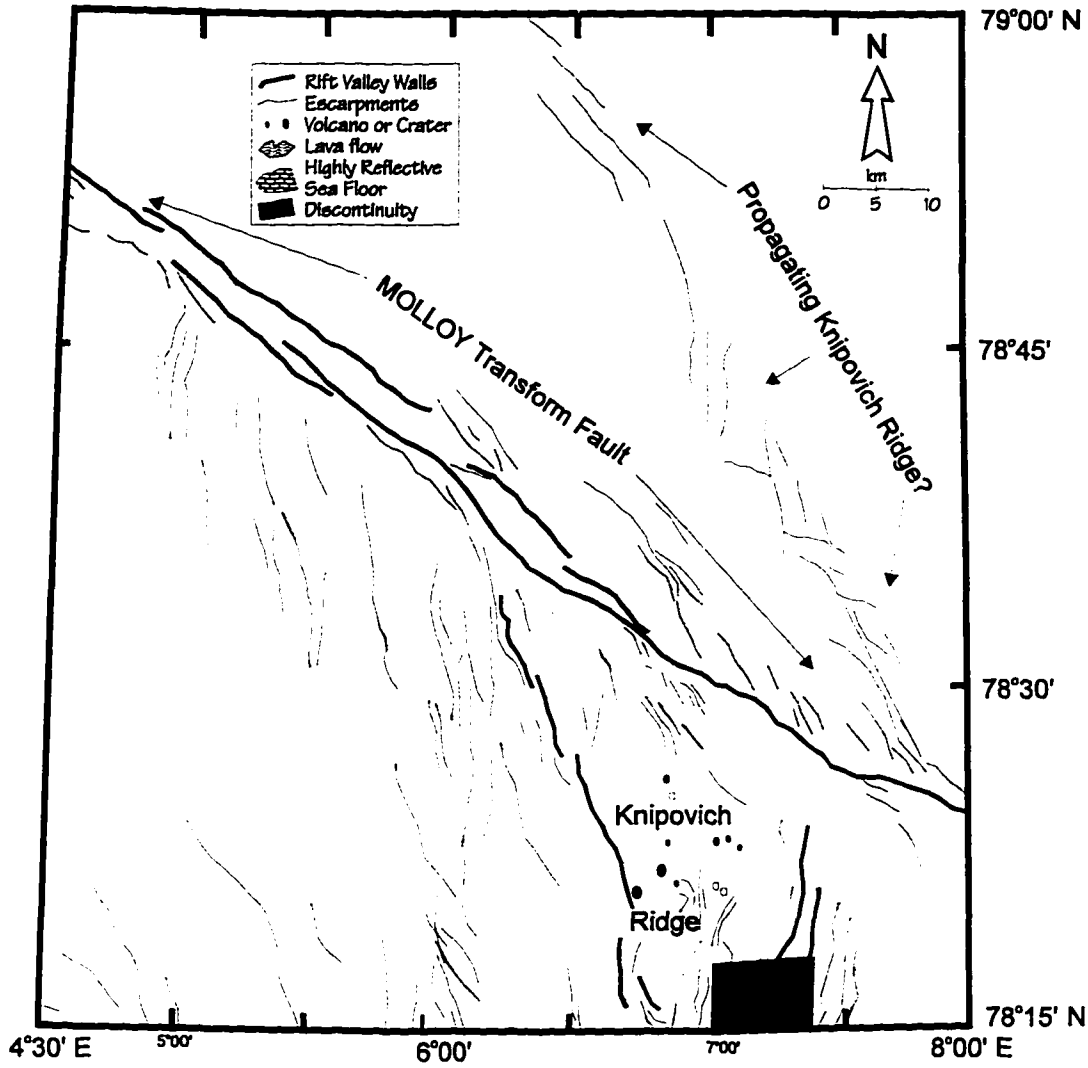

Figure 9B: Structural interpretations of the side-scan image illustrated in 9A. The Molloy Transform is well defined as a double fault system complicated by smaller anastomosing faults. Note the different trends between faults in the southwest section of the map (NW) compared to faults near the Knipovich Ridge (N) and faults at the intersection of the Knipovich Ridge and the Molloy Fracture Zone, which show a change in strike (to NW) along their length. Finally, note the faults to the northeast of the Molloy F.Z. which may indicate recent propagation of the rift valley.

Figure 10A: SeaMARC II side-scan image of the western flank of the northern Knipovich Ridge near the Hovgård Ridge (from 77°45'N to 78°30'N).

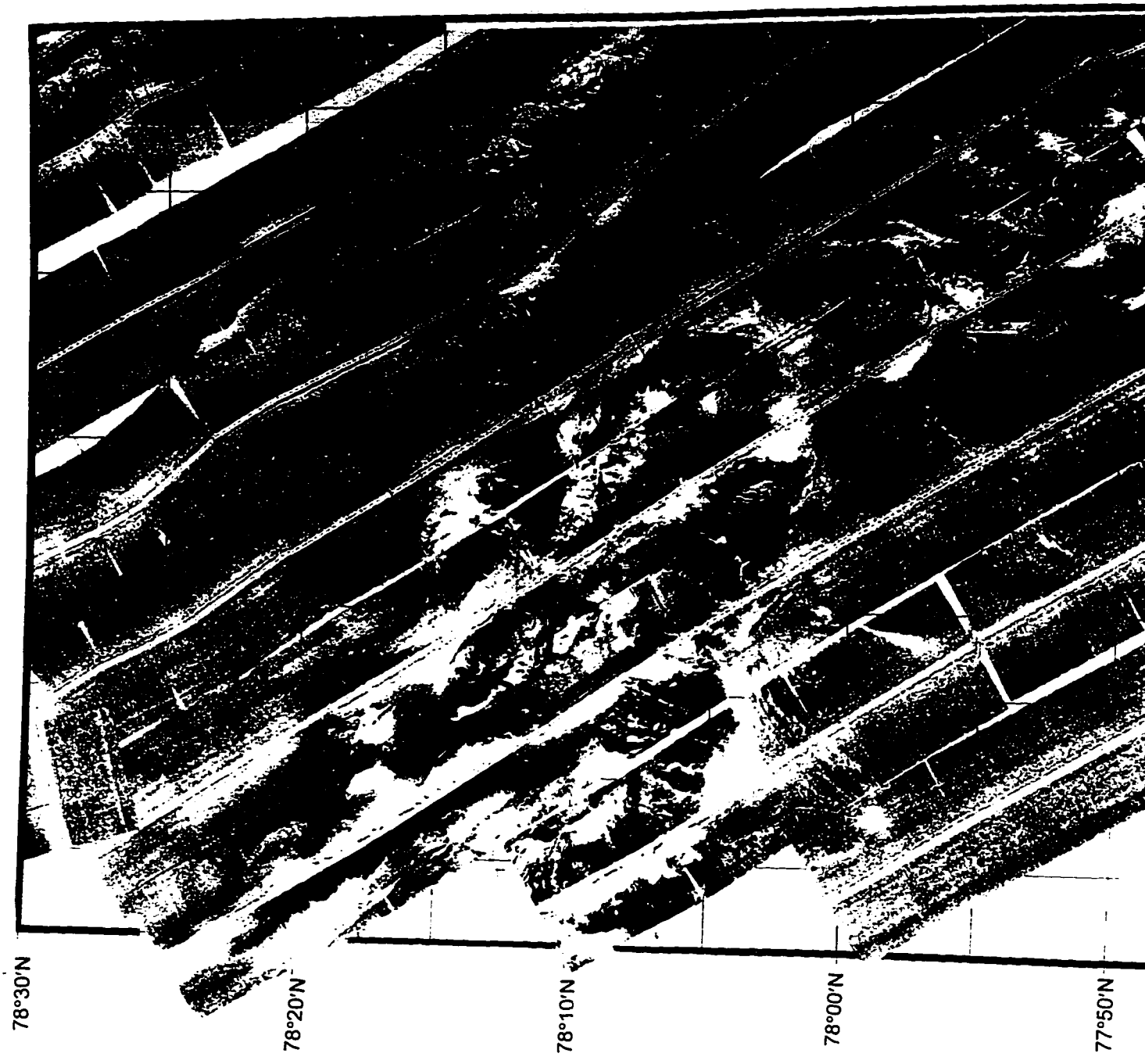

Figure 10A: SeaMARC II side-scan image of the western flank of the northern Knipovich Ridge near the Hovgård Ridge (from 77°45'N to 78°30'N).

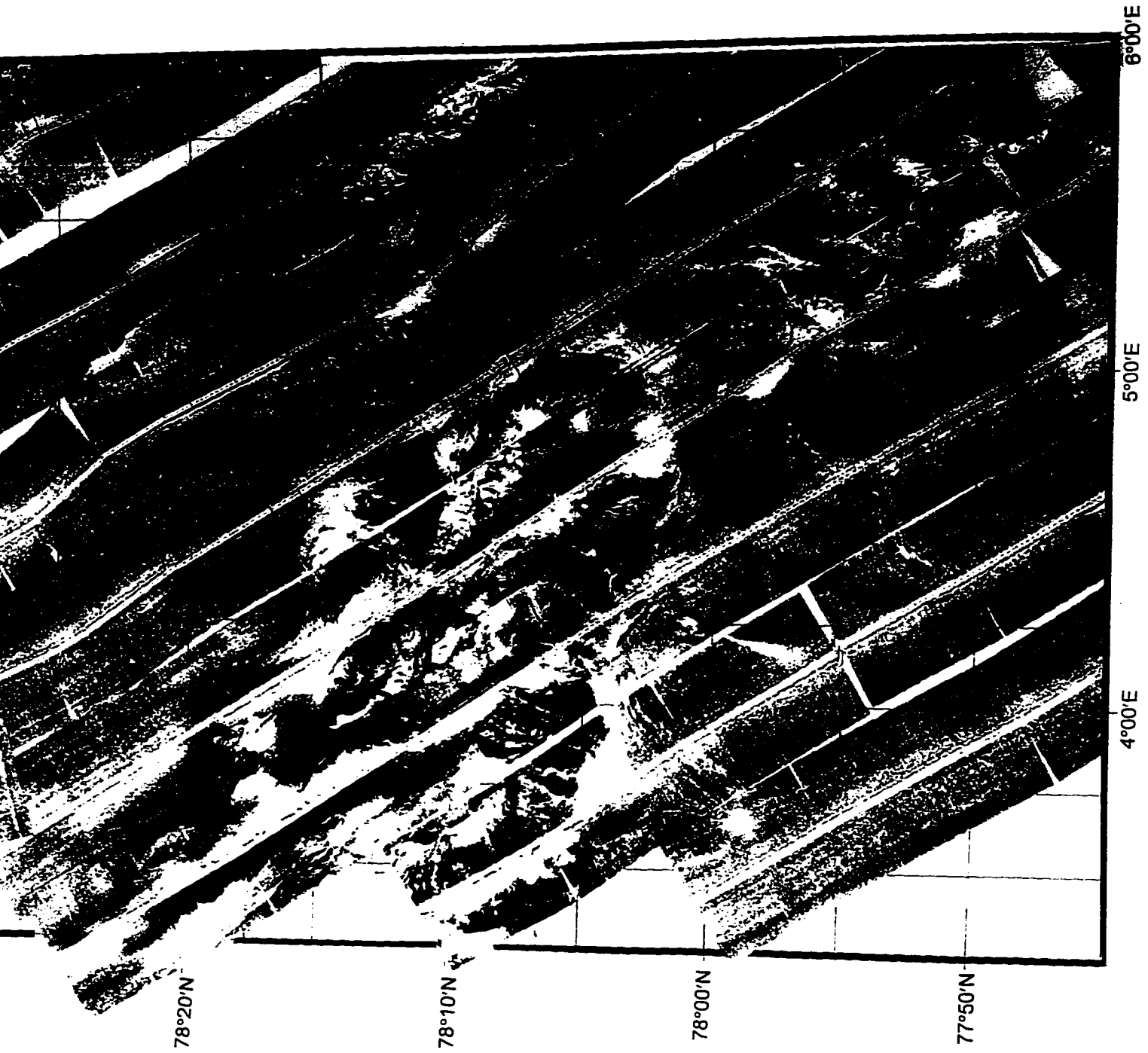

SeaMARC II side-scan image of the western flank of the northern Knipovich
ıe Hovgård Ridge (from 77°45'N to 78°30'N).

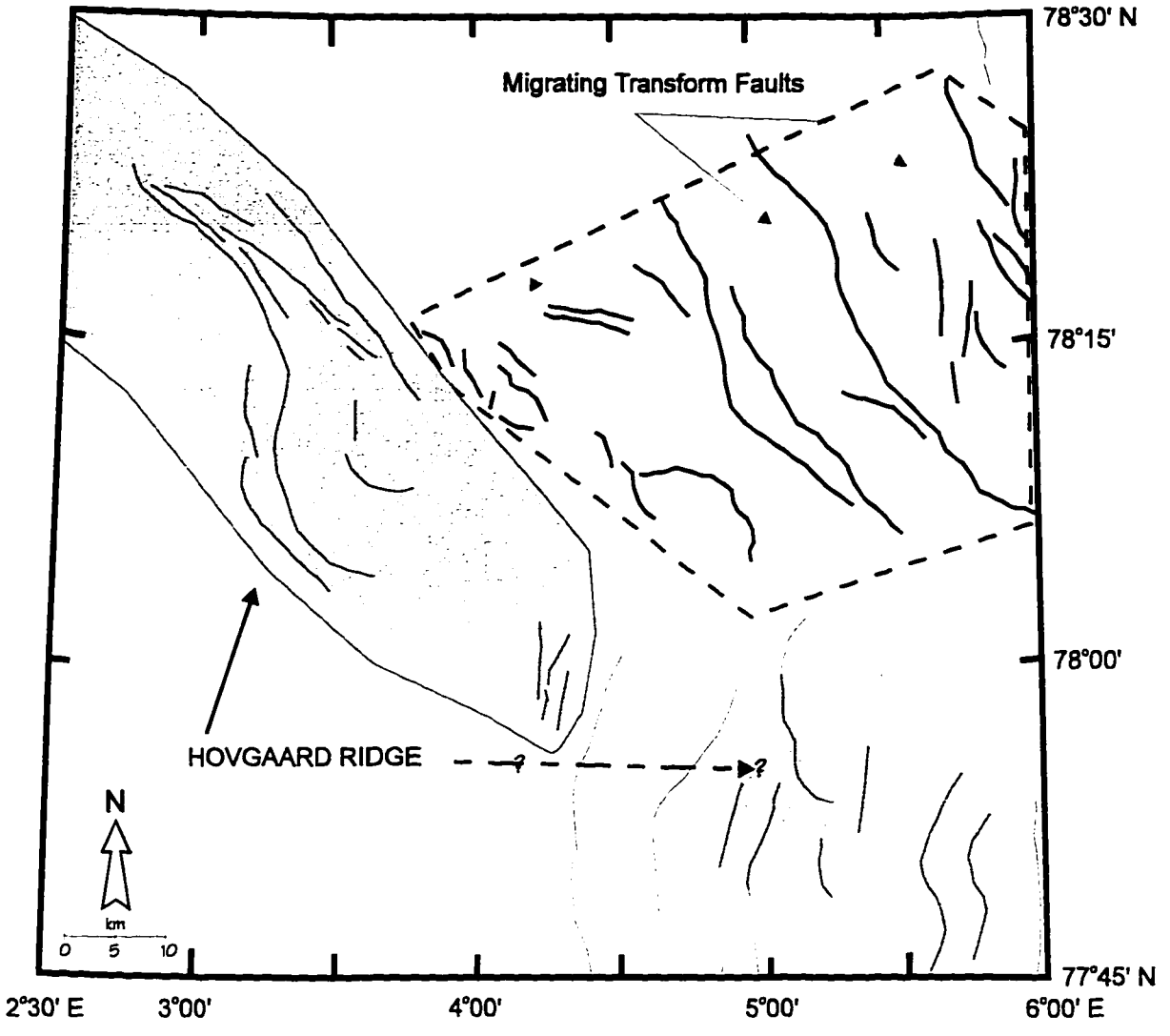

Figure 10B: Structural Interpretations of the side-scan image shown in 10A. Note the northwesterly trend of faults on and northeast of the Hovgård Ridge. The gray shaded area is probably a continuation of Seamount Belt 4. The boxed/dashed area shows highly anomalous fault trends northeast of the Hovgård Ridge indicative of a paleo-transform fault which was probably deactivated by a propagating Knipovich Ridge.

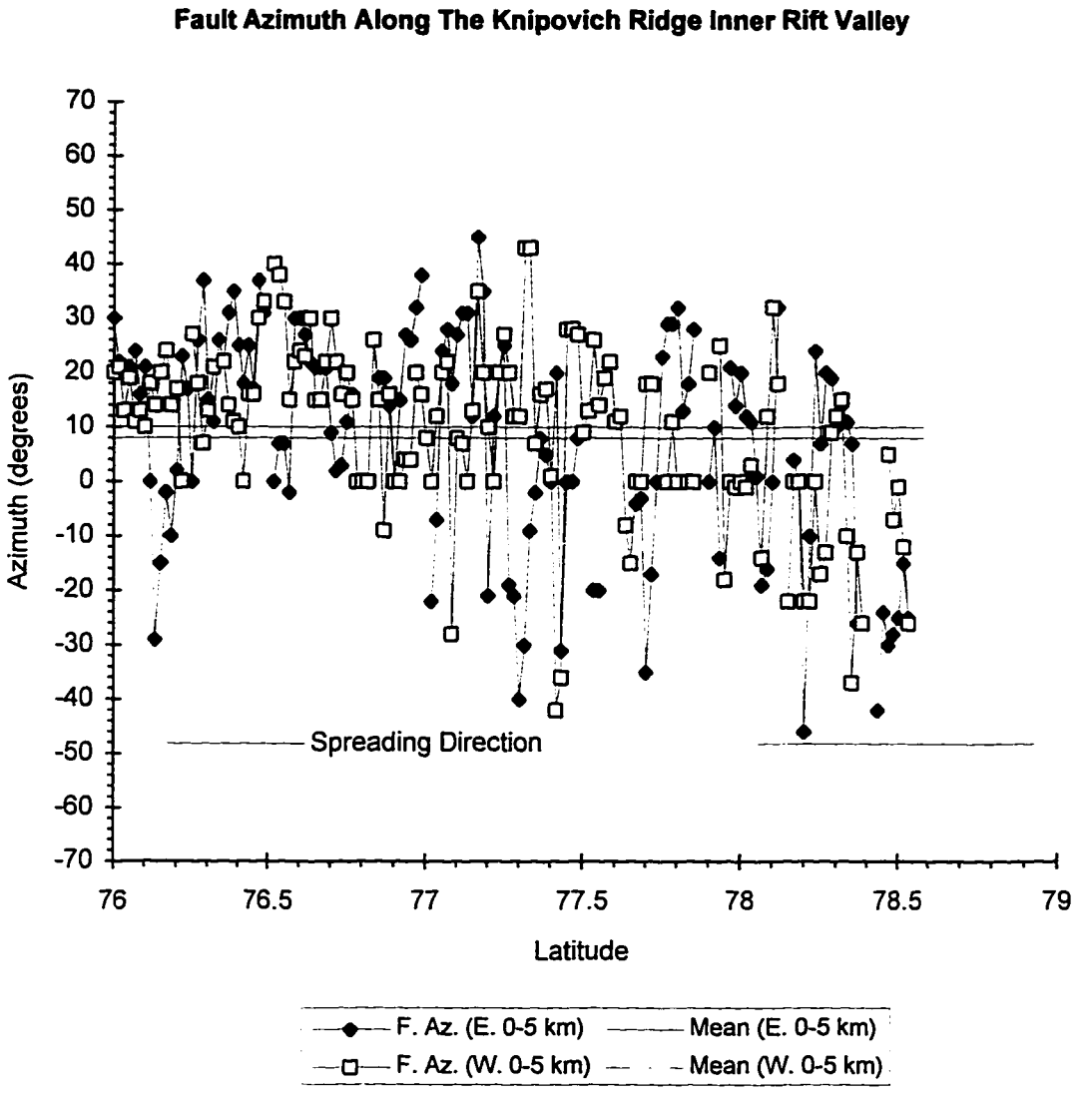

Figure 11A: Fault azimuth variability from south to north within the inner rift valley (10 km wide swath) of the Knipovich Ridge.

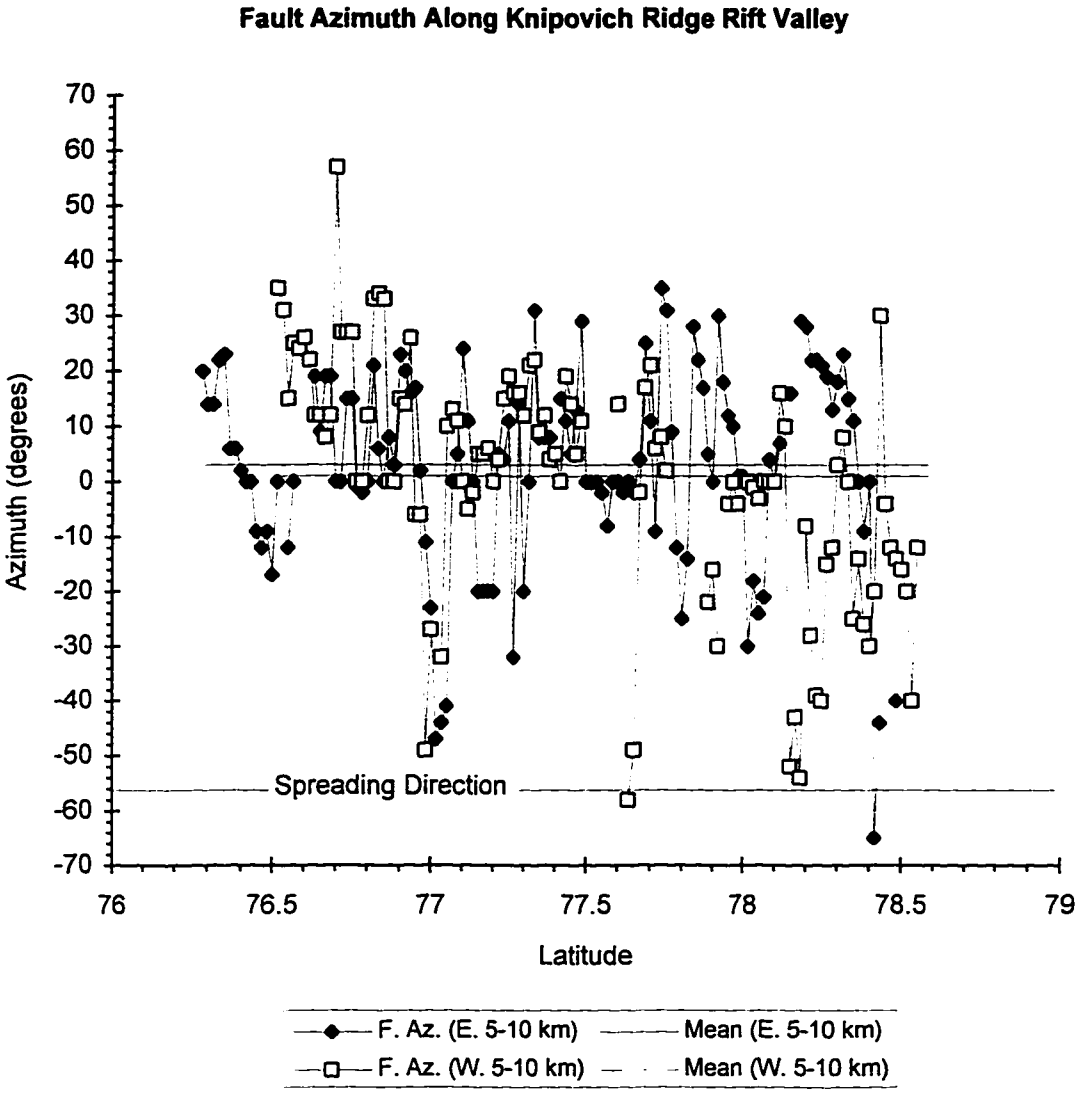

Figure 11B: Fault azimuth variability from south to north, 5-10 km away from the axis of the rift valley of the Knipovich Ridge.

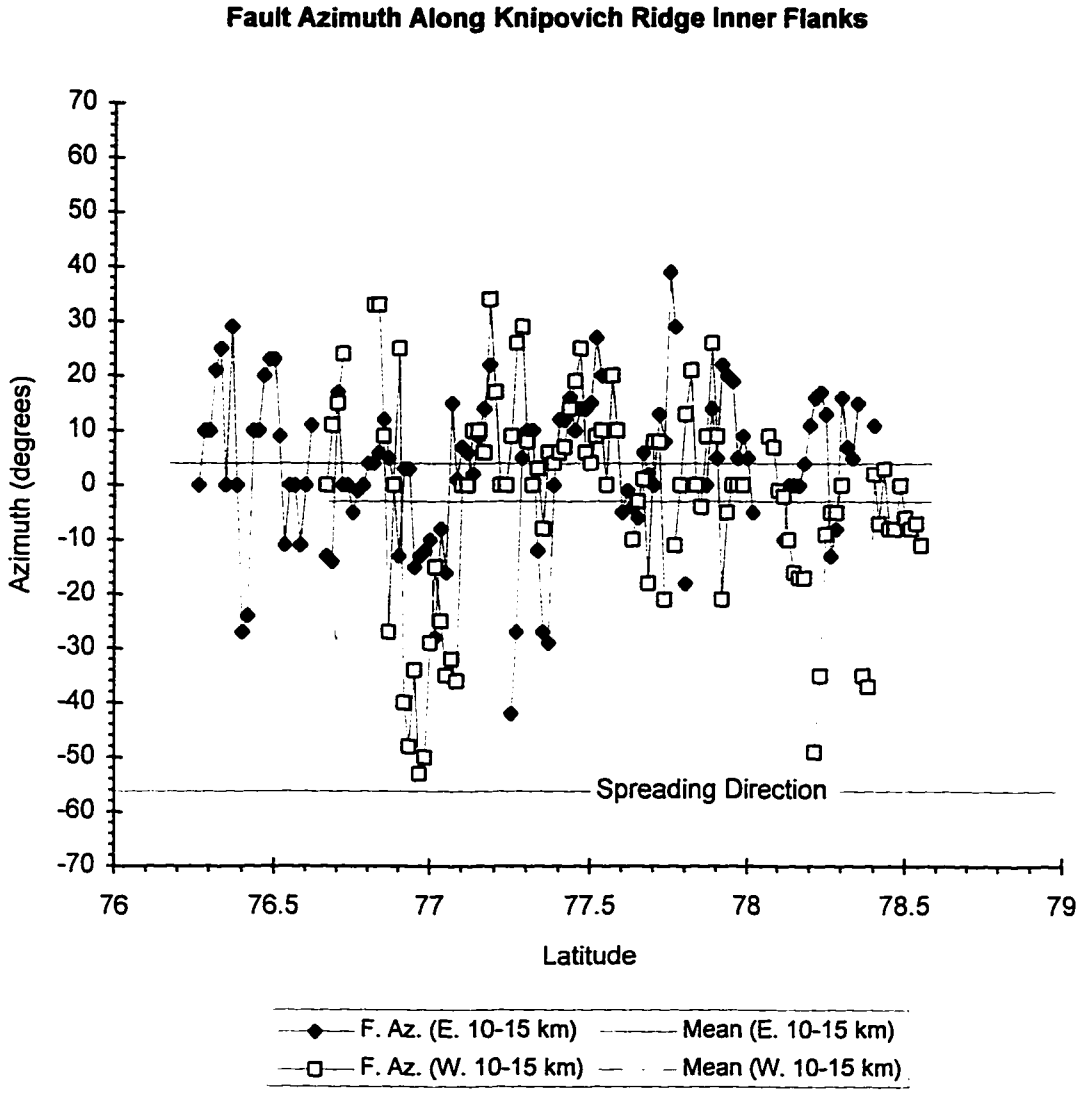

Figure 11C: Fault azimuth variability from south to north, 10-15 km away from the axis of the rift valley of the Knipovich Ridge.

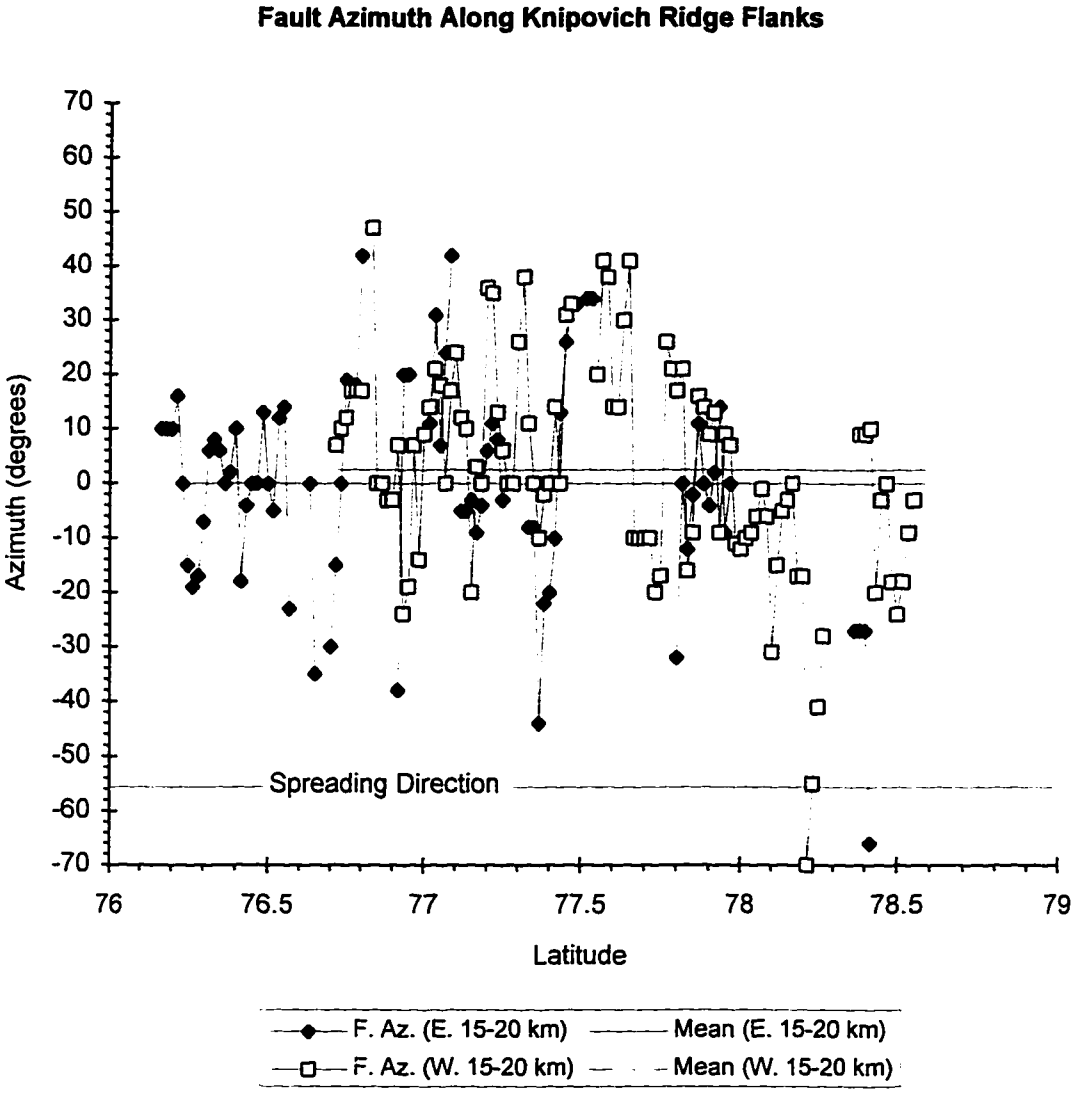

Figure 11D: Fault azimuth variability from south to north, 15-20 km away from the axis of the rift valley of the Knipovich Ridge.

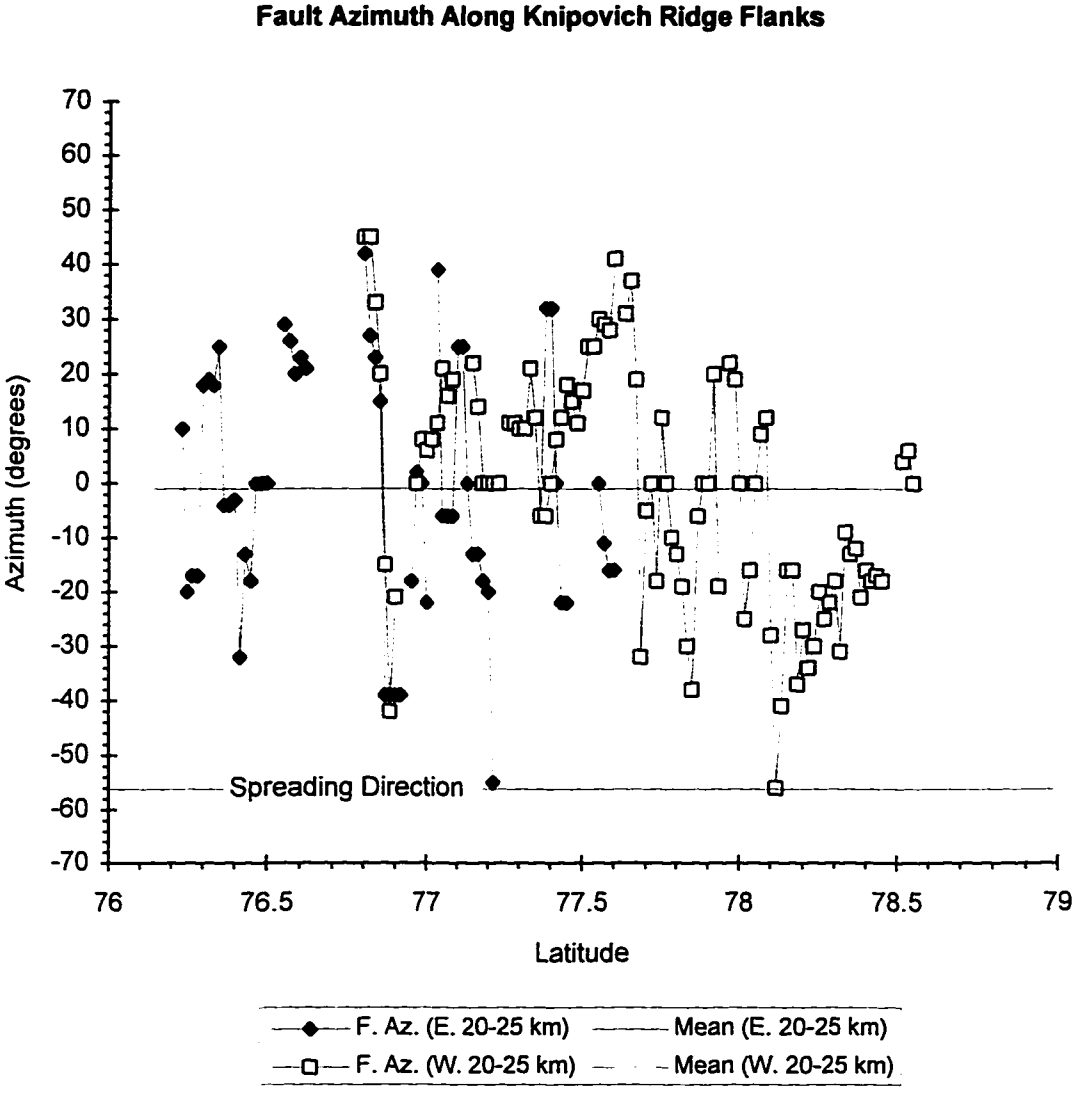

Figure 11E: Fault azimuth variability from south to north, 20-25 km away from the axis of the rift valley of the Knipovich Ridge.

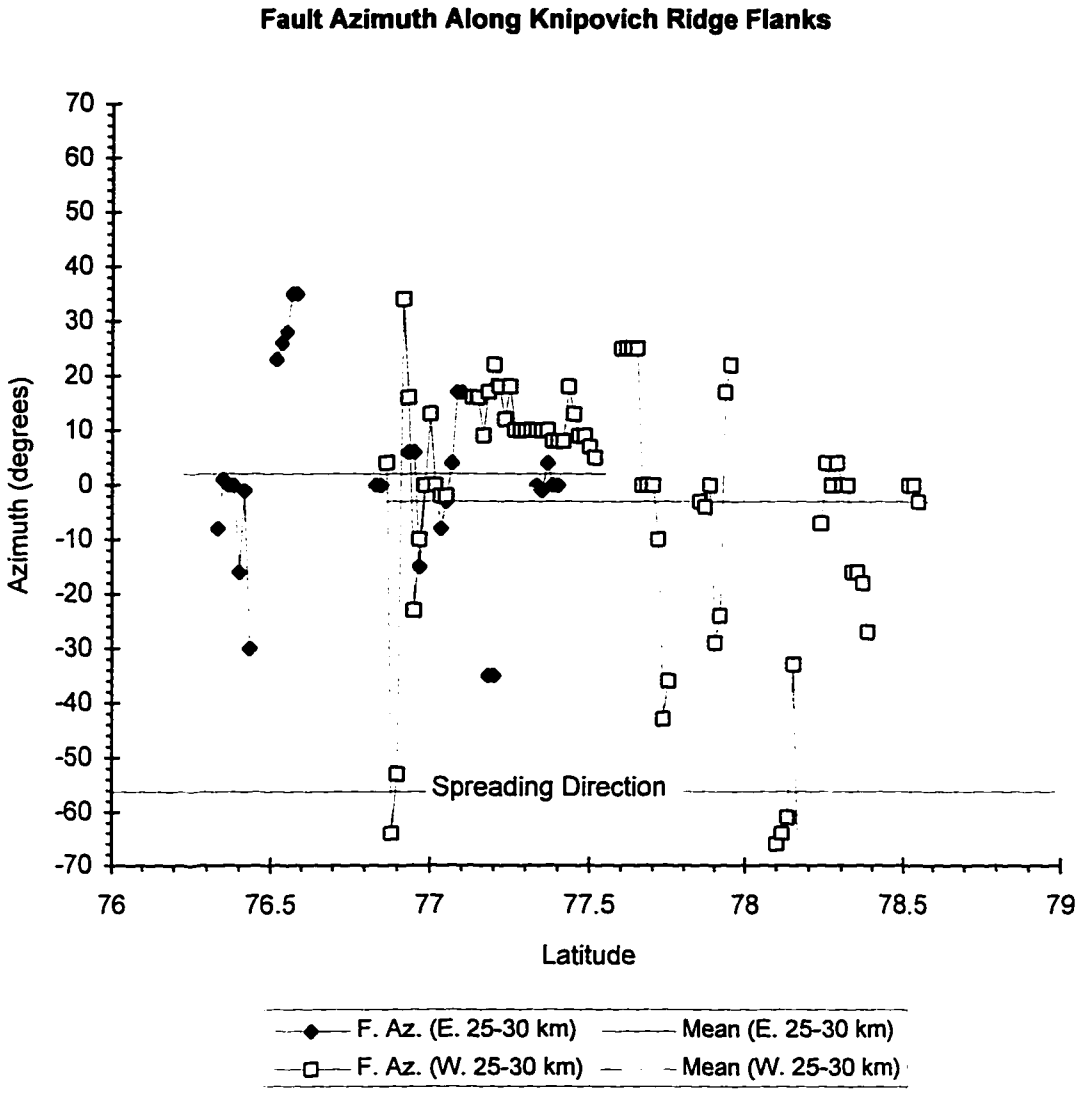

Figure 11F: Fault azimuth variability from south to north, 25-30 km away from the axis of the rift valley of the Knipovich Ridge.

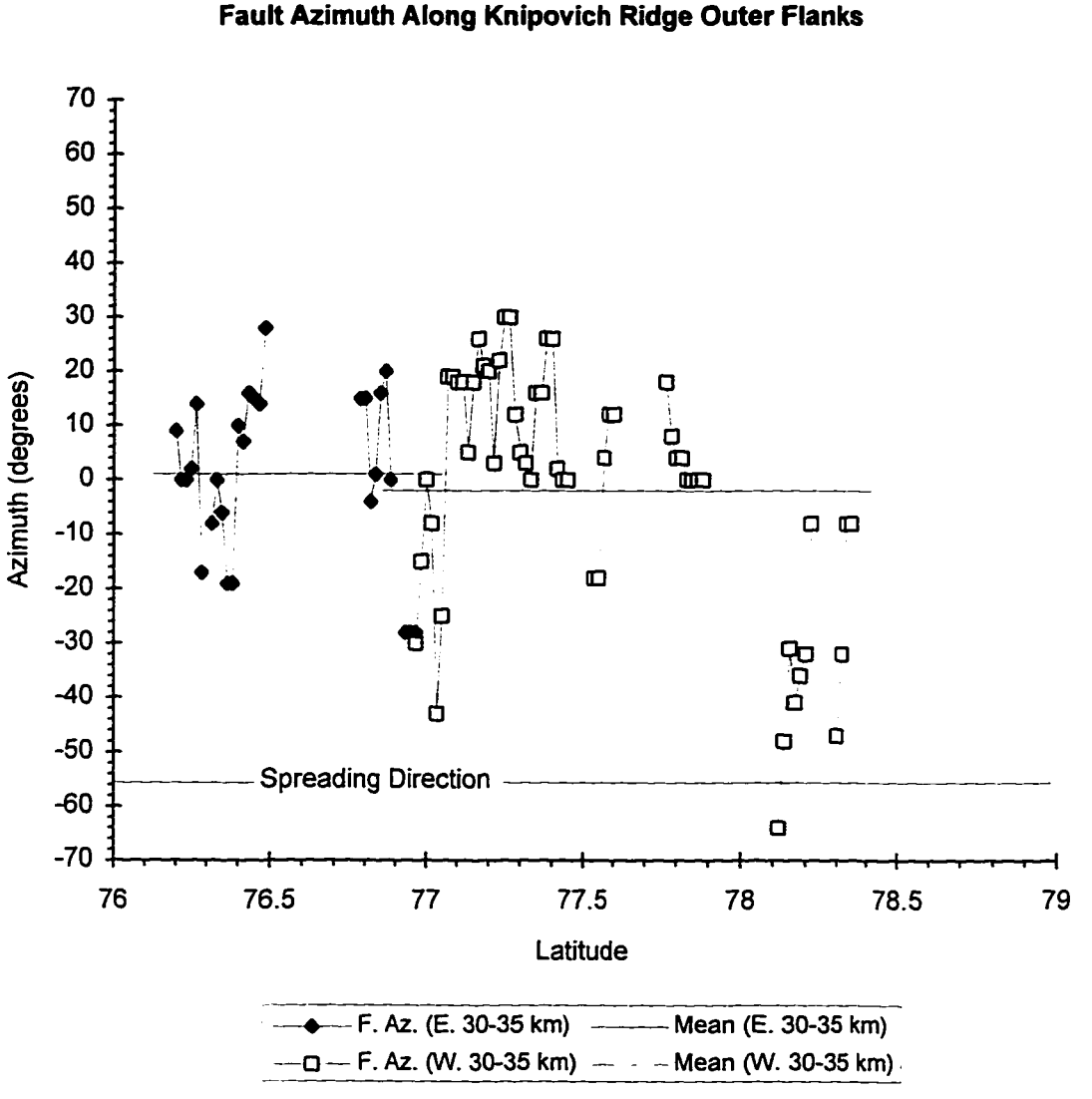

Figure 11G: Fault azimuth variability from south to north, 30-35 km away from the axis of the rift valley of the Knipovich Ridge.

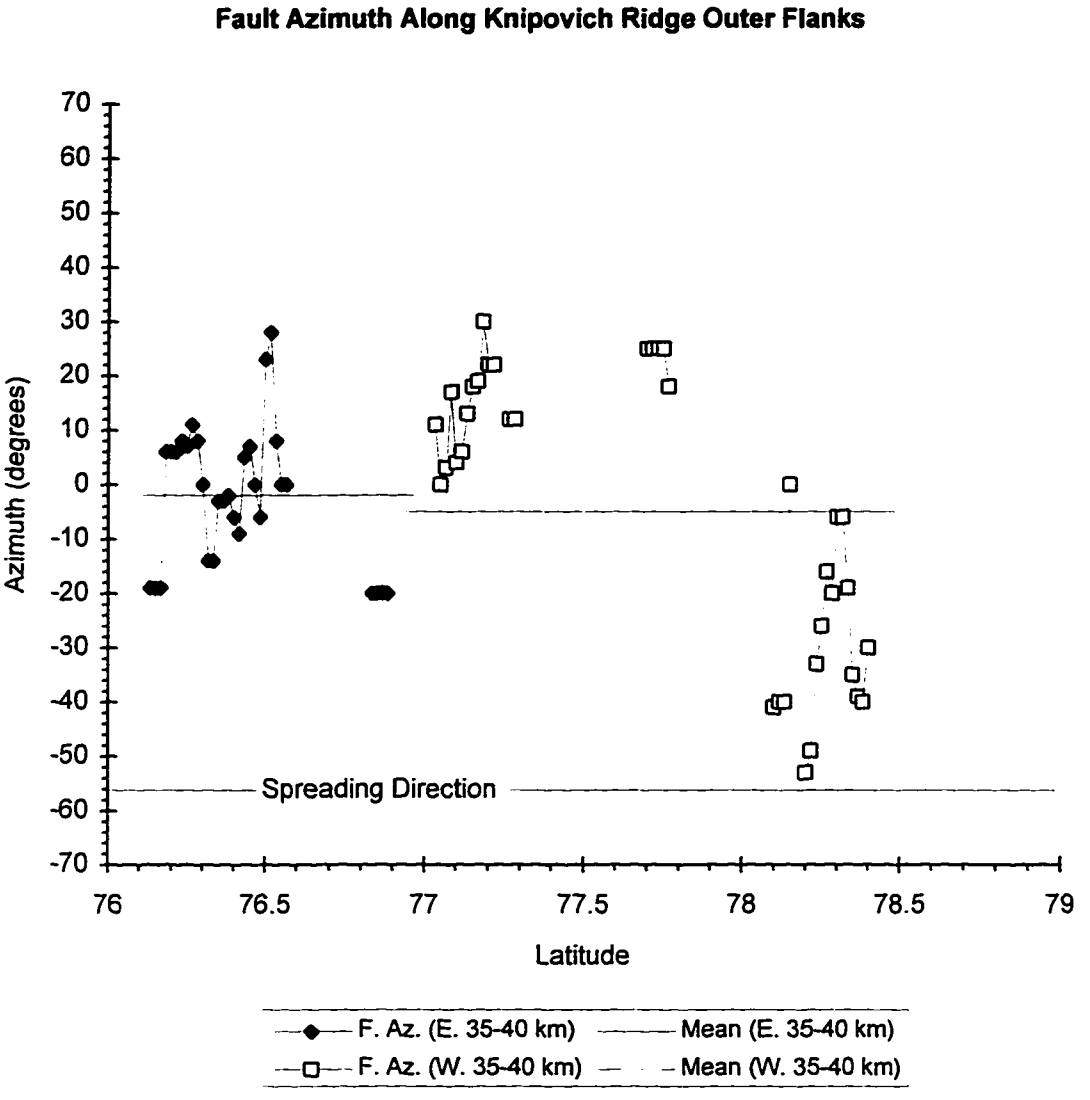

Figure 11H: Fault azimuth variability from south to north, 35-40 km away from the axis of the rift valley of the Knipovich Ridge.

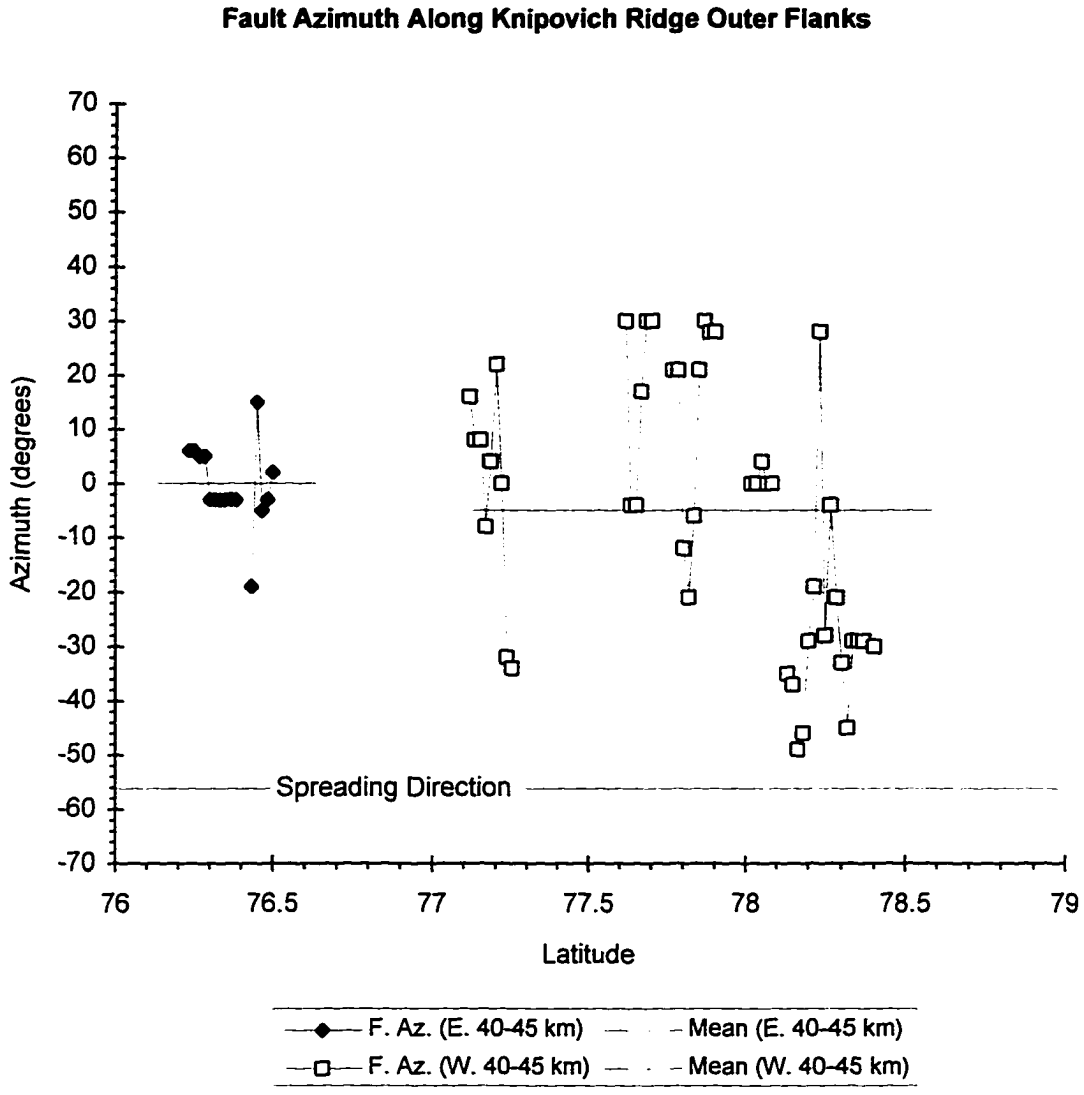

Figure 11I: Fault azimuth variability from south to north, 40-45 km away from the axis of the rift valley of the Knipovich Ridge.

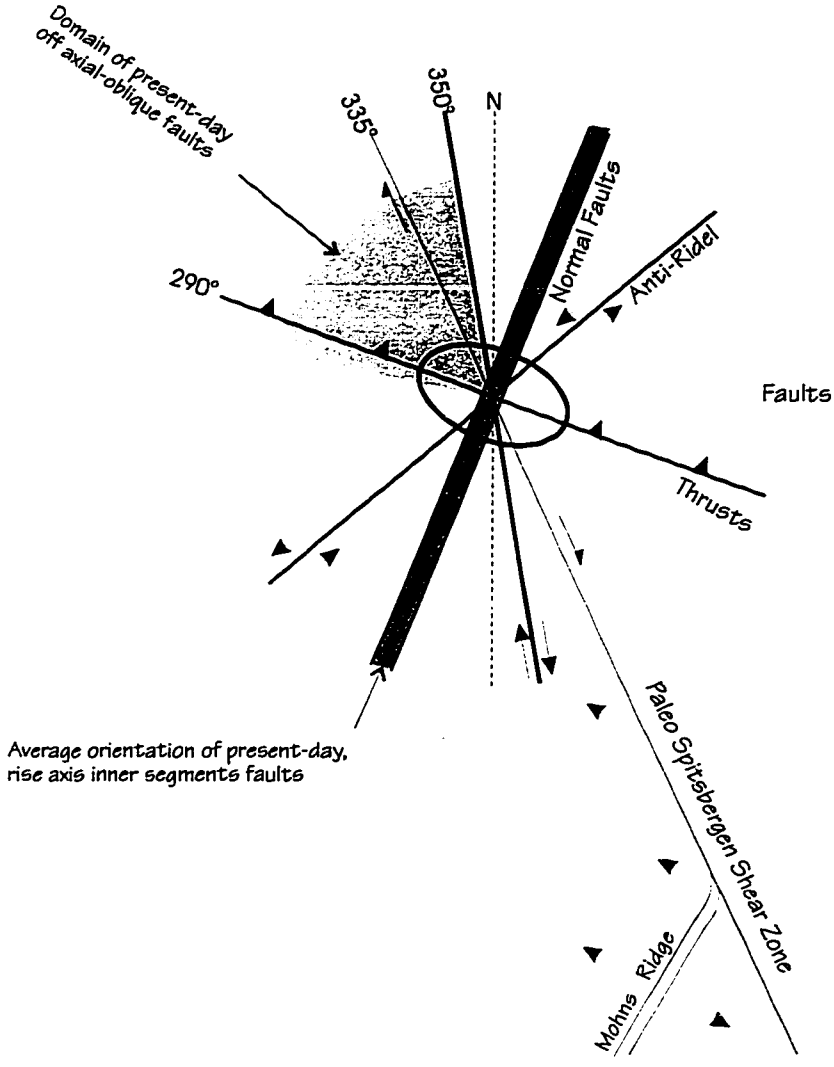

Paleo Spitsbergen Shear Couple Trends	Present Knipovich Ridge and Flank Trends
1) Normal faults (extensional) associate with shear zone trending 335° (022°)	1) Inner rift faults (024°)
2) Trend of Riedel Shears (350°)	2) Trend of Knipovich Ridge Axis (345°-005°)
3) Trend of major paleo shear zone faults (335°)	3) Trend of axial seamount chains and ridges (290°-340°)
4) Trend of compressional faults (283°-351°)	4) Trend of off axial oblique faults (283°-351°)

Figure 12: Diagram illustrating the relationship of the Paleo-Spitsbergen Shear Couple trends to the present Knipovich Ridge and flank trends.

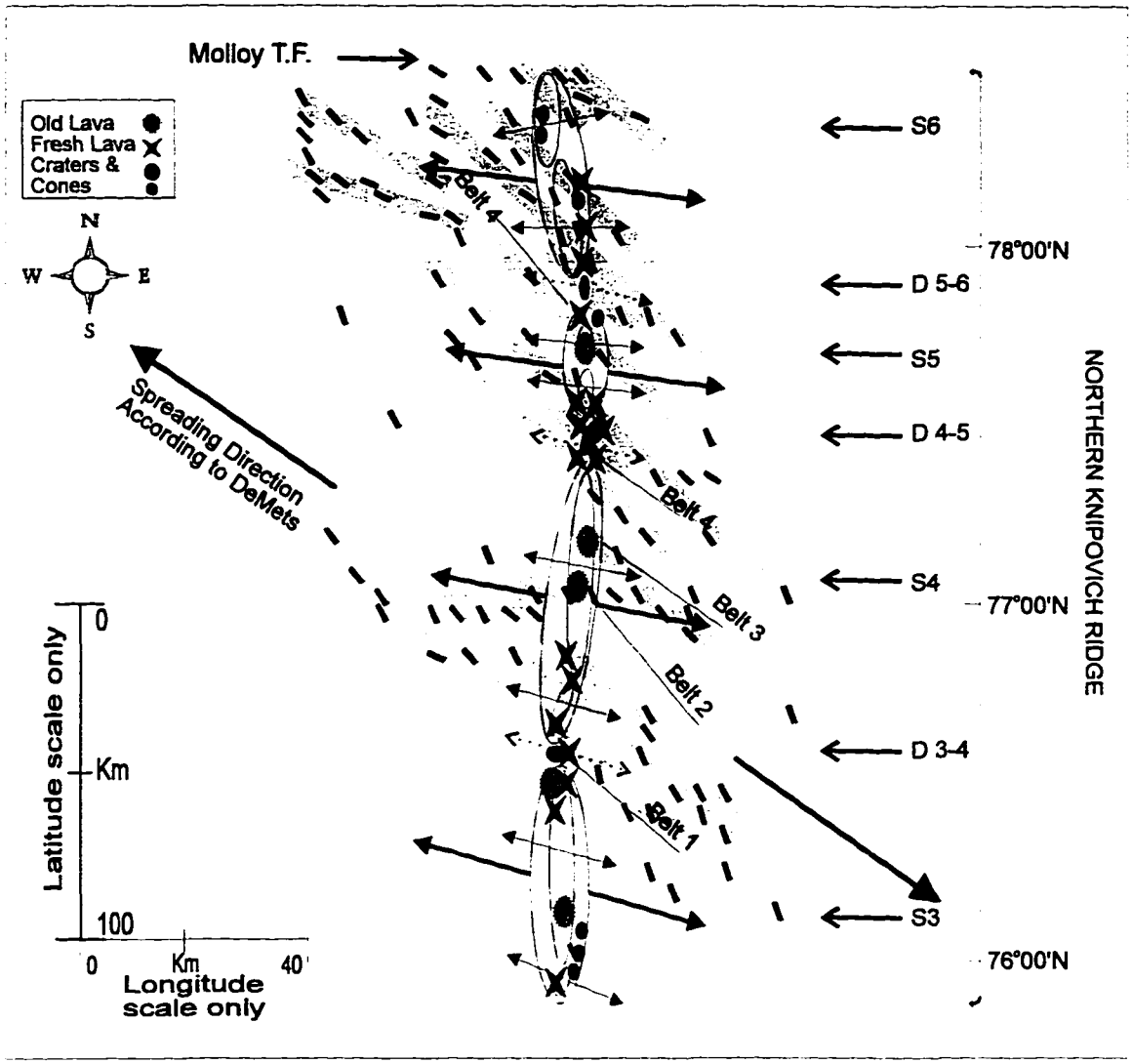

Figure 13: Diagram illustrating the distribution of second and third order segments along the northern Knipovich Ridge in comparison to proposed structural zones of weakness bands obliquely inherited from the Paleo-Spitsbergen Shear Zone. The short bold lines (exaggerated by a factor of three) within the gray bands represent the maximum anomalous orientations detected for a given location. Features are to scale along latitudes and exaggerated by a factor of three along longitudes. Along the rift valley segments, bold arrows represent spreading directions inferred from averaging fault azimuths in each second order segment, thin arrows represent inferred spreading directions for third order segments, and dashed arrows represent inferred spreading direction at major volcanic centers associated with a second order discontinuities. The flanks' shallow Seamount belts are marked. Note that there is ~10°-30° difference between the inferred spreading directions and the trends of these belts. Old and fresh lava flow locations are marked. Fresh lava flows dominate second and third order discontinuities while old lava flows tend to occur at segments' center.

BIBILIOGRAPHY

Chapter 1:

Appelgate, B., and Shor, A. N., 1993, The Northern Mid-Atlantic and Reykjanes Ridges: Spreading Center Morphology Between 55°50'N and 63°00'N (in press).

Bonatti, E., 1994, The Earth's Mantle below the Oceans, Scientific American, March 1994, 44-51.

Bonatti, E., and Crane, K., 1984, Oceanic Fracture Zones, Scientific American,, Vol. 250, No. 5, 40-51.

Bonatti, E., 1985, Punctiform initiation of seafloor spreading in the Red Sea during transition from a continental to an oceanic rift, Nature, Vol. 316, No. 6023, 33-37.

Cherkis, N. Z. and Vogt, P. R., 1994, Regional Bathymetry of the Norwegian-Greenland Sea, Naval Research Laboratory, Washington, D.C.

Cande, S. C. and Kent, D. V., 1992, A New Geomagnetic Polarity Time Scale for the Late Cretaceous and Cenozoic, Jour. Geophys. Res., 97, 13917-13951.

Chan, W. W., and B. J. Mitchell, 1985, Intraplate Earthquakes in Northern Svalbard, Tectonphysics, 114, 181-191.

Crane, K., Eldholm, O., Myhre, A. M., and Sundvor, E., 1982, Thermal Implications for the Evolution of the Spitsbergen Transform Fault, Tectonophysics, 89, 1-32.

Crane, K. and Bonatti, E., 1987, Fracture Zone Control on the Opening of the Red Sea: SIR A Data, Jour. of the Geological Soc. of London, 144, 407-420.

Crane, K., 1985, The spacing of rift axis highs: dependence upon diapiric processes in the underlying asthenosphere?, Earth and Planetary Science Letters, 72, 405-414.

Crane, K., Sundvor, E., Foucher, J. P., Hobart, M., Myhre, A. M., and LeDouran, S., 1988, Thermal Evolution of the Western Svalbard Margin, Mar. Geophys. Res., 9, 165-194.

Crane, K., Sundvor, E., Buck, R., and Martinez, F., 1991, Rifting in the Northern Norwegian-Greenland Sea: Thermal Tests of Asymmetric Spreading, Jour. Geophys. Res., 96, 14529-14550.

Desimon, A. I., and Karasik, A. M., 1979, Nekotoryye Osobennosti Morfologii I Razrastaiya Okeanicheskogo dna na Khrebte Knipovicha v Severnom Ledovitom Okeane, Dokl. Akad., Nauk SSSR, 247, 1215-1219 (in Russian), Some features of Bottom Relief and Seafloor Spreading on the Knipovich Ridge, Arctic Ocean, Dokl. Earth Science Section, 247, 73-77 (in English).

DeMets, C., Gordon, R. G., Argus, D. F., and Stein, S., 1990, Current Plate Motions, Geophys. J. Int., 101, 425-478

Detrick, R. S. and Humphris, S. E., 1994, Exploration of Global Oceanic Ridge System Unfolds, EOS, 75, 325-326.

Dore. A. G., and Gage, M. S., 1987, Crustal alignments and sedimentary domains in the evolution of the North Sea, North East Atlantic Margin and Barents Shelf. In: J. Brooks and K. Glennie (editors), Petroleum Geology of North West Europe. Graham and Trotman, London, 1131-1148.

Eldholm, O., Vogt, P., and Perry, R., 1978, Plate Tectonic Development of the Mid-Oceanic Ridge System North of the Jan Mayen Fracture Zone, A: Present Plate Boundaries, EOS 59, 371.

Eldholm, O. and Sundvor, E., 1980, The Continental Margins of the Norwegian-Greenland Sea: Recent Results and Outstanding Problems, Royal Society of London Phil. Trans., Ser. A: 294, 77-86.

Eldholm, O., Karasik, A. M., and Reksnes, P. A., 1986, The North American Plate Boundary, DNAG synthesis. Volume Geology of the Arctic Ocean Region Chapter 12.

Harland, W. B., 1969, Contribution of Spitsbergen to understanding of tectonic evolution of North Atlantic Region. In: M. Kay (Editor), North Atlantic: Geology and Continental Drift. American Association of Petroleum Geologists, Memoir 12, 817-851.

Horsfield, W. T. and Maton, P. I., 1970, Transform Faulting along the De Geer Line, Nature 226, 256-257.

Johnson, L. and Heezen, B. C., 1967, Morphology and Evolution of the Norwegian-Greenland Sea, Deep-Sea Research 14, 755-771.

Kovacs, L.C., Johnson, G. L., Srivastava, S. P., Taylor, P. T., and Vogt, P. R., 1987, Residual Magnetic Anomaly Chart of the Arctic Ocean Region (Naval research Laboratory and Naval Ocean research and Development Activity), In: The Arctic Ocean Region, Vol. L., The Geology of North America, edited by Arthur Gantz, L. Johnson, and J. F. Sweeny, 1990, 644p.

Macdonald, K. C., 1986, The Crest of the Mid-Atlantic Ridge: Models for crustal generation processes and tectonics, In: The Geology of North America, Vol. M for the Western north Atlantic Region, Edited by P. R. Vogt and B. E. Tuckolke, Geological Society of America, Boulder, CO.

Macdonald, K. C., Schierer, D. S., and Carbotte, S. M., 1991, Mid-Ocean ridges: Discontinuities, segments, and giant cracks, Science, 253, 986-994.

Minster, W. J., and T. H. Jordan, 1978, Present-Day Plate Motions, Jour. Geophys. Res., 83, 5331-5354.

Morgan, W. J., 1981, Hotspot Tracks and the Opening of the Atlantic and Indian Oceans, in The Sea, 7, edited by C. Emiliani, pp. 443-487, John Wiley, New York.

Okay, N., and Crane, K., 1993, Thermal Rejuvenation of the Yermak Plateau, Marine Geophysical Researches, 15, 243-263.

Okay, N., 1995, Thermal Rejuvenation in the Norwegian-Greenland Sea, Unpublished Ph.D. Thesis.

Ohta, Y., 1982, Morpho-Tectonic Studies Around Svalbard and the Northernmost Atlantic, in Embry, A. F. and Blackwell, H. R., Arctic Geology and Geophysics, Can. Soc. Petroleum Geol., Memoir 8,. 415-431.

Prestvik, T., 1977, Cenozoic plateau lavas of Spitsbergen - a geochemical study, Norsk Polarist, Arbok, 127-143.

Perry, R. K., Fleming, H. S., Weber, J. R., Kristoffersen, Y., Hall, J. K., Grantz, A., Johnson, G. L., Cherkis, N. Z., and Larsen, B., 1985, Bathymetry of the Arctic Ocean, Scale 1:6,000,000, Geol. Soc. Amer. Map Series, MC-56, Naval Research Laboratory, Washington, D.C.

Schouten, H., and Klitgord, K. D., 1982, The memory of the accreting plate boundary and the continuity of fracture zones, Earth Planet. Sci. Lett., 59, 255-266.

Schouten, H., and Klitgord, K. D., and Whitehead, J. A., 1985, Segmentation of mid-ocean ridges, Nature, 317, 225-229.

Searle, R. C., and Laughton, A. S., 1977, Sonar studies of the Mid-Atlantic Ridge and Kurchatov Fracture Zone, Jour. Geophys. Res., 82, 5313-5328.

Searle, R. C., 1984, GLORIA Survey of the East Pacific Rise near 3.5°S: Tectonic and volcanic characteristics of a fast spreading mid-ocean rise, Tectonophysics, 101, 319-344.

Sempere, J. C., and Macdonald, K. C., 1987, Marine Tectonics: Processes at Mid-Ocean Ridges, Reviews of Geophysics, 25, 6, 1313-1347.

Sempere, J. C., Purdy, G. M., and Schouten, H., 1990, Segmentation of the Mid-Atlantic Ridge between 24° N and 30°40N, Mar. Geophys. Res., 15, 153-200.

Sempere, J. C., J. Lin, H. S. Brown, H. Schouten, and G. M. Purdy., 1993, Segmentation and morphotectonic variations along a slow-spreading center: The Mid-Atlantic Ridge (24° N-30°40N, Nature, 344, 427-431.

Shor, A., 1990, SeaMARC II seafloor mapping system: Seven years of Pacific research, Pacific Rim Congress Vol. III; Australian Institute of Mining and Metallogenesis, 49-59.

Skjelkvale, B. L., Amundsen, H. E. F., O'Reilly, S. Y., Griffin, W. L., and Gjelsvik, T., 1989, A primitive alkali basaltic stratovolcano and associated eruptive centers, Northwestern Spitsbergen,: Volcanology and Tectonic Significance, 1989, Journal of Volcanology and Geothermal Research, 37, 1-19.

Sobczak, L. W., and Hearty, D. B., with contributions by R. Forsberg, Y. Kristoffersen, O. Eldholm and S. D. May), 1987, Gravity of the Arctic Ocean, In: The Arctic Ocean Region, Vol. L., The Geology of North America, edited by Arthur Gantz, L. Johnson, and J. F. Sweeny, 1990, 644p.

Stein, S., Melosh, H. J., and Minster, J. B., 1977, Ridge Migration and Asymmetric Sea-floor Spreading, Earth Planet. Sci. Lett., 36, 51-62.

Sundvor, E. and O. Eldholm, 1979, The Western and Northern Margin off Svalbard, Tectonophysics, 59, 239-250.

Talwani, M. and Eldholm, O., 1977, Evolution of the Norwegian-Greenland Sea, Geol. Soc. America Bull. 88, 969-999.

Thiede, J., S. Pfirman, H-W Schenke, and W. Reil, 1990, Bathymetry of the Molloy Deep: Fram Strait between Greenland and Svalbard, Marine Geophysical Researches, 12, 197-214.

Vogt, P. R., and Avery, O. E., 1974, Tectonic History of the Arctic Basins: Partial Solutions and Unsolved Mysteries, in Marine Geology and Oceanography of the Arctic Seas, edited by Herman, Y., 83-117, Springer-Verlag, New York.

Vogt, P. R., R. H. Feden, O. Eldholm, and E. Sundvor, 1978, The Ocean Crust West and North of the Svalbard Archipelago: Synthesis and Review of New Results, Polarforschung, 48, 1-19.

Vogt, P. R., G. L. Johnson, and L. Kristjansson, 1980, Morphology and Magnetic Anomalies North of Iceland, Journal of Geophysics, 47, 67-80

Vogt, P. R., R. K. Perry, R. H. Feden, H. S. Fleming, and N. Z. Cherkis, 1981, The Greenland-Norwegian Sea and Iceland Environment: Geology and Geophysics; In: The Ocean Basins and Margins, Vol. 5, The Arctic Ocean, Edited by A. E. M. Nairn and M. Churkin, pp. 493-598, Plenum, New York, 1981.

Vogt, P. R., L. C. Kovacs, L. C. Bernero, and S. P. Srivastava, 1982, Asymmetric geophysical signatures in the Greenland-Norwegian and southern Labrador Seas and the Eurasia Basin, Tectonophysics, 89, 95-160.

Vogt, P. R., 1986b, Geophysical and Geochemical Signatures and Plate Tectonics, Chapter 11, in The Nordic Seas, edited by B. G. Hurdle, Springer Verlag.

Vogt, P. R., 1986a, Seafloor Topography, Sediments, and Paleoenvironments, Chapter 11, in The Nordic Seas, edited by B. G. Hurdle, Springer Verlag.

Vogt, P. R., K. Crane, E. Sundvor, M. D. Max, and S. L. Pfirman, 1994, Methane-Generated(?) Pockmarks on young thickly sedimented oceanic crust in the Arctic: Vestnesa Ridge, Fram Strait, Geology, 22, 255-258.

Wernicke, B., 1985, Uniform sense normal simple shear of the continental lithosphere, Canadian Journal of Earth Sciences, 22, 108-125.

Chapter2:

Appelgate, B., and Shor, A. N., 1993, The Northern Mid-Atlantic and Reykjanes Ridges: Spreading Center Morphology Between 55°50'N and 63°00'N, in press.

Bonatti, E., 1985, Punctiform initiation of seafloor spreading in the Red Sea during transition from a continental to an oceanic rift, Nature, Vol. 316, No. 6023, 33-37.

Bonatti, E., G. Ottonello, and P. R. Hamlyn, 1986, Peridotites from the island of Zabargad (St. John) Red Sea: Petrology and Geochemistry, Jour. Geophys. Res., 91, 599-631.

Cherkis, N. Z. and Vogt, P. R., 1994, Regional Bathymetry of the Norwegian-Greenland Sea, Naval Research Laboratory, Washington, D.C.

Courtillot, V., 1982, Propagating Rifts and Continental Breakup, Tectonics, 1, 239-250.

Crane, K., 1985, The spacing of rift axis highs: dependence upon diapiric processes in the underlying asthenosphere?, Earth and Planetary Science Letters, 72, 405-414.

Crane, K., and E. Bonatti, 1987, The role of fracture zones during early Red Sea rifting: structural analysis using Space Shuttle radar and LANDSAT imagery, Jour. Geol. Soc., 144, 407-420.

Crane, K., Sundvor, E., Foucher, J. P., Hobart, M., Myhre, A. M., and LeDouran, S., 1988, Thermal Evolution of the Western Svalbard Margin, Mar. Geophys. Res., 9, 165-194.

Crane, K., Sundvor, E., Buck, R., and Martinez, F., 1991, Rifting in the Northern Norwegian-Greenland Sea: Thermal Tests of Asymmetric Spreading, Jour. Geophysical. Res., 96, 14529-14550.

Dore. A. G., and Gage, M. S., 1987, Crustal alignments and sedimentary domains in the evolution of the North Sea, North East Atlantic Margin and Barents Shelf. In: J. Brooks and K. Glennie (editors), Petroleum Geology of North West Europe. Graham and Trotman, London, 1131-1148.

Eldholm, O., Vogt, P., and Perry, R., 1978, Plate Tectonic Development of the Mid-Oceanic Ridge System North of the Jan Mayen Fracture Zone, A: Present Plate Boundaries, EOS 59, 371.

Eldholm, O. and Sundvor, E., 1980, The Continental Margins of the Norwegian-Greenland Sea: Recent Results and Outstanding Problems, Royal Society of London Phil. Trans., Ser. A: 294, 77-86.

Eldholm, O., Karasik, A. M., and Reksnes, P. A., 1986, The North American Plate Boundary, DNAG synthesis. Volume Geology of the Arctic Ocean Region Chapter 12.

Geli, L., 1993, "Volcano-tectonic breathing" and Sedimentation since late Miocene times at the Mohns Ridge in the Norwegian-Greenland Sea, unpublished work.

Harland, W. B., 1969, Contribution of Spitsbergen to understanding of tectonic evolution of North Atlantic Region. In: M. Kay (Editor), North Atlantic: Geology and Continental Drift. American Association of Petroleum Geologists, Memoir 12, 817-851

Horsfield, W. T. and Maton, P. I., 1970, Transform Faulting along the De Geer Line, Nature 226, 256-257

Johnson, L. and Heezen, B. C., 1967, Morphology and Evolution of the Norwegian-Greenland Sea, Deep-Sea Research 14, 755-771.

Kent, D. V., and Gradstein, F. M., 1986, A Jurassic to recent Chronology, In P. Vogt and B. Tucholke (editors), 1986, The Western North Atlantic Region, Vol. M, Decade of North American Geology (DNAG) series, Geological Society of America, Boulder.

Kovacs, L.C., Johnson, G. L., Srivastava, S. P., Taylor, P. T., and Vogt, P. R., 1987, Residual Magnetic Anomaly Chart of the Arctic Ocean Region (Naval research Laboratory and Naval Ocean research and Development Activity), In: The Arctic Ocean Region, Vol. L., The Geology of North America, edited by Arthur Gantz, L. Johnson, and J. F. Sweeny, 1990, 644p.

LaBrecque, J. L., Kent D. V., and Cande S. C., 1977, Revised Magnetic Polarity Time Scale for Late Cretaceous and Cenozoic Time, Geology, 5, 330-335.

Macdonald, K. C., Scheirer, D. S., and Carbotte, S. M., 1991, Mid-Ocean ridges: Discontinuities, segments, and giant cracks, Science, 253, 986-994,

Nishenko, S., 1986, Compilation (digital file) of earthquake epicenters etc. In the North

Atlantic area prepared for Zoback et al. (1986) and Einarrson (1986).

Okay, N., and Crane, K., 1993, Thermal Rejuvenation of the Yermak Plateau, Marine Geophysical Researches, 15, 243-263.

Palmer, A. R., 1983, The Decade of North American Geology 1983 Geologic Time Scale, Geological Society of America, Boulder

Perry, R. K., Fleming, H. S., Weber, J. R., Kristoffersen, Y., Hall, J. K., Grantz, A., Johnson, G. L., Cherkis, N. Z., and Larsen, B., 1985, Bathymetry of the Arctic Ocean, Scale 1:6,000,000, Geol. Soc. Amer. Map Series, MC-56, Naval Research Laboratory, Washington, D.C.

Schouten, H., and Klitgord, K. D., and Whitehead, J. A., 1985, Segmentation of mid-ocean ridges, Nature, 317, 225-229.

Sempere, J. C., Purdy, G. M., and Schouten, H., 1990, Segmentation of the Mid-Atlantic Ridge between 24° N and 30°40N, Nature, 344, 427-431.

Shor, A., 1990, SeaMARC II seafloor mapping system: Seven years of Pacific research, Pacific Rim Congress Vol. III; Australian Institute of Mining and Metallogenesis, 49-59.

Sobczak, L. W., and Hearty, D. B., with contributions by R. Forsberg, Y. Kristoffersen, O. Eldholm and S. D. May), 1987, Gravity of the Arctic Ocean, In: The Arctic Ocean Region, Vol. L., The Geology of North America, edited by Arthur Gantz, L. Johnson, and J. F. Sweeny, 1990, 644p.

Sundvor, E. and O. Eldholm, 1979, The Western and Northern Margin off Svalbard, Tectonophysics, 59, 239-250.

Sundvor, E., and Austegard, A., 1990, The Evolution of the Svalbard Margins: Synthesis and new results, In: Geological History of the Polar Oceans: Arctic Versus Antarctic, U. Bleil and J. Thiede (editors), Kluwer Academic Publishing, 77-94.

Talwani, M. and Eldholm, O., 1977, Evolution of the Norwegian-Greenland Sea, Geol. Soc. America Bull. 88, 969-999.

Vogt, P. R., and Avery, O. E., 1974, Tectonic History of the Arctic Basins: Partial Solutions and Unsolved Mysteries, in Marine Geology and Oceanography of the Arctic Seas, edited by Herman, Y., 83-117, Springer-Verlag, New York.

Vogt, P. R., Perry R. K., Feden R. H., Fleming H. S., and Cherkis N. Z., 1981, 'The Greenland-Norwegian Sea and Iceland Environment: Geology and Geophysics, in: The Ocean Basins and Margins, 5, Nairn, A. E. M. and Churkin, M. (editors), pp. 493-598.

Vogt, P. R., L. C. Kovacs, L. C. Bornero, and S. P. Srivastava, 1982, Asymmetric geophysical signatures in the Greenland-Norwegian and southern Labrador Seas and the

Eurasia Basin, Tectonophysics, 89, 95-160.

Vogt, P. R., 1986, Geophysical and Geochemical Signatures and Plate Tectonics, Chapter 11, in The Nordic Seas, edited by B. G. Hurdle, Springer Verlag.

Chapter 3:

Chan, W. W., and B. J. Mitchell, 1985, Intraplate Earthquakes in Northern Svalbard, Tectonphysics, 114, 181-191.

Cande, S. C. and Kent, D. V., 1992, A New Geomagnetic Polarity Time Scale for the Late Cretaceous and Cenozoic, Jour. Geophys. Res., 97, 13917-13951.

Crane, K., Eldholm, O., Myhre, A. M., and Sundvor, E., 1982, Thermal Implications for the Evolution of the Spitsbergen Transform Fault, Tectonophysics, 89, 1-32.

Crane, K. and Bonatti, E., 1986, Fracture Zone Control on the Opening of the Red Sea: SIR A Data, Jour. of the Geological Soc. of London, 144, 407-420.

Crane, K., 1985, The spacing of rift axis highs: dependence upon diapiric processes in the underlying asthenosphere?, Earth and Planetary Science Letters, 72, 405-414.

Crane, K., Sundvor, E., Foucher, J. P., Hobart, M., Myhre, A. M., and LeDouran, S., 1988, Thermal Evolution of the Western Svalbard Margin, Mar. Geophys. Res., 9, 165-194.

Crane, K., Sundvor, E., Buck, R., and Martinez, F., 1991, Rifting in the Northern Norwegian-Greenland Sea: Thermal Tests of Asymmetric Spreading, Jour. Geophys. Res., 96, 14529-14550.

DeMets, C., Gordon, R. G., Argus, D. F., and Stein, S., 1990, Current Plate Motions, Geophys. J. Int., 101, 425-478

Dore. A. G., and Gage, M. S., 1987, Crustal alignments and sedimentary domains in the evolution of the North Sea, North East Atlantic Margin and Barents Shelf. In: J. Brooks and K. Glennie (editors), Petroleum Geology of North West Europe. Graham and Trotman, London, 1131-1148.

Eldholm, O., Vogt, P., and Perry, R., 1978, Plate Tectonic Development of the Mid-Oceanic Ridge System North of the Jan Mayen Fracture Zone, A: Present Plate Boundaries, EOS 59, 371.

Eldholm, O. and Sundvor, E., 1980, The Continental Margins of the Norwegian-Greenland Sea: Recent Results and Outstanding Problems, Royal Society of London Phil. Trans., Ser. A: 294, 77-86.

Eldholm, O., Karasik, A. M., and Reksnes, P. A., 1986, The North American Plate Boundary, DNAG synthesis. Volume Geology of the Arctic Ocean Region Chapter 12.

Harland, W. B., 1969, Contribution of Spitsbergen to understanding of tectonic evolution of North Atlantic Region. In: M. Kay (Editor), North Atlantic: Geology and Continental Drift. American Association of Petroleum Geologists, Memoir 12, 817-851.

Horsfield, W. T. and Maton, P. I., 1970, Transform Faulting along the De Geer Line, Nature 226, 256-257.

Johnson, L. and Heezen, B. C., 1967, Morphology and Evolution of the Norwegian-Greenland Sea, Deep-Sea Research 14, 755-771.

Kovacs, L.C., Johnson, G. L., Srivastava, S. P., Taylor, P. T., and Vogt, P. R., 1987, Residual Magnetic Anomaly Chart of the Arctic Ocean Region (Naval research Laboratory and Naval Ocean research and Development Activity), In: The Arctic Ocean Region, Vol. L., The Geology of North America, edited by Arthur Gantz, L. Johnson, and J. F. Sweeny, 1990, 644p.

Minster, W. J., and T. H. Jordan, 1978, Present-Day Plate Motions, Jour. Geophys. Res., 83, 5331-5354.

Morgan, W. J., 1981, Hotspot Tracks and the Opening of the Atlantic and Indian Oceans, in The Sea, 7, edited by C. Emiliani, pp. 443-487, John Wiley, New York.

Okay, N., and Crane, K., 1993, Thermal Rejuvenation of the Yermak Plateau, Marine Geophysical Researches, 15, 243-263.

Shor, A., 1990, SeaMARC II seafloor mapping system: Seven years of Pacific research, Pacific Rim Congress Vol. III; Australian Institute of Mining and Metallogenesis, 49-59.

Sobczak, L. W., and Hearty, D. B., with contributions by R. Forsberg, Y. Kristoffersen, O. Eldholm and S. D. May), 1987, Gravity of the Arctic Ocean, In: The Arctic Ocean Region, Vol. L., The Geology of North America, edited by Arthur Gantz, L. Johnson, and J. F. Sweeny, 1990, 644p.

Stein, S., Melosh, H. J., and Minster, J. B., 1977, Ridge Migration and Asymmetric Sea-floor Spreading, Earth Planet. Sci. Lett., 36, 51-62.

Sundvor, E. and O. Eldholm, 1979, The Western and Northern Margin off Svalbard, Tectonophysics, 59, 239-250.

Talwani, M. and Eldholm, O., 1977, Evolution of the Norwegian-Greenland Sea, Geol. Soc. America Bull. 88, 969-999.

Thiede, J., S. Pfirman, H-W Schenke, and W. Reil, 1990, Bathymetry of the Molloy Deep: Fram Strait between Greenland and Svalbard, Marine Geophysical Researches, 12, 197-214.

Vogt, P. R., 1986b, Geophysical and Geochemical Signatures and Plate Tectonics, Chapter 11, in The Nordic Seas, edited by B. G. Hurdle, Springer Verlag.

Vogt, P. R., 1986a, Seafloor Topography, Sediments, and Paleoenvironments, Chapter 11, in The Nordic Seas, edited by B. G. Hurdle, Springer Verlag.

Vogt, P. R., and Avery, O. E., 1974, Tectonic History of the Arctic Basins: Partial Solutions and Unsolved Mysteries, in Marine Geology and Oceanography of the Arctic Seas, edited by Herman, Y., 83-117, Springer-Verlag, New York.

Vogt, P. R., R. K. Perry, R. H. Feden, H. S. Fleming, and N. Z. Cherkis, 1981, The Greenland-Norwegian Sea and Iceland Environment: Geology and Geophysics; In: The Ocean Basins and Margins, Vol. 5, The Arctic Ocean, Edited by A. E. M. Nairn and M. Churkin, pp. 493-598, Plenum, New York, 1981.

Vogt, P. R., L. C. Kovacs, L. C. Bernero, and S. P. Srivastava, 1982, Asymmetric geophysical signatures in the Greenland-Norwegian and southern Labrador Seas and the Eurasia Basin, Tectonophysics, 89, 95-160.